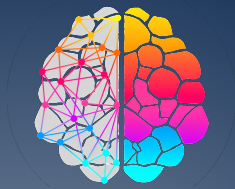

MATHEMATICAL AND NUMERICAL MODELING OF THE HUMAN BRAIN: FROM PHYSIOLOGY TO NEURODEGENERATIVE DISEASES

Paola F. Antonietti

Università degli Studi di Roma Tor Vergata

January 2025

Acknowledgements

https://brainum.mox.polimi.it/

The BraiNum Team

lymph

Francesca Bonizzoni

Ivan Fumagalli

Stefano Pagani

Nicola Parolini

Mattia Corti

Niteen Kumar

Caterina B. Leimer Saglio

The plan

1. Elements of brain's physiology and Neurodegenerative Disorders

2. A quick introduction to (conforming) FEM and polytopal Discontinuous Galerkin methods

3. Mathematical and numerical modelling of the misfolding process in NDs

4. Mathematical and numerical modelling of the brain's perfusion and waste clearance mechanisms

5. Mathematical and numerical modelling of epileptic seizures

lymph - discontinuous poLYtopal methods for Multi-PHysics

lymph

lymph.bitbucket.io

Physics

Laplacian

$$-\nabla \cdot (\mu \nabla u) = f$$

- **Assembly**
- **InputData**
- **MainFunctions**
- **PostProcessing**
- RunSetup.m
- RunMainLaplacian.m
- ...

Heat

$$\frac{\partial u}{\partial t} - \nabla \cdot (\mu \nabla u) + \sigma u = f$$

- **Assembly**
- **InputData**
- **MainFunctions**
- **PostProcessing**
- **TimeIntegration**
- RunSetup.m
- RunMainParabolic.m
- ...

Elastodynamics

$$\frac{\partial^2 \boldsymbol{u}}{\partial t^2} - \nabla \cdot \boldsymbol{\sigma}(\boldsymbol{u}) = \boldsymbol{f}$$

- **Assembly**
- **InputData**
- **MainFunctions**
- **PostProcessing**
- **TimeIntegration**
- RunSetup.m
- RunMainEla.m
- ...

Poroelastoacoustics

$$\begin{cases} \rho_p \frac{\partial^2 \boldsymbol{u}_p}{\partial t^2} + \rho_f \frac{\partial^2 \boldsymbol{u}_f}{\partial t^2} - \nabla \cdot \boldsymbol{\sigma}_p(\boldsymbol{u}_p, \boldsymbol{u}_f) = \boldsymbol{f}_p \\ \rho_f \frac{\partial^2 \boldsymbol{u}_p}{\partial t^2} + \rho_w \frac{\partial^2 \boldsymbol{u}_f}{\partial t^2} + \frac{\eta}{k} \frac{\partial \boldsymbol{u}_f}{\partial t} - \nabla \cdot \boldsymbol{\sigma}_f(\boldsymbol{u}_p, \boldsymbol{u}_f) = \boldsymbol{f}_f \end{cases}$$

$$c^{-2} \frac{\partial^2 \varphi_a}{\partial t^2} - \rho_a^{-1} \nabla \cdot (\rho_a \nabla \varphi_a) = f_a$$

- **Assembly**
- **InputData**
- **MainFunctions**
- **PostProcessing**
- **TimeIntegration**
- RunSetup.m
- RunMainPoroAcuEla.m
- ...

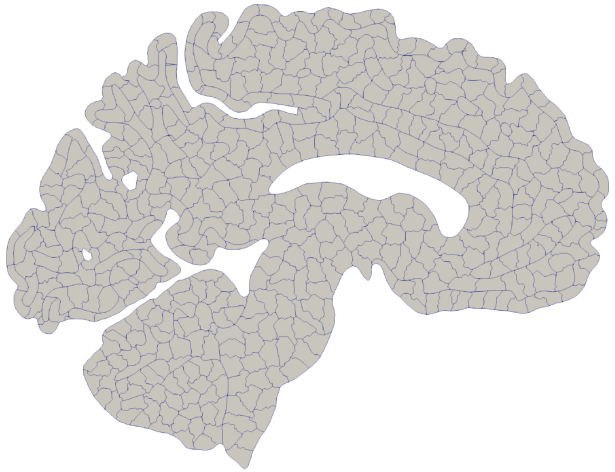

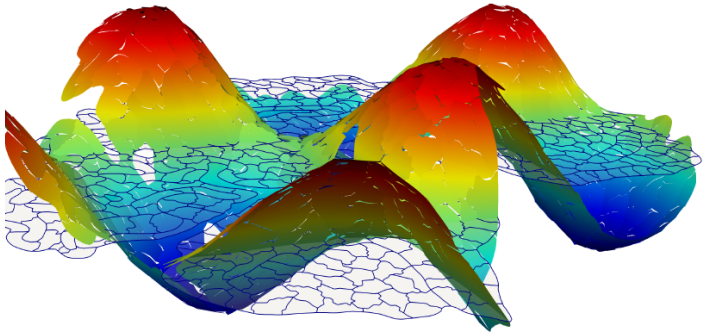

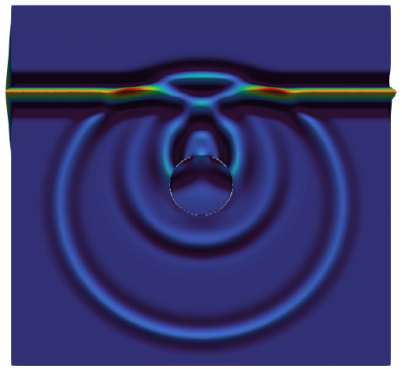

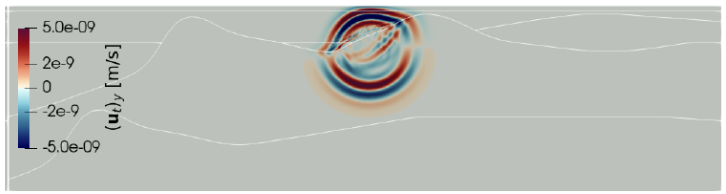

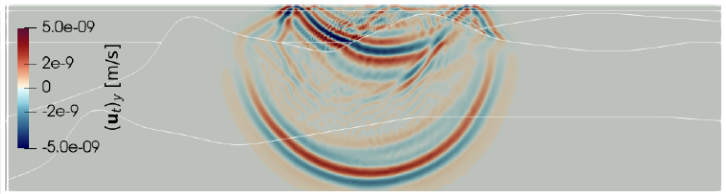

lymph – discontinuous poLYtopal methods for Multi-PHysics

[Antonietti, Bonetti, Botti, Corti, Fumagalli, Mazzieri, *Transactions on Mathematical Software* (2025)]

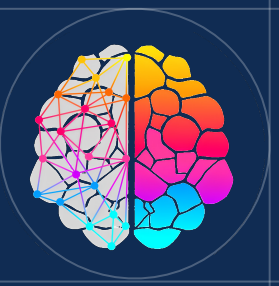

1 - Elements of brain’s physiology and neurodegenerative disorders

01

Overview of brain anatomy

The brain is the largest organ and part of the Central Nervous System (CNS). Its major divisions are the cerebrum, cerebellum, brain stem, and diencephalon.

Cerebrum

It is associated with higher functions like reasoning and memory.

Cerebellum

It is associated with motor control and coordination.

Brain stem

It is associated with vital functions such as breathing and heart rate.

Diencephalon

It is the relay center for sensory information and homeostatic functions.

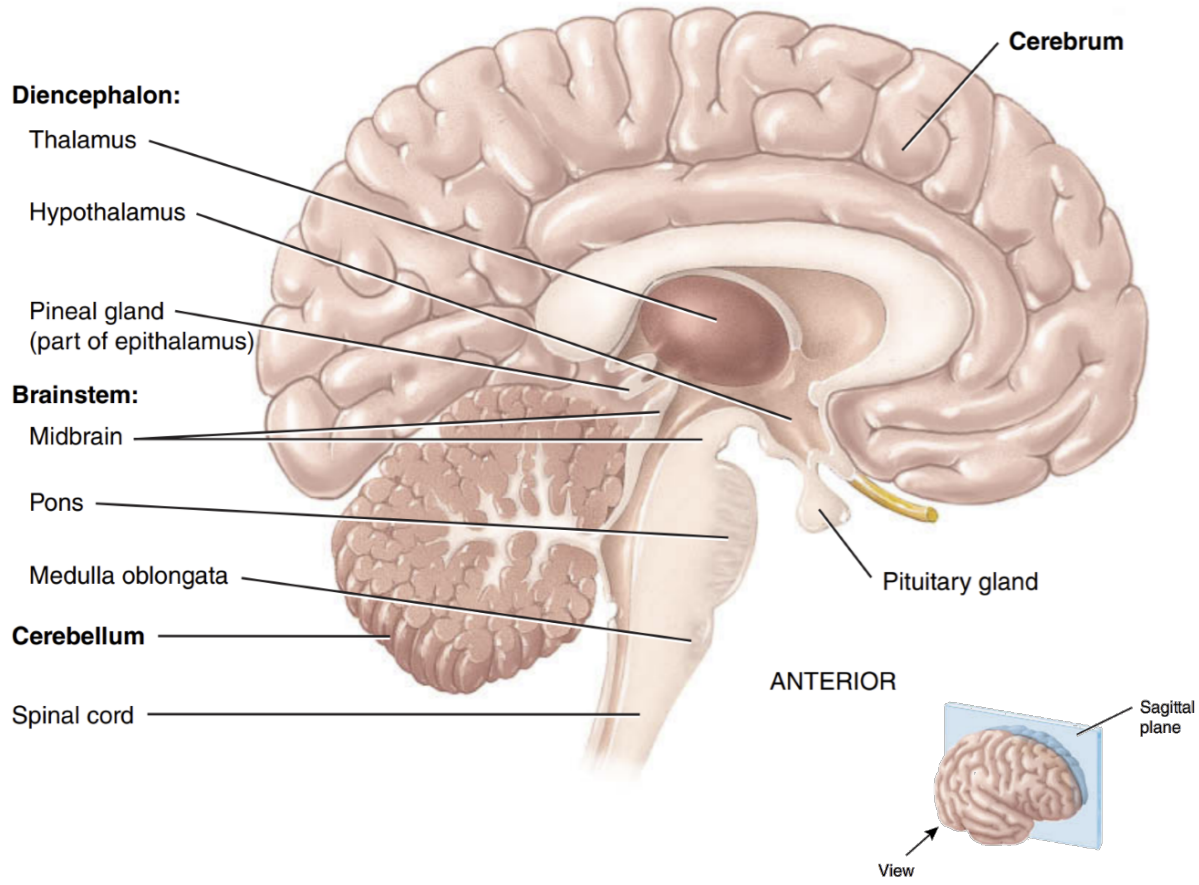

G. J. Tortora, and B. Derrickson – Principles of Anayomy & Physiology (2017)

Cerebrum and lobes

The cerebrum is divided into two hemispheres, connected by the corpus callosum. The outer layer is composed of grey matter and divided into four lobes associated with different abilities.

Frontal Lobe

- Decision making
- Motor Control

Parietal Lobe

- Positioning
- Sensory information integration
- Calculus capacity

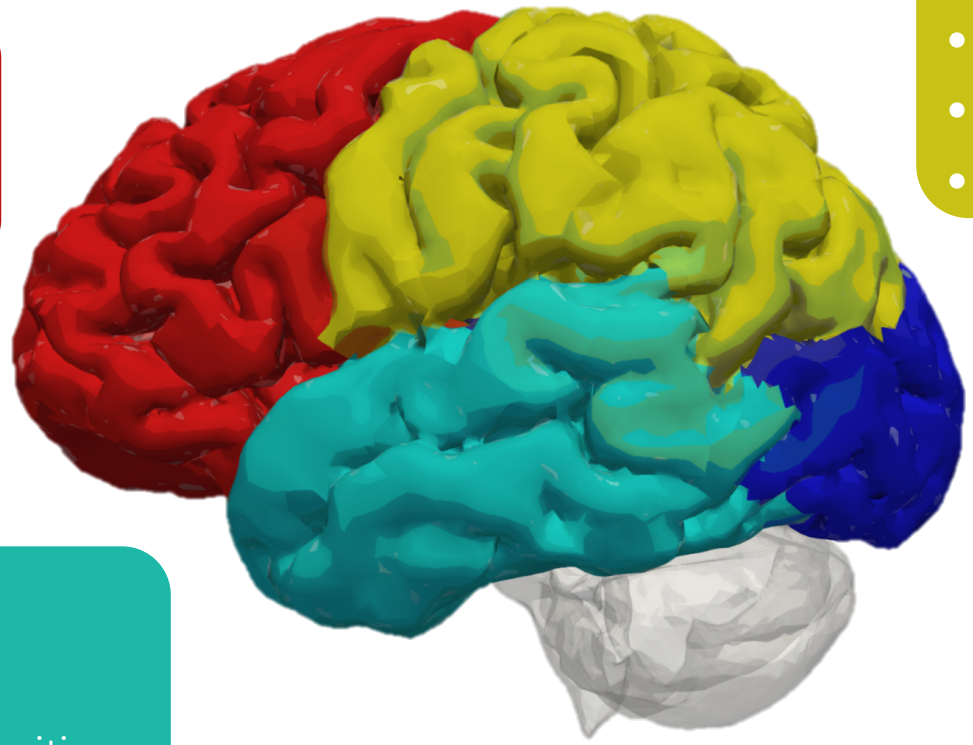

Temporal Lobe

- Sounds perception
- Object/language recognition
- Long-term memory.

Occipital Lobe

Interpretation of visual stimuli (presence of primary and secondary visual cortex).

G. J. Tortora, and B. Derrickson – Principles of Anayomy & Physiology (2017)

Ventricular system

The ventricular system is a complex network of interconnected cavities within the brain, filled with cerebrospinal fluid (CSF). It comprises two lateral ventricles located in the cerebral hemispheres, the third ventricle in the midline, and the fourth ventricle, positioned between the brain stem and the cerebellum.

Functions of Cerebrospinal Fluid

- Cushioning: Provides mechanical protection, acting as a shock absorber for the brain.
- Nutrient Transport: Facilitates the distribution of nutrients and removal of waste products.
- Homeostasis: Maintains stable intracranial pressure and ionic balance, critical for neuronal function.

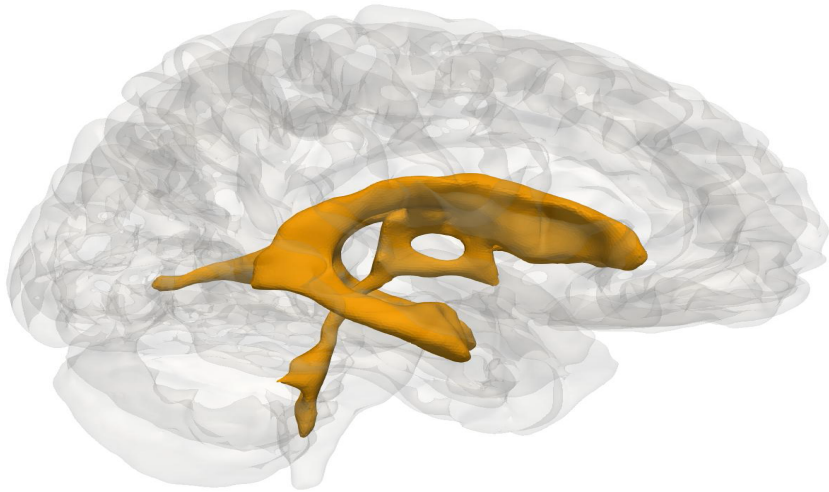

L. Sakka, G. Coll, and J. Chazal – European Annals of Otorhinolaryngology (2011)

Circulatory system

Neurons are the most sensitive cell type to the interruption of oxygen supply.

The brain's oxygen consumption is incredibly high (15% of the cardiac output at rest).

Large arteries provide the oxygenated blood to the brain. At the base of the brain, there is a connection on each side between the middle and posterior cerebral arteries, known as the circle of Willis. This allows the compensation of occlusions of main arterial trunks.

The large cerebral veins can be divided into deep and superficial types. The latter accompany the arteries on the brain's surface. All of the veins empty into large venous sinuses formed by folds of the dura.

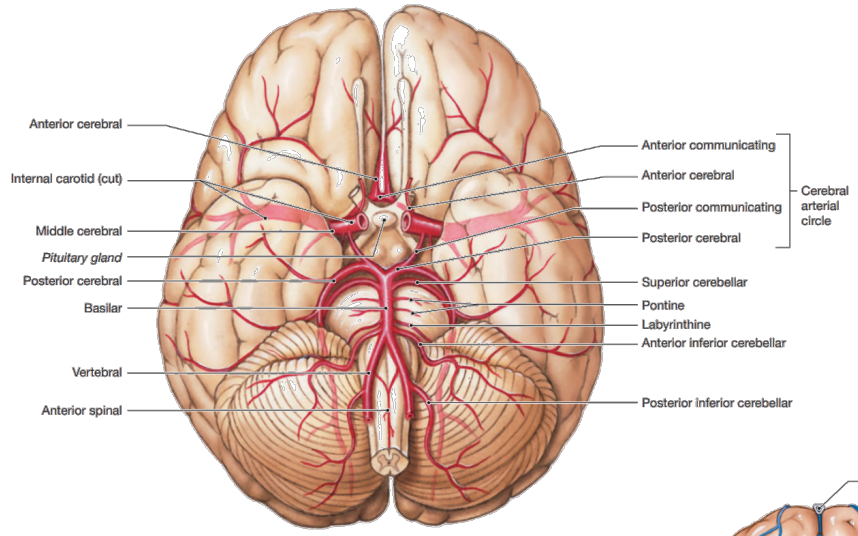

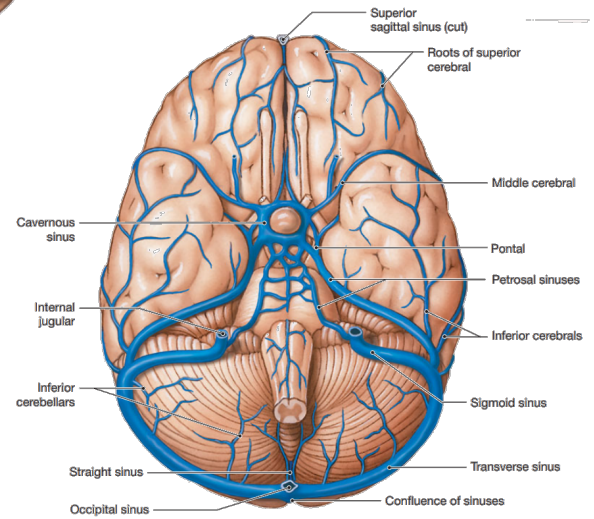

F.H. Martini, M.J. Timmons, and R.B. Tallitsch – Human Anatomy (2012)

Neuronal structure

From a microscopical point of view, the nervous system is composed of neurons and glial cells. The first ones are responsible for the main functions of the nervous system, whereas the glial cells primarily support and protect the neurons.

A neuron is a cell with a body (or soma) that has a nucleus surrounded by cytoplasm containing various organelles. It is also composed of an axon and some dendrites that connect it to different neurons.

Neuronal cells respond to stimuli with an electrical discharge and can conduct nerve impulses quickly over long distances. In most cases, the nerve impulse reaches the synapse, where communication with the next neuron occurs.

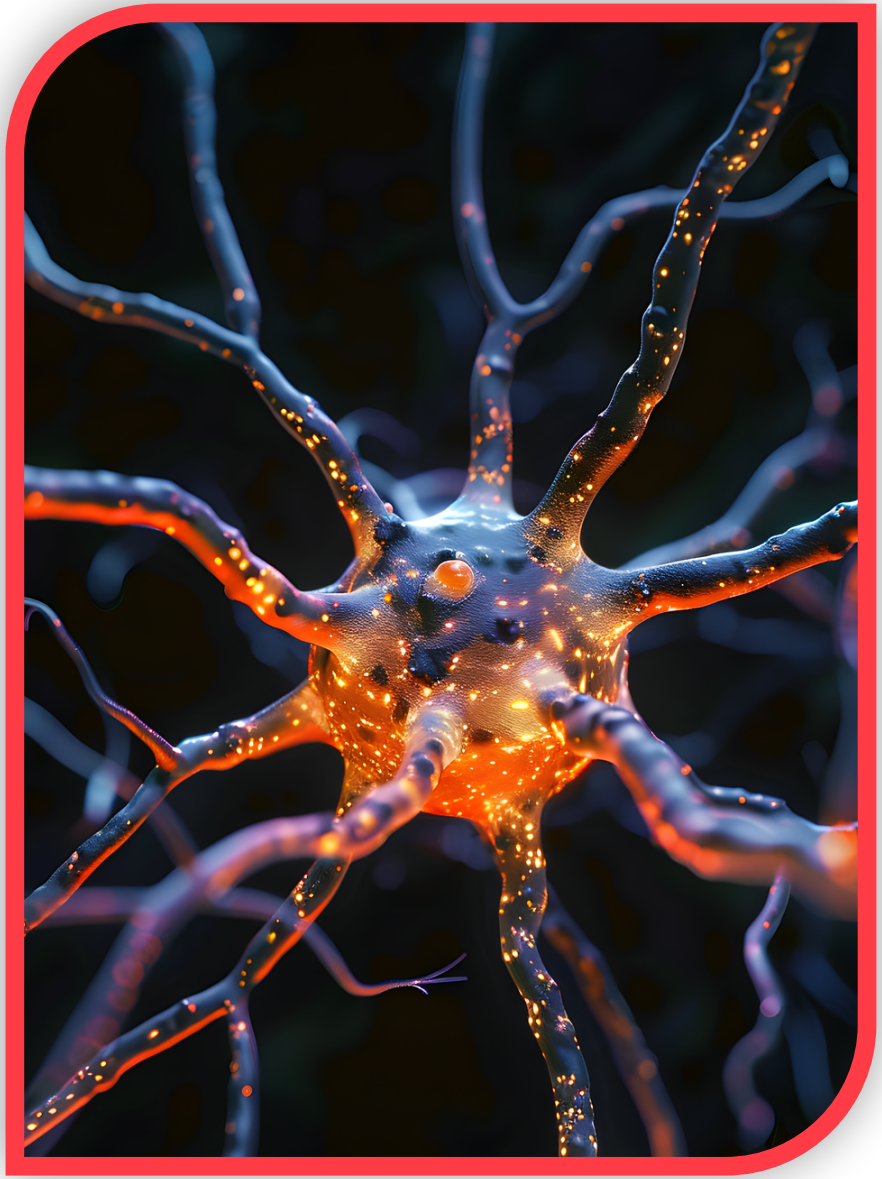

P. Brodal – The Central Nervous System (2010)

Neurodegenerative diseases

Some neurodegenerative diseases involve abnormal protein conformations that resist normal degradation. These pathologies are known as protheinopathies.

Misfolded proteins tend to aggregate, can disrupt cell function, and cause neuronal toxicity, leading to neuronal death. Moreover, proteins may spread through neural pathways, affecting distant brain regions.

This process is called the prion-like paradigm. The prion effect is not limited to classic prion diseases; similar mechanisms are observed in other proteinopathies.

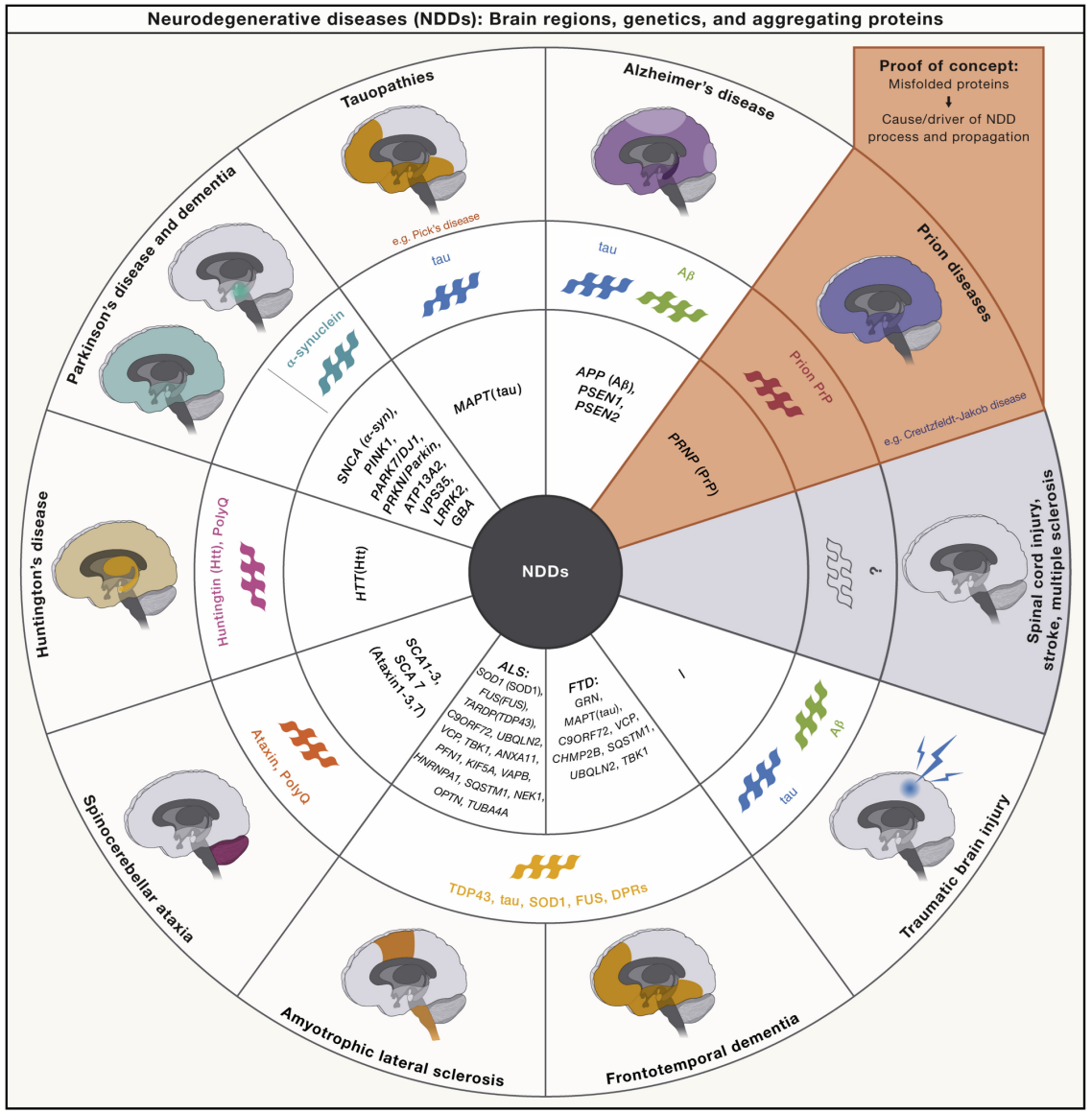

D. M. Wilson et al. – Cell (2023)

Alzheimer's disease

Alzheimer's disease is the most common dementia. It is characterized by a progressive neurodegeneration accompanied by cognitive impairments. Alzheimer's disease is predicted to affect more than 139 million people in 2050.

The earliest manifestations are normally associated to a subjective decline in mental abilities without impaired performance on objective cognitive testing. This first symptomatic stage is named Mild Cognitive Impairment (MCI).

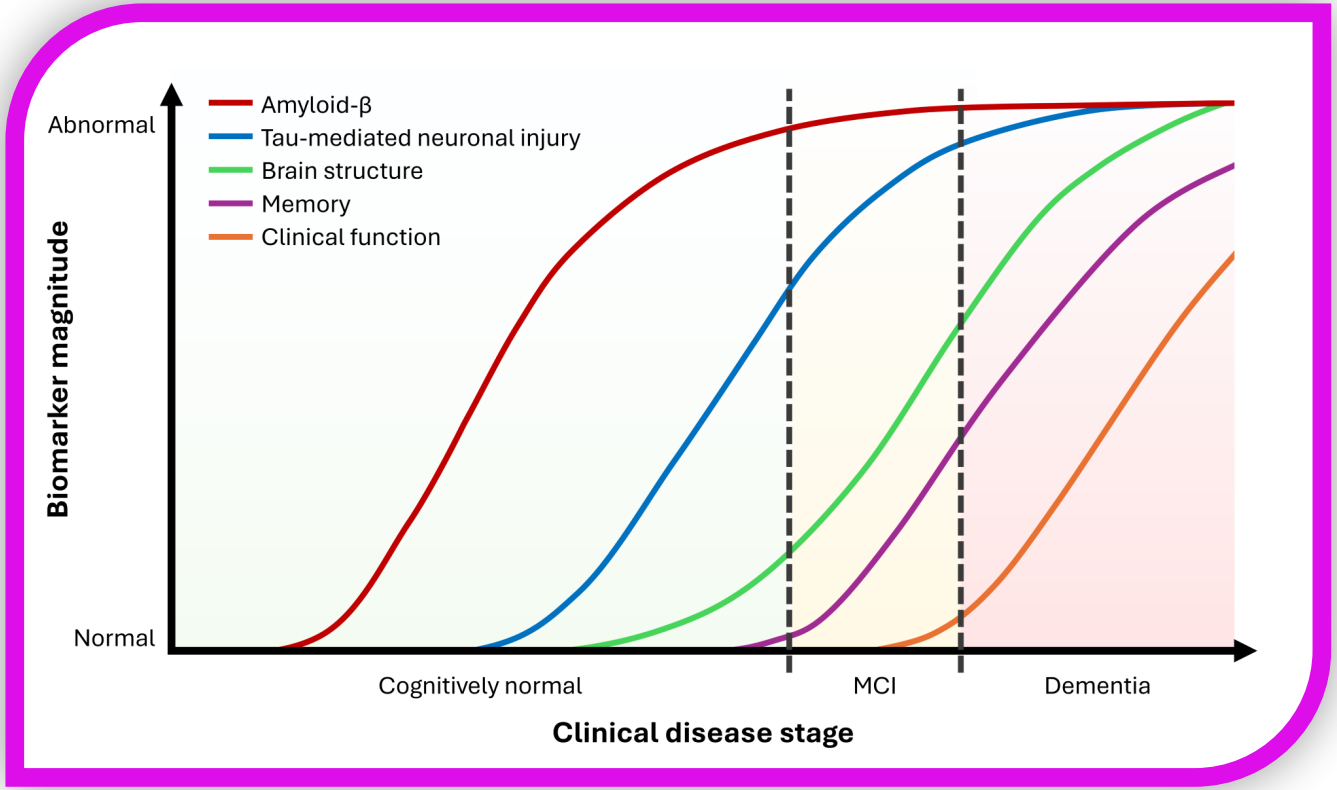

Alzheimer's disease is characterized by accumulating two abnormal proteins: amyloid-β and tau protein. Deposits of aggregated amyloid plaques and induce aggregation of tau protein, by forming neurofibrillary tangles. The created inflammatory state contribute to neuronal death, leading to brain atrophy.

D. S. Knopman et al. – Nature Reviews. Disease Primers (2021)

Parkinson's disease

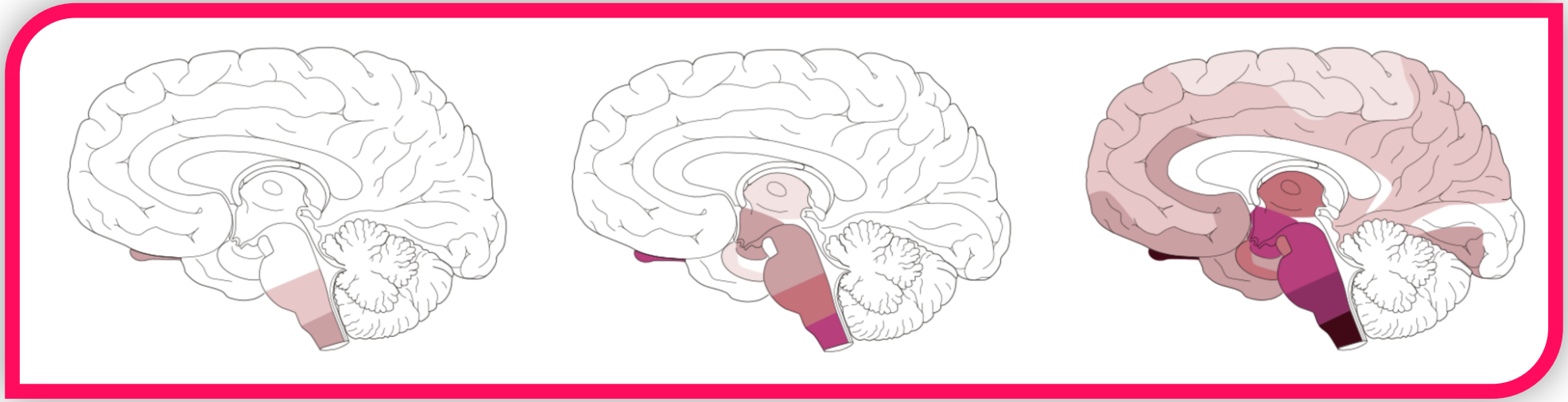

Parkinson's disease is the second most common neurodegenerative disorder. Overall, the global prevalence of the disease is estimated at around 0.3%. Parkinson's disease is clinically defined by bradykinesia, namely movements slower than expected, and at least one additional cardinal motor feature (rigidity or rest tremor).

Characteristic features of Parkinson's disease include neuronal death in specific areas of the substantia nigra and the widespread α-synuclein accumulation in Lewy bodies. Gross macroscopic atrophy of the brain is not detected in Parkinson's disease. Neurodegeneration occurs only in certain types of neurons within particular brain regions.

W. Poewe et al. – Nature Reviews. Disease Primers (2017)

Epilepsy

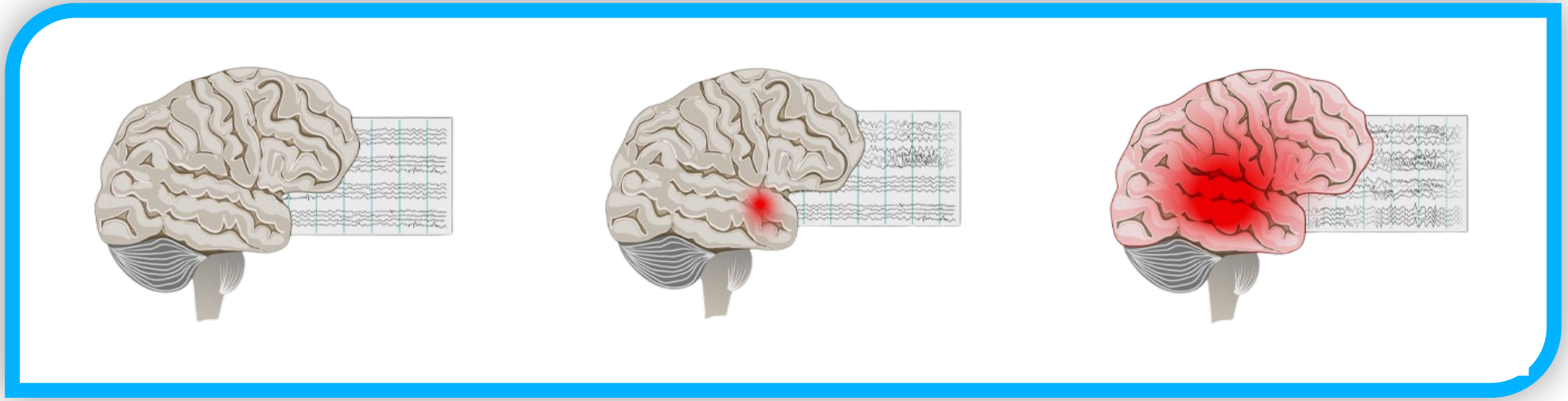

Epilepsy is a brain condition that causes recurring seizures. There are many types of epilepsy, and in some cases, the cause is not known. Epilepsy is common. It's estimated that 1.2% of people in the United States have active epilepsy.

Seizure symptoms can vary widely. Some people may lose awareness during a seizure. Some people stare blankly for a few seconds during a seizure. Others may repeatedly twitch their arms or legs, movements known as convulsions. Treatment with medicines or sometimes surgery can control seizures for most people with epilepsy.

O. Devinsky et al. – Nature Reviews. Disease Primers (2018)

The mathematical and computational challenges

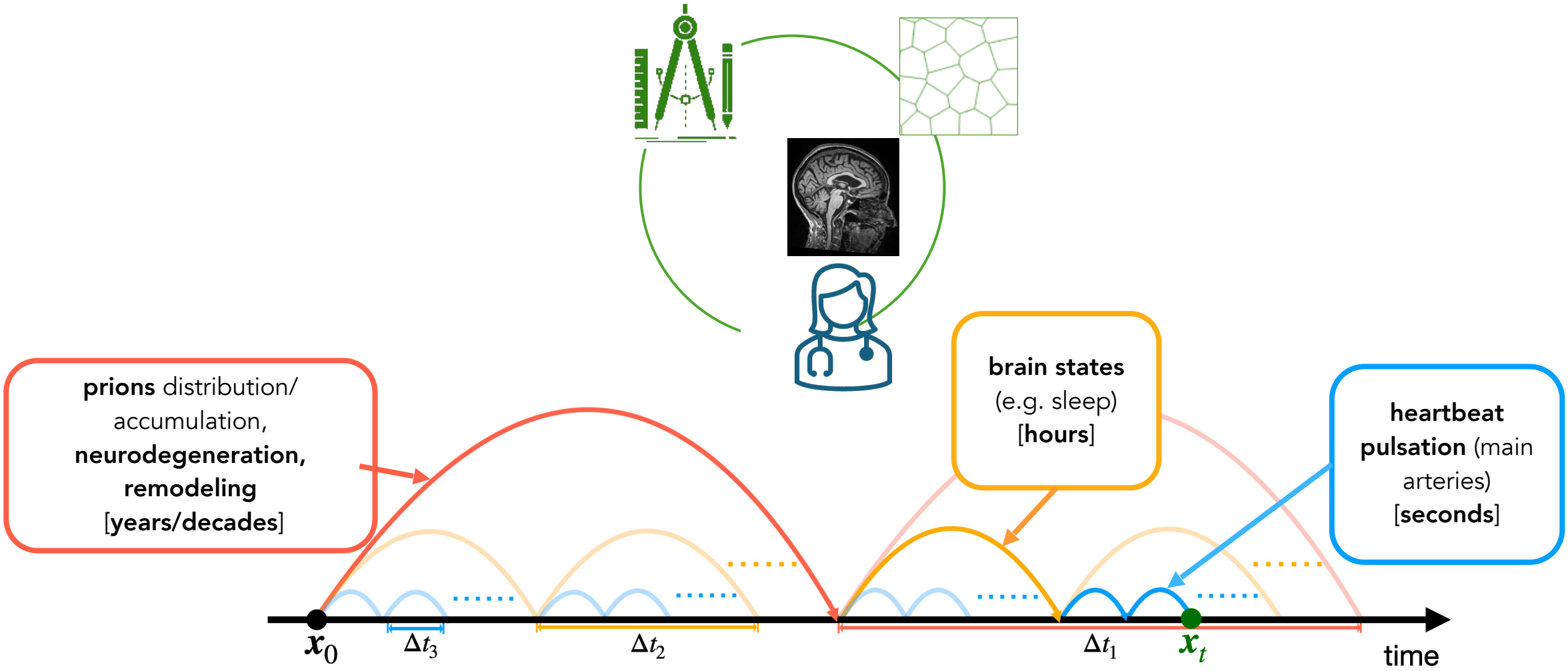

Challenges (and opportunities)

Modelling

- Transport/agglomeration of misfolded proteins
- CSF production: still discussed in the medical literature [Orešković, Brinker, MacAulay, …]
- The brain is an extremely soft material [Goriely, Holzapfel, Kuhl, …]
- Effects of tissue nonlinear elasticity on clearance/atrophy
- Interstitial CSF flow in perivascular space [Iliff, Mardal, Rognes, …]

Computational

- Generation and parallel partition brain meshes
- Structure-preserving numerical schemes
- Robust & scalable solvers
- Complicated geometries, moving domains (ALE) CFD, embedded interfaces,
- Energy conservation at the interfaces in time-discrete settings
- Machine-learning enhanced acceleration algorithms

Clinical

- Integration of physics-based and data-driven approaches
- Machine learning surrogate models
- Latent dynamics
- Uncertainty in the data

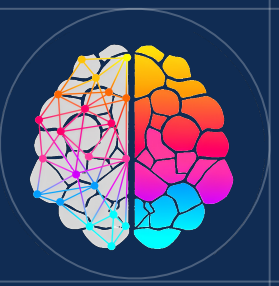

2 - A quick introduction to (conforming) FEM and polytopal Discontinuous Galerkin methods

02

2a - Conforming FEMs

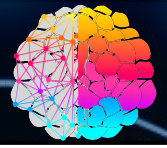

Model (Toy) Problem: the Poisson Equation

Let $\Omega \subset \mathbb{R}^d$ $(d = 2, 3)$ be an convex, polygonal domain. Given $f \in L^2(\Omega)$ find $u \in H^2(\Omega)$ such that

$$\begin{cases} -\Delta u = f & \text{in } \Omega \\ u = 0 & \text{on } \partial\Omega \end{cases}$$

Variational formulation

Find $u \in H_0^1(\Omega)$ such that

$$\int_\Omega \nabla u \cdot \nabla v = \int_\Omega fv \quad \forall\, v \in H_0^1(\Omega)$$

General setting

$$\text{Find } u \in V \equiv H_0^1(\Omega) \text{ such that} \quad \mathcal{A}(u, v) = \mathcal{F}(v) \quad \forall\, v \in V \quad (P)$$

Model (Toy) Problem: the Poisson Equation

Let V an Hilbert space endowed with the norm $\|\cdot\|_V$.Consider the following problem

$$\text{Find } u \in V \text{ such that} \quad \mathcal{A}(u,v) = \mathcal{F}(v) \quad \forall\, v \in V \quad (\star)$$

- $\mathcal{A} : V \times V \longrightarrow \mathbb{R}$ is a bilinear form that satisfies

$$\begin{aligned} &\text{Continuity} && |\mathcal{A}(w,v)| \lesssim \|w\|_V \|v\|_V && \forall w, v \in V \\ &\text{Coercivity} && \mathcal{A}(v,v) \gtrsim \|v\|_V \|v\|_V && \forall v \in V \end{aligned}$$

- $\mathcal{F} : V \longrightarrow \mathbb{R}$ is a linear, continuous functional.

Then, problem $(\star)$ admits a unique solution $u \in V$ and

$$\|u\|_V \lesssim \|\mathcal{F}\|_{V^*} .$$

Our model problem (P) satisfies the Lax-Milgam lemma.

Discretization. Step 1: the mesh

- Let $\mathcal{T}_h$ be a *shape-regular*, *conforming* triangulation of Ω into triangles/tetrahedra
  - A triangulation $\mathcal{T}_h$ is called *conforming* if the intersection of any pair of neghboring elements is either empty, or a complete face or a complete edge or a vertex.
  - A triangulation $\mathcal{T}_h$ is called *shape-regular* if there exists a number $\rho > 0$ such that every $\mathcal{K} \in \Omega_h$ contains a circle of radius $\rho_{\mathcal{K}}$ with

$$\rho_{\mathcal{K}} \geq h_{\mathcal{K}}/\rho$$

    where h_K is the diameter of K.
- Define the mesh-size h as $h = \max_{\mathcal{K} \in \mathcal{T}_h}$

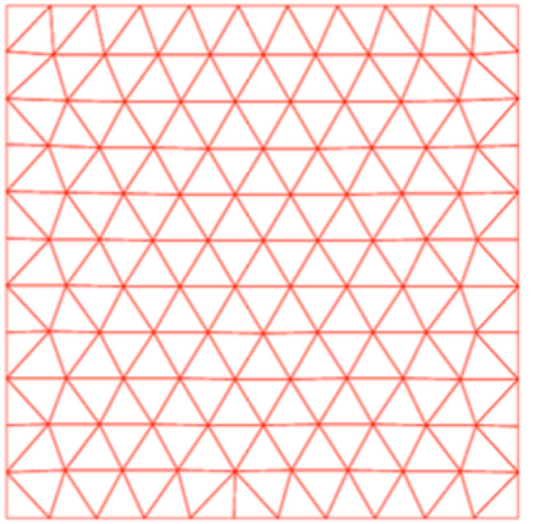

Discretization. Step 2: the discrete space

For $p \geq 1$, define

$$V_h^p = \left\{ v_h \in C^0(\Omega) : v_h|_{\mathcal{K}} \in \mathbb{P}^p(\mathcal{K}) \quad \forall K \in \mathcal{T}_h,\ v_h = 0 \text{on } \partial\Omega \right\} \subseteq H_0^1(\Omega)$$

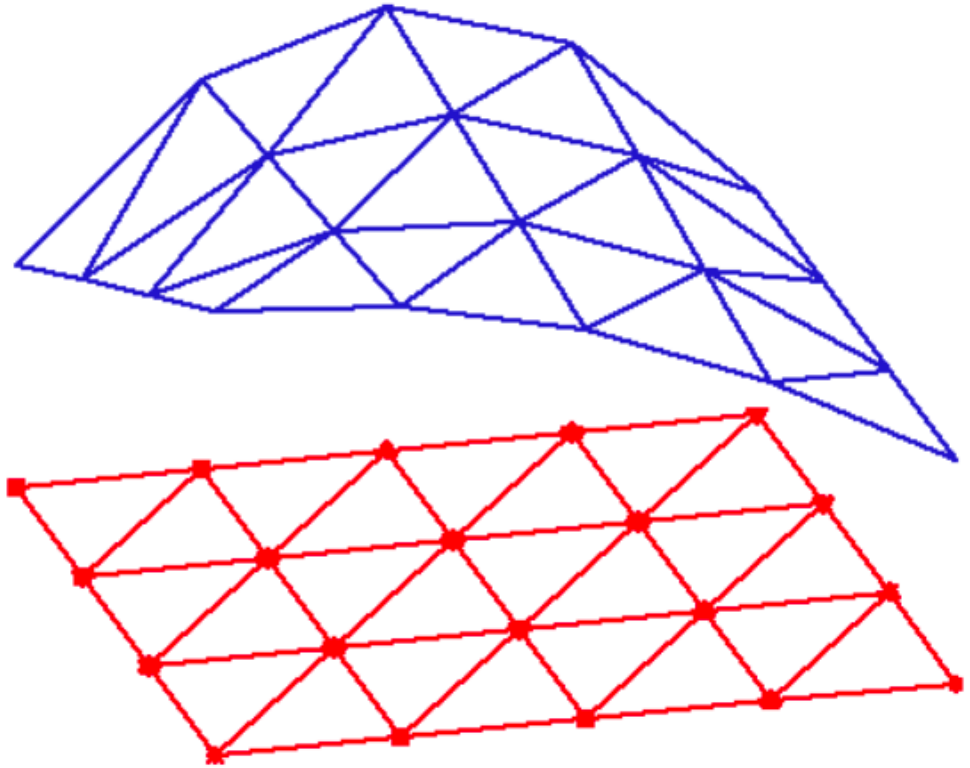

Example ot $v_h \in V_h^p$

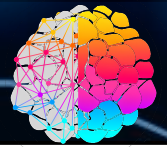

Discretization. Step 3: the discrete formulation

Find $u_h \in V_h^p$ such that

$$\int_\Omega \nabla u_h \cdot \nabla v_h = \int_\Omega f v_h \quad \forall\, v_h \in V_h^p$$

General setting

Find $u_h \in V_h^p$ such that

$$\mathcal{A}(u_h, v_h) = \mathcal{F}(v_h) \quad \forall\, v_h \in V_h^p \quad (P_h)$$

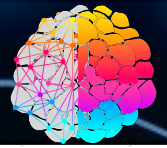

Algebraic form

- Chose a basis for V_h^p, i.e. $V_h^p = \text{span}\left\{\varphi_j,\, j = 1, \ldots, N_h^p\right\}$
- Express the discrete solution u_h in terms of the basis $\{\varphi_j\}$, i.e.

$$u_h = \sum_{j=1}^{N_h^p} u_j \varphi_j$$

- Impose that (P_h) is verified for any basis function, i.e.

$$\sum_{j=1}^{N_h^p} u_j \mathcal{A}(\varphi_j, \varphi_i) = \mathcal{F}(\varphi_i) \quad \forall\, i = 1, \ldots N_h^p$$

- Rewrite (P_h) as a system of N_h^p linear equations in N_h^p unknowns

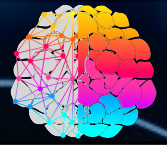

Algebraic form (cont'd)

$$\text{Find } \mathbf{u} = [u_1, u_2, \ldots, u_{N_h^p}]^T \in \mathbb{R}^{N_h^p} \quad \text{such that} \quad \mathbf{Au} = \mathbf{F}$$

- $\mathbf{A} \in \mathbb{R}^{N_h^p \times N_h^p}$ is defined as

$$\mathbf{A}(i,j) = \mathcal{A}(\varphi_j, \varphi_i) \quad \forall\, i,j = 1, \ldots N_h^p$$

- $\mathbf{F} \in \mathbb{R}^{N_h^p}$ is defined as

$$\mathbf{F}(i) = \mathcal{F}(\varphi_i) \quad \forall\, i = 1, \ldots N_h^p$$

Properties of the matrix $\mathbf{A}$

The matrix $\mathbf{A}$ is symmetric and positive definite (spd).

Example: $p = 1$, triangular grid, Lagrangian shape functions

- Any $v_h \in V_h^1$ is characterized by the values it takes at the internal vertexes $\mathbf{V}_j$, $j = 1, \ldots, N_h^p$, of the grid $\mathcal{T}_h$
- On the boundary $v_h = 0$
- $V_h^1 = \text{span}\left\{\varphi_j, j = 1, \ldots, N_h^p\right\}$ (Lagrangian functions)

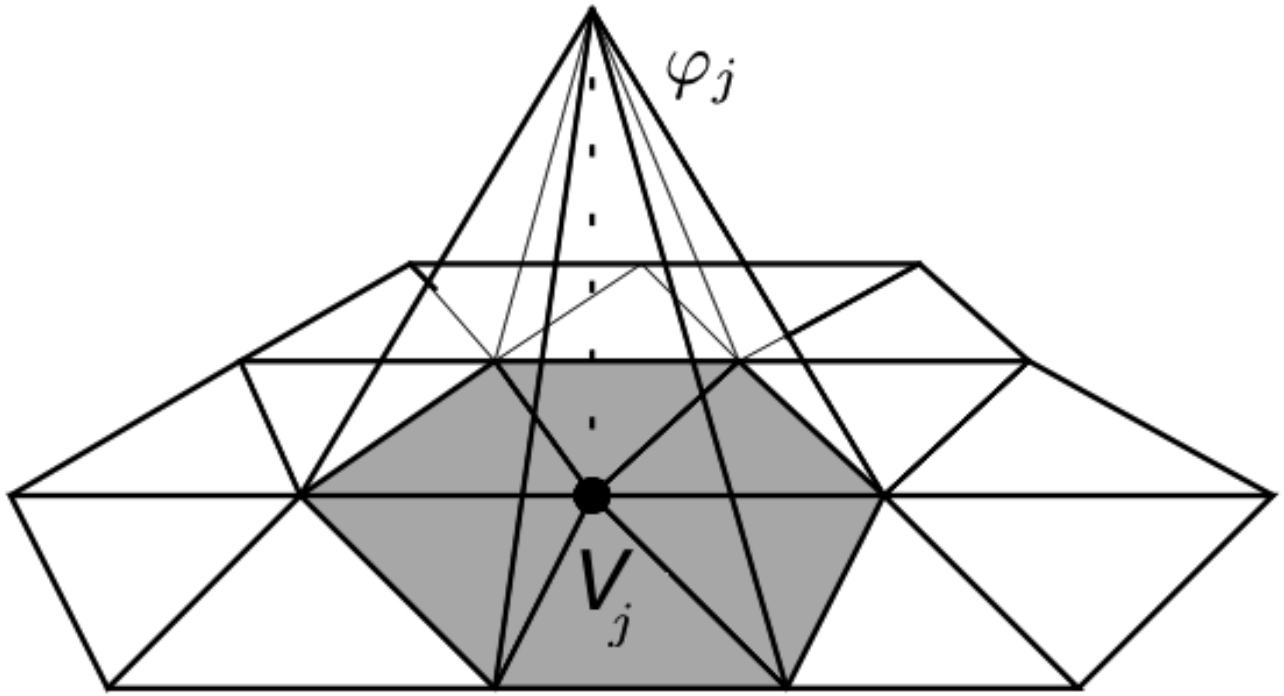

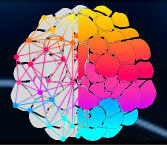

Condition number of the stiffness matrix A

Since **A** is spd, its spectral condition number is given by

$$\kappa_2(\mathbf{A}) = \frac{\lambda_{\max}(\mathbf{A})}{\lambda_{\min}(\mathbf{A})}$$

where $\lambda_{\max}(\mathbf{A})$ and $\lambda_{\min}(\mathbf{A})$ are the maximum and minimum eigenvalue of **A**, respectively.

It can be shown that

$$\kappa_2(\mathbf{A}) \leq C(p)h^{-2}$$

- as the grid-size h decreases the associated system becomes more and more ill-conditioned
- the higher the conditioning number is, the more the solution of the linear system resents from the perturbation on the data
- the constant $C(p)$ depends (dramatically) on p.

Convergence analysis

Recall that $V_h^p \subset V \equiv H_0^1(\Omega)$ and that $\|\cdot\|_V \equiv |\cdot|_{H^1(\Omega)}$ is a norm on V (thanks to the Poincaré inequality).

To estimate the error $\|u - u_h\|_V$ we need four ingredients

1. Continuity: $\mathcal{A}(w, v) \lesssim \|w\|_V \|v\|_V$ for all $w, v \in V$
2. Coercivity: $\mathcal{A}(v_h, v_h) \gtrsim \|v_h\|_V^2$ for all $v_h \in V_h^p$
3. Consistency: $\mathcal{A}(u, v_h) = \mathcal{F}(v_h)$ for all $v_h \in V_h^p$
4. Interpolation estimates:

$$\|u - u_I\|_V \lesssim ?$$

for a suitable interpolant u_I of the exact solution u (see later)

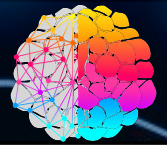

Convergence analysis

$$\|u - u_h\|_V \leq \|u - u_I\|_V + \|u_I - u_h\|_V \quad \text{(triangle inequality)}$$

$$\begin{aligned}
\|u_I - u_h\|_V^{\cancel{2}} &\lesssim \mathcal{A}(u_I - u_h, u_I - u_h) && \text{(coercivity)} \\
&\lesssim \mathcal{A}(u_I - u, u_I - u_h) && \text{(consistency)} \\
&\lesssim \|u_I - u\|_V \cancel{\|u_I - u_h\|_V} && \text{(continuity)}
\end{aligned}$$

$$\|u - u_h\|_V \lesssim \|u - u_I\|_V$$

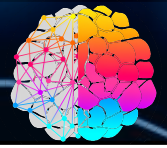

Convergence analysis

Interpolation estimates

Let $\{\mathcal{T}_h\}_h$ be a family of regular grids with granularity $h > 0$. Then, there exists a constant $C(p)$ such that

$$|v - v_I|_{H^m(\Omega)} \leq C(p)\, h^{p+1-m}\, |v|_{H^{p+1}(\Omega)} \quad \forall v \in H^{p+1}(\Omega) \quad m = 0, 1$$

where $v_I : C^0(\Omega) \longrightarrow V_h^p$ is the Lagrangian interpolation operator interpolating v in the degrees of freedom.

Error estimates in the V-norm

If the exact solution u of problem (P) is such that $u \in H^{p+1}(\Omega)$ then

$$\|u - u_h\|_V \leq C(p)\, h^p\, |u|_{H^{p+1}(\Omega)},$$

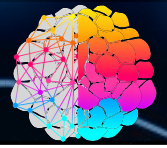

Convergence analysis (cont'd)

Elliptic regularity

Let Ω be a convex polygon and let $g \in L^2(\Omega)$. Consider the homogeneous Dirichlet problem

$$\begin{cases} -\Delta\varphi = g & \text{in } \Omega \\ \varphi = 0 & \text{on } \partial\Omega \end{cases} \qquad (P^*)$$

Then, the solution $\varphi \in H^2(\Omega)$ and $\|\varphi\|_{2,\Omega} \lesssim \|g\|_{0,\Omega}$

Suppose that the following property holds

Adjoint consistency

$$\mathcal{A}^*(v,\varphi) = \mathcal{A}(v,\varphi) = \mathcal{F}(v) \quad \forall\, v \in V$$

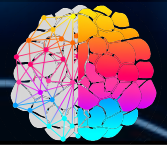

Eror estimates in the L^2norm: the Aubin-Nitsche trick

Take $g = u - u_h$ in (P^*), then

$$
\begin{aligned}
\|u - u_h\|_{0,\Omega}^2 &= \int_\Omega (u - u_h)^2 \\
&= \mathcal{A}(u - u_h, \varphi) \\
&= \mathcal{A}(\varphi, u - u_h) && \text{(adjoint consistency)} \\
&= \mathcal{A}(\varphi - \varphi_I, u - u_h) && \text{(consistency)} \\
&\lesssim \|\varphi - \varphi_I\|_V \, \|u - u_h\|_V && \text{(continuity)} \\
&\lesssim h \, \|\varphi\|_{2,\Omega} \, \|u - u_h\|_V && \text{(interpolation)} \\
&\lesssim h \, \|u - u_h\|_{0,\Omega} \, \|u - u_h\|_V && \text{(elliptic regularity)}
\end{aligned}
$$

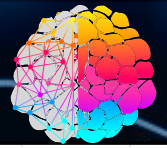

Eror estimates in the L^2 norm: the Aubin-Nitsche trick (cont'd)

Take $g = u - u_h$ in (P^*), then

$$
\begin{aligned}
\|u - u_h\|_{0,\Omega}^2 &= \int_\Omega (u - u_h)^2 \\
&= \mathcal{A}(u - u_h, \varphi) \\
&= \mathcal{A}(\varphi, u - u_h) && \text{(adjoint consistency)} \\
&= \mathcal{A}(\varphi - \varphi_I, u - u_h) && \text{(consistency)} \\
&\lesssim \|\varphi - \varphi_I\|_V \, \|u - u_h\|_V && \text{(continuity)} \\
&\lesssim h \, \|\varphi\|_{2,\Omega} \, \|u - u_h\|_V && \text{(interpolation)} \\
&\lesssim h \cancel{\|u - u_h\|_{0,\Omega}} \, \|u - u_h\|_V && \text{(elliptic regularity)}
\end{aligned}
$$

Error estimates in the L^2 norm

If the exact solution u of problem (P) is such that $u \in H^{p+1}(\Omega)$ then

$$\|u - u_h\|_{0,\Omega} \leq C(p) \, h^{p+1} \, |u|_{H^{p+1}(\Omega)}$$

2b - (Polytopal) Discontinuous Galerkin methods

What are DG methods?

Discontinuous Galerkin (DG) methods are a family of finite element methods for the approximation of partial differential equations

The idea

The discrete solution is seek in a discrete space made of polynomials that are completely discontinuous across mesh elements

$$V_h \not\subseteq V$$

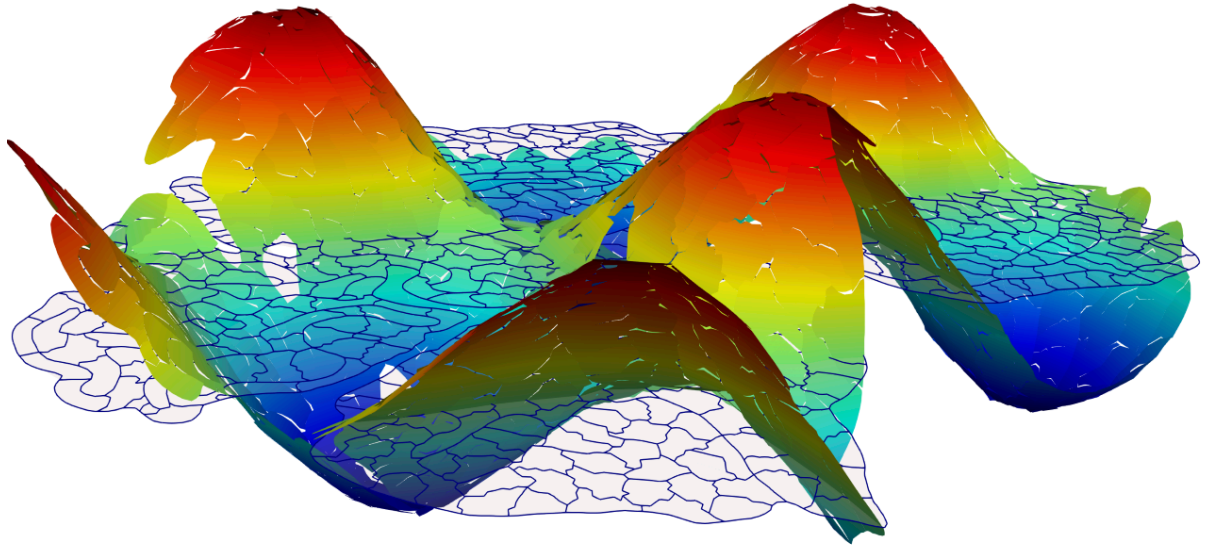

Feature of DG methods

- √ Wide range of PDE's treated within the same unified framework
- √ Weak approximation of boundary conditions
- √ Flexibility in mesh design
- √ Flexibility in polynomial degree distribution

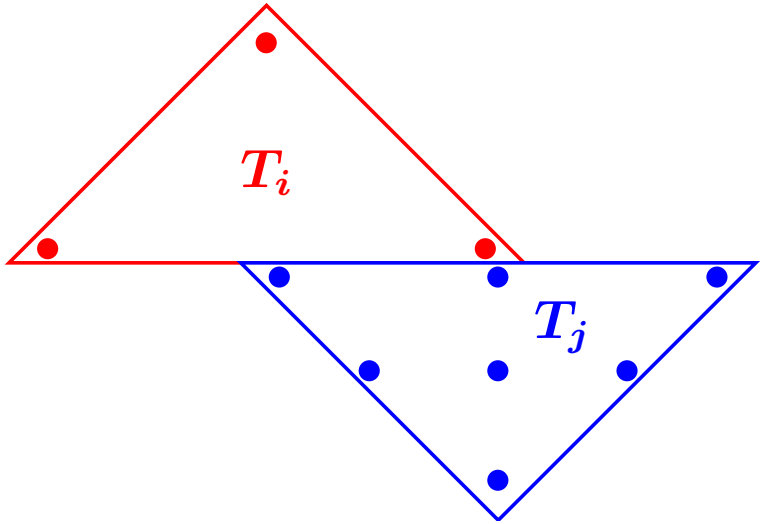

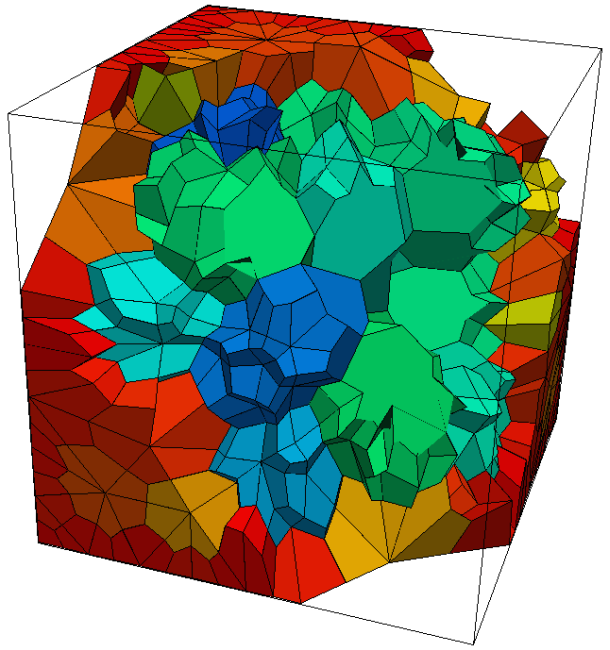

- X Higher number of degrees of freedom
- X Larger algebraic linear systems to be solved (need of fast solvers)

Essential bibliography

- B. Rivière. Discontinuous Galerkin Methods for Solving Elliptic and Parabolic Equations: Theory and Implementation, SIAM, 2008.
- J.S. Hesthaven, T. Warburton, Discontinuous Galerkin Methods. Algorithms, Analysis, and Applications, Springer, 2008.
- H. Fahs, High-order discontinuous Galerkin methods for the Maxwell equations, 2010, Editions Universitaires Europ`eennes,
- D. A. Di Pietro, A. Ern, Mathematical Aspects of Discontinuous Galerkin Methods, Springer, 2012
- A. Cangiani , Z. Dong , E. H. Georgoulis , P. Houston, hp-Version Discontinuous Galerkin Methods on Polygonal and Polyhedral Meshes, SpringerBriefs in Mathematics, 2017

Discretization. Step 1: the mesh

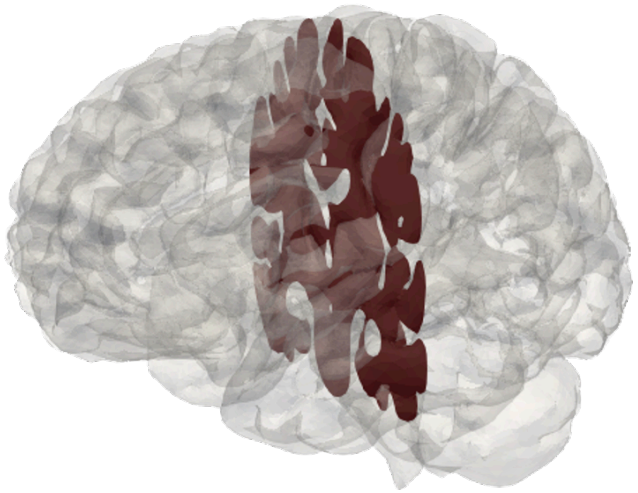

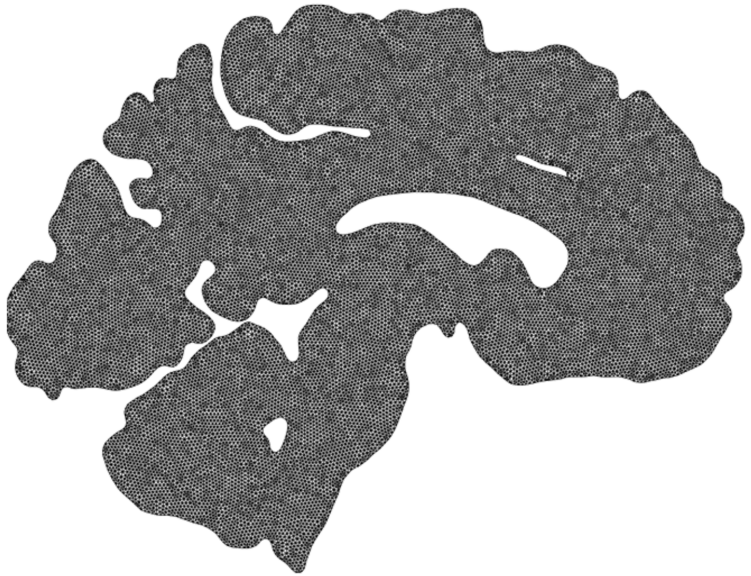

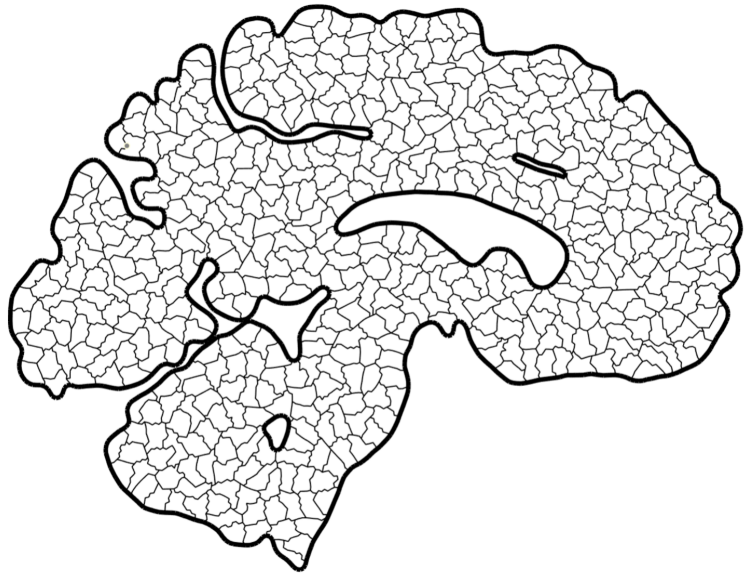

Let $\mathcal{T}_h$ be a polytopal mesh (very mild regularity assumption)

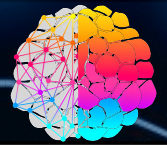

A first look at DG Finite Element methods

$$\text{Model problem} \quad \longrightarrow \quad \begin{cases} -\Delta u = f & \text{in } \Omega \\ u = 0 & \text{on } \partial\Omega \end{cases}$$

- Take the equation $-\Delta u = f$, multiply it by a (elementwise smooth) test function v and integrate over an element $\mathcal{K} \in \mathcal{T}_h$

$$\int_{\mathcal{K}} -\Delta u v = \int_{\mathcal{K}} f v$$

- Integrate by parts and sum over all the elements $\mathcal{K} \in \mathcal{T}_h$

$$\sum_{\mathcal{K} \in \mathcal{T}_h} \int_{\mathcal{K}} \nabla u \cdot \nabla v - \boxed{\sum_{\mathcal{K} \in \mathcal{T}_h} \int_{\partial \mathcal{K}} \nabla u \cdot \mathbf{n}_{\mathcal{K}} v} = \int_{\Omega} f v$$

Trace operators & magic formula (Arnold '82)

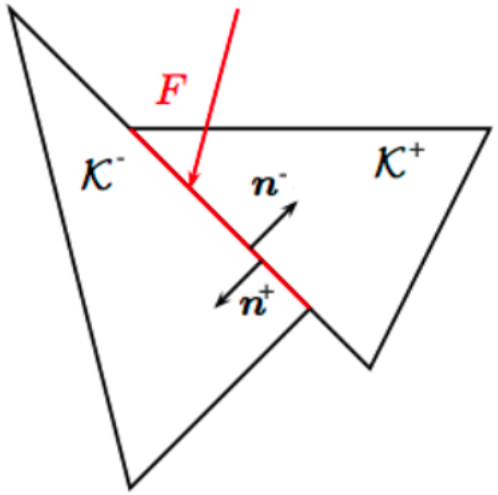

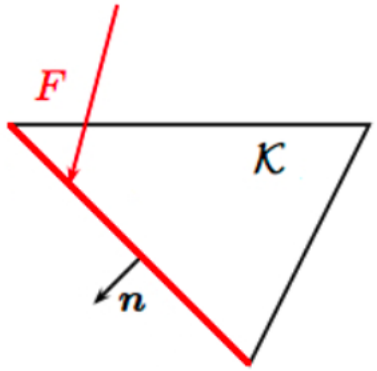

- for any $F \in \mathcal{F}^I$(= set of interior faces) shared by $\mathcal{K}^{\pm}$

$$\{\{v\}\} = (v^+ + v^-)/2 \qquad [\![v]\!] = v^+ n^+ + v^- n^-$$
$$\{\{\tau\}\} = (\tau^+ + \tau^-)/2 \qquad [\![\tau]\!] = \tau^+ \cdot n^+ + \tau^- \cdot n^-$$

- for any $F \in \mathcal{F}^B$(= set of boundary faces)

$$\{\{v\}\} = v \qquad [\![v]\!] = vn \qquad \{\{\tau\}\} = \tau \qquad [\![\tau]\!] = \tau \cdot n$$

$$\sum_{\mathcal{K}\in\mathcal{T}_h} \int_{\partial\mathcal{K}} \tau \cdot \mathbf{n}_{\mathcal{K}} v = \sum_{F\in\mathcal{F}} \int_F \{\{\tau\}\} \cdot [\![v]\!] + \sum_{F\in\mathcal{F}^I} \int_F [\![\tau]\!] \{\{v\}\}$$

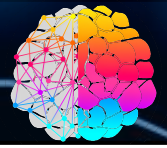

A first look at DG Finite Element methods (cont'd)

- Use that $[\![u]\!] = 0 \; \forall F \in \mathcal{F}$ (since $u \in H_0^1(\Omega)$) to add a symmetry term

$$\sum_{\mathcal{K}\in\mathcal{T}_h} \int_{\mathcal{K}} \nabla u \cdot \nabla v - \sum_{F\in\mathcal{F}} \int_F \{\!\{\nabla u\}\!\} \cdot [\![v]\!] - \sum_{F\in\mathcal{F}} \int_F \{\!\{\nabla_h v\}\!\} \cdot [\![u]\!] = \int_\Omega fv$$

  where ∇_h is the elementwise gradient (v is only piecewise smooth).

- We also add a stabilization term that controls the jumps

$$\sum_{\mathcal{K}\in\mathcal{T}_h} \int_{\mathcal{K}} \nabla u \cdot \nabla v - \sum_{F\in\mathcal{F}} \int_F \{\!\{\nabla u\}\!\} \cdot [\![v]\!] - \sum_{F\in\mathcal{F}} \int_F [\![u]\!] \cdot \{\!\{\nabla_h v\}\!\} + \sum_{F\in\mathcal{F}} \int_F \gamma [\![u]\!] \cdot [\![v]\!] = \int_\Omega fv$$

  where γ is a stabilization function (that might depend on the discretization parameters) [Douglas-Dupont, Wheeler, Arnold], see later .....

Discretization. Step 2: the discrete space

- For $p \geq 1$, define the DG discrete space

$$V_h^p = \left\{ v_h \in L^2(\Omega) : v_h|_{\mathcal{K}} \in \mathbb{P}^p(\mathcal{K}) \quad \forall \mathcal{K} \in \mathcal{T}_h \right\} \boxed{\not\subset H_0^1(\Omega)}$$

- Discretize $u \rightsquigarrow u_h$, $v \rightsquigarrow v_h$

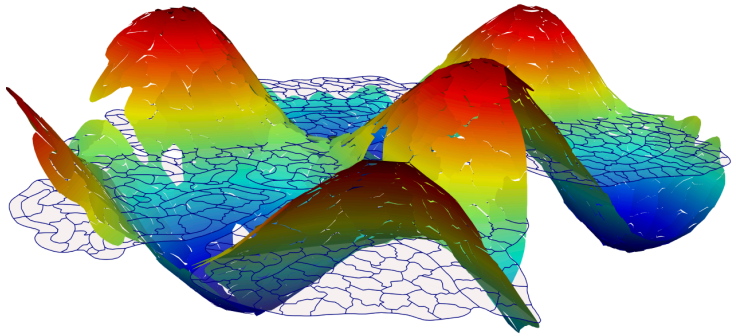

Example of $\mathrm{v_h} \in \mathrm{V_h^p}$

$$\text{Find } u_h \in V_h^p \quad \text{s.t.} \quad \mathcal{A}(u_h, v_h) = \int_\Omega f v_h \quad \forall\, v_h \in V_h^p$$

$$\mathcal{A}(w, v) = \sum_{\mathcal{K} \in \mathcal{T}_h} \int_{\mathcal{K}} \nabla w \cdot \nabla v - \sum_{F \in \mathcal{F}} \int_F \{\!\{\nabla_h w\}\!\} \cdot [\![v]\!]$$

$$- \sum_{F \in \mathcal{F}} \int_F [\![w]\!] \cdot \{\!\{\nabla_h v\}\!\} + \sum_{F \in \mathcal{F}} \int_F \gamma\, [\![w]\!] \cdot [\![v]\!]$$

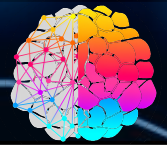

Interior Penalty DG methods

$$\text{Find } u_h \in V_h^p \quad \text{s.t.} \quad \mathcal{A}(u_h, v_h) = \int_\Omega f v_h \quad \forall\, v_h \in V_h^p$$

$$\mathcal{A}(w, v) = \sum_{\mathcal{K} \in \mathcal{T}_h} \int_{\mathcal{K}} \nabla w \cdot \nabla v - \sum_{F \in \mathcal{F}} \int_F \{\!\{\nabla_h w\}\!\} \cdot [\![v]\!]$$
$$- \theta \sum_{F \in \mathcal{F}} \int_F [\![w]\!] \cdot \{\!\{\nabla_h v\}\!\} + \sum_{F \in \mathcal{F}} \int_F \gamma\, [\![w]\!] \cdot [\![v]\!]$$

- $\theta = 1$: Symmetric Interior Penalty (SIP). [Wheeler, 78],[Arnold, 82]
- $\theta = -1$: Non-symmetric Interior Penalty (NIP). [Riviére, Wheeler & Girault, 99]
- $\theta = 0$: Incomplete Interior Penalty (IIP). [Dawson, Sun, Wheeler, 04]

The stabilization function

$$\sum_{F\in\mathcal{F}}\int_F \gamma\,[\![w]\!]\cdot[\![v]\!] \qquad \gamma=\alpha\,\frac{\mathrm{p}^2}{\mathrm{h}}$$

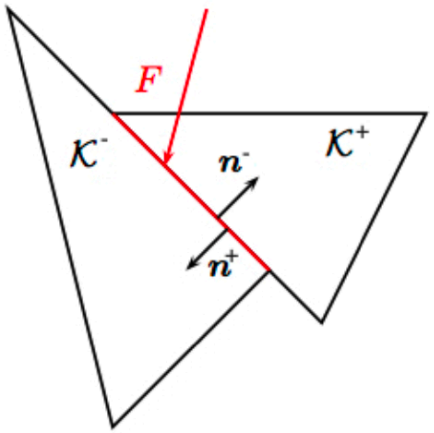

$$\mathrm{p}=\begin{cases}\max\{p_{\mathcal{K}^-},p_{\mathcal{K}^-}\} & \text{if } F\in\mathcal{F}_h^I\\ p_{\mathcal{K}} & \text{if } F\in\mathcal{F}^B\end{cases}\qquad \mathrm{h}=\begin{cases}\min\{h_{\mathcal{K}^+},h_{\mathcal{K}^-}\} & \text{if } F\in\mathcal{F}^I\\ h_{\mathcal{K}} & \text{if } F\in\mathcal{F}^B\end{cases}$$

Assumptions

$$p_{\mathcal{K}^+}\approx p_{\mathcal{K}^-}\qquad h_{\mathcal{K}^+}\approx h_{\mathcal{K}^-}$$

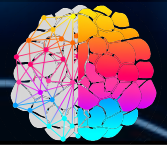

A bit of theory: error bounds in the "DG" norm

If $u \in H^s(\mathcal{T}_h)$, $s \geq 2$, then

$$\|u - u_h\|_{\mathrm{DG}} \lesssim \frac{h^{\min(p+1,s)-1}}{p^{s-1/2}} \|u\|_{H^s(\mathcal{T}_h)}$$

For the SIP and IIP methods the above estimate holds provided that the penalty constant α is chosen sufficiently large.

- The bound is optimal in h and suboptimal in p by a factor $p^{1/2}$. See, for example, [Houston, Schwab, Suli, 2001], [Riviere, Wheeler, Girault, 1999], [Perugia, Schotzau, 2001].
- Optimal error estimates with respect to p can be shown using the projector of [Georgoulis & Suli, 2005] provided the solution belongs to a suitable augmented space, or whenever a continuous interpolant can be built; cf. [Stamm & Wihler, 2010].

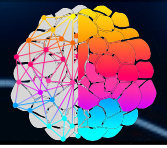

A bit of theory: error bounds in the L^2 norm

If the exact solution $u \in H^s(\mathcal{T}_h)$, $s \geq 2$ and if u_h is the solution obtained with the SIP method ($\theta = 1$), it holds

$$\|u - u_h\|_{L^2(\Omega)} \lesssim \frac{h^{\min(p+1,s)}}{p^{s+1/2}} \|u\|_{H^s(\mathcal{T}_h)}$$

The essential ingredient in the duality argument for proving L^2 estimates is the following adjoint consistency property

$$\mathcal{A}(v_h, z) = \int_\Omega f v_h \quad \forall\, v_h \in V_h^p$$

A practical example

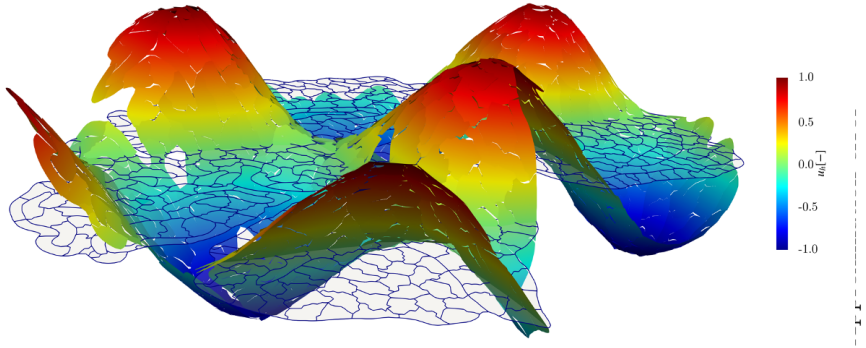

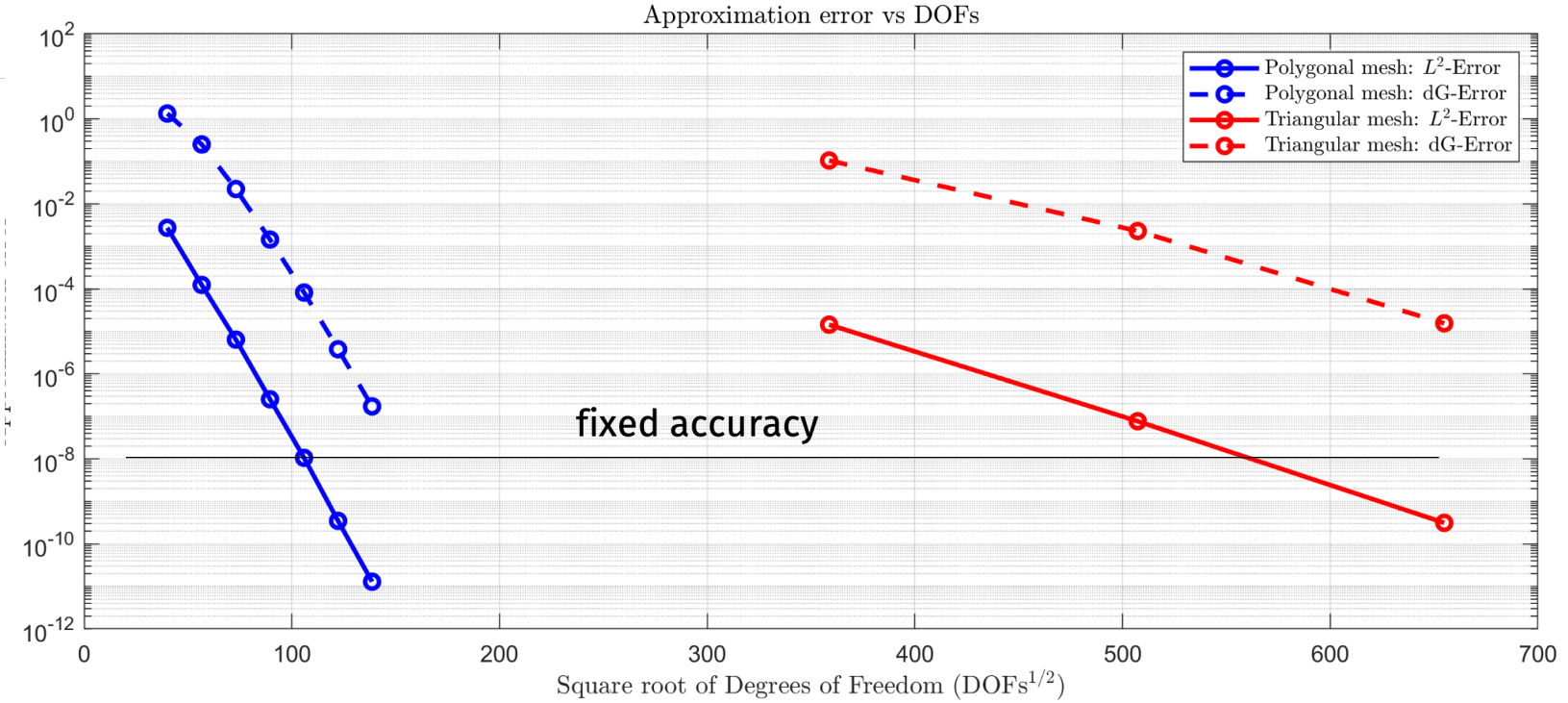

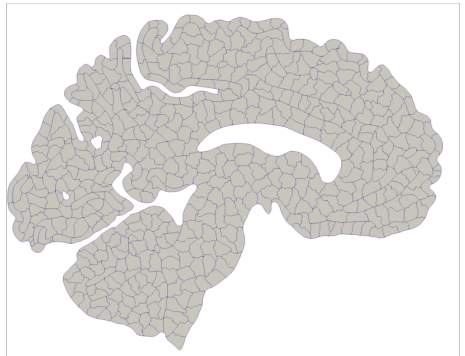

534 polygons (aggl.)
polynomial deg. 1-7

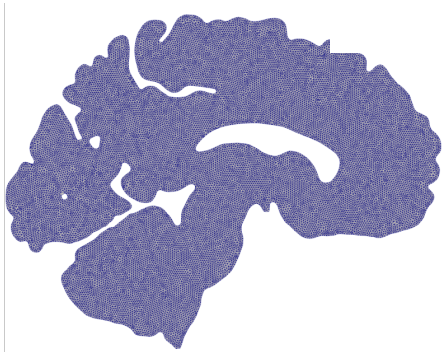

42 891 triangles
polynomial deg. 1-3

- Agglomerated grids outperform triangular grids
- High-order polynomials on an agglomerated mesh is more advantageous (smooth solution)

3 - Mathematical and numerical modeling of the misfolding process in NDs.

03

Modeling misfolded protein dynamics

- Diffusion: Captures the spread of pathological agents (e.g., misfolded proteins like tau or alpha-synuclein) through the brain.
- Reaction terms: Represent local processes such as protein aggregation, clearance, or neuronal damage.
- Neuroanatomical structure: Incorporates the geometry of the brain or specific regions, possibly derived from imaging data.
- Anisotropic Diffusion: Incorporate anisotropic diffusion to account for the directional spread along axonal pathways.
- Neuronal Damage: Include neuronal density as another variable.
- Feedback Mechanisms: Model interactions between neuronal death and further aggregation:Coupled PDEs: Represent multiple interacting species, such as different forms of misfolded proteins.

Increasingly informative mathematical models: FK model

$$\begin{cases} \dfrac{\partial c}{\partial t} = \nabla \cdot (\mathbf{D}\nabla\, c) + \alpha\, c(1-c) + f, & \text{in } \Omega \times (0,T], \\ (\mathbf{D}\nabla c) \cdot \boldsymbol{n} = 0, & \text{on } \Gamma_N \times (0,T], \\ c = c_{\mathrm{D}}, & \text{on } \Gamma_D \times (0,T], \\ c(0) = c_0, & \text{in } \Omega, \end{cases}$$

Solutions

$$c = c(\boldsymbol{x}, t)$$

Relative protein concentration

Bounds: $c \in [0,1]$

Diffusion tensor

$$\mathbf{D} = \mathbf{D}(\boldsymbol{x}) = d_{\mathrm{ext}}\mathbf{I} + d_{\mathrm{axn}}\boldsymbol{a}(\boldsymbol{x}) \otimes \boldsymbol{a}(\boldsymbol{x})$$

•S. Fornari, A. Schafer, M. Jucker, A. Goriely, E. Kuhl – Journal of the Royal Society Interface (2019)

•M. Corti, F. Bonizzoni, L. Dede', A.M. Quarteroni, P.F. Antonietti – Computer Methods in Applied Mechanics and Engineering (2023)

Increasingly informative mathematical models: heterodimer model

$$
\begin{cases}
\dfrac{\mathrm{d}c}{\mathrm{d}t} = \nabla \cdot (\mathbf{D}\nabla c) - k_1\, c - k_{12}\, c\, q + k_0 & \text{in } \Omega \times (0,T], \\
\dfrac{\mathrm{d}q}{\mathrm{d}t} = \nabla \cdot (\mathbf{D}\nabla q) - \tilde{k}_1\, q + k_{12}\, q\, c & \text{in } \Omega \times (0,T], \\
c = c_{\mathrm{D}}, \quad q = q_{\mathrm{D}} & \text{on } \Gamma_{\mathrm{D}} \times (0,T], \\
(\mathbf{D} \cdot \nabla c) \cdot \boldsymbol{n} = 0, \quad (\mathbf{D} \cdot \nabla q) \cdot \boldsymbol{n} = 0 & \text{on } \Gamma_{\mathrm{N}} \times (0,T], \\
c(0,\boldsymbol{x}) = c_0, \quad q(0,\boldsymbol{x}) = q_0 & \text{in } \Omega.
\end{cases}
$$

Solutions

$c = c(\boldsymbol{x}, t)$

Healthy protein concentration

Bounds: $c \geq 0$

$q = q(\boldsymbol{x}, t)$

Misfolded protein concentration

Bounds: $q \geq 0$

S. Fornari, A. Schafer, M. Jucker, A. Goriely, E. Kuhl – Journal of the Royal Society Interface (2019)
P.F. Antonietti, F. Bonizzoni, M. Corti, A. Dall'Olio – Computer Methods in Applied Mechanics and Engineering (2024)

Increasingly informative mathematical models: Smoluchowski model

$$
\begin{cases}
\dfrac{\partial c_1}{\partial t} = \nabla \cdot (\mathbf{D}_1 \nabla c_1) + k_0 - k_1 c_1 - 2\kappa c_1^2 - a\, c_1 \displaystyle\sum_{j=2}^{n-1} c_j, \\
\dfrac{\partial c_2}{\partial t} = \nabla \cdot (\mathbf{D}_2 \nabla c_2) - k_2 c_2 + \kappa c_1^2 - a c_1 c_2 + 2f \displaystyle\sum_{j=2}^{n-3} c_{2+j}, \\
\dots \\
\dfrac{\partial c_i}{\partial t} = \nabla \cdot (\mathbf{D}_i \nabla c_i) - k_i c_i - a c_1 c_i + a c_1 c_{i-1} + 2f \displaystyle\sum_{j=2}^{n-i-1} c_{i+j} - (i-3) f c_i, \\
\dots \\
\dfrac{\partial c_n}{\partial t} = \nabla \cdot (\mathbf{D}_n \nabla c_n) + a c_1 c_{n-1}, \\
+\mathrm{BCs} + \mathrm{ICs}.
\end{cases}
$$

Solutions

$$c_j = c_j(\boldsymbol{x}, t)$$

Concentration of agglomerate of *j* proteins

Bounds: $c_j \geq 0$

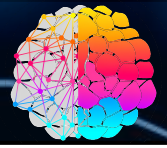

FK: semidiscrete formulation

$$\text{For any } t > 0, \text{ find } c_h(t) \in W_h^{DG} \text{ s.t.}$$

$$\left(\frac{\partial c_h}{\partial t}, w_h\right)_\Omega + \mathcal{A}(c_h, w_h) - r_L(c_h, w_h) + r_N(c_h, c_h, w_h) = F_h(w_h) \qquad \forall w_h \in W_h^{DG}$$

Diffusion Term

Linear reaction term

Nonlinear reaction term

$$\mathcal{A}(c_h, w_h) = \int_\Omega \mathbf{D}\nabla_h c_h \cdot \nabla_h w_h - \sum_{F \in \mathcal{F}_h} (\eta [[c_h]] \cdot [[w_h]] - \{\{\mathbf{D}\nabla_h c_h\}\} \cdot [[w_h]] - [[c_h]] \cdot \{\{\mathbf{D}\nabla_h w_h\}\})$$

$$r_L(c_h, w_h) = \int_\Omega \alpha c_h w_h$$

$$r_N(v_h, c_h, w_h) = \int_\Omega \alpha v_h c_h w_h$$

Theoretical analysis of the semi discrete formulation

ENERGY NORM

$$||c_h(t)||_\epsilon^2 := ||c_h(t)||^2 + \int_0^t ||c_h(s)||_{\mathrm{DG}}^2 \mathrm{d}s$$

STABILITY: Under suitable assumptions on the mesh and provided the penalty parameter is large enough

$$\| c_h(t) \|_\epsilon \lesssim \text{data}$$

ERROR BOUNDS: Under suitable assumptions on the mesh and provided the penalty parameter is large enough, if the exact solution is sufficiently regular

$$|||c(t) - c_h(t)|||_\epsilon^2 \lesssim \sum_{K \in \mathcal{T}_h} C_K(c, \dot{c}, n, t, \ldots) h_K^{2min(p+1,n)-2}$$

Theoretical analysis of the semi discrete formulation

DEFINITION: ENERGY NORM

$$||c_h(t)||_\epsilon^2 := ||c_h(t)||^2 + \int_0^t ||c_h(s)||_{\mathrm{DG}}^2 \mathrm{d}s$$

THEOREM: STABILITY ESTIMATE

Under suitable assumptions on the mesh regularity and let $c_h(t)$ be the solution of semi-discrete problem for any $t \in (0, \hat{t}]$, with $\hat{t} \leq T$ introduced by Perov inequality. Let the stability parameter η be large enough. Then:

$$||c_h(t)||_\epsilon^2 \leq \frac{\left(||c_h^0||^2 + \int_0^T ||f(s)||^2 \mathrm{d}s\right) e^{\frac{2\tilde{\alpha}+1}{\tilde{\mu}} t}}{\left(\tilde{\mu}^{d-1} - \frac{\tilde{\alpha} C_{\mathrm{G}_d}^3}{2^{d-1}(2\tilde{\alpha}+1)\varepsilon}\left(||c_h^0||^2 + \int_0^T ||f(s)||^2 \mathrm{d}s\right)^{d-1}\left(e^{\left(\frac{2\tilde{\alpha}+1}{\tilde{\mu}}\right)(d-1)t} - 1\right)\right)^{\frac{1}{d-1}}}, \tag{1}$$

where $\tilde{\mu} = \min\left\{1, 2\mu - \frac{d\varepsilon\tilde{\alpha}C_{\mathrm{G}_d}^3}{(2^{d-2})}\right\} > 0$ and $\varepsilon > 0$ is small enough, $\tilde{\alpha} = ||\alpha||_{L^\infty}$ and C_{G_d} defined in discrete Gagliardo-Nirenberg inequality.

Numerical results: Verification

Known (smooth) exact solution. Computed errors and expected convergence rates

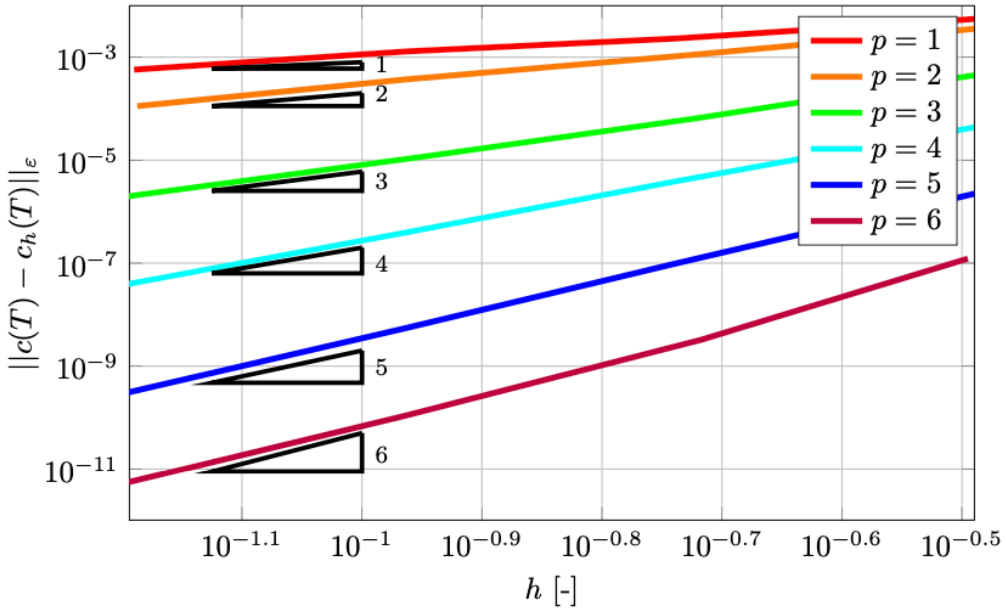

semi-implicit treatment of the nonlinear term

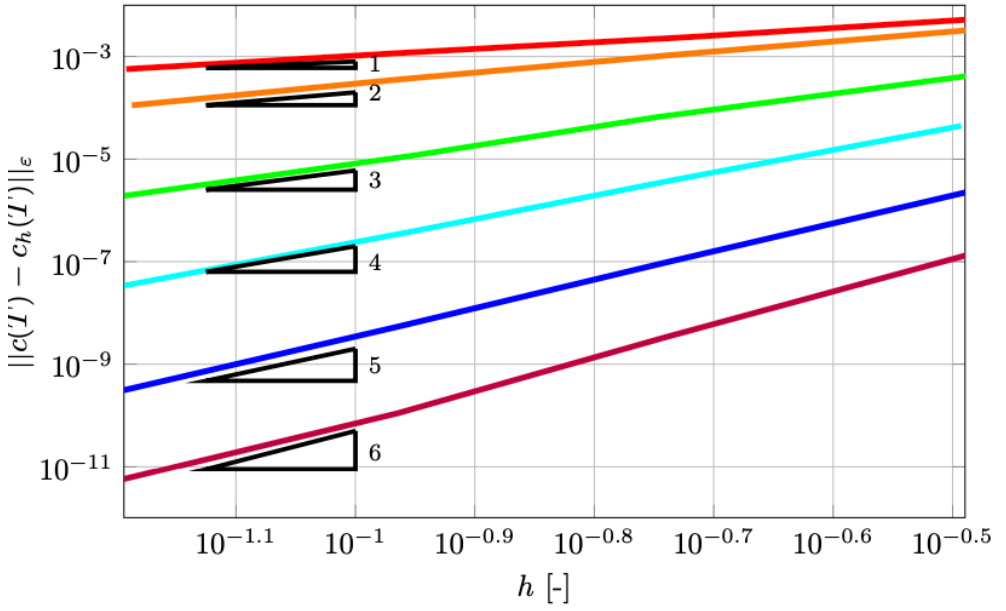

implicit treatment of the nonlinear term

Patterns of α-synuclein concentration at different stages of parkinson's disease (2D)

Initial Triangular Mesh:
41 194 Elements

Agglomerated Mesh:
500 Elements

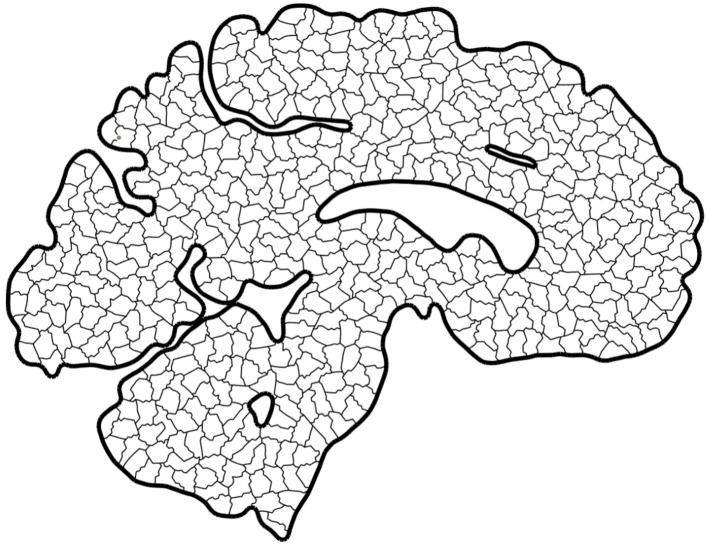

Fibres principal directions from Diffusion-weighted magnetic resonance (DWI) images

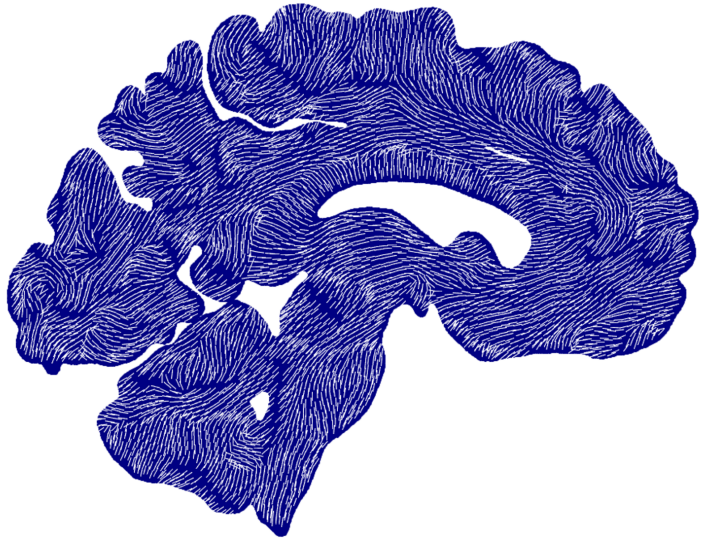

Patterns of α-synuclein concentration at different stages of parkinson's disease (2D)

- $\mathbf{D}$ has the following structure: $\mathbf{D} = d_{ext} I + d_{axn}(\mathbf{n} \otimes \mathbf{n})$ where $\mathbf{n} = \mathbf{n}(x)$ is the axonal fibres direction in the point $x \in \Omega$ and $d_{ext}, d_{axn} > 0$.

- We derive the diffusion tensor from DTI medical images. By computing the principal eigenvector $\mathbf{n}$ of the imaging- derived tensor, we find the directions of the fibres.

- We impose an axonal diffusion, which is 10 times faster than the isotropic one: $d_{ext} = 8\text{mm}^2/\text{year}$ and $d_{axn} = 80\text{mm}^2/\text{year}$.

- Conversion factor: $\alpha = 0.9/\text{year}$.

Fibres principal directions from Diffusion-weighted magnetic resonance (DWI) images

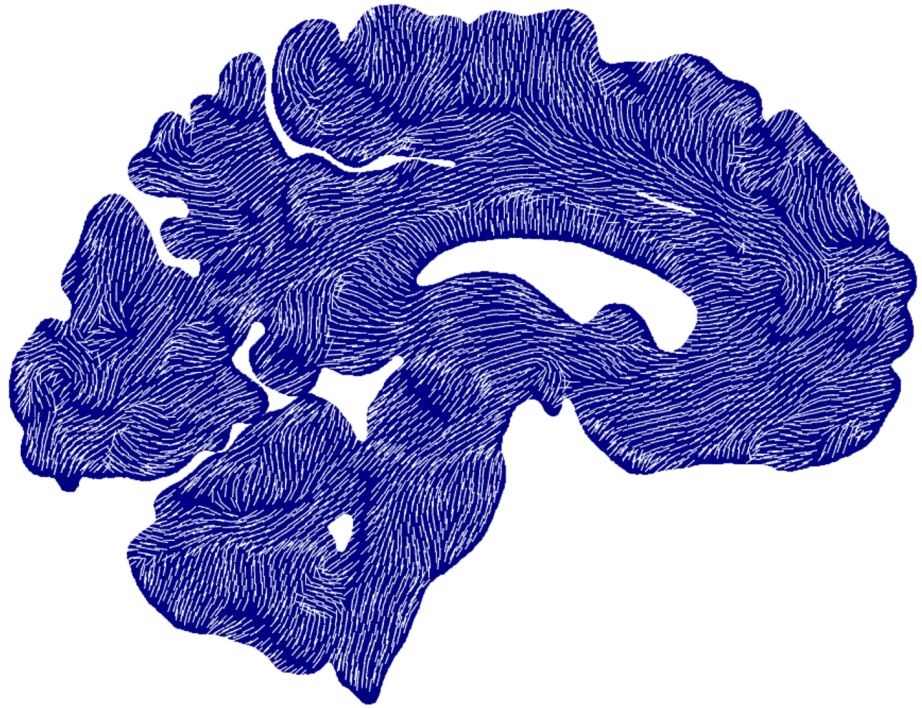

A. Schafer, J. Weickenmeier, and E. Kuhl, CMAME, 2019.

Patterns of α-synuclein concentration at different stages of parkinson's disease (2D)

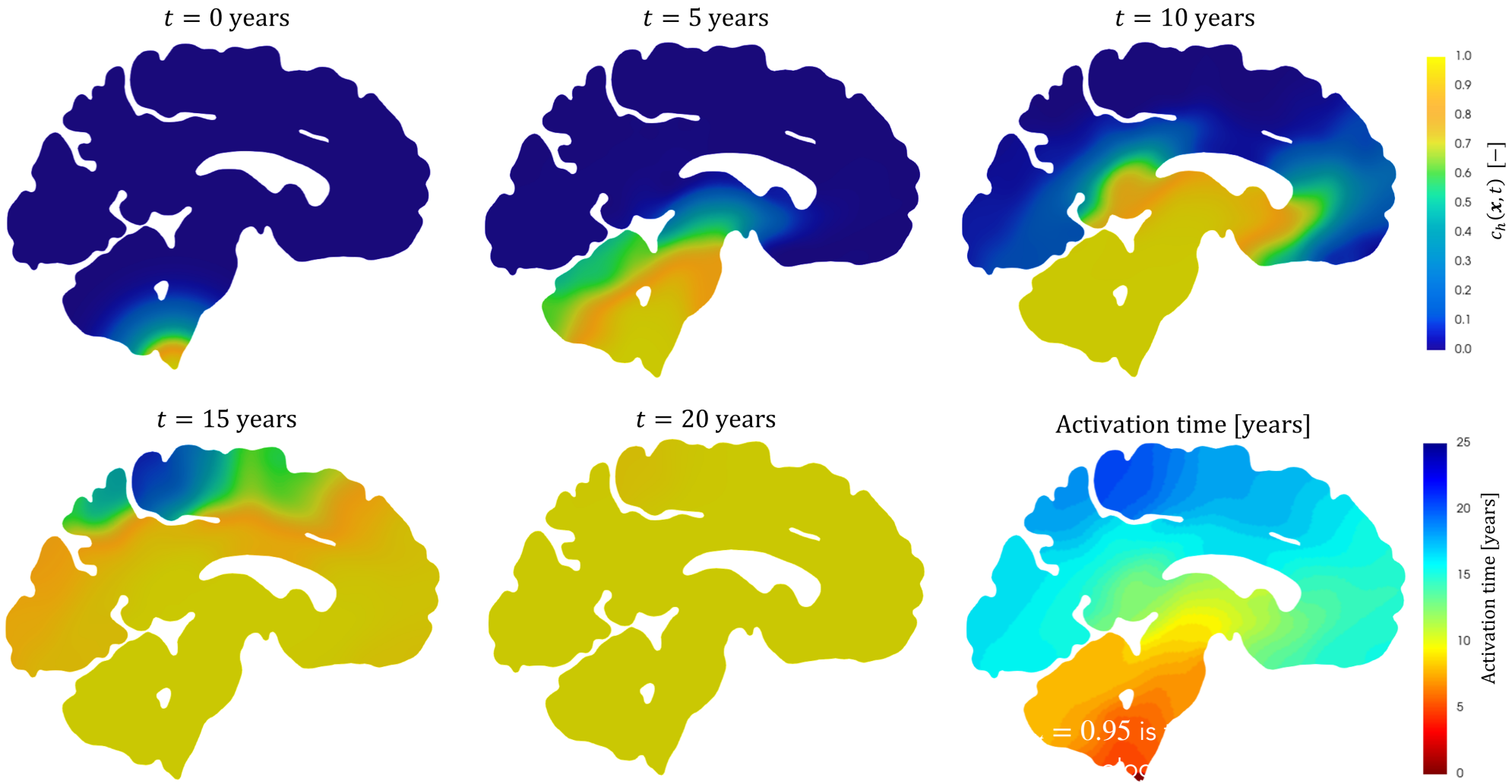

Patterns of α-synuclein concentration at different stages of parkinson's disease (2D)

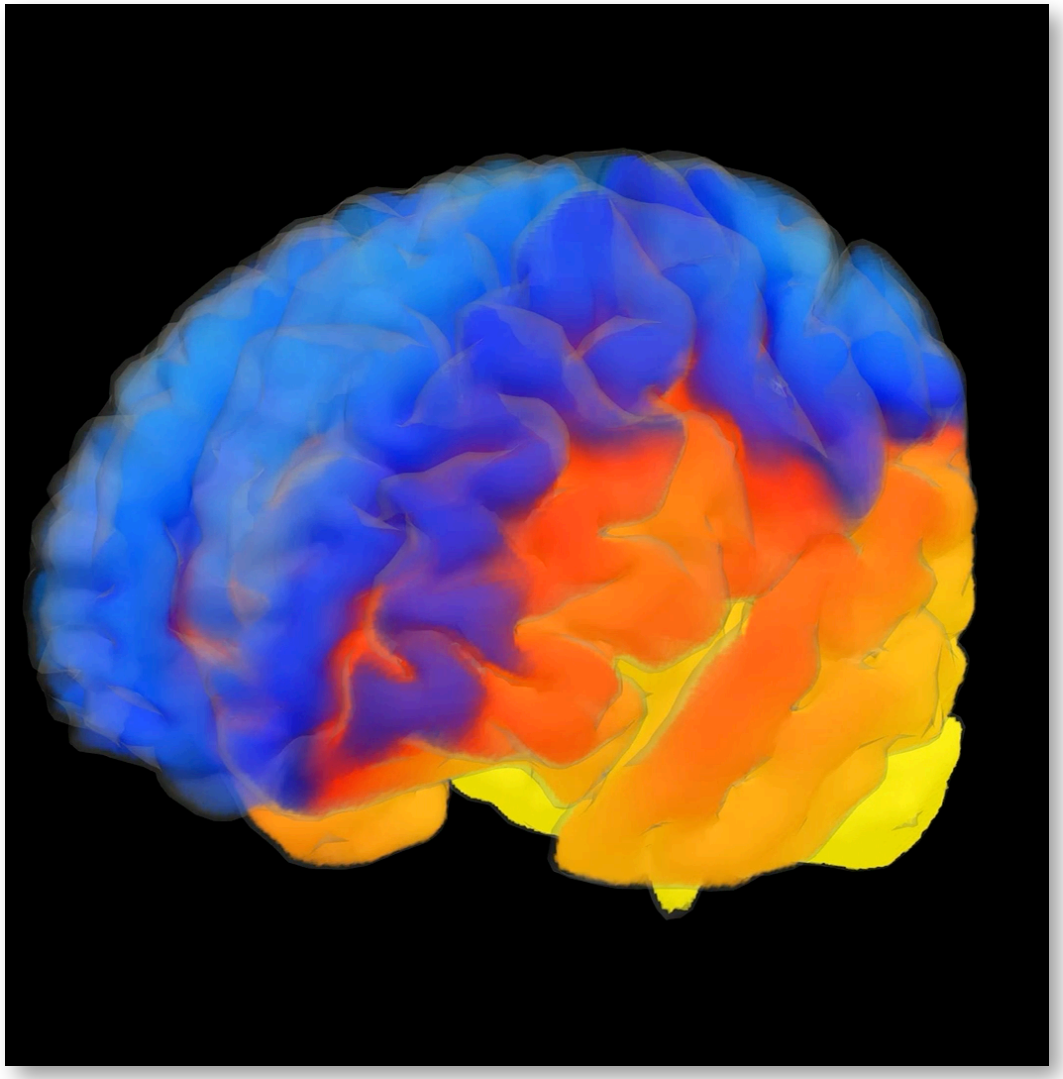

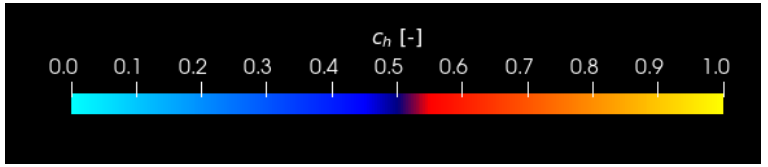

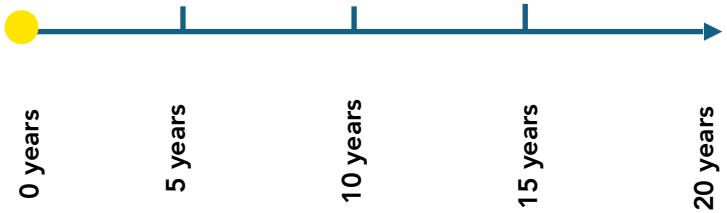

The issue of positivity preserving

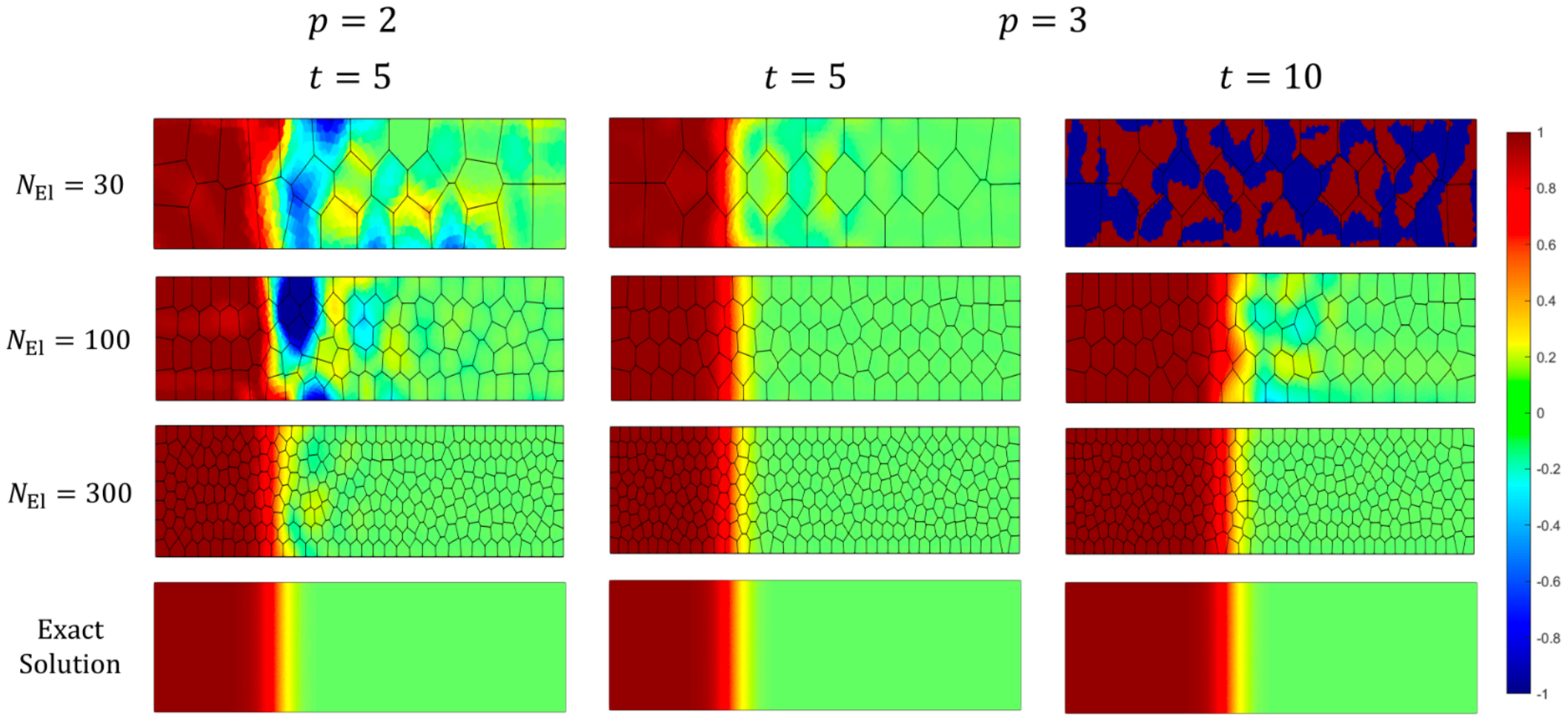

A positivity – preserving polydg scheme

To preserve the positivity of the solution, we introduce a change of variable in the equation:

FK equation in original variable

$$\begin{cases} \dfrac{\partial c}{\partial t} = \nabla \cdot (\mathbf{D}\nabla c) + \alpha\, c(1-c) + f, & \text{in } \Omega \times (0,T], \\ (\mathbf{D}\nabla c) \cdot \boldsymbol{n} = 0, & \text{on } \Gamma_N \times (0,T], \\ c = c_{\mathrm{D}}, & \text{on } \Gamma_D \times (0,T], \\ c(0) = c_0, & \text{in } \Omega, \end{cases}$$

FK equation in new variable

$$\begin{cases} \dfrac{\partial e^{\lambda}}{\partial t} = \nabla \cdot (e^{\lambda}\mathbf{D}\nabla \lambda) + \alpha\, e^{\lambda}(1-e^{\lambda}) + f, & \text{in } \Omega \times (0,T], \\ (\mathbf{D}\nabla \lambda) \cdot \boldsymbol{n} = 0, & \text{on } \Gamma_N \times (0,T], \\ \lambda = \lambda_{\mathrm{D}}, & \text{on } \Gamma_D \times (0,T], \\ \lambda(0) = \lambda_0, & \text{in } \Omega, \end{cases}$$

$$c = e^{\lambda}$$

Francesca Bonizzoni, Marcel Braukhoff, Ansgar Jüngelm Ilaria Perugia , 2020

A structure-preserving polyDG method for the FK equation

DG SEMIDISCRETE FORMULATION

For any $t \in (0,T]$, find $\lambda_h(t) \in W_{h,p}^{\mathrm{DG}}$ such that:

$$\begin{cases} \left(\dfrac{\partial e^{\lambda_h(t)}}{\partial t}, \varphi_h\right)_\Omega + \mathscr{A}(\lambda_h(t); \lambda_h(t), \varphi_h) - \left(\alpha e^{\lambda_h}\left(1 - e^{\lambda_h}\right), \varphi_h\right)_\Omega = F(\varphi_h) \quad \forall \varphi_h \in W_{h,p}^{\mathrm{DG}}, \\ \lambda_h(0) = \lambda_{0h} \end{cases}$$

FULLY DISCRETE FORMULATION

Given the initial condition $\lambda_h^0 = \lambda_{0h}$, find λ_h^{k+1} for $k = 0, ..., N_t - 1$, such that:

$$\begin{aligned} &\left(\frac{e^{\lambda_h^{k+1}} - e^{\lambda_h^k}}{\Delta t}, \varphi_h\right)_\Omega - \left(\alpha\left(\vartheta e^{\lambda_h^{k+1}} + (1-\vartheta)e^{\lambda_h^k}\right)\left(1 - \left(\vartheta e^{\lambda_h^{k+1}} + (1-\vartheta)e^{\lambda_h^k}\right)\right), \varphi_h\right)_\Omega \\ &\quad + \frac{\varepsilon}{\Delta t}(\lambda_h^{k+1}, \varphi_h)_\Omega + \frac{\varepsilon}{\Delta t}(\mathbf{D}\nabla_h \lambda_h^{k+1}, \nabla_h \varphi_h)_\Omega + \frac{\varepsilon}{\Delta t}(\zeta[\![\lambda_h^{k+1}]\!], [\![\varphi_h]\!])_{\mathscr{F}_h^{\mathrm{I}} \cup \mathscr{F}_h^D} \\ &\quad + \vartheta \mathscr{A}(\lambda_h^{k+1}; \lambda_h^{k+1}, \varphi_h) + (1-\vartheta)\mathscr{A}(\lambda_h^k; \lambda_h^k, \varphi_h) = \vartheta F^{k+1}(\varphi_h) + (1-\vartheta)F^k(\varphi_h), \qquad \text{in } \Omega. \end{aligned}$$

Convergence of the discrete solution

THEOREM: CONVERGENCE OF DISCRETE SOLUTION

Let data and mesh be sufficiently regular and let η_0 be sufficiently large. Let $\varepsilon > 0$, $\vartheta = 1$, $\Delta t \in (0,1)$, and let $\lambda_h^{k+1} \in W_{h,p}^{\mathrm{DG}}$ be a solution of fully-discrete solution with homogeneous forcing term $f = 0$. Assume that $\lambda_h^k \in W_{h,p}^{\mathrm{DG}}$ is such that $e^{\lambda_h^k} \to c^k$ strongly in $L^2(\Omega)$ as $(\varepsilon, h) \to 0$. Then there exists a unique strong solution $c^{k+1} \in H^2(\Omega)$ to:

$$
\begin{cases}
\dfrac{c^{k+1} - c^k}{\Delta t} = \nabla \cdot (\mathbf{D} \nabla\, c^{k+1}) + \alpha\, c^{k+1}(1 - c^{k+1}), & \text{in } \Omega, \\
c^{k+1} = c_{\mathrm{D}} = e^{\lambda_{\mathrm{D}}}, & \text{on } \Gamma_D, \\
(\mathbf{D} \nabla c^{k+1}) \cdot \boldsymbol{n} = 0, & \text{on } \Gamma_N,
\end{cases}
$$

2D verification

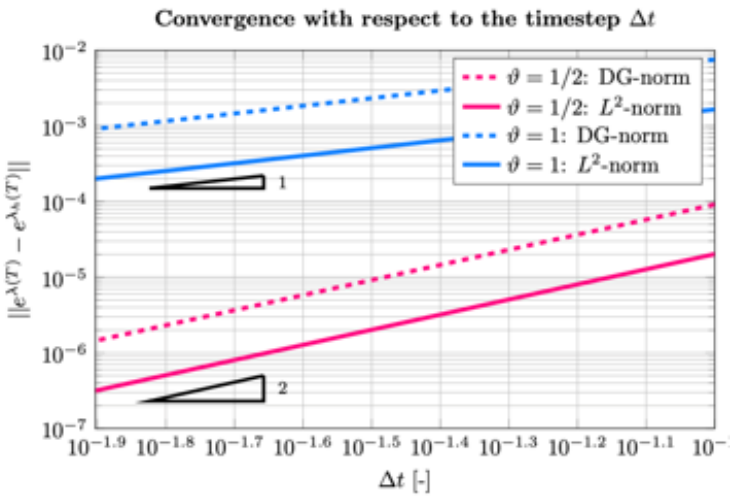

(a) Convergence in time with $p = 1$.

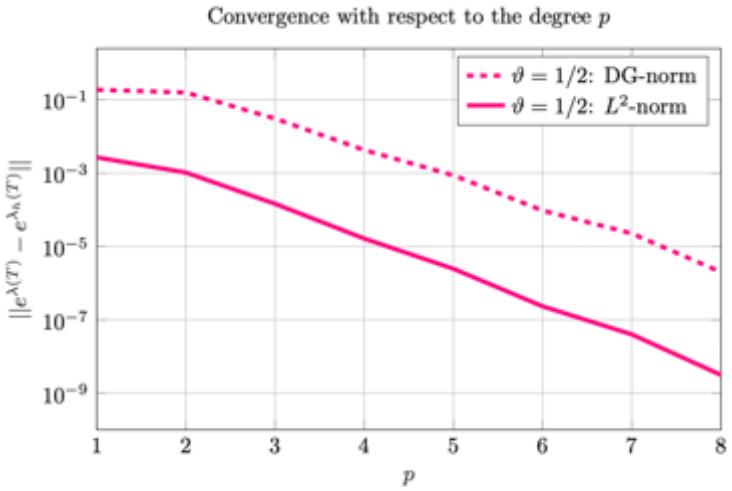

(b) Convergence in p with $\Delta t = 10^{-6}$.

Travelling wave

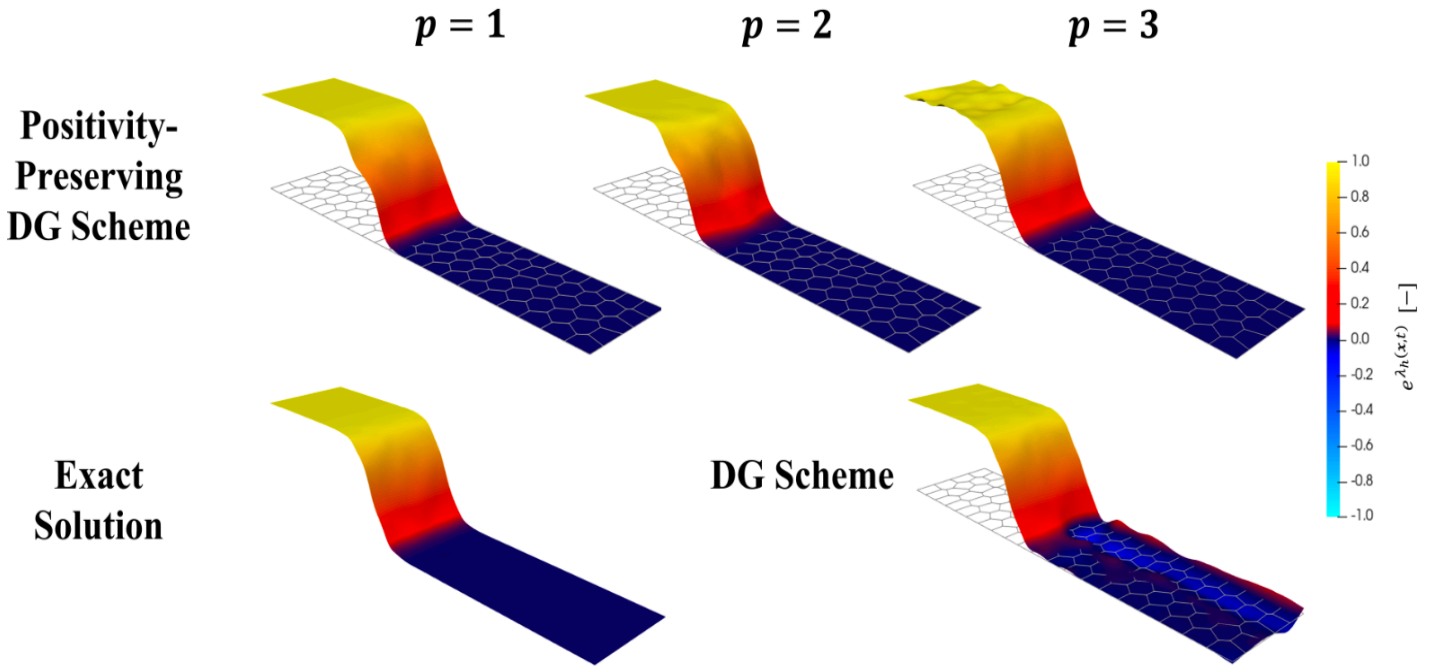

2D Simulation: Parkinson's disease

Initial Triangular Mesh:
White-Grey Matters Distinction

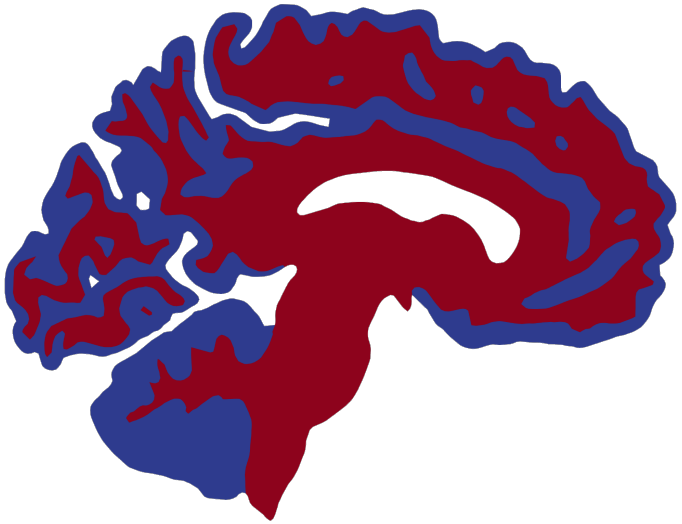

Agglomerated Mesh:
534 Elements

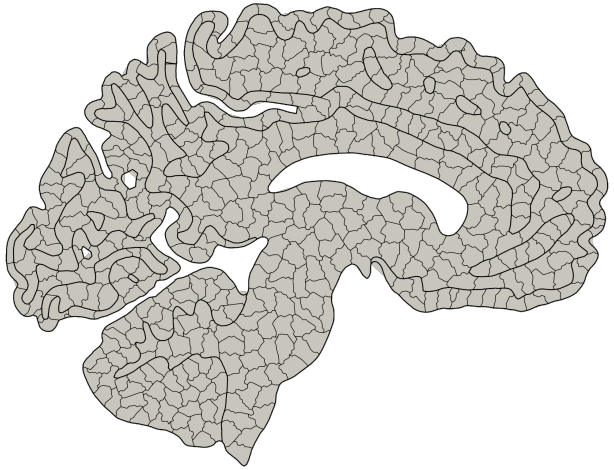

Fibres principal directions from DWI images

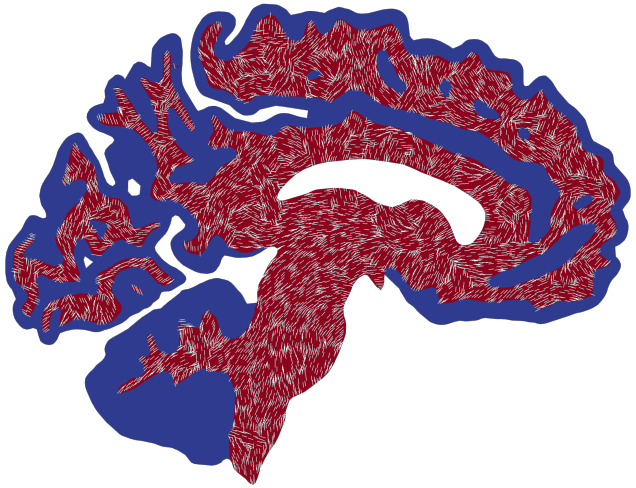

2D Simulation: Parkinson's disease

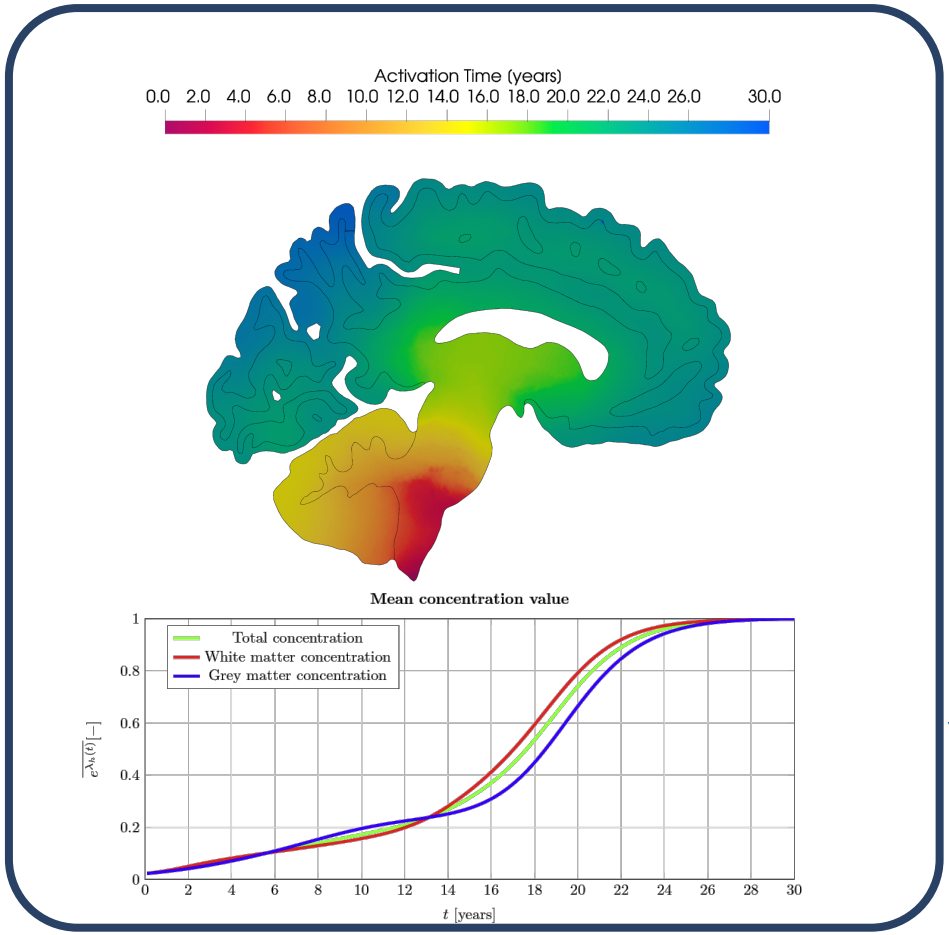

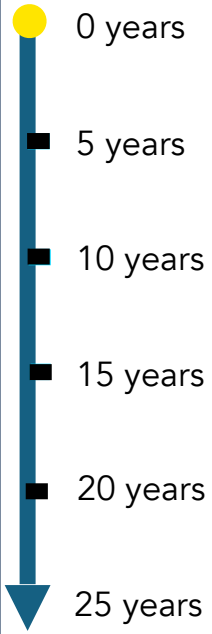

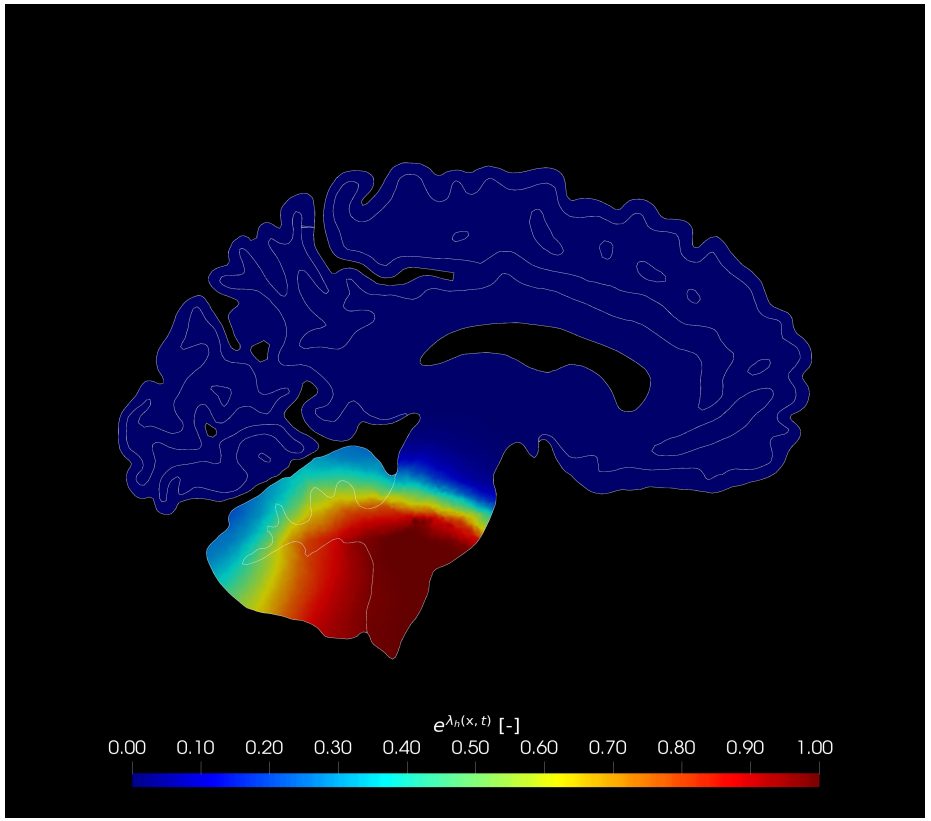

Alzheimer's disease: 3D simulation

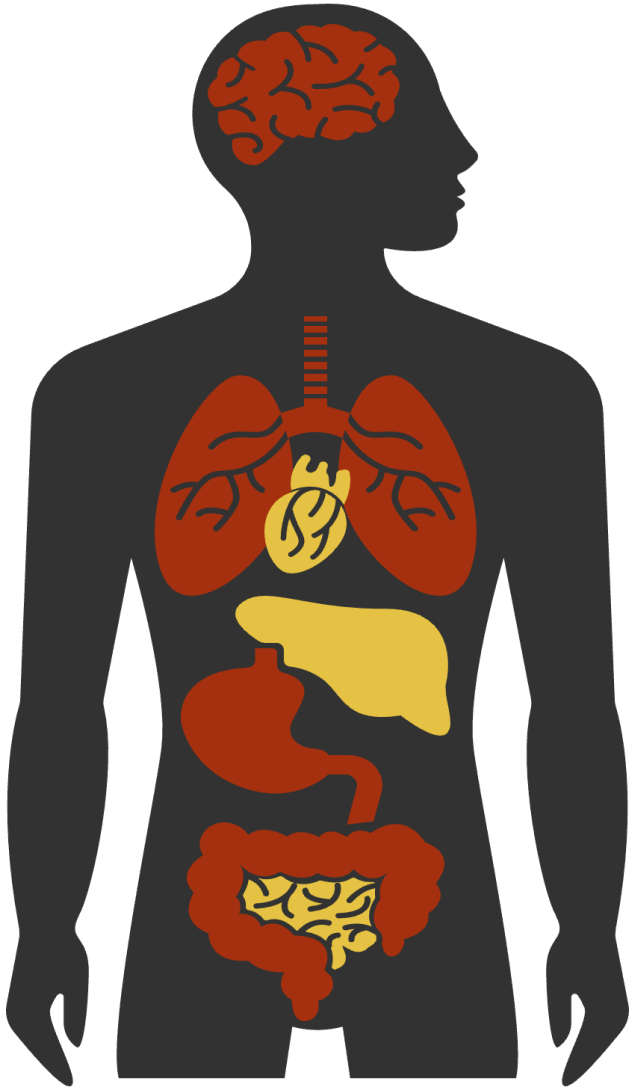

Age	83 Years	**P**hatology	Alzheimer's Disease
Gender	Male		

Structural MRI

Brain geometry to construct the numerical mesh grid.

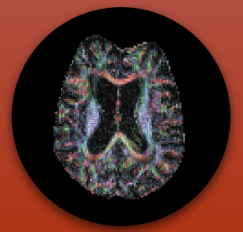

DWI-MRI

Axonal diffusion directions to derive the diffusion tensor.

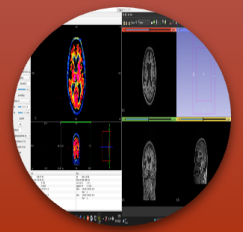

PIB-PET

Initial concentration of β-Amyloid proteins in the brain (83 years).

Alzheimer's disease: 3D simulation

Tetrahedral Mesh:

323 014 Elements

Initial Condition Derived from PET-PiB Medical Image:

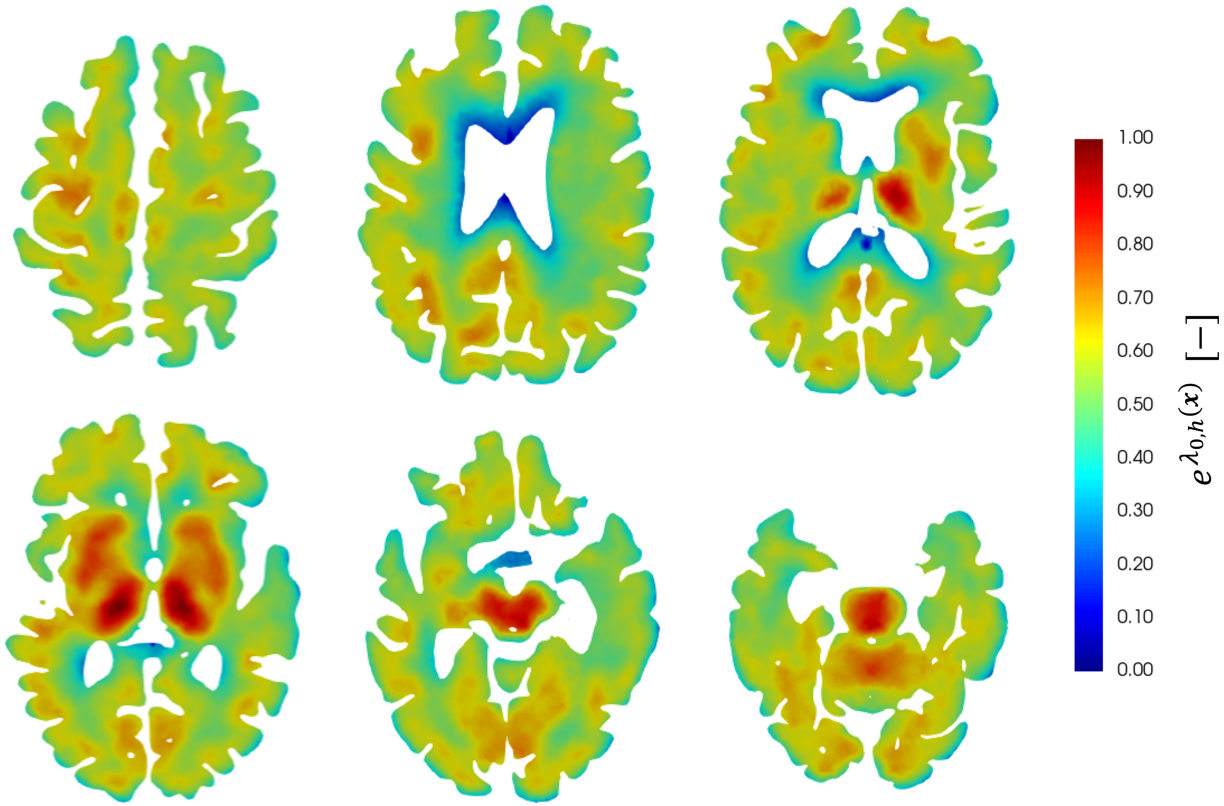

Alzheimer's disease: 3D simulation

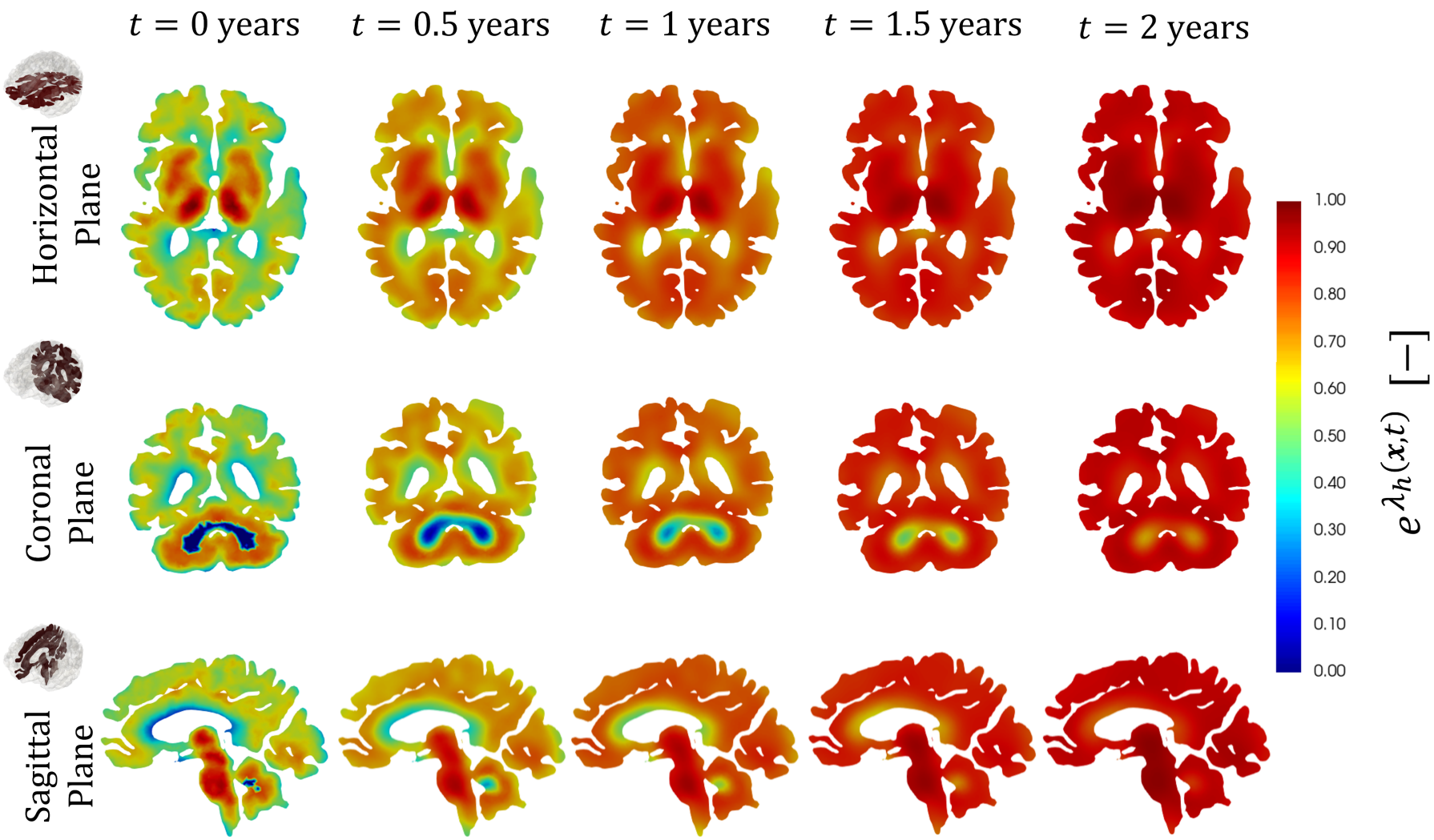

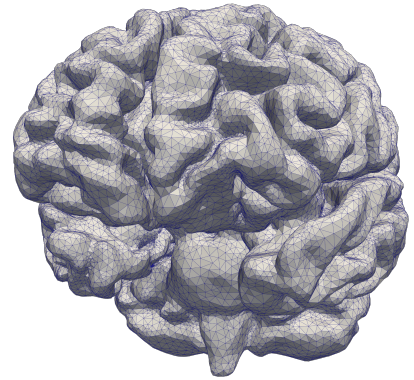

PolyDG methods for the heterodimer model

$$
\begin{cases}
\dfrac{\mathrm{d}c}{\mathrm{d}t} = \nabla \cdot (\mathbf{D}\nabla c) - k_1\, c - k_{12}\, c\, q + k_0 & \text{in } \Omega \times (0,T], \\
\dfrac{\mathrm{d}q}{\mathrm{d}t} = \nabla \cdot (\mathbf{D}\nabla q) - \tilde{k}_1\, q + k_{12}\, q\, c & \text{in } \Omega \times (0,T], \\
c = c_{\mathrm{D}}, \quad q = q_{\mathrm{D}} & \text{on } \Gamma_{\mathrm{D}} \times (0,T], \\
(\mathbf{D} \cdot \nabla c) \cdot \boldsymbol{n} = 0, \quad (\mathbf{D} \cdot \nabla q) \cdot \boldsymbol{n} = 0 & \text{on } \Gamma_{\mathrm{N}} \times (0,T], \\
c(0,\boldsymbol{x}) = c_0, \quad q(0,\boldsymbol{x}) = q_0 & \text{in } \Omega.
\end{cases}
$$

$c = c(\boldsymbol{x}, t)$

Healthy proteins concentration

$q = q(\boldsymbol{x}, t)$

Misfolded proteins concentration

Theorem: stability estimate

Under suitable assumptions on the mesh regularity and let $c_h(t)$ and $q_h(t)$ be the solutions of semi-discrete problem for any $t \in (0, \hat{t}]$, with $\hat{t} \leq T$ maximum time of validity of Perov inequality, that can be computed from the data. Let the stability parameter η be large enough. Then:

$$\|c_h\|_\varepsilon^2 + \|q_h\|_\varepsilon^2 \leq \frac{\left(\|c_{0h}\|^2 + \|q_{0h}\|^2 + \int_0^T \left(\|f_c(s)\|^2 + \|f_q(s)\|^2 \right) \mathrm{d}s \right)}{\left(\widetilde{\mu}^{d-1} - \widetilde{\mu}^{-1} \xi t \left(\|c_{0h}\|^2 + \|q_{0h}\|^2 + \int_0^T \left(\|f_c(s)\|^2 + \|f_q(s)\|^2 \right) \right)^{d-1} \right)^{\frac{1}{d-1}}}$$

where

$$\widetilde{\mu} = \min\{1, \mu, K_1, \tilde{K}_1\} \qquad \xi = \frac{C_{\mathrm{G}_d}^3 K_{12}^2}{2^{d-2}\mu}$$

having defined $K_{12} = \|k_{12}\|_{L^\infty}$, $K_1 = \|k_1\|_{L^\infty}$, $\widetilde{K}_1 = \|\tilde{k}_1\|_{L^\infty}$, and C_{G_d} from discrete Gagliardo-Nirenberg inequality.

Theorem: a-priori error estimate

Let us introduce the following norm:

$$|||u|||_{\mathrm{DG}} = ||u||_{\mathrm{DG}} + \left|\left|\eta^{-\frac{1}{2}}\{\{\mathbf{D}\nabla_h u\}\}\right|\right|_{\mathrm{L}^2(\mathscr{F}_h^{\mathrm{I}}\cup\mathscr{F}_h^{\mathrm{D}})} \qquad \forall u \in H^2(\mathscr{T}_h).$$

Let us consider the heterodimer problem with $f_c = f_q = 0$ and $c_{\mathrm{D}} = q_{\mathrm{D}} = 0$. Let us introduce suitable assumptions on the model parameters and on the mesh regularity. Let c and q be the weak solutions of heterodimer problem for any $t \in (0,T]$ and assume that $c, q \in C^1([0,T], H^n(\Omega))$ with $n \geq 2$. Let c_h and q_h be the solution of DG formulation for any $t \in (0,T]$. Then, the following estimate holds:

$$|||c(t) - c_h(t)|||_\varepsilon^2 + |||q(t) - q_h(t)|||_\varepsilon^2 \lesssim \sum_{K\in\mathscr{T}_h} h_K^{2\min(p+1,n)-2}\Big(\|c(t)\|_{H^n(K)}^2 + \|q(t)\|_{H^n(K)}^2 + \int_0^t \Big(\|c(s)\|_{H^n(K)}^2 + \|\dot{c}(s)\|_{H^n(K)}^2 + \|q(s)\|_{H^n(K)}^2 + \|\dot{q}(s)\|_{H^n(K)}^2\Big)\,\mathrm{d}s\Big).$$

Numerical results (2D)

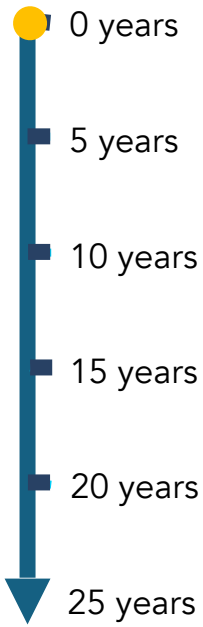

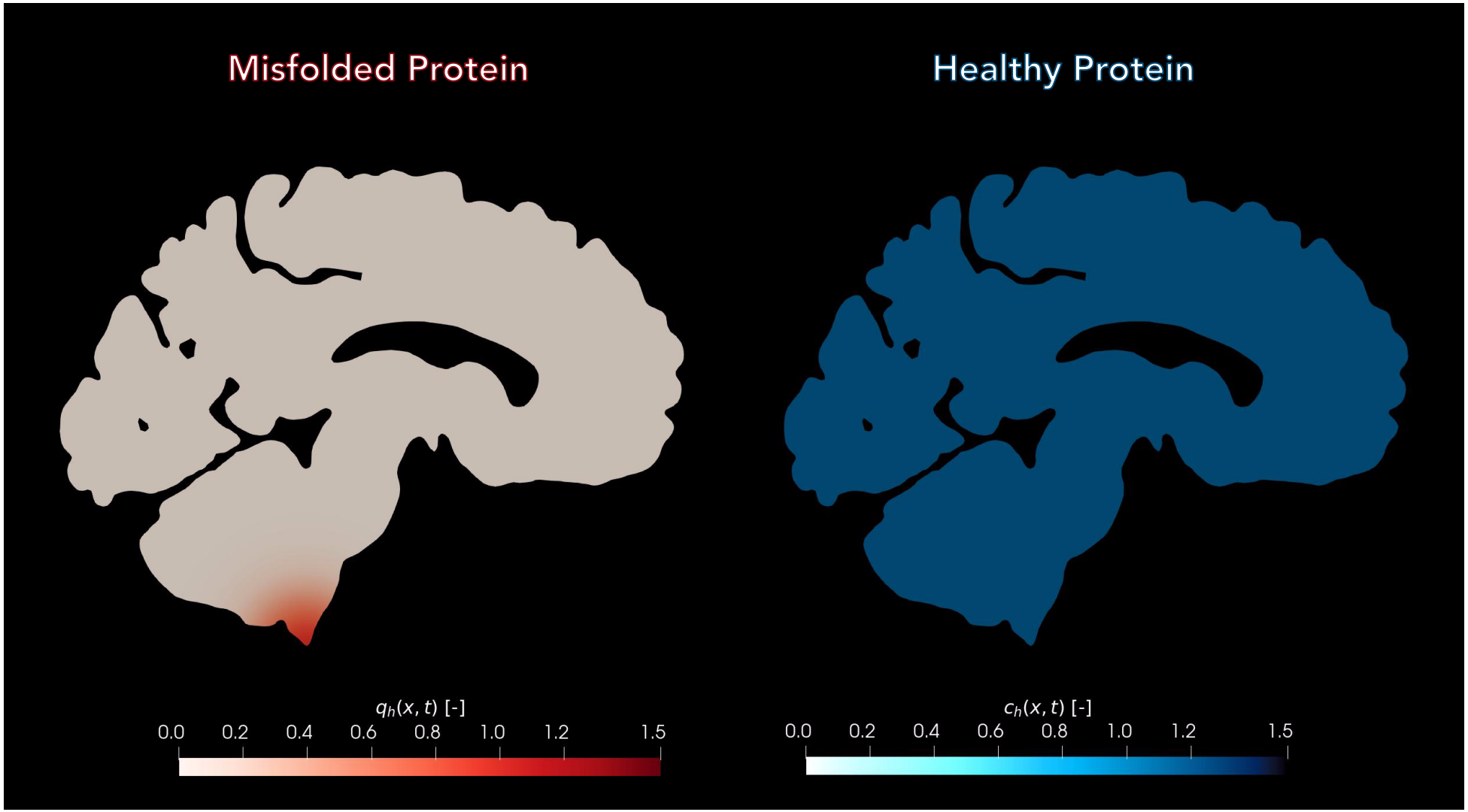

Antonietti, P.F., Bonizzoni, F., Corti, M., Dall'Olio, A. (2024)

Fisher – Kolmogorov vs. Heterodimer

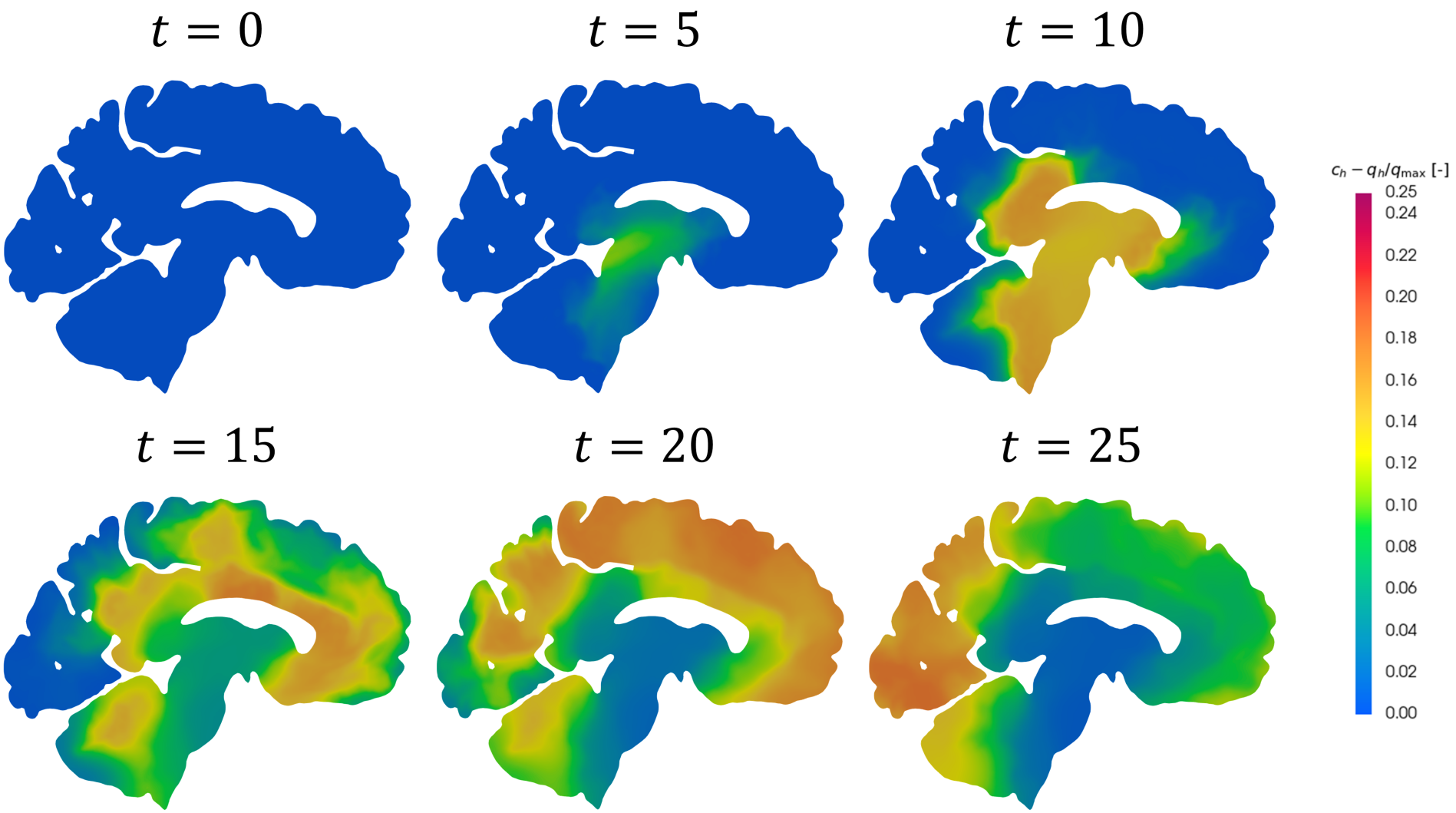

Antonietti, P.F., Corti, M. (2024)

Fisher – Kolmogorov vs. Heterodimer

Heterodimer Model

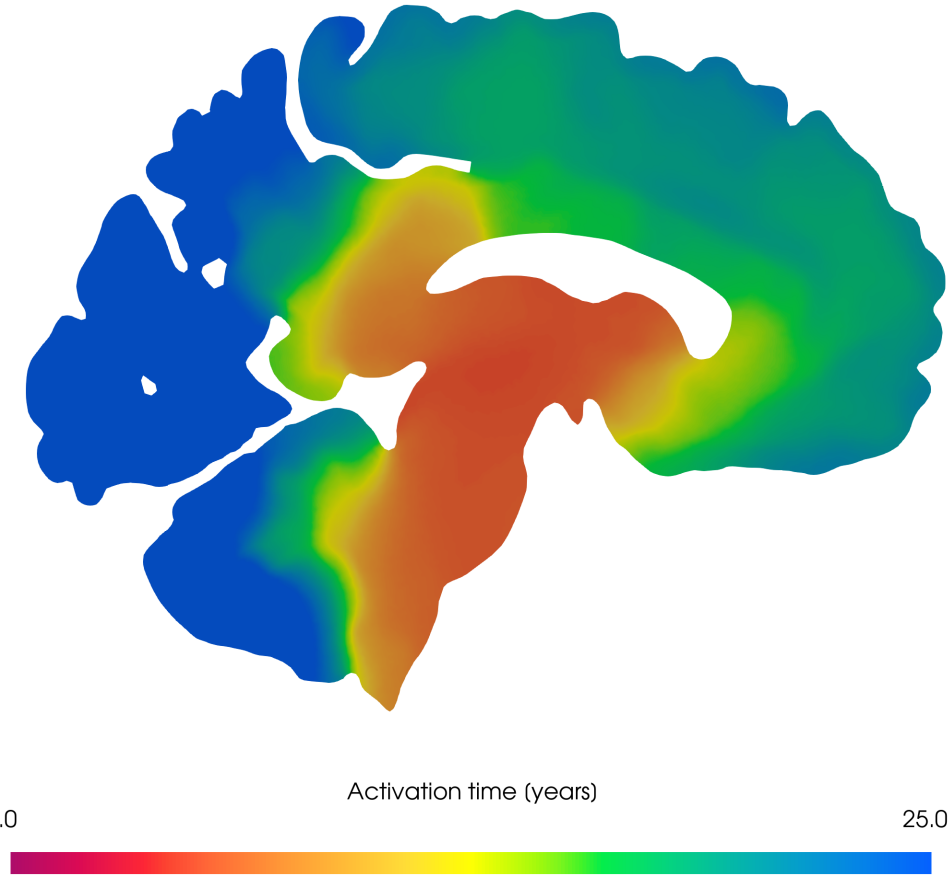

Fisher-Kolmogorov Model

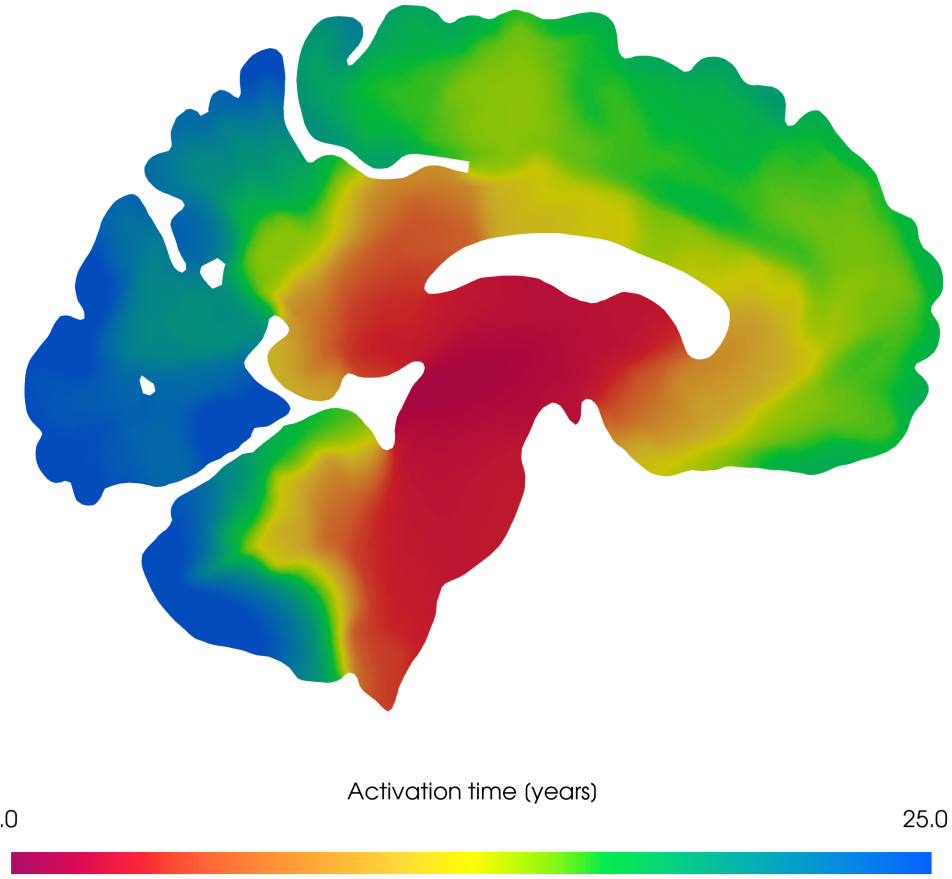

Heterodimer model: Parkinson's diseases - verification

$$\begin{cases} \dfrac{\partial c}{\partial t} = \nabla \cdot (\mathbf{D}\nabla c) - k_1 c - k_{12} c q + k_0, & \text{in } \Omega \times (0, T], \\ \dfrac{\partial q}{\partial t} = \nabla \cdot (\mathbf{D}\nabla q) - \widetilde{k}_1 q + k_{12} c q, & \text{in } \Omega \times (0, T]. \end{cases}$$

Coeff. non-neg., $\boldsymbol{a} : \Omega \to \mathbb{R}^N$ unit. $N = 2, 3$.

Axonal connection

$$\mathbf{D}(\boldsymbol{x}) = d_{\text{ext}}\mathbf{I} + \underbrace{d_{\text{axn}}\boldsymbol{a}(\boldsymbol{x}) \otimes \boldsymbol{a}(\boldsymbol{x})}_{\textit{Anisotropic}}$$

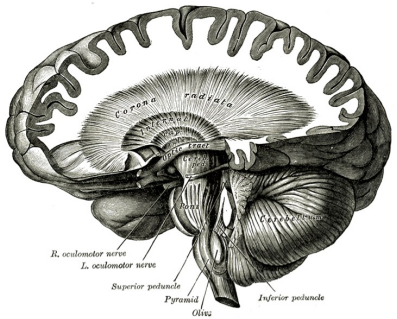

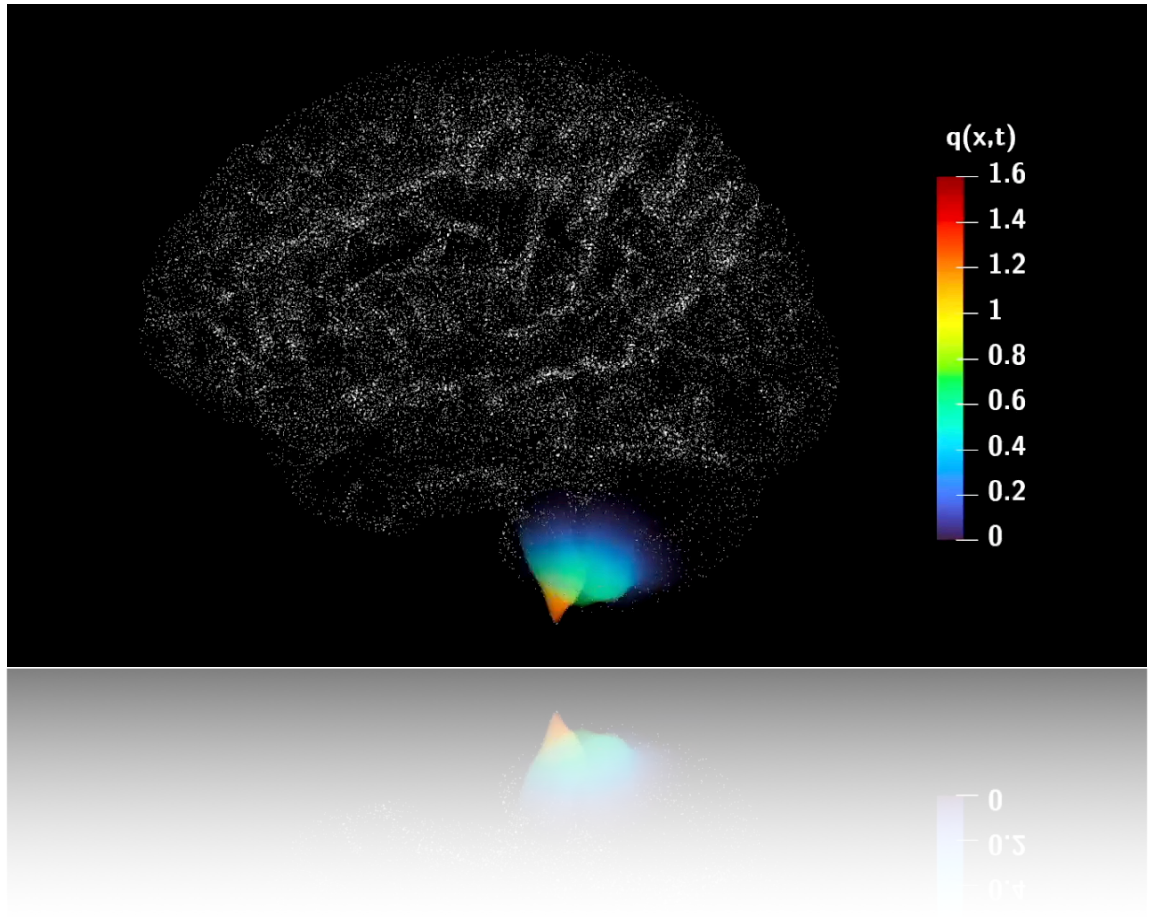

Heterodimer model: Parkinson's diseases - verification

Misfolded proteins

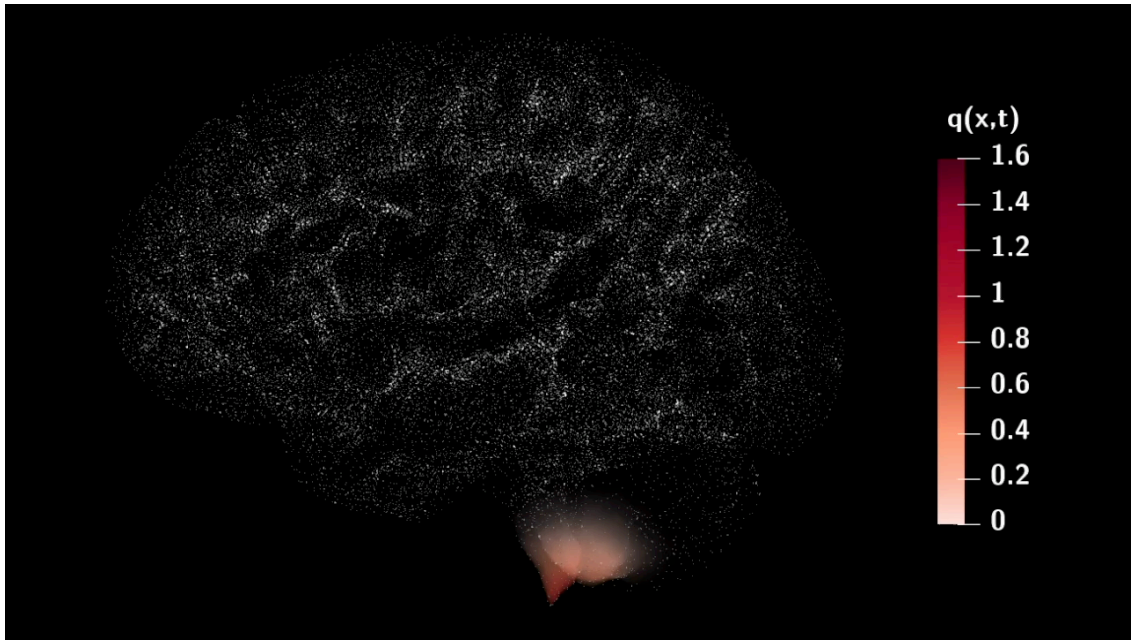

Native proteins

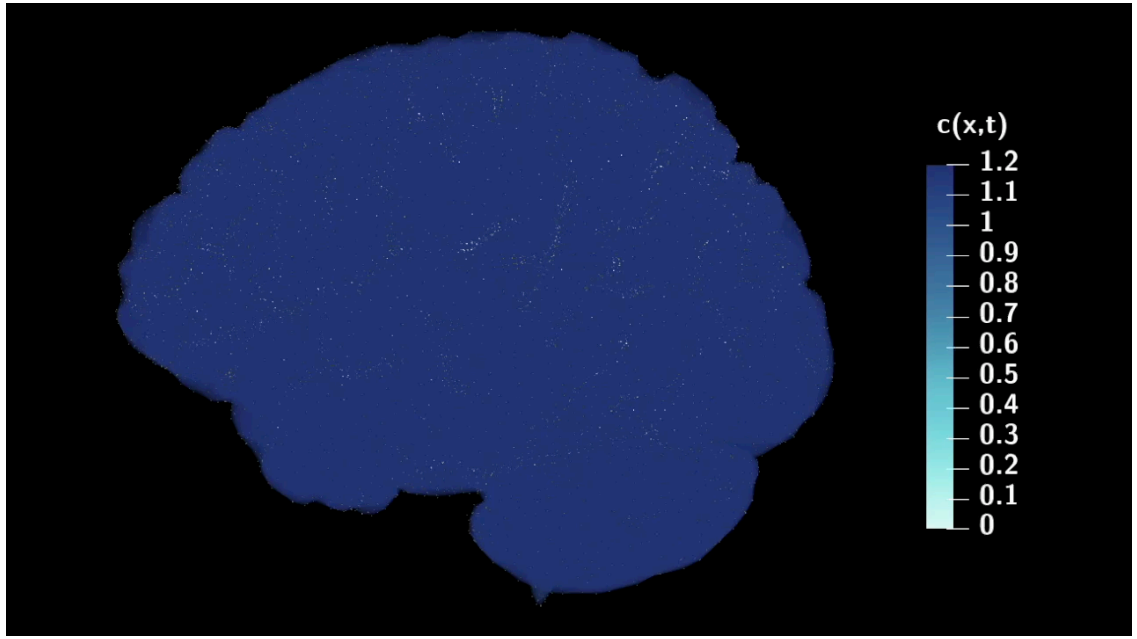

- Stable pathological equilibrium reached.
- Stereotipical topological evolution pattern
- *lower brainstem → mesocortex → neocortex*

Heterodimer model: Parkinson's diseases - verification

Transverse section

Frontal section

Sagittal section

Heterodimer model: Parkinson's diseases - verification

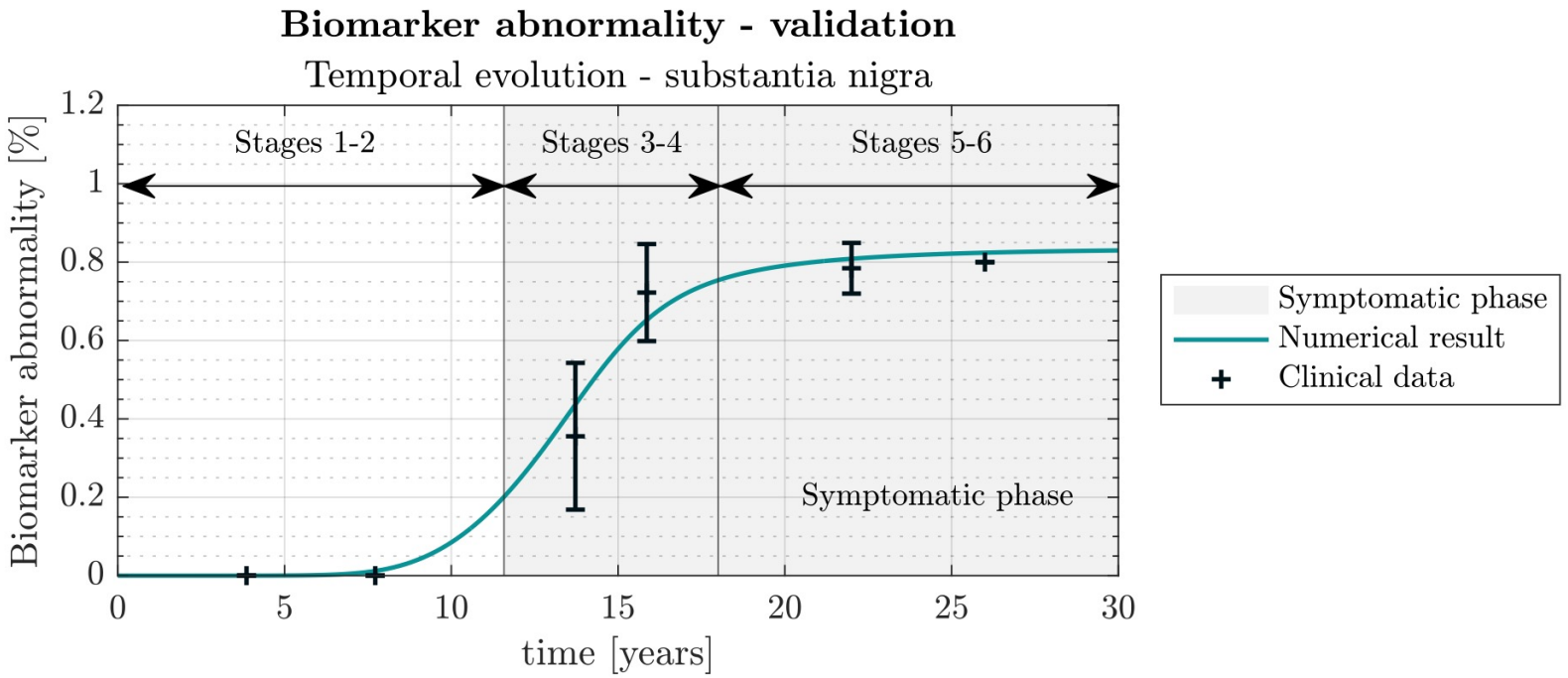

$$B_i^{\alpha}(t) = \frac{\int_{R_i} q(\boldsymbol{x}, t)\mathrm{d}\boldsymbol{x}}{\int_{R_i} c(\boldsymbol{x}, t) + q(\boldsymbol{x}, t)\mathrm{d}\boldsymbol{x}}$$

Biomarker Abnormality Curve (BAC) for **substantia nigra**. Data from Braak et al. (2003). Averages (110 patients) for each disease stage $\pm\sigma$.

Fisher – Kolmogorov on graphs

1

DWI-MRI

DWI-MRI determines the **Brownian motion** of water molecules, we can approximate axonal directions.

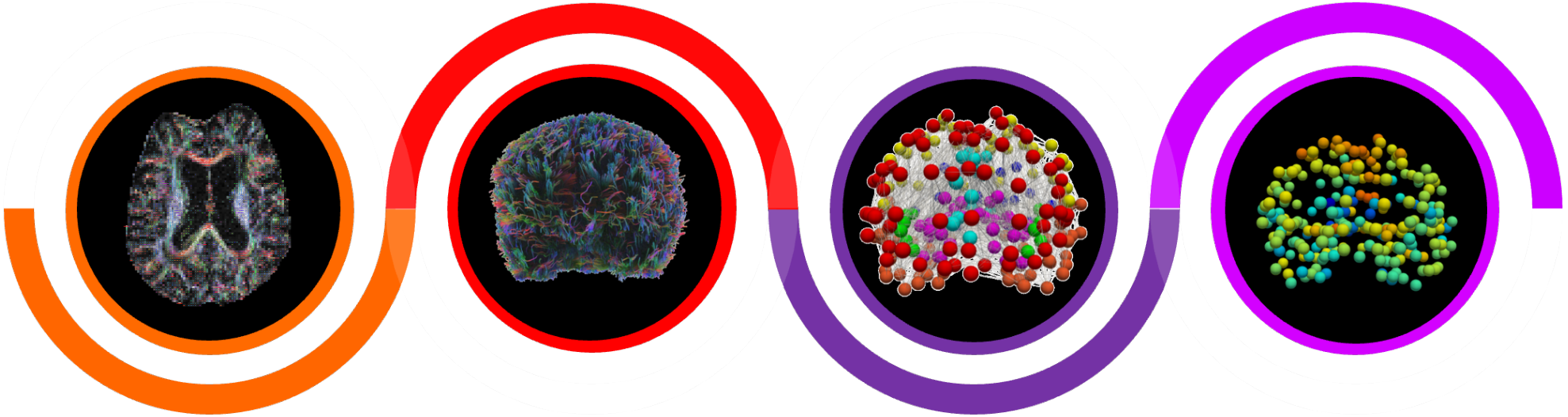

TRACTOGRAPHY

2

Brain tractography approximates the **principal axonal directions** at any point.

3

CONNECTOME

From tractography we reconstruct a **graph** with the principal brain regions and their connections.

PiB-PET

4

PiB-PET is able to identify the presence of **Amyloid-β** inside the brain.

Fisher – Kolmogorov on graphs

$$\begin{cases} \dfrac{\partial c}{\partial t} = \nabla \cdot (\mathbf{D}\nabla\, c) + \alpha\, c(1-c) + f, & \text{in } \Omega \times (0,T], \\ (\mathbf{D}\nabla c) \cdot \boldsymbol{n} = 0, & \text{on } \Gamma_N \times (0,T], \\ c = c_{\mathrm{D}}, & \text{on } \Gamma_D \times (0,T], \\ c(0) = c_0, & \text{in } \Omega, \end{cases}$$

$$\alpha(\boldsymbol{x}, \boldsymbol{p}) = \sum_{j=1}^{N} p_j \chi_{\Omega_j}(\boldsymbol{x})$$

Stochastic reaction parameter

$$\mathbf{D} = \mathbf{D}(\boldsymbol{x}) = d_{\mathrm{ext}}\mathbf{I} + d_{\mathrm{axn}}\boldsymbol{a}(\boldsymbol{x}) \otimes \boldsymbol{a}(\boldsymbol{x})$$

Diffusion tensor

Fisher – Kolmogorov on graphs

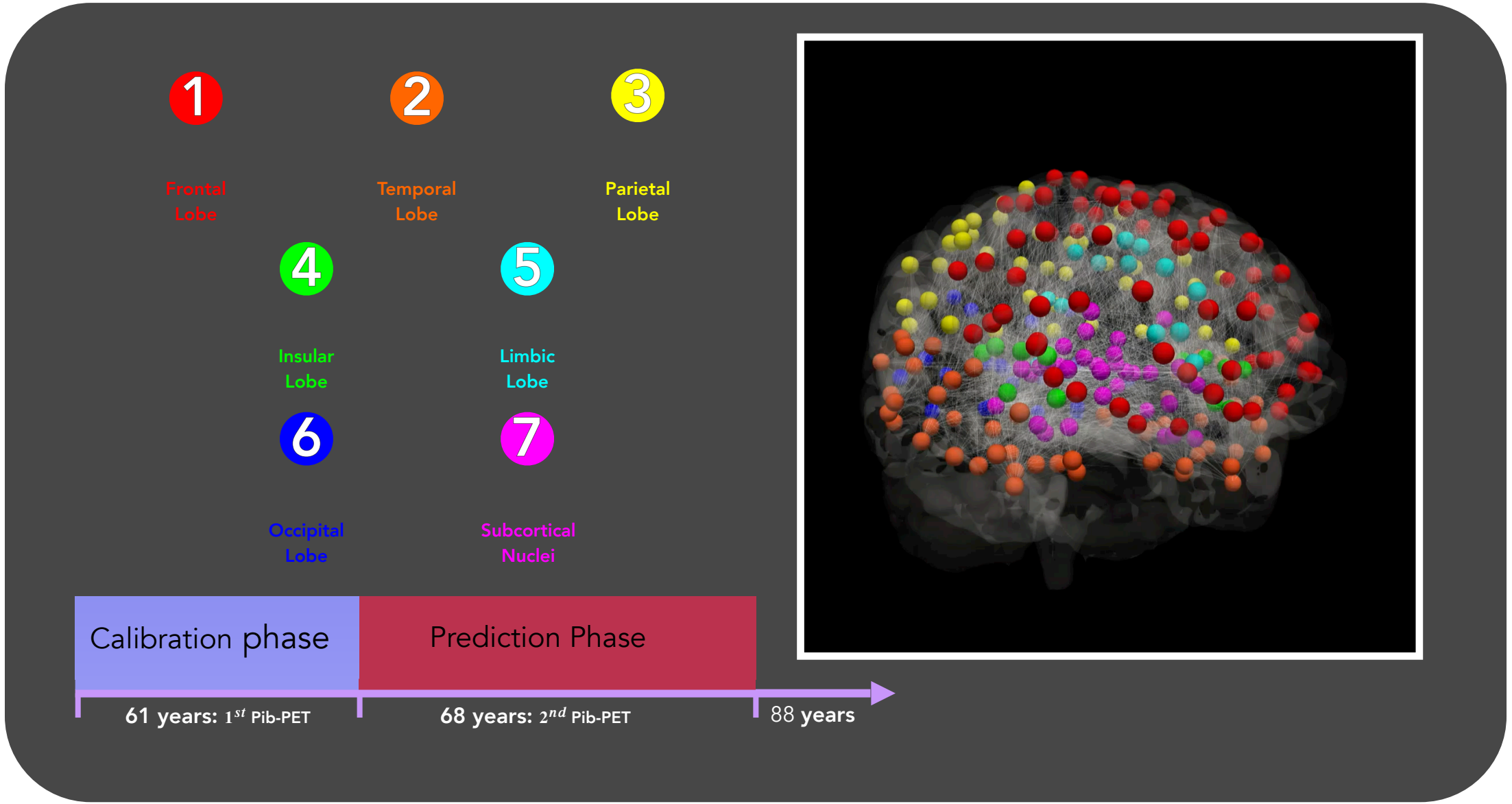

Fisher – Kolmogorov on graphs

Continuous formulation

$$\frac{\partial c}{\partial t} = \nabla \cdot (\mathbf{D}\nabla c) + \alpha c(1-c)$$

+ Graph Space-Discretization

+ Crank-Nicolson Time-Discretization

Discrete formulation

Given the initial conditions $\boldsymbol{c}_0$ and $\boldsymbol{c}_{-1}$, find $\boldsymbol{c}^{k+1} = \boldsymbol{c}^{k+1}(\boldsymbol{p})$, such that

$$\begin{cases} \dfrac{\boldsymbol{c}^{k+1} - \boldsymbol{c}^{k}}{\Delta t} = -\dfrac{1}{2}\mathbf{L}\left(\boldsymbol{c}^{k+1} + \boldsymbol{c}^{k}\right) + \boldsymbol{\alpha} \odot \left(\dfrac{1}{2}\boldsymbol{c}^{k+1} + \dfrac{1}{2}\boldsymbol{c}^{k}\right) \odot \left(\mathbf{1} - \left(\dfrac{3}{2}\boldsymbol{c}^{k} - \dfrac{1}{2}\boldsymbol{c}^{k-1}\right)\right) \quad k = 0, ..., N_t - 1, \\ \boldsymbol{c}^{0} = \boldsymbol{c}_0, \qquad \boldsymbol{c}^{-1} = \boldsymbol{c}_{-1}, \end{cases}$$

Numerical Result

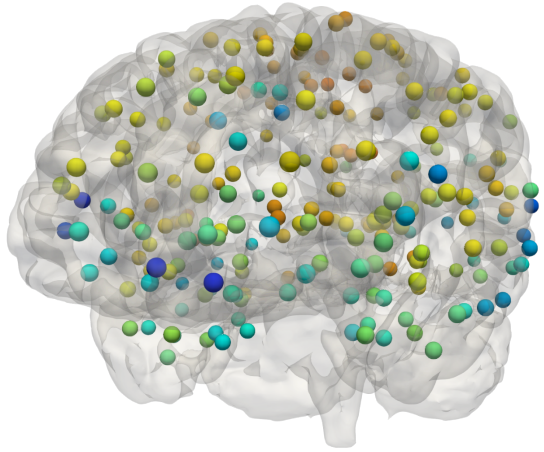

$c_h(T)$ [-]

0.0 0.1 0.2 0.3 0.4 0.5 0.6 0.7 0.8 0.9 1.0

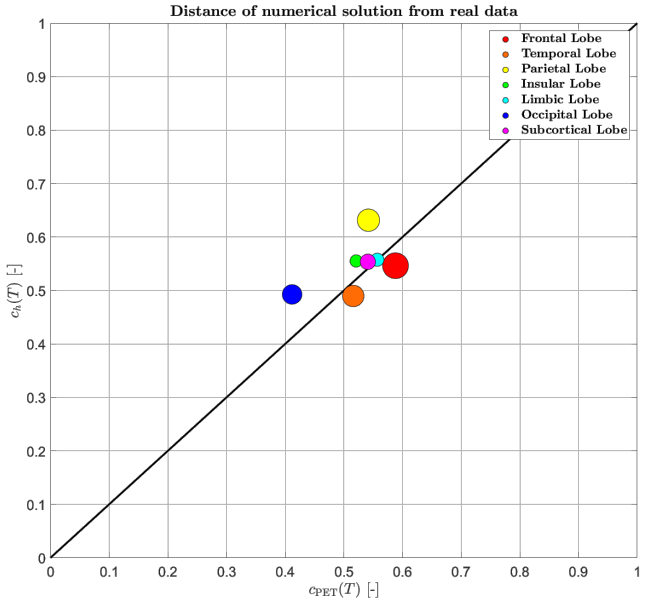

PET Data

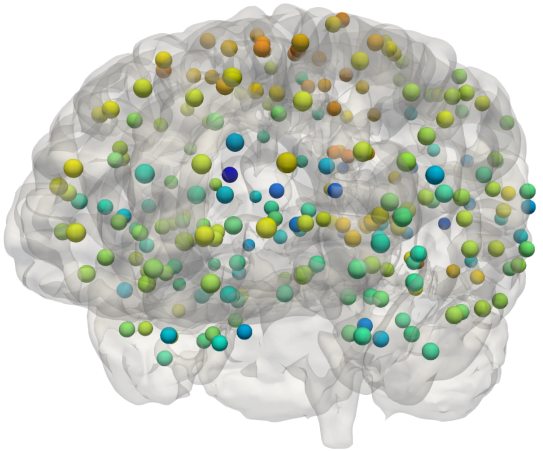

$c_{\mathrm{PET}}(T)$ [-]

0.0 0.1 0.2 0.3 0.4 0.5 0.6 0.7 0.8 0.9 1.0

Alzheimer's diseases

- We consider a patient affected by Alzheimer's diseases (medical data: 61 years olds, 68 years old)
- **Calibration phase**: the distribution of the reaction parameters in the different regions of the brain is obtained by solving an inverse UQ problem.
- **Forward UQ analysis** to determine the evolution of the Amyloid-β protein for the next twenty years, taking as initial condition the data provided from the corresponding PET images.

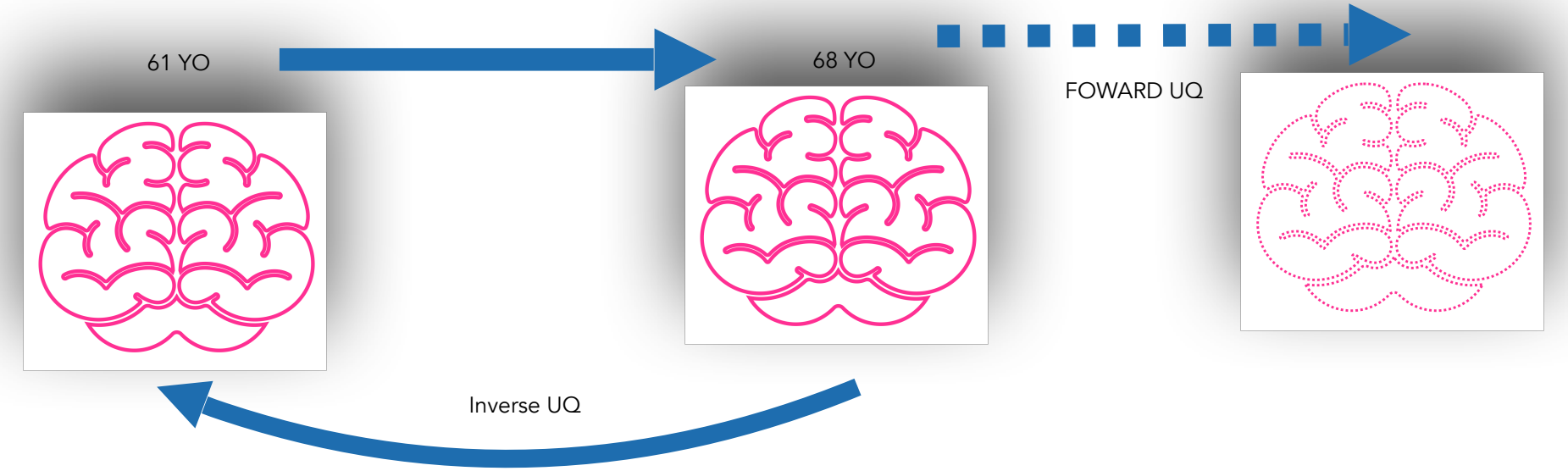

Calibration phase (Estimation of parameter distributions)

- Employ DWI data, a Magnetic Resonance Imaging, which determines the Brownian motion of the water molecules (axonal nature of the neuronal connections creates directional paths for the motion).
- Determine the brain's tractography, highlighting the axons' principal direction (Figure 2b).
- The tractography is used to derive a weighted graph G, where the nodes in V are associated with a parcellation of the brain regions and the connecting edges E are weighted taking into account both the number of connections and the length of the paths.

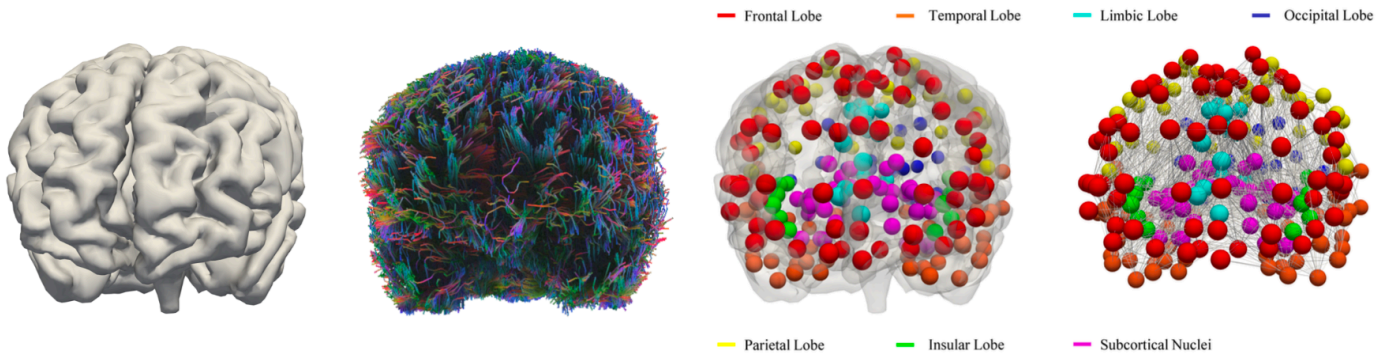

(a) Brain surface (b) Tractography (c) Nodes of the graph (d) Graph

We group the nodes in 7 regions: frontal lobe, temporal lobe, parietal lobe, insular lobe, limbic lobe, occipital lobe, and subcortical nuclei.

Alzheimer's diseases

Local graphs of the seven regions of the brain and brain connectogram between different regions (excluding the connections with weight lower than 5% of the principal one)

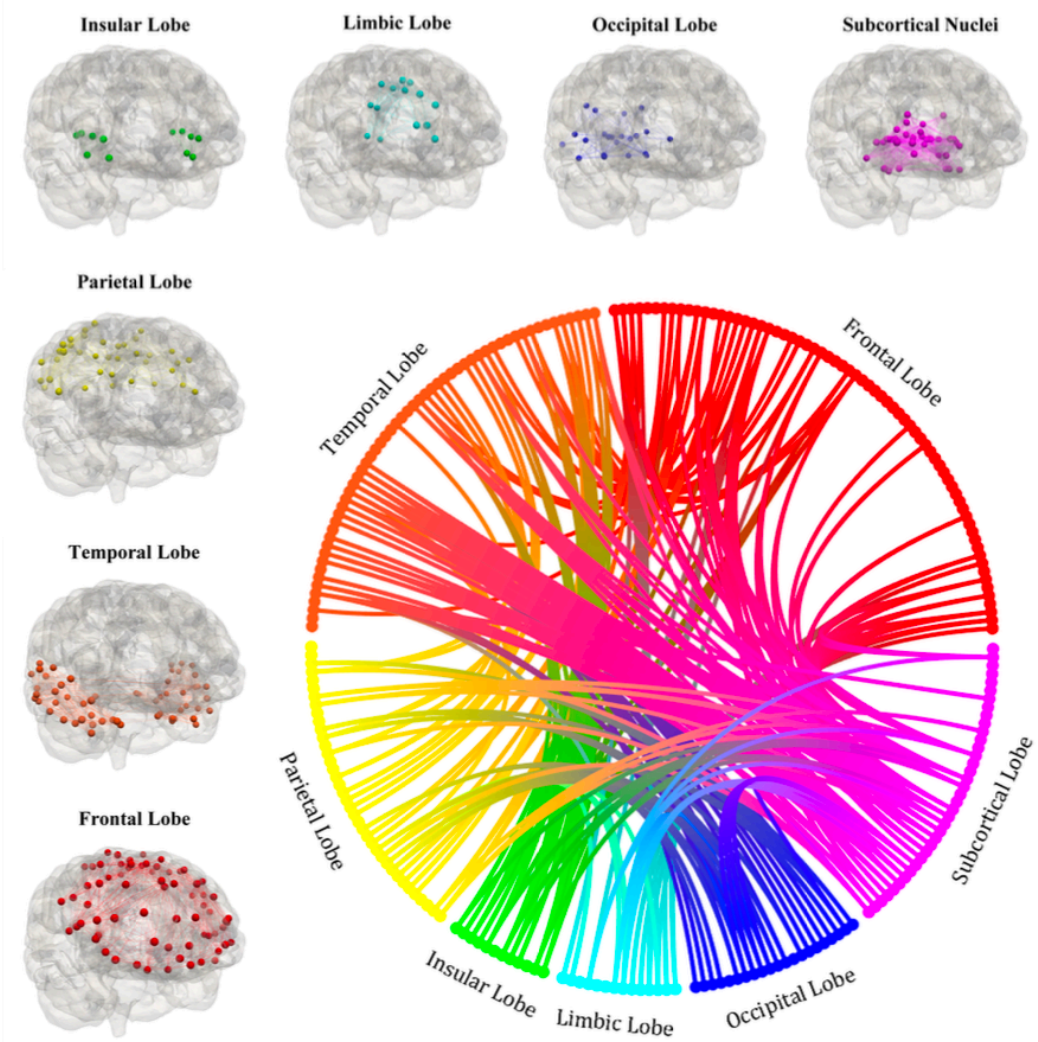

- We estimate the concentration c of Amyloid-β protein at two different time instances (61 Y, 68 Y), to estimate the reaction parameter and initial conditions for the (patient-specific) FK problem.
- PET-PiB data, which uses a radioligand able to identify the presence of Amyloid-β plaques.
- The output of the process is the projection of the medical images (at 61 and 68 years of the patient)

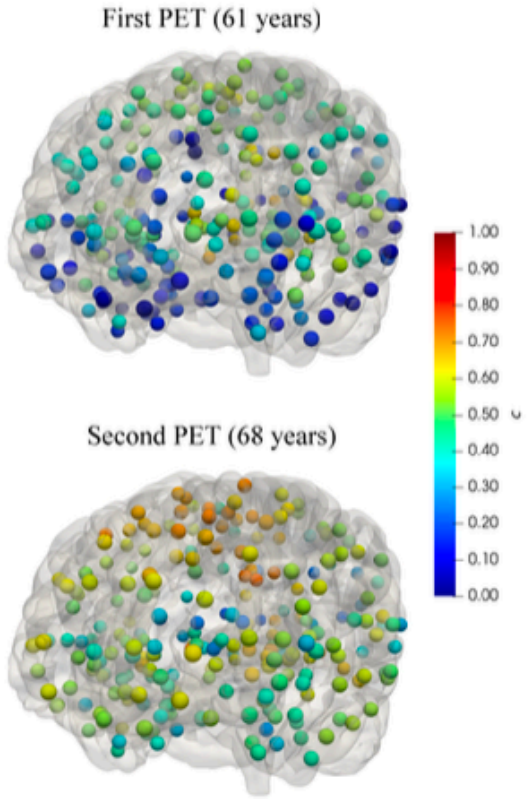

Projection of PET-PiB images on the reconstructed graph

The scatter plot confirms the increase of the concentration in most of the nodes.
However, it seems that a few nodes exhibit a decrease in the concentration of misfolded proteins. This is non-physical, we also observe that such a non-physical behaviour is mainly located in the subcortical lobe. We attribute this inconsistency to the atrophy of the region, which can be observed in the MRI images around the ventricles, and which is typical of AD

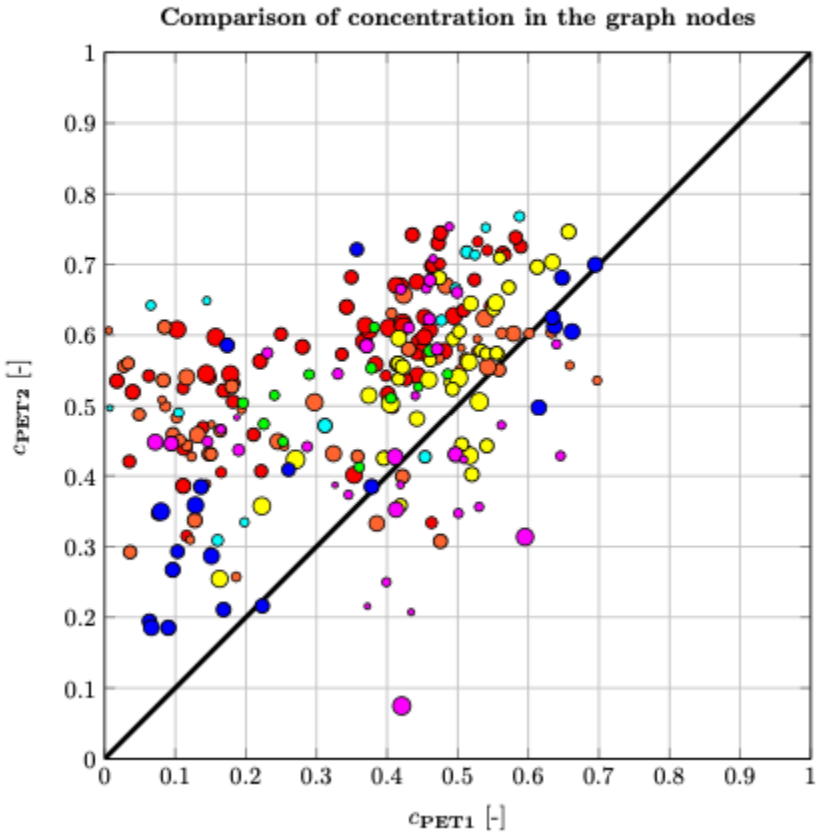

concentration of the second PET (at 68 years) versus that of the first (at 61 years).

Results of the MCMC algorithm. Histogram and Gaussian distribution associated with each lobe of the brain and comparison between the medical data and the numerical results

- comparison between the average concentration $\mathcal{Q}$ of the protein in each region of the graph computed starting from the numerical solution, obtained using the mean values of the parameters and the corresponding $\mathcal{Q}$ derived from the medical images (neglecting the outliers).
- the size of the bullets is proportional to the volume of the lobes.
- The accuracy of the estimating algorithm for the parameters can be measured by the distance from the bisecting line

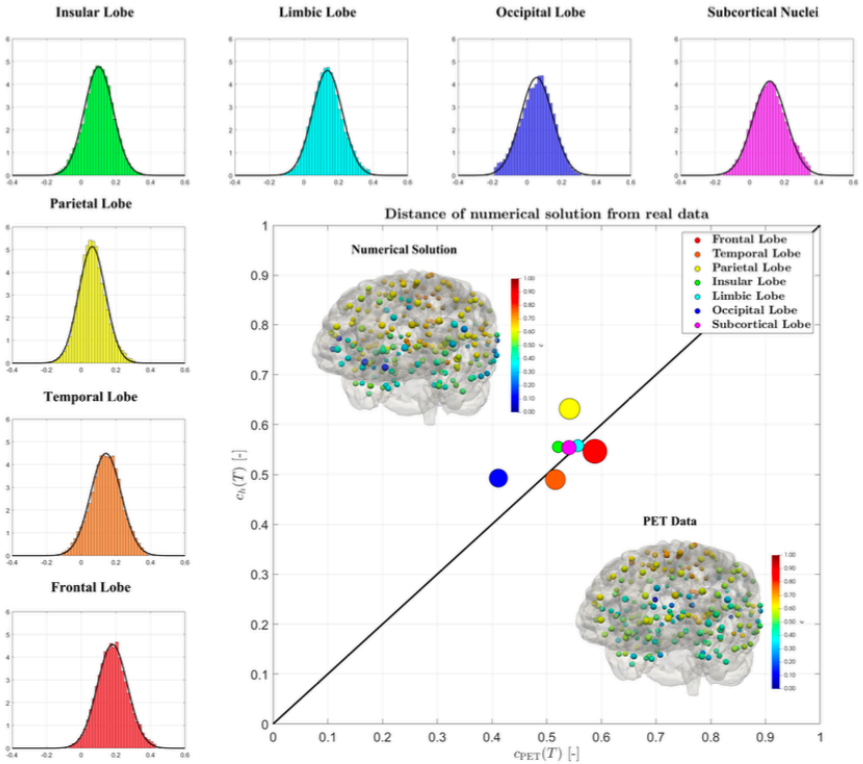

4 - Mathematical and numerical modelling of brain's perfusion and waste clearance mechanisms

04

Fluid flow(s) in the brain

Multiple fluids system in the brain

- **Arterial blood** - supply of oxygen and nutrients
- **Capillaries** - exchange substances with the tissue
- **Venous blood** - removal of CO_2
- **Interstitial/Cerebrospinal fluid** (CSF)

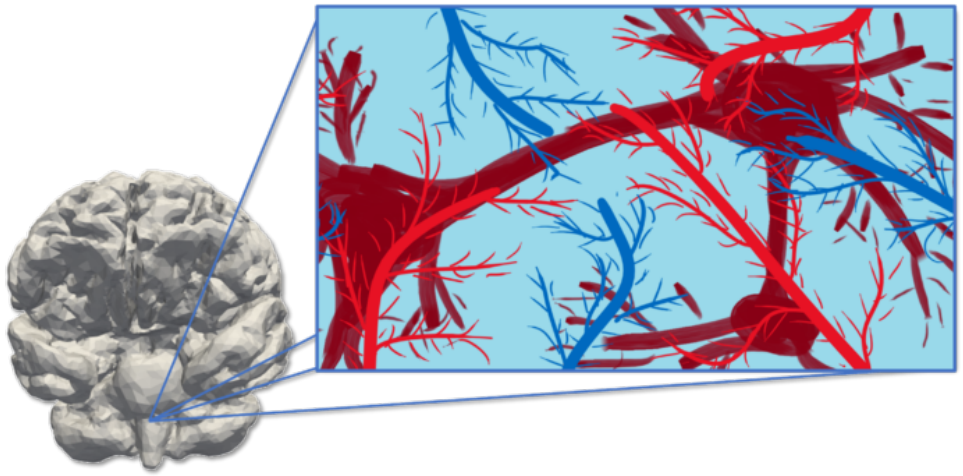

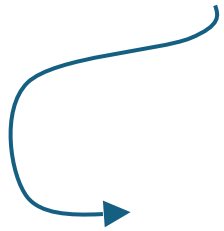

- generated in **choroid plexus** (80%) and **whole organ**
- **exchanging mass with blood capillaries** and **PVS**
- **flows in brain ventricles**
- **clears waste proteins** generated by brain activity

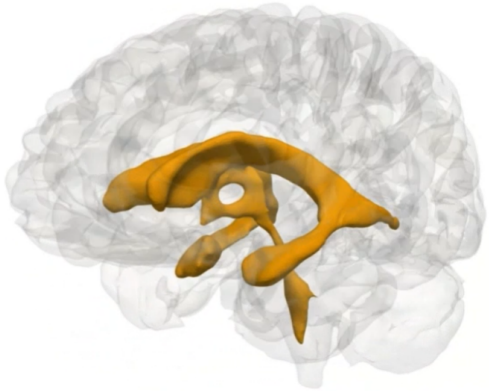

4a - Modeling brain’s perfusion

The brain as a poroelastic medium

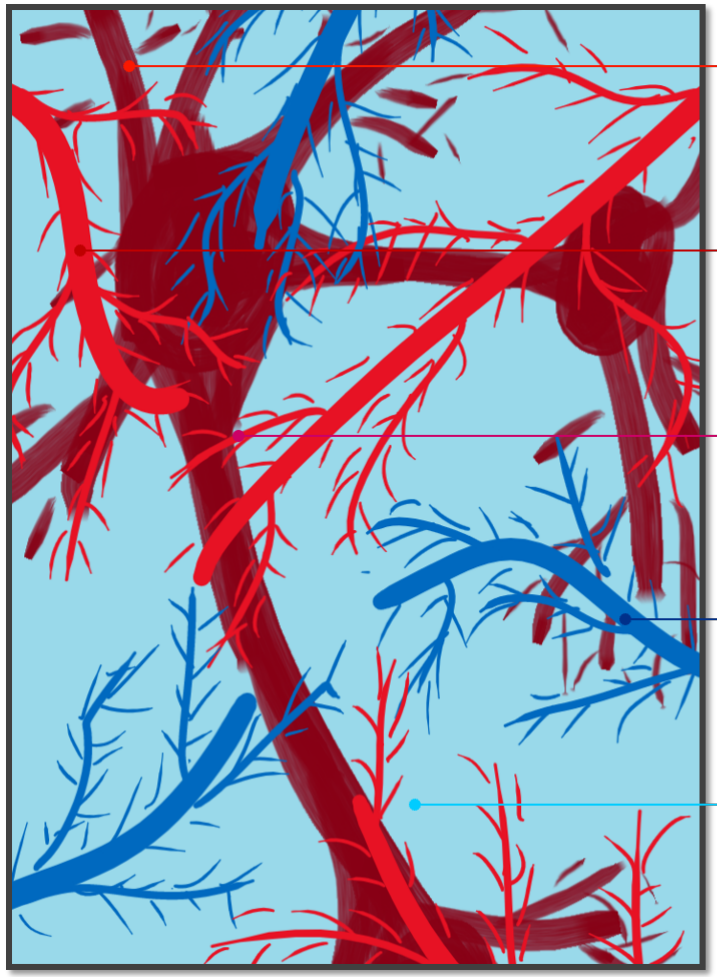

PARENCHYMAL TISSUE
Tissue is mainly composed by neurons and glial cells.

ARTERIES (A)
Vessels which transports the oxygenated blood from heart to the brain.

CAPILLARIES (C)
Vessels which exchange oxygen with the cells and produce CSF-ISF.

VEINS (V)
Vessels which transports the de-oxygenated blood from brain to the heart.

CSF-ISF (E)

Tully, B. et al. «Cerebral water transport using multiple-network poroelastic theory: application to normal pressure hydrocephalus» Journal of Fluid Mechanics, 2011
K.-A. Mardal, Vegard Vinje, Bastian Zapf, Geir Ringstad, Per Kristian Eide, and Marie E Rognes, Fluids and Barriers of the CNS, 2023.
M. Corti, P. F. Antonietti, L. Dede', A. Quarteroni, M3AS, 2023

The brain as a poroelastic medium

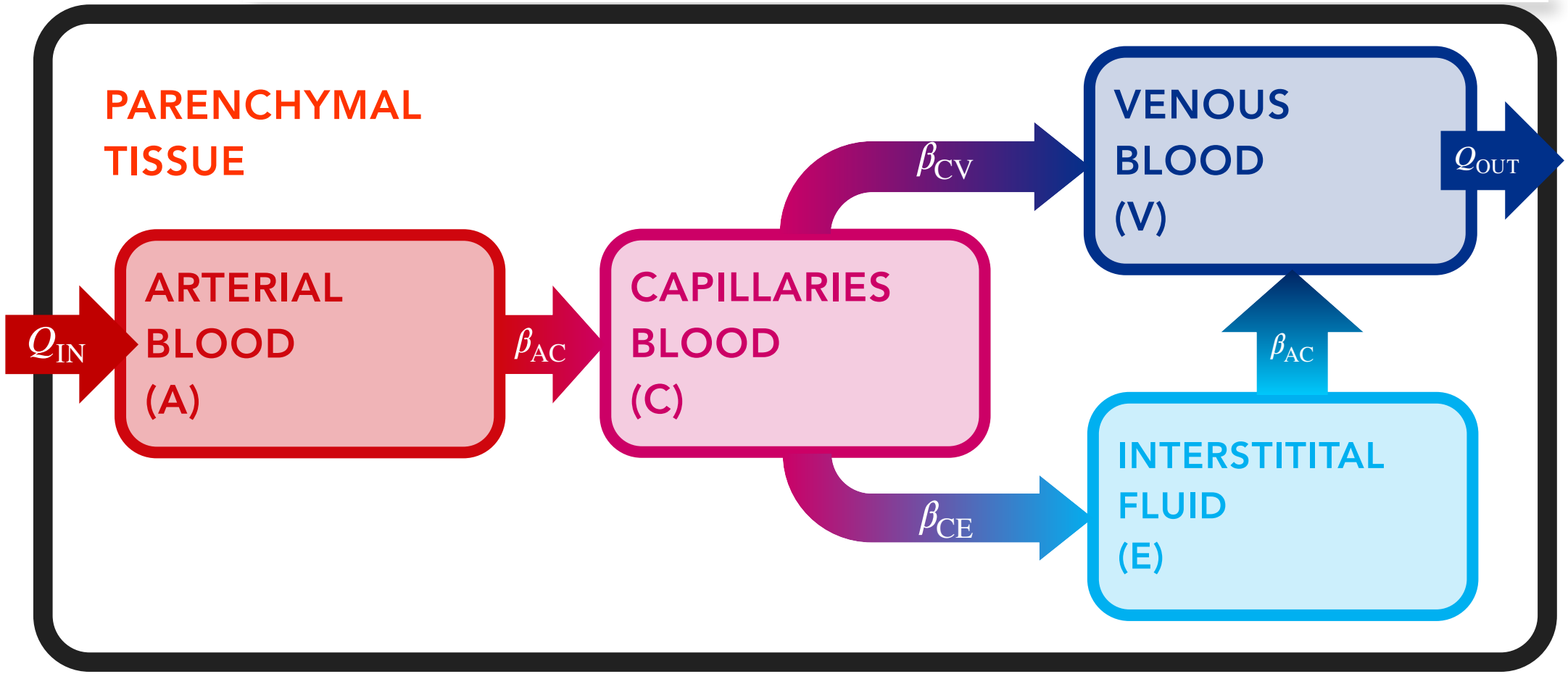

The brain as a poroelastic medium

PARENCHYMAL TISSUE
$$\rho\frac{\partial^2 \boldsymbol{u}}{\partial t^2} - \nabla\cdot(\mu\boldsymbol{\varepsilon}(\boldsymbol{u}) + \lambda(\nabla\cdot\boldsymbol{u})\mathbf{I}) + \alpha_{\mathrm{A}}\nabla p_{\mathrm{A}} + \alpha_{\mathrm{C}}\nabla p_{\mathrm{C}} + \alpha_{\mathrm{V}}\nabla p_{\mathrm{V}} + \alpha_{\mathrm{E}}\nabla p_{\mathrm{E}} = \boldsymbol{f}$$

ARTERIES (A)
$$c_{\mathrm{A}}\frac{\partial p_{\mathrm{A}}}{\partial t} + \nabla\cdot\left(\alpha_{\mathrm{A}}\frac{\partial \boldsymbol{u}}{\partial t} - \frac{\mathbf{K}_{\mathrm{A}}}{\mu_{\mathrm{A}}}\nabla p_{\mathrm{A}}\right) + \beta_{\mathrm{AC}}(p_{\mathrm{A}} - p_{\mathrm{C}}) = g_{\mathrm{A}}$$

CAPILLARIES (C)
$$c_{\mathrm{C}}\frac{\partial p_{\mathrm{C}}}{\partial t} + \nabla\cdot\left(\alpha_{\mathrm{C}}\frac{\partial \boldsymbol{u}}{\partial t} - \frac{\mathbf{K}_{\mathrm{C}}}{\mu_{\mathrm{C}}}\nabla p_{\mathrm{C}}\right) + \beta_{\mathrm{AC}}(p_{\mathrm{C}} - p_{\mathrm{A}}) + \beta_{\mathrm{CV}}(p_{\mathrm{C}} - p_{\mathrm{V}}) + \beta_{\mathrm{CE}}(p_{\mathrm{C}} - p_{\mathrm{E}}) = g_{\mathrm{C}}$$

VEINS (V)
$$c_{\mathrm{V}}\frac{\partial p_{\mathrm{V}}}{\partial t} + \nabla\cdot\left(\alpha_{\mathrm{V}}\frac{\partial \boldsymbol{u}}{\partial t} - \frac{\mathbf{K}_{\mathrm{V}}}{\mu_{\mathrm{V}}}\nabla p_{\mathrm{V}}\right) + \beta_{\mathrm{CV}}(p_{\mathrm{V}} - p_{\mathrm{C}}) + \beta_{\mathrm{VE}}(p_{\mathrm{V}} - p_{\mathrm{E}}) + \beta^{\mathrm{e}}_{\mathrm{V}}(p_{\mathrm{V}} - \tilde{p}_{\mathrm{Vein}}) = g_{\mathrm{V}}$$

CSF-ISF (E)
$$c_{\mathrm{E}}\frac{\partial p_{\mathrm{E}}}{\partial t} + \nabla\cdot\left(\alpha_{\mathrm{E}}\frac{\partial \boldsymbol{u}}{\partial t} - \frac{\mathbf{K}_{\mathrm{E}}}{\mu_{\mathrm{E}}}\nabla p_{\mathrm{E}}\right) + \beta_{\mathrm{CE}}(p_{\mathrm{E}} - p_{\mathrm{C}}) + \beta_{\mathrm{VE}}(p_{\mathrm{E}} - p_{\mathrm{V}}) = g_{\mathrm{E}}$$

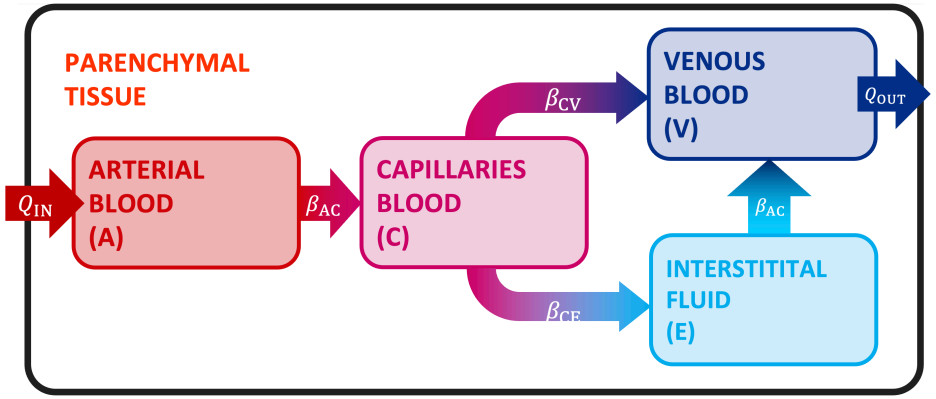

PolyDG discretization

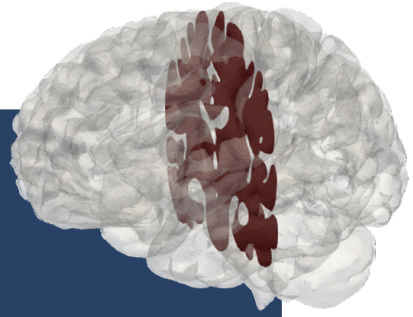

ELASTODYNAMICS

$$\rho\frac{\partial^2 \boldsymbol{u}}{\partial t^2} - \nabla\cdot(\mu\boldsymbol{\varepsilon}(\boldsymbol{u}) + \lambda(\nabla\cdot\boldsymbol{u})\mathbf{I}) + \sum_{i\in J}\alpha_i\nabla p_i = \boldsymbol{f}$$

FLUID NETWORKS

$$c_j\frac{\partial p_j}{\partial t} + \nabla\cdot\left(\alpha_j\frac{\partial \boldsymbol{u}}{\partial t} - \frac{\mathbf{K}_j}{\mu_j}\nabla p_j\right) + \sum_{k\in J}\beta_{jk}(p_j - p_k) + \beta_j^{\mathrm{e}}p_j = g_j$$

We introduce the polyDG discrete spaces V_h^{DG} and Q_h^{DG} on a polygonal/ polyhedral mesh

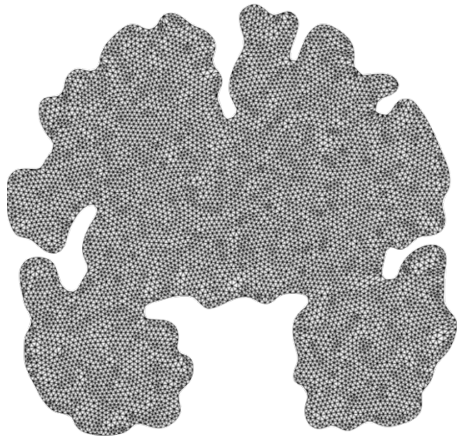

[Antonietti, Manuzzi, Corti et al., 2022, 2023, 2024]

PolyDG semidiscrete formulation

Find $\boldsymbol{u}_h(t) \in V_h^{\mathrm{DG}}$ and $p_{jh}(t) \in Q_h^{\mathrm{DG}}$ with $j \in J$ such that $\forall t > 0$:

$$\rho\left(\ddot{\boldsymbol{u}}_h(t), \boldsymbol{v}_h\right)_\Omega + \mathscr{A}_{\mathrm{E}}(\boldsymbol{u}_h(t), \boldsymbol{v}_h) + \sum_{k \in J} \Bigg(-\mathscr{B}_k(p_{kh}(t), \boldsymbol{v}_h) + c_k\left(\dot{p}_{kh}(t), q_{kh}\right)_\Omega + \mathscr{A}_{\mathrm{P}_k}(p_{kh}(t), q_{kh}) + \mathscr{B}_k\left(q_{kh}, \dot{\boldsymbol{u}}_h(t)\right) + C_k\left((p_{jh})_{j \in J}, q_{kh}\right) \Bigg) = F(\boldsymbol{v}_h) + \sum_{k \in J} G_k(q_{kh}) \quad \forall \boldsymbol{v_h} \in V_h^{\mathrm{DG}}\ \forall q_{kh} \in Q_h^{\mathrm{DG}}$$

$\mathscr{A}_{\mathrm{E}}(\boldsymbol{u}, \boldsymbol{v})$ Elliptic elasticity terms

$\mathscr{B}_k(p_k, \boldsymbol{u})$ Elasticity-pressure coupling

$\mathscr{A}_{\mathrm{P}_k}(p_k, q_k)$ Elliptic pressures terms

$\mathscr{C}_k((p_j)_{j \in J}, q_k)$ Pressure-pressure coupling

The temporal discretisation is based on a coupling between a Newmark β-method for the momentum equation and a θ-method for the pressur equations

DEFINITION: ENERGY NORM

$$||(\boldsymbol{u}_h,(p_{kh})_{k\in J})(t)||_{\varepsilon}^2 = ||\sqrt{\rho}\dot{\boldsymbol{u}}_h(t)||^2+|||\boldsymbol{u}_h(t)|||_{\mathrm{DG,E}}^2+\sum_{k\in J}\left(||\sqrt{c_k}p_{kh}(t)||^2+\int_0^t\left(||p_{kh}(s)||_{\mathrm{DG,P}_k}^2+||\sqrt{\beta_k^{\mathrm{e}}}\,p_{kh}(s)||^2\right)\mathrm{d}s\right)$$

THEOREM: STABILITY ESTIMATE

Under suitable assumptions on the mesh regularity, let $(\boldsymbol{u}_h(t),(p_{kh}(t))_{k\in J})$ be the solution of the semi-discrete problem for any $t\in(0,\hat{t}]$. Let the stability parameters be large enough for any $k\in J$. then, it holds:

$$||(\boldsymbol{u}_h,(p_{kh})_{k\in J})(\hat{t})||_{\varepsilon}\lesssim\vartheta_0+\int_0^{\hat{t}}\left(\frac{1}{\sqrt{\rho}}||\boldsymbol{f}(t)||+\sum_{k\in J}\frac{1}{\sqrt{c_k}}||g_k(t)||\right)\mathrm{d}t,$$

where ϑ_0 is a function of the initial conditions, defined as:

$$\vartheta_0^2:=||\sqrt{\rho}\dot{\boldsymbol{u}}_h^0||^2+||\boldsymbol{u}_h^0||_{\mathrm{DG,E}}^2+\sum_{k\in J}||\sqrt{c_k}p_{kh}^0||^2$$

Numerical results: verification

Parameter	Value	Parameter	Value
ρ	1.00 [Kg/m^3]	k_j $(j = 1, ..., 4)$	1.00 [m^2]
λ	1.00 [Pa]	μ_j $(j = 1, ..., 4)$	1.00 [Pa · s]
μ	1.00 [Pa]	β_{12}, β_{34}	1.00 [m^2/(N · s)]
α_j $(j = 1, ..., 4)$	0.25 [–]	β_{13}, β_{14}, β_{23}, β_{24}	0.00 [m^2/(N · s)]
c_j $(j = 1, ..., 4)$	0.10 [m^2/N]	β_j^{e} $(j = 1, ..., 4)$	0.00 [m^2/(N · s)]

Table 1: Physical parameter values used in the 3D simulation.

EXACT SOLUTION

$$\boldsymbol{u}(x,y,z,t) = \sin(\pi t)\begin{bmatrix} -\cos(\pi x)\cos(\pi y) \\ \sin(\pi x)\sin(\pi y) \\ z \end{bmatrix}$$

$$p_1(x,y,z,t) = p_3(x,y,z,t) = \pi\sin(\pi t)(\cos(\pi y)\sin(\pi x) + \cos(\pi x)\sin(\pi y))z$$

$$p_2(x,y,z,t) = p_4(x,y,z,t) = \pi\sin(\pi t)(\cos(\pi y)\sin(\pi x) - \cos(\pi x)\sin(\pi y))z$$

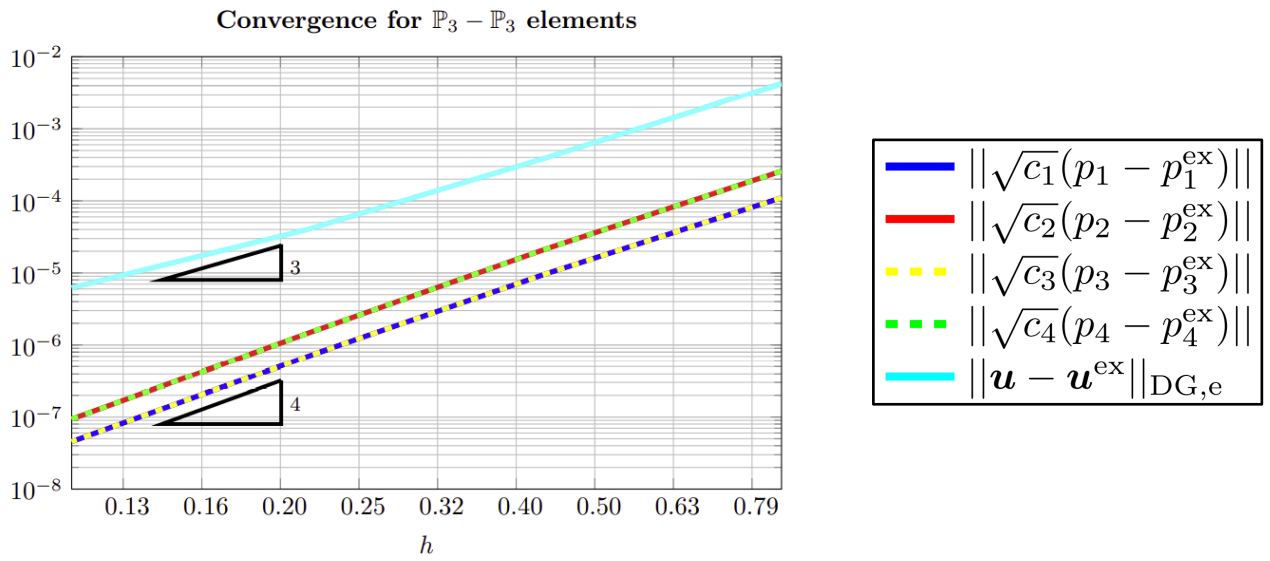

Numerical results: verification

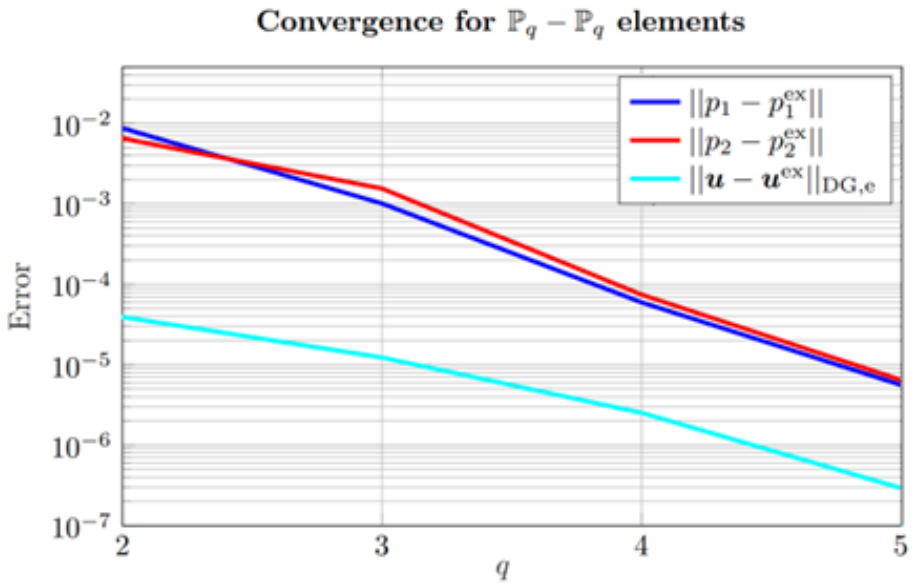

- Realistic equations' parameters
- Analytical solution to assess $p-$convergence
- Agglomerated meshes of brain section via GNN

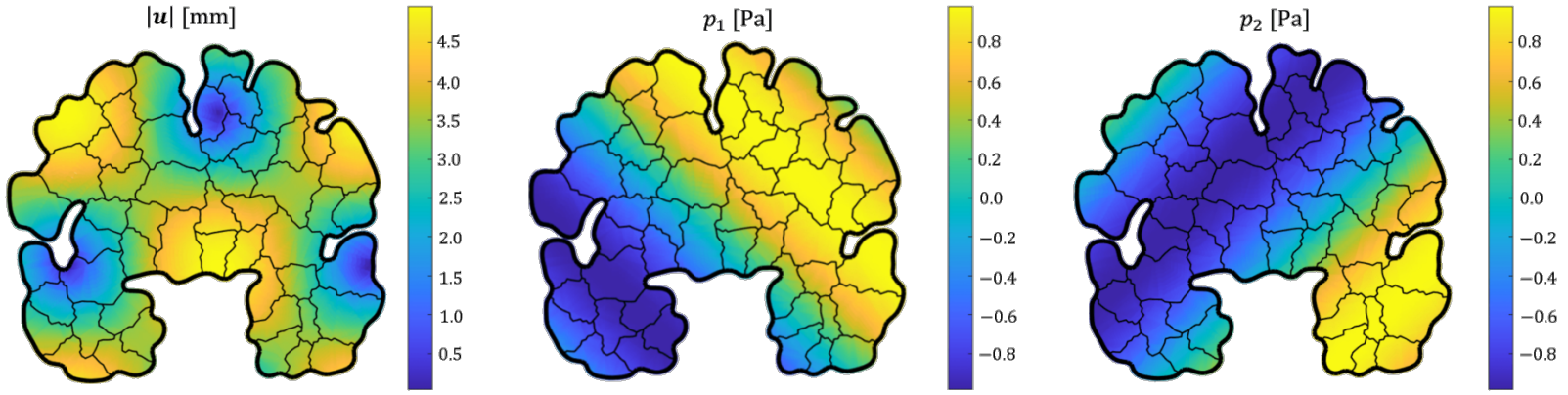

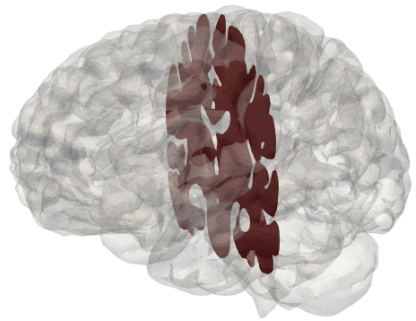

PATIENT-SPECIFIC SIMULATION: FROM MEDICAL IMAGES TO MODEL CALIBRATION

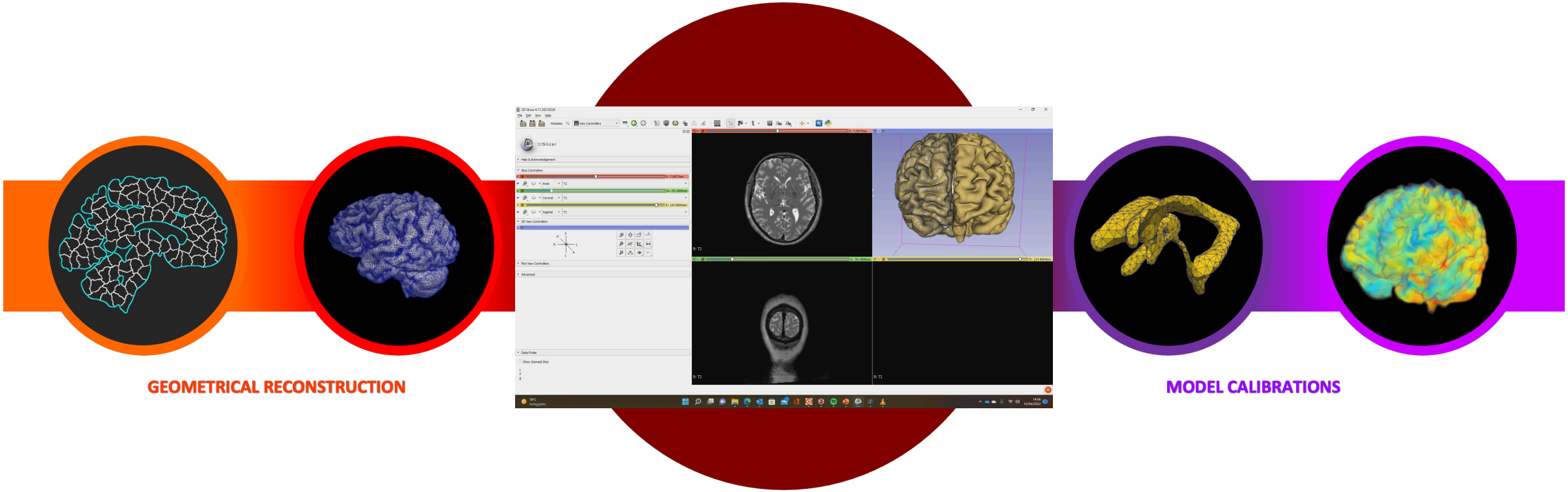

GEOMETRICAL RECONSTRUCTION

MODEL CALIBRATIONS

Medical images are essential to derive the **geometrical domain** for the simulation of physiological and pathological processes.

The **patient-specificity** of the domain can impact on the system development.

A **customized** mathematical model using parameters based on **clinical images and biomarkers** is of primary importance.

The model **calibration** requires to analyse different types of inputs with structured procedures.

Numerical results: 3d test case

$p_E \rightarrow$ CSF-ISF pressure

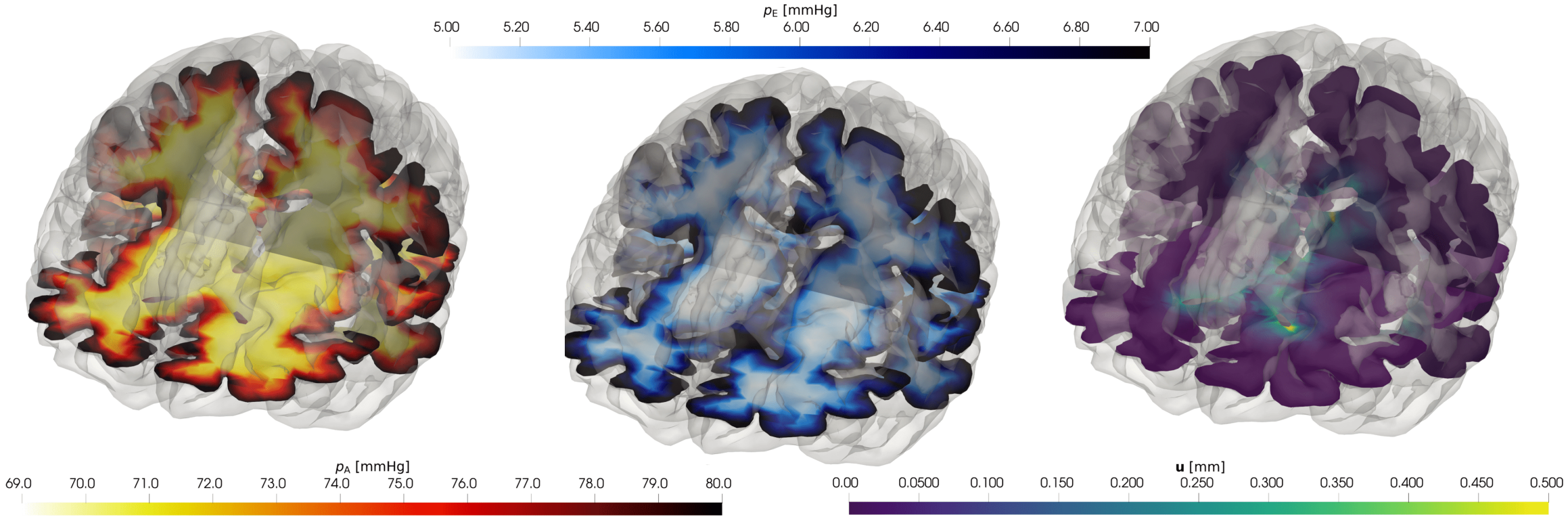

$p_A \rightarrow$ Arterial pressure

$u \rightarrow$ Displacement

4b - Modeling waste clearance by CSF flow

A multiphysics model of the CSF and the brain

$$
\begin{cases}
\rho_{\mathrm{f}}\partial_t \boldsymbol{u} - \nabla\cdot\sigma_{\mathrm{f}}(\boldsymbol{u}) + \nabla p_{\mathrm{f}} = \boldsymbol{f}_{\mathrm{f}} & \text{in } \Omega_{\mathrm{f}} \\
\nabla\cdot\boldsymbol{u} = 0 & \text{in } \Omega_{\mathrm{f}} \\
\rho_{\mathrm{el}}\partial_{tt}^2 \boldsymbol{d} - \nabla\cdot\sigma_{\mathrm{el}}(\boldsymbol{d}) + \sum_{\mathrm{k}\in J}\alpha_{\mathrm{k}}\nabla p_{\mathrm{k}} = \boldsymbol{f}_{\mathrm{el}} & \text{in } \Omega_{\mathrm{el}} \\
c_{\mathrm{j}}\partial_t p_{\mathrm{j}} + \nabla\cdot\left(\alpha_{\mathrm{j}}\partial_t \boldsymbol{d} - \frac{1}{\mu_{\mathrm{j}}}K_{\mathrm{j}}\nabla p_{\mathrm{j}}\right) + \sum_{\mathrm{k}\in J}\beta_{\mathrm{jk}}(p_{\mathrm{j}} - p_{\mathrm{k}}) + \beta_{\mathrm{j}}^{\mathrm{e}} p_{\mathrm{j}} = g_{\mathrm{j}} & \text{in } \Omega_{\mathrm{el}} \quad \forall \mathrm{j}\in J
\end{cases}
$$

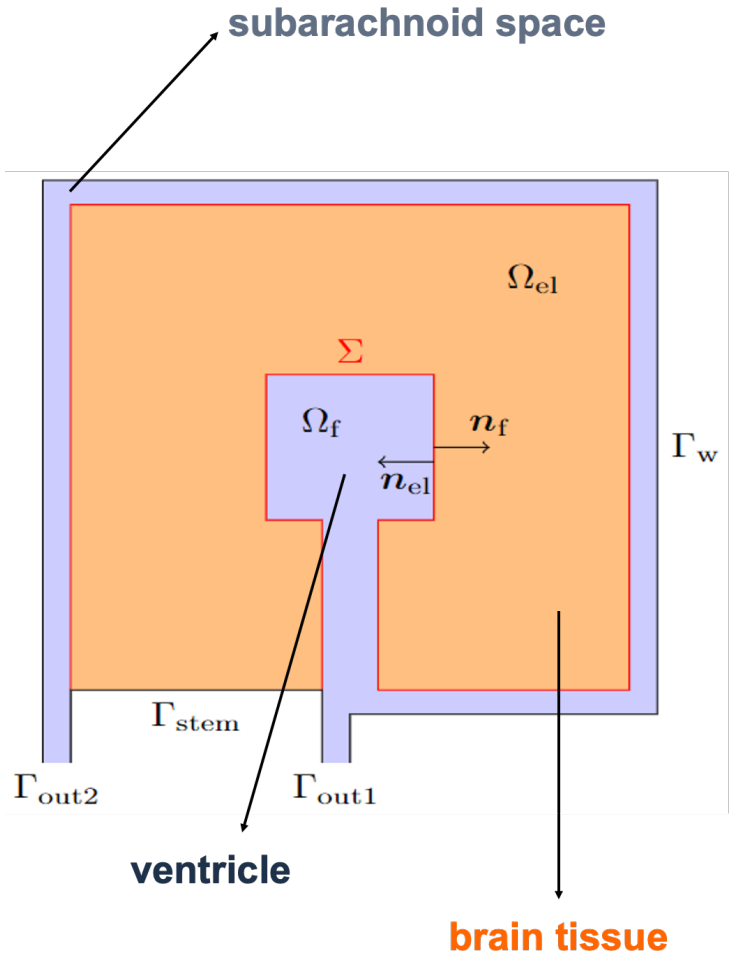

Stokes equations in the brain cavities

Multi-compartment Poro-Elasticity (MPE) eq's - dynamic formulation

- wave equations of linear elasticity
- multi-compartment Darcy problems $J = \{\mathrm{A}, \mathrm{C}, \mathrm{V}, \mathrm{E}\}$
  - A : arterial blood
  - V : venous blood
  - C : blood capillaries
  - E : CSF in permeating the extracellular space

[Fumagalli et al. (2024) J Comp Phys 513; Causemann et al. (2022) Fluid Barr CNS 19; Hornkjøl et al. (2022) Front Bioeng Biotech 10; Boon et al. (2022) J Comp Phys 467]

A multiphysics model of the CSF and the brain

Boundary conditions

Γ_{w} skull
Γ_{stem} brain stem
Γ_{out} 4th ventricle outlets

$$\begin{cases} \boldsymbol{d} = \boldsymbol{0} & \text{on } \Gamma_{\mathrm{stem}} \\ \frac{1}{\mu_{\mathrm{j}}} K_{\mathrm{j}} \nabla p_{\mathrm{j}} \cdot \boldsymbol{n} = 0 & \text{on } \Gamma_{\mathrm{stem}} \quad \forall \mathrm{j} \in J \\ \boldsymbol{u} = \boldsymbol{0} & \text{on } \Gamma_{\mathrm{w}} \\ (\sigma_{\mathrm{f}}(\boldsymbol{u}) - p_{\mathrm{f}} I)\boldsymbol{n} = -\overline{p}^{\mathrm{out}} \boldsymbol{n} & \text{on } \Gamma_{\mathrm{out}} \end{cases}$$

Interface conditions on Σ

$$\begin{cases} \frac{1}{\mu_{\mathrm{j}}} K_{\mathrm{j}} \nabla p_{\mathrm{j}} \cdot \boldsymbol{n}_{\mathrm{el}} = 0 \qquad \mathrm{j} \in \{\mathbf{A},\mathbf{C},\mathbf{V}\} \\ \boldsymbol{u} \cdot \boldsymbol{n}_{\mathrm{f}} + \left(\partial_t \boldsymbol{d} - \frac{1}{\mu_{\mathrm{E}}} K_{\mathrm{E}} \nabla p_{\mathrm{E}} \right) \cdot \boldsymbol{n}_{\mathrm{el}} = 0 \\ \sigma_{\mathrm{el}}(\boldsymbol{d}) \boldsymbol{n}_{\mathrm{el}} - \sum_{\mathrm{k} \in J} \alpha_{\mathrm{k}} p_{\mathrm{k}} \boldsymbol{n}_{\mathrm{el}} + \sigma_{\mathrm{f}}(\boldsymbol{u}) \boldsymbol{n}_{\mathrm{f}} - p_{\mathrm{f}} \boldsymbol{n}_{\mathrm{f}} = \boldsymbol{0} \\ p_{\mathrm{E}} = p_{\mathrm{f}} - \sigma_{\mathrm{f}}(\boldsymbol{u}) \boldsymbol{n}_{\mathrm{f}} \cdot \boldsymbol{n}_{\mathrm{f}}, \quad (\sigma_{\mathrm{f}}(\boldsymbol{u}) \boldsymbol{n}_{\mathrm{f}} - p_{\mathrm{f}} \boldsymbol{n}_{\mathrm{f}}) \wedge \boldsymbol{n}_{\mathrm{f}} = \boldsymbol{0} \end{cases}$$

Beavers-Joseph-Saffman condition

$$(\sigma_{\mathrm{f}}(\boldsymbol{u}) \boldsymbol{n}_{\mathrm{f}} - p_{\mathrm{f}} \boldsymbol{n}_{\mathrm{f}}) \wedge \boldsymbol{n}_{\mathrm{f}} = \frac{\gamma \mu_{\mathrm{f}}}{\sqrt{k_{\mathrm{E}}}} (\boldsymbol{u} - \partial_t \boldsymbol{d}) \wedge \boldsymbol{n}_{\mathrm{f}}$$

for the moment: $\gamma = 0$ (no tangential stress)

- stress balance **at pores** (only normal)

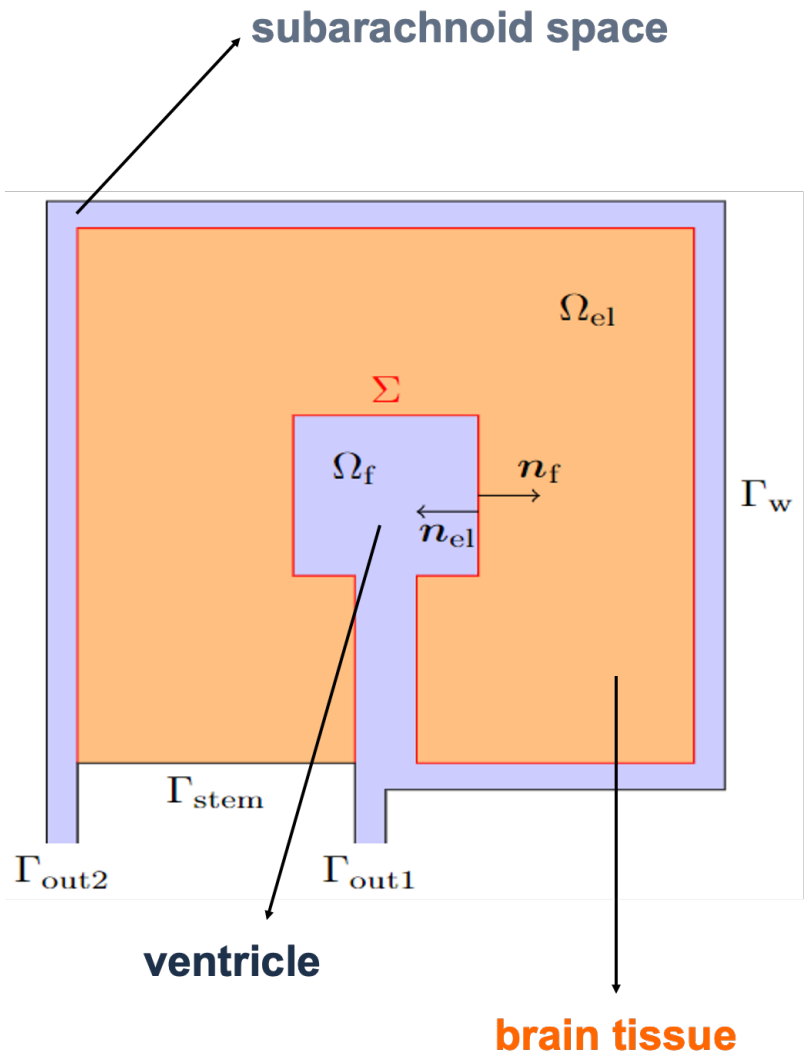

[Fumagalli et al. (2024) J Comp Phys 513; Causemann et al. (2022) Fluid Barr CNS 19; Hornkjøl et al. (2022) Front Bioeng Biotech 10; Boon et al. (2022) J Comp Phys 467]

PolyDG discretisation

WHY

- naturally account for **complex geometries**
- compliant to **local refinement** (*h*,*p*,*hp*)
- **elements with general shape** admitted

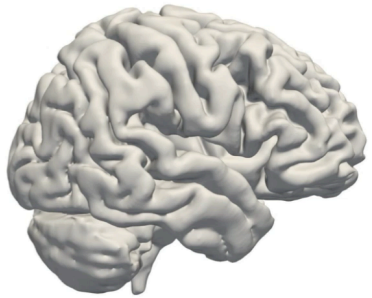

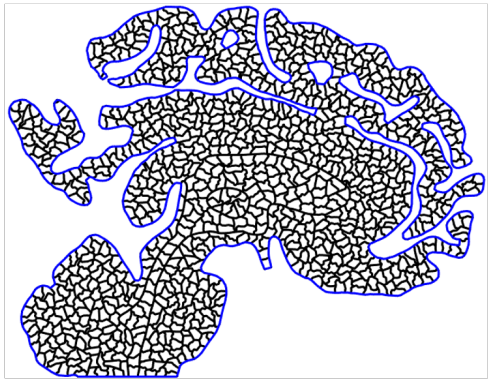

HOW

interface

$$\Omega_\ell \to \mathscr{T}_\ell \qquad \mathscr{F}^\Sigma \cup \mathscr{F}_\ell = \begin{cases} \mathscr{F}_\ell^{\mathrm{I}} & \text{internal} \\ \mathscr{F}_\ell^{\mathrm{D}} & \text{Dirichlet} \\ \mathscr{F}_\ell^{\mathrm{N}} & \text{Neumann} \end{cases} \qquad \ell = \mathrm{el}, \mathrm{f}$$

mesh — faces

FE spaces (degree *m*)

$$Q_{\mathrm{j},h}^{\mathrm{DG}} = \{q \in L^2(\Omega_{\mathrm{el}}) : q|_K \in \mathbb{P}_m(K) \quad \forall K \in \mathscr{T}_{\mathrm{el}}\}$$
$$Q_h^{\mathrm{DG}} = \{q \in L^2(\Omega_{\mathrm{f}}) : q|_K \in \mathbb{P}_m(K) \quad \forall K \in \mathscr{T}_{\mathrm{f}}\}$$
$$\boldsymbol{W}_h^{\mathrm{DG}} = \{\boldsymbol{w} \in [L^2(\Omega_{\mathrm{el}})]^d : \boldsymbol{w}|_K \in [\mathbb{P}_m(K)]^d \quad \forall K \in \mathscr{T}_{\mathrm{el}}\}$$
$$\boldsymbol{V}_h^{\mathrm{DG}} = \{\boldsymbol{v} \in [L^2(\Omega_{\mathrm{f}})]^d : \boldsymbol{v}|_K \in [\mathbb{P}_m(K)]^d \quad \forall K \in \mathscr{T}_{\mathrm{f}}\}$$

on $\mathscr{F}_{\mathrm{el}}^{\mathrm{I}}, \mathscr{F}_{\mathrm{f}}^{\mathrm{I}}$

$$\text{mean:} \quad \{\!\{q\}\!\} = \frac{1}{2}(q^+ + q^-), \quad \{\!\{\boldsymbol{w}\}\!\} = \frac{1}{2}(\boldsymbol{w}^+ + \boldsymbol{w}^-)$$
$$\text{jump:} \quad [\![q]\!] = q^+\boldsymbol{n}^+ + q^-\boldsymbol{n}^-, \quad [\![\boldsymbol{w}]\!] = \boldsymbol{w}^+ \odot \boldsymbol{n}^+ + \boldsymbol{w}^- \odot \boldsymbol{n}^-$$
$$(\text{where} \quad \boldsymbol{a} \odot \boldsymbol{b} = {}^1\!/_2(\boldsymbol{a} \otimes \boldsymbol{b} + \boldsymbol{b} \otimes \boldsymbol{a}))$$

on $\mathscr{F}^\Sigma$

$$\{\!\{q_{\mathrm{el}}\}\!\} = q_{\mathrm{el}}, \quad [\![\boldsymbol{w}_{\mathrm{el}}, \boldsymbol{v}_{\mathrm{f}}]\!] = \boldsymbol{w}_{\mathrm{el}} \odot \boldsymbol{n}_{\mathrm{el}} + \boldsymbol{v}_{\mathrm{f}} \odot \boldsymbol{n}_{\mathrm{f}}$$

Remarks

- mesh made of **polygons/polyhedra**
- variational formulation of the pb (Galerkin)
- **discontinuous** functions

  → **jump and average** operators defined on faces (internal and on boundary)

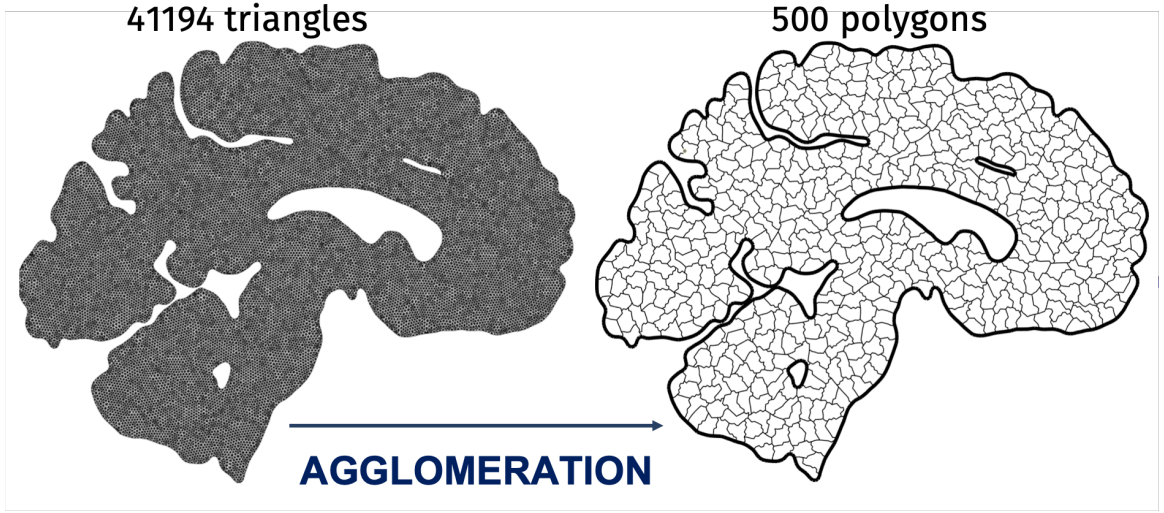

graph neural networks to comply with **media heterogeneity** and preserve mesh quality

Advantages w.r.t. simplicial/tensorial mesh

- naturally account for **complex geometries**
- compliant to **local refinement** (*h*,*p*,*hp*)
- **elements with general shape** admitted

⬇

combine computational efficiency and geometric accuracy

[Antonietti-Manuzzi, 2022, 2023, Feder-Cangiani-Heltai 2024]

Semidiscrete formulation: bilinear forms

$$\mathcal{A}_{\mathrm{el}}(\boldsymbol{d},\boldsymbol{w}) = \int_{\Omega_{\mathrm{el}}} \sigma_{\mathrm{el}}(\boldsymbol{d}) : \varepsilon(\boldsymbol{w}) - \sum_{F\in\mathscr{F}_{\mathrm{el}}^{\mathrm{I}}\cup\mathscr{F}_{\mathrm{el}}^{\mathrm{D}}} \int_F (\{\!\{\sigma_{\mathrm{el}}(\boldsymbol{d})\}\!\} : [\![\boldsymbol{w}]\!] + [\![\boldsymbol{d}]\!] : \{\!\{\sigma_{\mathrm{el}}(\boldsymbol{w})\}\!\} + \eta [\![\boldsymbol{d}]\!] : [\![\boldsymbol{w}]\!])$$

$$\mathcal{B}_{\mathrm{j}}(p_{\mathrm{j}},\boldsymbol{w}) = -\int_{\Omega_{\mathrm{el}}} \alpha_{\mathrm{j}} p_{\mathrm{j}} \operatorname{div}\boldsymbol{w} + \sum_{F\in\mathscr{F}_{\mathrm{el}}^{\mathrm{I}}\cup\mathscr{F}_{\mathrm{el}}^{\mathrm{D_j}}} \int_F \alpha_{\mathrm{j}} \{\!\{p_{\mathrm{j}} I\}\!\} : [\![\boldsymbol{w}]\!], \qquad \mathrm{j}\in J$$

poroel. coupling

$$A_{\mathrm{j}}(p_{\mathrm{j}},q_{\mathrm{j}}) = \int_{\Omega_{\mathrm{el}}} \frac{1}{\mu_{\mathrm{j}}} K_{\mathrm{j}} \nabla p_{\mathrm{j}} \cdot \nabla q_{\mathrm{j}} - \sum_{F\in\mathscr{F}_{\mathrm{el}}^{\mathrm{I}}\cup\mathscr{F}_{\mathrm{el}}^{\mathrm{D_j}}} \int_F \left(\left\{\!\!\left\{ \frac{1}{\mu_{\mathrm{j}}} K_{\mathrm{j}} \nabla p_{\mathrm{j}} \right\}\!\!\right\} \cdot [\![q_{\mathrm{j}}]\!] + [\![p_{\mathrm{j}}]\!] \cdot \left\{\!\!\left\{ \frac{1}{\mu_{\mathrm{j}}} K_{\mathrm{j}} \nabla q_{\mathrm{j}} \right\}\!\!\right\} + \zeta_{\mathrm{j}} [\![p_{\mathrm{j}}]\!] \cdot [\![q_{\mathrm{j}}]\!] \right), \qquad \mathrm{j}\in J$$

compartments' mass exchange

$$\mathcal{C}_{\mathrm{j}}(\{p_{\mathrm{k}}\}_{\mathrm{k}\in J}, q_{\mathrm{j}}) = \int_{\Omega_{\mathrm{el}}} \sum_{\mathrm{k}\in J} \beta_{\mathrm{kj}} (p_{\mathrm{j}} - p_{\mathrm{k}}) q_{\mathrm{j}} + \int_{\Omega_{\mathrm{el}}} \beta_{\mathrm{j}}^{\mathrm{e}} p_{\mathrm{j}} q_{\mathrm{j}}, \qquad \mathrm{j}\in J$$

$$\mathcal{A}_{\mathrm{f}}(\boldsymbol{u},\boldsymbol{v}) = \int_{\Omega_{\mathrm{f}}} \sigma_{\mathrm{f}}(\boldsymbol{u}) : \varepsilon(\boldsymbol{v}) - \sum_{F\in\mathscr{F}_{\mathrm{f}}^{\mathrm{I}}\cup\mathscr{F}_{\mathrm{f}}^{\mathrm{D}}} \int_F (\{\!\{\sigma_{\mathrm{f}}(\boldsymbol{u})\}\!\} : [\![\boldsymbol{v}]\!] + [\![\boldsymbol{u}]\!] : \{\!\{\sigma_{\mathrm{f}}(\boldsymbol{v})\}\!\} + \gamma_{\boldsymbol{v}} [\![\boldsymbol{u}]\!] : [\![\boldsymbol{v}]\!])$$

$$\mathcal{B}_{\mathrm{f}}(p,\boldsymbol{v}) = -\int_{\Omega_{\mathrm{f}}} p \operatorname{div}\boldsymbol{v} + \sum_{F\in\mathscr{F}_{\mathrm{f}}^{\mathrm{I}}\cup\mathscr{F}_{\mathrm{f}}^{\mathrm{D}}} \int_F \{\!\{pI\}\!\} : [\![\boldsymbol{v}]\!]$$

$$\mathcal{S}(p,q) = \sum_{F\in\mathscr{F}_{\mathrm{f}}^{\mathrm{I}}} \int_F \gamma_p [\![p]\!] \cdot [\![q]\!]$$

inf-sup stabilization

$$\mathcal{J}(p_{\mathrm{E}},\boldsymbol{w},\boldsymbol{v}) = \sum_{F\in\mathscr{F}^{\Sigma}} \int_F (\{\!\{p_{\mathrm{E}} I\}\!\} : [\![\boldsymbol{w},\boldsymbol{v}]\!])$$

interface coupling

$$\sum_{F\in\mathscr{F}^{\Sigma}} \int_F [\{\!\{p_{\mathrm{E}} I\}\!\} : [\![\boldsymbol{w},\boldsymbol{v}]\!] - [\![\partial_t \boldsymbol{d},\boldsymbol{u}]\!] : \{\!\{q_{\mathrm{E}} I\}\!\}]$$

element-wise integration by parts

BC

[Antonietti et al. 2022, Corti et al, 2023, Fumagalli, 2024]

Semidiscrete formulation

$$\text{Find } (\boldsymbol{d}, \{p_{\mathrm{j}}\}_{\mathrm{j}\in J}, \boldsymbol{u}, p) \in H^2(0,T;\boldsymbol{W}_h^{\mathrm{DG}}) \times \left(\bigtimes_{\mathrm{j}\in J} H^1(0,T;Q_{\mathrm{j},h}^{\mathrm{DG}}) \right) \times H^1(0,T;\boldsymbol{V}_h^{\mathrm{DG}}) \times L^2(0,T;Q_h^{\mathrm{DG}})$$

$$\text{such that } \boldsymbol{d}(0) \simeq \boldsymbol{d}_0, \partial_t \boldsymbol{d}(0) \simeq \dot{\boldsymbol{d}}_0, \boldsymbol{u}(0) \simeq \boldsymbol{u}_0, p_{\mathrm{j}}(0) \simeq p_{\mathrm{j}0}, \forall \mathrm{j} \in J, \text{ and, for all } t \in (0,T],$$

$$(\rho_{\mathrm{el}} \partial_{tt}^2 \boldsymbol{d}, \boldsymbol{w})_{\Omega_{\mathrm{el}}} + \mathcal{L}_{\mathrm{el}}(\boldsymbol{d}, \{p_{\mathrm{k}}\}_{\mathrm{k}\in J}; \boldsymbol{w}) - \mathcal{F}_{\mathrm{el}}(\boldsymbol{w}) + \sum_{\mathrm{j}\in J} \left[(c_{\mathrm{j}} \partial_t p_{\mathrm{j}}, q_{\mathrm{j}})_{\Omega_{\mathrm{el}}} + \mathcal{L}_{\mathrm{j}}(\{p_{\mathrm{k}}\}_{\mathrm{k}\in J}, \partial_t \boldsymbol{d}; q_{\mathrm{j}}) - \mathcal{F}_{\mathrm{j}}(q_{\mathrm{j}}) \right]$$

MPE (poromech.)

Stokes (fluid)

$$+ (\rho_{\mathrm{f}} \partial_t \boldsymbol{u}, \boldsymbol{v})_{\Omega_{\mathrm{f}}} + \mathcal{L}_{\mathrm{f}}(\boldsymbol{u}, p; \boldsymbol{v}, q) - \mathcal{F}_{\mathrm{f}}(\boldsymbol{v})$$

$$+ \mathcal{J}(p_{\mathrm{E}}, \boldsymbol{w}, \boldsymbol{v}) - \mathcal{J}(q_{\mathrm{E}}, \partial_t \boldsymbol{d}, \boldsymbol{u}) = 0 \qquad \forall \boldsymbol{w} \in \boldsymbol{W}_h^{\mathrm{DG}}, \boldsymbol{v} \in \boldsymbol{V}_h^{\mathrm{DG}}, q \in Q_h^{\mathrm{DG}}, q_{\mathrm{j}} \in Q_{\mathrm{j},h}^{\mathrm{DG}},$$

Interface coupling

Ingredients for the analysis

Broken DG norms

$$\|\boldsymbol{d}\|^2_{\mathrm{DG,el}} = \|\sqrt{\mathbb{C}_{\mathrm{el}}}[\varepsilon_h(\boldsymbol{d})]\|^2 + \|\sqrt{\eta}[\![\boldsymbol{d}]\!]\|^2_{\mathscr{F}^{\mathrm{I}}_{\mathrm{el},h}\cup\mathscr{F}^{\mathrm{D}}_{\mathrm{el},h}} \qquad \|p\|^2_{\mathrm{DG},P_{\mathrm{j}}} = \left\|\sqrt{\frac{1}{\mu_{\mathrm{j}}}K_{\mathrm{j}}}\nabla_h p\right\|^2 + \left\|\sqrt{\zeta_{\mathrm{j}}}[\![p]\!]\right\|^2_{\mathscr{F}^{\mathrm{I}}_{\mathrm{el},h}\cup\mathscr{F}^{\mathrm{D_j}}_{\mathrm{el},h}}$$

$$\|\boldsymbol{u}\|^2_{\mathrm{DG},\boldsymbol{u}} = \|\sqrt{2\mu}\nabla^S_h\boldsymbol{u}\|^2 + \|\sqrt{\gamma_{\boldsymbol{v}}}[\![\boldsymbol{u}]\!]\|^2_{\mathscr{F}^{\mathrm{I}}_{\mathrm{f},h}} \qquad \|q\|^2_{\mathrm{DG},P_{\mathrm{f}}} = \|q\|^2 + \|\sqrt{\gamma_p}[\![q]\!]\|^2_{\mathscr{F}^{\mathrm{I}}_{\mathrm{f},h}\cup\mathscr{F}^{\mathrm{D}}_{\mathrm{f},h}}$$

Energy norms

$$\|(\boldsymbol{d},\{p_{\mathrm{j}}\}_{\mathrm{j}\in J})\|^t_{\mathrm{el}} = \left[\|\sqrt{\rho_{\mathrm{el}}}\partial_t\boldsymbol{d}(t)\|^2_{\Omega_{\mathrm{el}}} + \|\boldsymbol{d}(t)\|^2_{\mathrm{DG,el}} + \sum_{\mathrm{j}\in J}\left(\|\sqrt{c_{\mathrm{j}}}p_{\mathrm{j}}(t)\|^2_{\Omega_{\mathrm{el}}} + \int_0^t\left(\|p_{\mathrm{j}}(s)\|^2_{\mathrm{DG},P_{\mathrm{j}}} + \|\sqrt{\beta^{\mathrm{e}}_{\mathrm{j}}}p_{\mathrm{j}}(s)\|^2_{\Omega_{\mathrm{el}}}\right)ds\right)\right]^{1/2}$$

$$\|(\boldsymbol{u},p)\|^t_{\mathrm{f}} = \left[\|\sqrt{\rho_{\mathrm{f}}}\boldsymbol{u}(t)\|^2_{\Omega_{\mathrm{f}}} + \int_0^t\left(\|\boldsymbol{u}(s)\|^2_{\mathrm{DG},\boldsymbol{v}} + \|p(s)\|^2_{\mathrm{DG},P_{\mathrm{f}}}\right)ds\right]^{1/2}$$

$$\|(\boldsymbol{d},\{p_{\mathrm{j}}\}_{\mathrm{j}\in J},\boldsymbol{u},p)\|^t_{\mathrm{EN}} = \left[\left(\|(\boldsymbol{d},\{p_{\mathrm{j}}\}_{\mathrm{j}\in J}\|^t_{\mathrm{el}}\right)^2 + \left(\|(\boldsymbol{u},p)\|^t_{\mathrm{f}}\right)^2\right]^{1/2}.$$

Analysis of the semi-discrete formulation

Stability estimate at time t [Fumagalli et al. JCP 2024]

$$\|(\boldsymbol{d}, \{p_{\mathrm{j}}\}_{\mathrm{j}\in J}, \boldsymbol{u}, p)\|_{\mathrm{EN}}^{t} \lesssim \|(\boldsymbol{d}, \{p_{\mathrm{j}}\}_{\mathrm{j}\in J}, \boldsymbol{u}, 0)\|_{\mathrm{EN}}^{0} + \int_0^t \left(\frac{1}{\sqrt{\rho_{\mathrm{el}}}} \|\boldsymbol{f}_{\mathrm{el}}(s)\|_{\Omega_{\mathrm{el}}} + \sum_{\mathrm{j}\in J} \frac{1}{\sqrt{c_{\mathrm{j}}}} \|g_{\mathrm{j}}(s)\|_{\Omega_{\mathrm{el}}} + \frac{1}{\sqrt{\rho_{\mathrm{f}}}} \|\boldsymbol{f}_{\mathrm{f}}(s)\|_{\Omega_{\mathrm{f}}} \right) ds$$

Regularity of solution

$$\boldsymbol{d} \in C^2((0,T]; [H^r(\Omega_{\mathrm{el}})]^d), \qquad \boldsymbol{u} \in C^1((0,T]; [H^r(\Omega_{\mathrm{el}})]^d),$$
$$p \in C^0((0,T]; H^r(\Omega_{\mathrm{el}})), \qquad p_{\mathrm{j}} \in C^1((0,T]; [H^r(\Omega_{\mathrm{el}})]^d), \quad \mathrm{j} \in J$$

Same results with BJS condition [Fumagalli, 2024, arXiv:2406.14041]

Optimal convergence

[Fumagalli et al. JCP 2024]

$$\left\|(\boldsymbol{e}^{\boldsymbol{d}}, \{e^{P_{\mathrm{j}}}\}_{\mathrm{j}\in J}, \boldsymbol{e}^{\boldsymbol{u}}, e^{P_{\mathrm{f}}})\right\|_{\mathrm{EN}'}^{t} \lesssim h^m$$

Modified energy norm for smooth functions; interface forms do not cancel out.

Assumptions

- $\Omega_{\mathrm{el}}, \Omega_{\mathrm{f}}$ domains geometrically conforming at the interface Σ
- There is NO assumption on the number of edges of mesh elements
- shape-regular simplicial covering of the meshes
- The sequence of meshes fare uniformly polytopic-regular
- Local bounded variation in h

Analysis of the semi-discrete formulation

Regularity assumptions

$$\boldsymbol{d} \in C^2((0,T];[H^r(\Omega_{\mathrm{el}})]^d), \qquad \boldsymbol{u} \in C^1((0,T];[H^r(\Omega_{\mathrm{el}})]^d),$$
$$p \in C^0((0,T];H^r(\Omega_{\mathrm{el}})), \qquad p_{\mathrm{j}} \in C^1((0,T];[H^r(\Omega_{\mathrm{el}})]^d), \quad \mathrm{j} \in J$$

Optimal convergence

$$\left\|(\boldsymbol{e}^{\boldsymbol{d}}, \{e^{P_{\mathrm{j}}}\}_{\mathrm{j}\in J}, \boldsymbol{e}^{\boldsymbol{u}}, e^{P_{\mathrm{f}}})\right\|_{\mathrm{EN}}^t \lesssim h^m$$

where $\boldsymbol{e}^{\boldsymbol{d}} = \boldsymbol{d} - \boldsymbol{d}_h, e^{P_{\mathrm{j}}} = p_{\mathrm{j}} - p_{\mathrm{j},h}\ \forall \mathrm{j} \in J, \boldsymbol{e}^{\boldsymbol{u}} = \boldsymbol{u} - \boldsymbol{u}_h, e^{P_{\mathrm{f}}} = p - p_h$

Same results with Beavers-Joseph-Saffman interface condition

[Fumagalli, submitted – arXiv:2406.14041]

Optimal convergence

$$\left\|(\boldsymbol{e}^{\boldsymbol{d}}, \{e^{P_{\mathrm{j}}}\}_{\mathrm{j}\in J}, \boldsymbol{e}^{\boldsymbol{u}}, e^{P_{\mathrm{f}}})\right\|_{\mathrm{EN}'}^t \lesssim h^m$$

Modified energy norm for smooth functions; interface forms do not cancel out.

Fumagalli, Corti, Parolini, Antonietti (2024)
Fumagalli (2024)

Verification

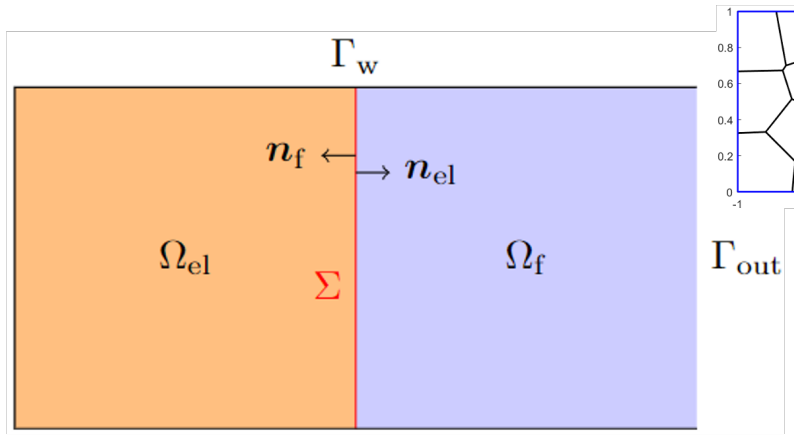

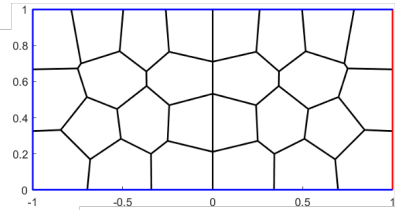

- exact solution:

  sinusoidal in *x*, *y*, *t*

- all parameters = 1
- Dirichlet BC on Γ_w
  Neumann BC on Γ_{out}
- **same polynomial order *m*** for all variables

Convergence of relative error in the energy norm

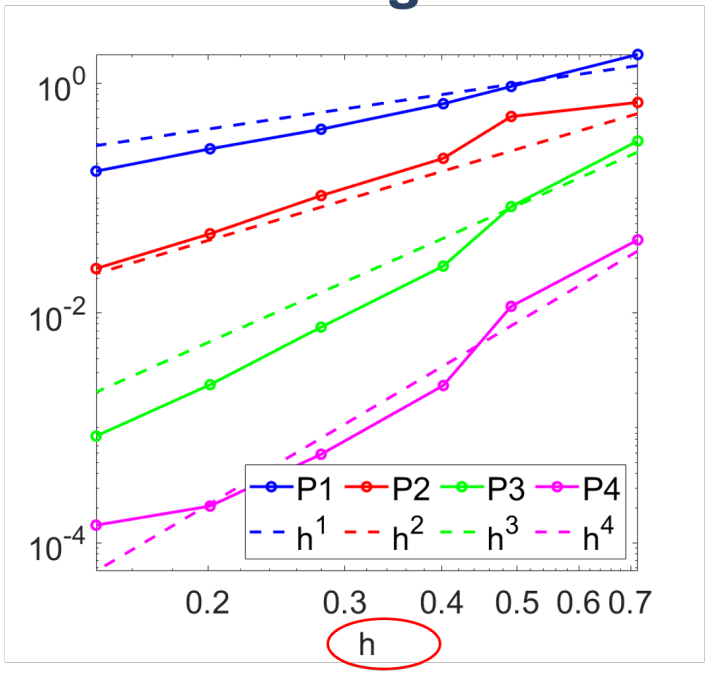

theoretical estimate verified (**optimal order**)

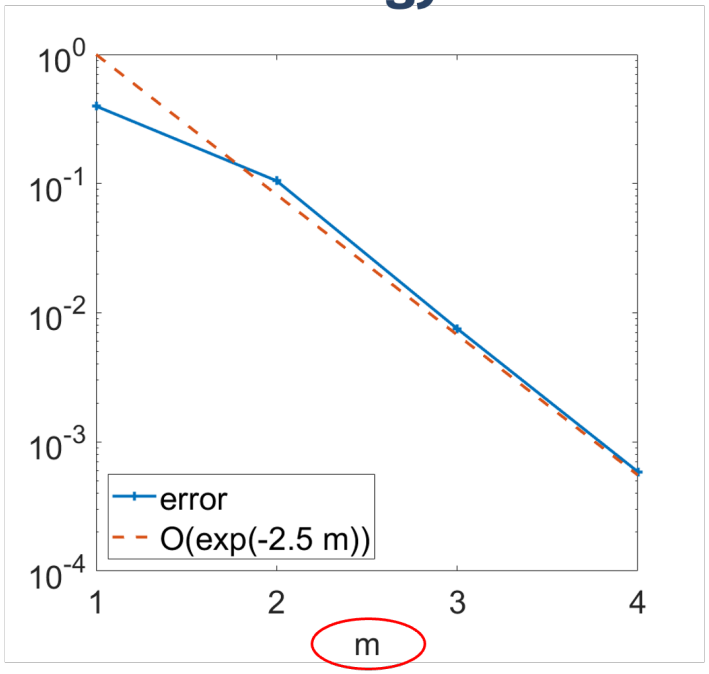

spectral convergence w.r.t. polynomial degree *m*

Patient-specific simulations in 3D

Tetrahedral geometry – FEniCS solver
(3D-lymph for PolyDG under development)

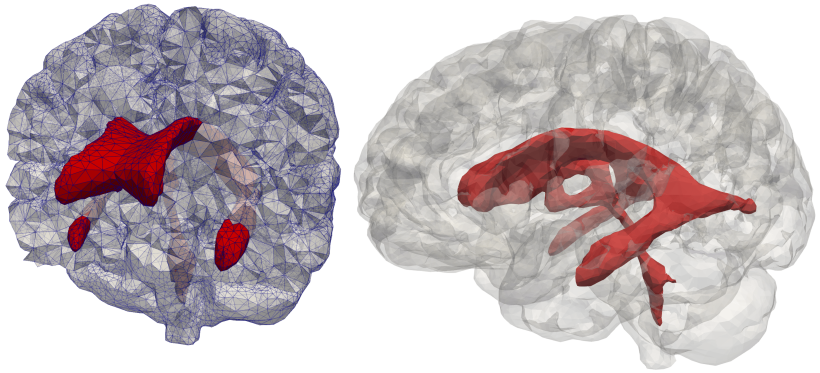

CSF generation inflow in choroid plexus
[Howden et al CMBBE (2008)]

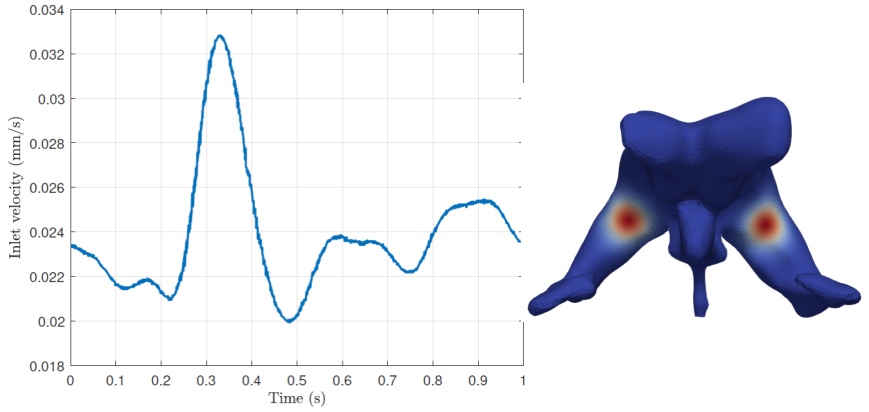

- flow analysis in the cerebral ventricles
- physiological peak velocity in the aqueduct: 2 mm/s

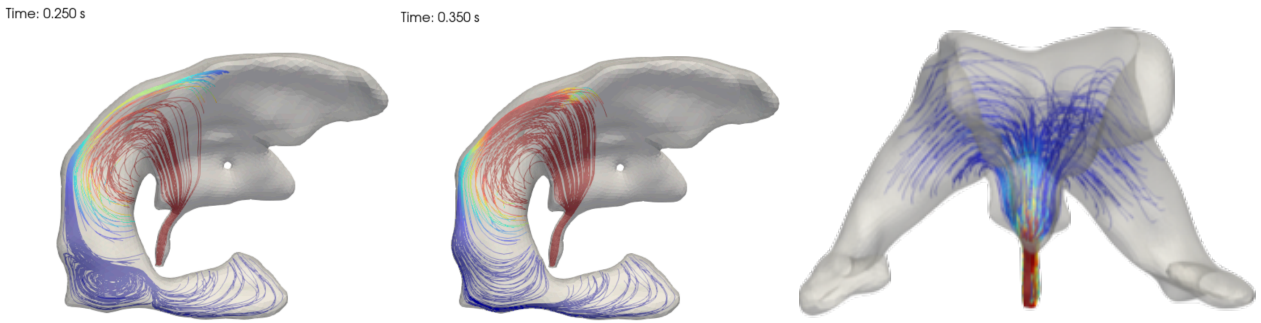

Patient-specific geometries

Imaging data

MRI

angiography

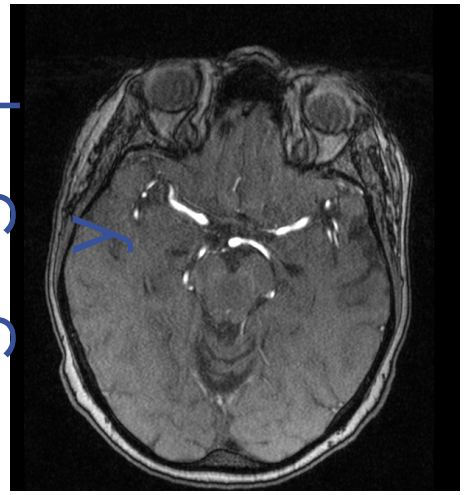

SVMTK

github.com/SVMTK/SVMTK

[Mardal, Rognes, Thompson, Valnes (2022)]

vmtk

vmtk.org

github.com/checkrenzi/vmtk

Domain reconstruction and mesh generation

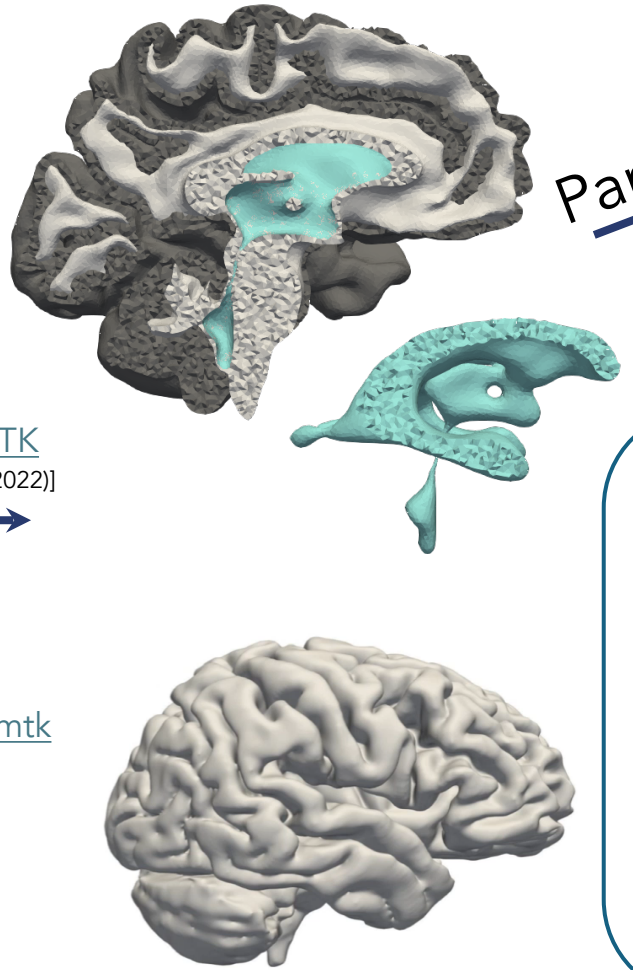

ParMETIS

Agglomerated poly grid

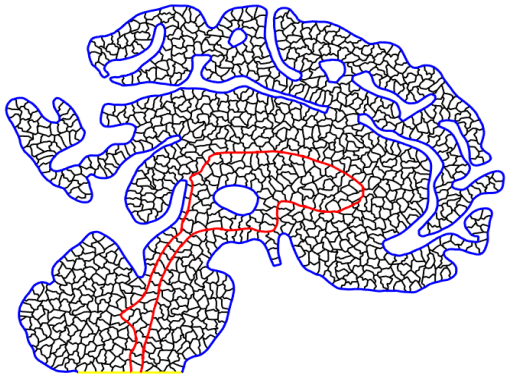

Ongoing developments

- **automatization** of segmentation (fine details e.g. aqueduct of Sylvius)
- h/p/hp **refinement & adaptivity** in polytopal grids
- parellization: **partitioning** of 3D polyhedral mesh

OASIS-3 database https://oasis-brains.org/ [LaMontagne, Benzinger, Morris et al. 2019]

Fluid-Poroelastic Structure Interaction (FPSI)

- Multi-physics: Stokes (CSF) + poroelasticity (tissue)
- Polygonal mesh of 2D slice of patient-specific brain (no subarachnoid space, corpus callosus)
- Physiological parameters – 1 por. compartment (CSF)
- BCs: no flow through dura mater, imposed outlet stress (spine)
- 1011 polygons (aggl. from >29'000 triangles) → h ~ 8 mm, polynomial degree 3
- Newmark (for displacement) + Crank-Nicolson (for others)

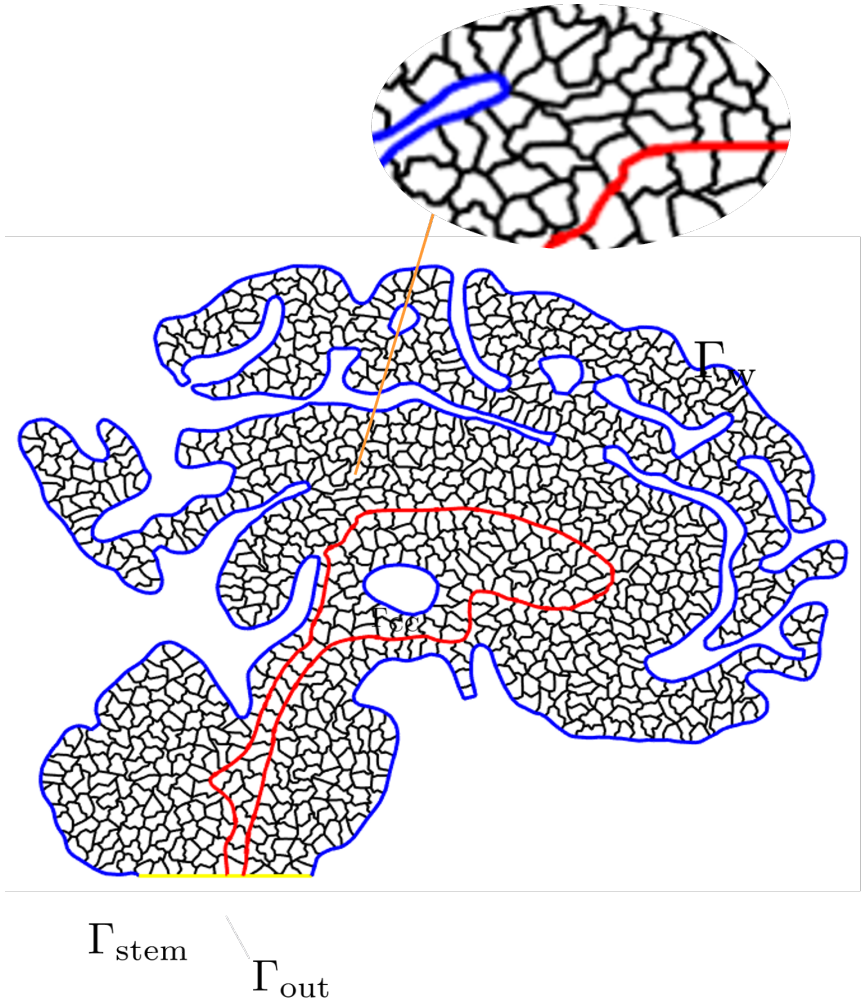

[Fumagalli, 2024], [Corti et al. M3AS 2023, Causemann et al. Flu Barr CNS 2022]

Results: Brain 2D slice

- displacement and Stokes source terms $f_{el} = 0 = 0$, $\boldsymbol{f}_f = 0$
- distributed interstitial CSF source: $g_E = c_P \, 2\pi \, 10^3 \sin(2\pi t)$ [s^{-1}]
- BCs: no flow through pia mater (no subarachnoid space), imposed outlet stress (spine)
- displacement ~ 0.01 mm
- (-) pressure gradient towards brain ventricles until t ~ 0.7s
- ~ continuous pressure at the interface
-

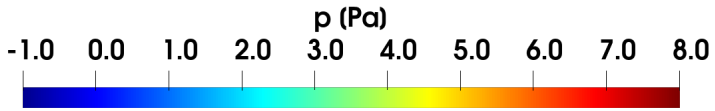

- Test in simplified geometry (sphere in sphere with duct)
- distributed CSF source:
  $\boldsymbol{g}_{el} = c_P\, 2\pi \cdot 10^3 \sin(2\pi t)$ [s^{-1}]

BJ ⟹ flat instead of parabolic profile

S ⟹ magnitude and phase of pressure

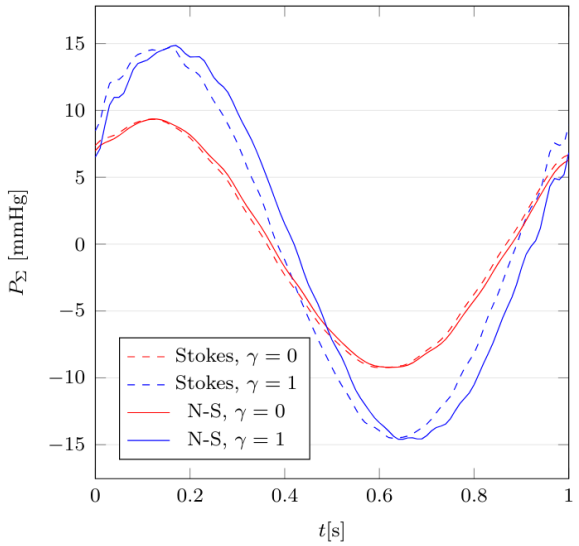

Beavers-Joseph-Saffman interface condition

$$(\sigma_f(\boldsymbol{u})\boldsymbol{n}_f - p_f\boldsymbol{n}_f) \wedge \boldsymbol{n}_f = \frac{\gamma\mu_f}{\sqrt{k_E}}(\boldsymbol{u} - \partial_t\boldsymbol{d}) \wedge \boldsymbol{n}_f$$

$\gamma = 0$ $\gamma = 1$

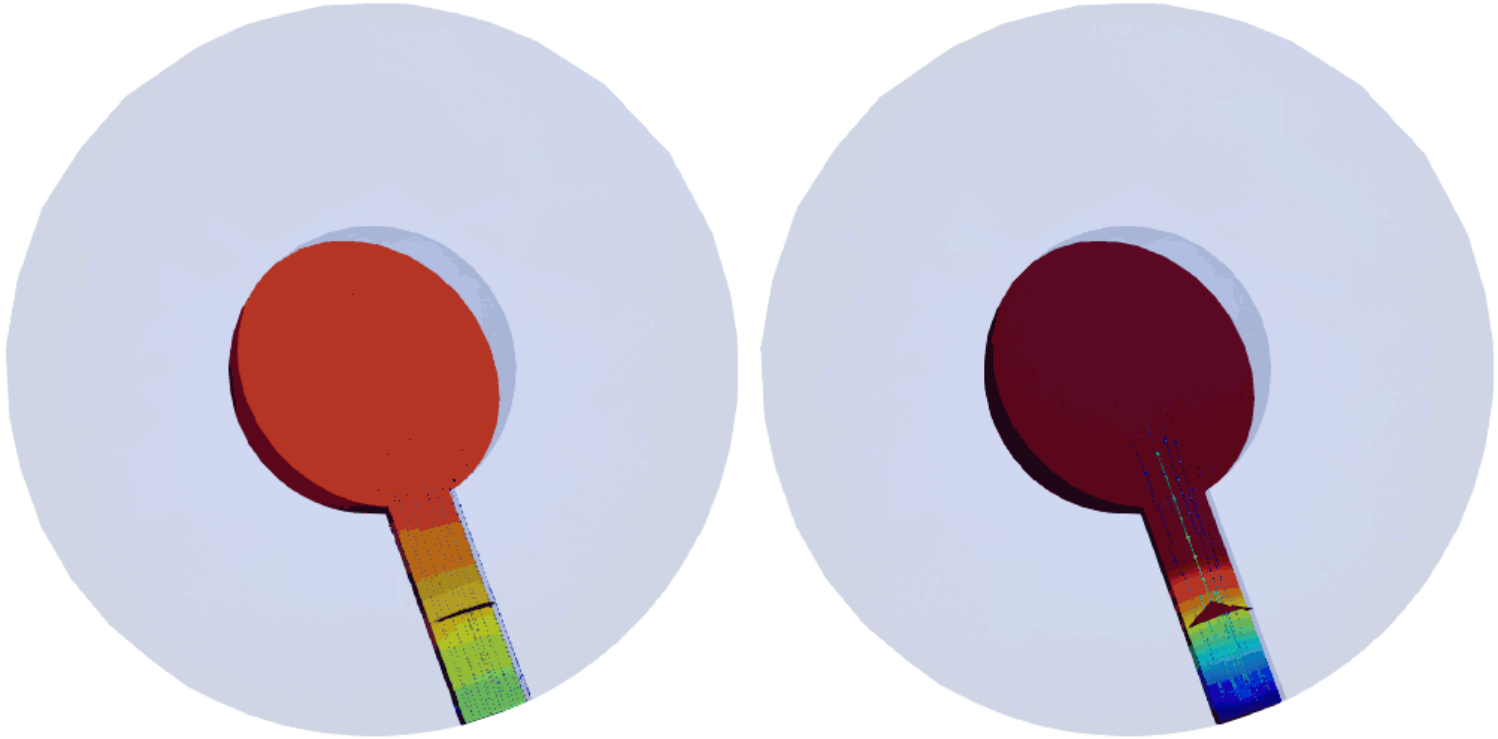

[Fumagalli (2024) *submitted* – arXiv:2406.14041]

Patient-specific simulations in 3D – with ventricles

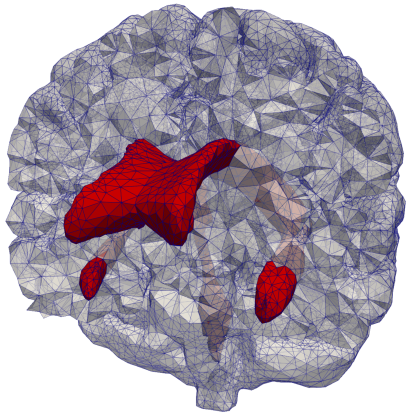

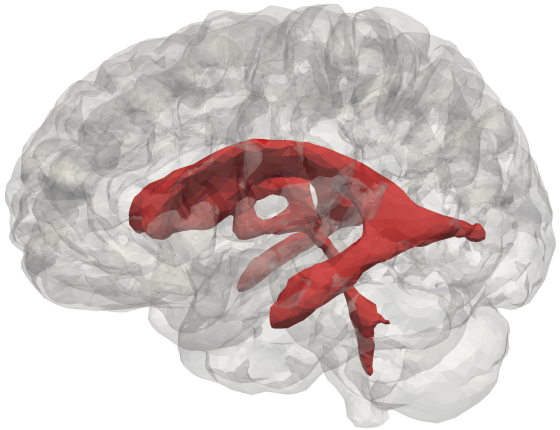

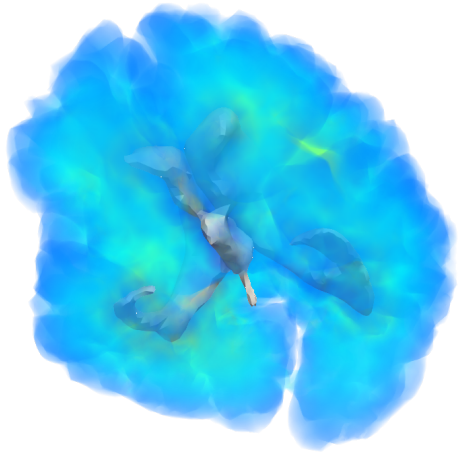

- physiological pulsatile data (literature)

- flow analysis in the cerebral ventricles
- role of the lateral ventricles:
  ~ 80% of CSF generation
  (choroid plexus)

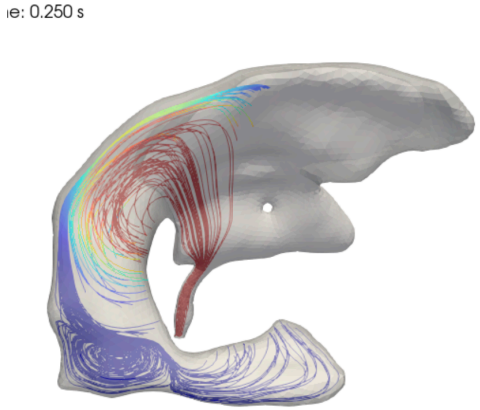

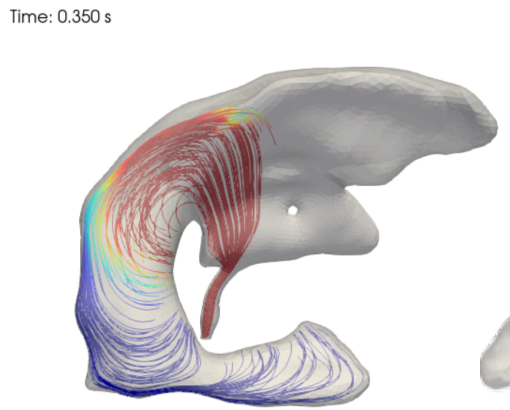

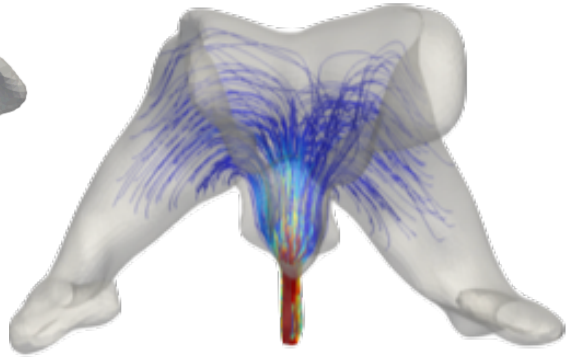

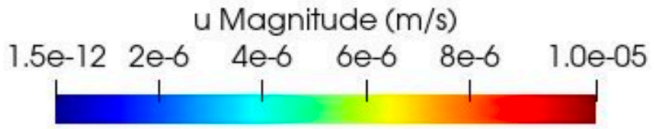

multiphenics

Credits: I. De Vittori

Blood flow in the circle of Willis

- **Circle of Willis from internal carotid + basilar** (⌀ 0.8-2.0 mm)
- 3D model: Stokes discretised by PolyDG (FEniCS)
  - computationally expensive but naturally dealing with branching
- 1D model: hyperbolic conservation laws for Q and A (Taylor-Galerkin disc.)
  - computationally cheaper but requires assumptions on branching (pressure drop due to branching angles)

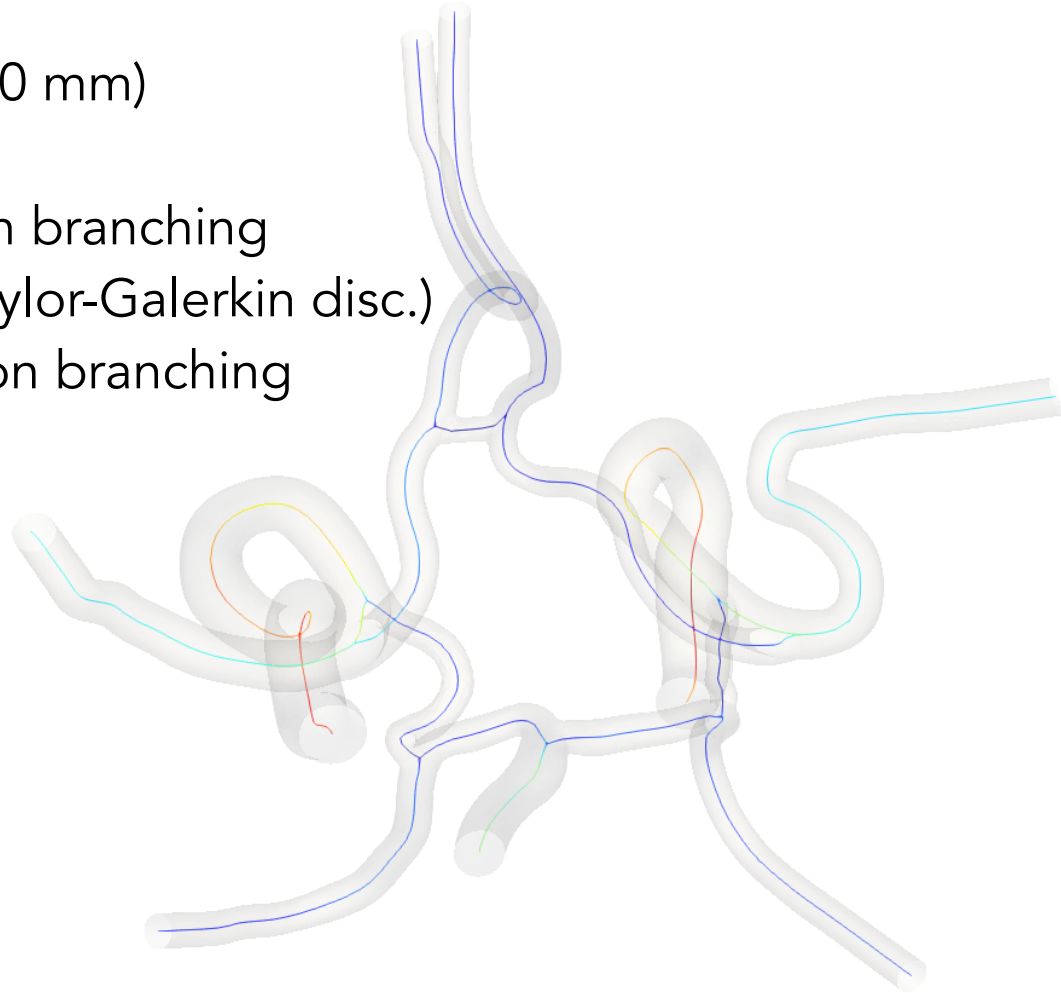

Output:

- blood flowrate in different perfusion regions: suitable input for MPE

[Formaggia, Quarteroni, Veneziani, 2009; Müller, Toro 2014, Figueroa 2020, Di Gregorio et al. 2021]

5 - Mathematical and numerical modelling of epileptic seizures

05

Pathophysilogical context - Epilepsy

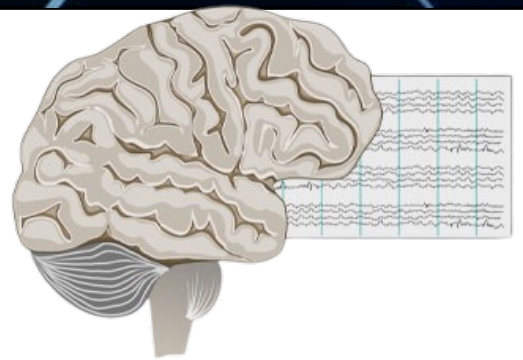

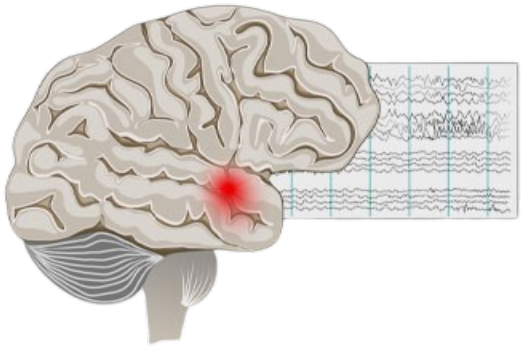

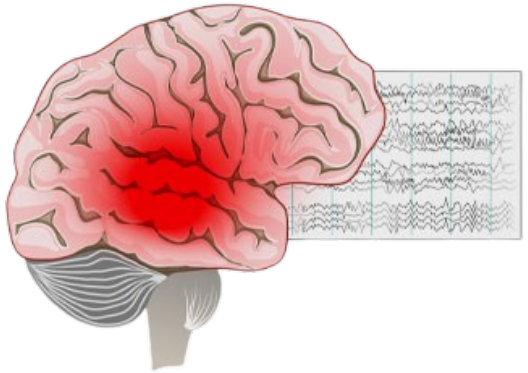

Epilepsy

Repetition of sudden, excessive, and synchronous discharges in cortical neurons of the brain.

Epilepsy is the most common chronic brain disease and affects people of all ages. More than **65 million people** worldwide have epilepsy.

Single condition

Other conditions: cerebral palsy, intellectual disability, autism, Alzheimer's disease, and traumatic brain injury

Aim of the research

Present an **accurate and high-order** computational framework for modeling pathological epileptic events.

In-silico analisy of mechanism of seizures and study of possible treatments

Treatments for epilepsy

Anti-epileptic drugs stimulation

Act on ionic conductances in order to control the ion unbalance inside the cell membrane

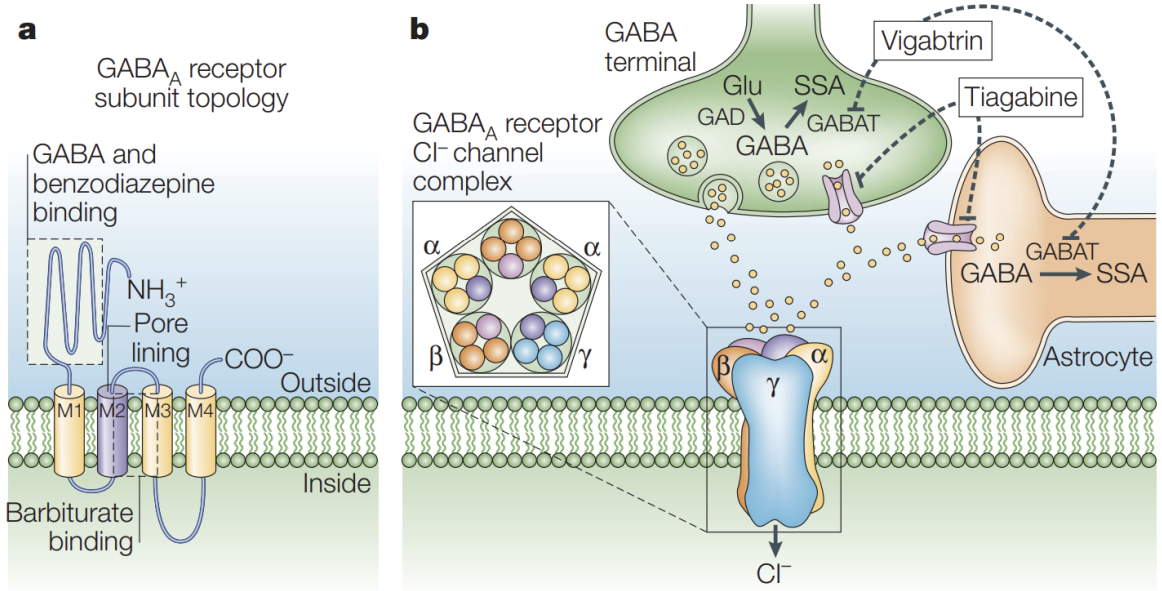

Deep Brain Stimulation

Release of electrical stimuli via internal electrostimulators governed by pulse generator

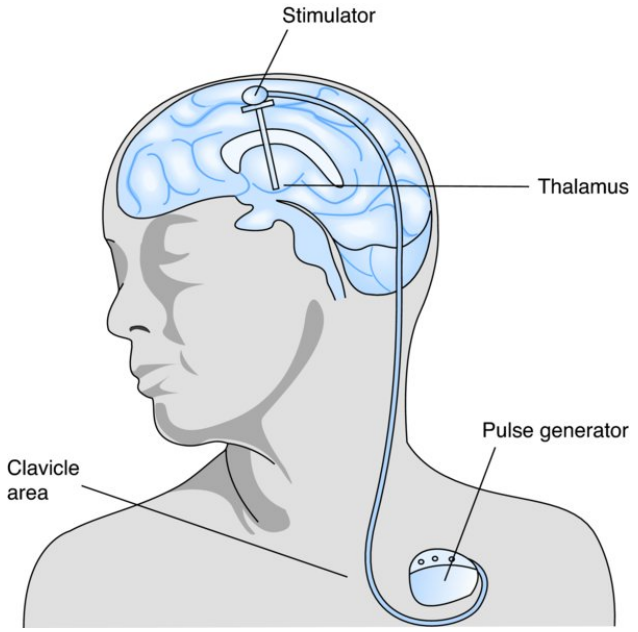

Rogawski MA, Löscher W. *The neurobiology of antiepileptic drugs*. Nat Rev Neurosci. 2004 Jul;5(7):553-64. doi: 10.1038/nrn1430. PMID: 15208697.

Anti-epileptic drugs simulation

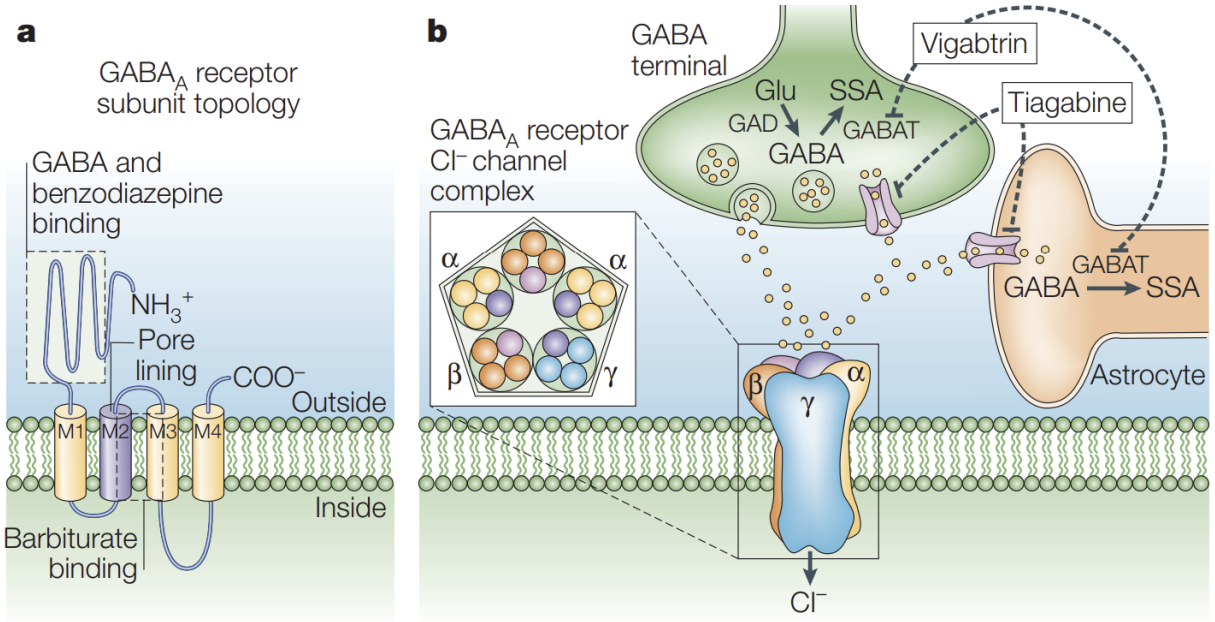

Act on ionic conductances in order to control the ion unbalance inside the cell membrane

$$
\begin{cases}
C_m \dfrac{dV_m}{dt} = -(I_{\mathrm{Cl}} + I_{\mathrm{Na}} + I_{\mathrm{K}}), \\
\dfrac{d[Ca]_i}{dt} = -\dfrac{[Ca]_i}{80} - G_{\mathrm{Ca}} \dfrac{0.002(V_m - E_{\mathrm{Ca}})}{1 + \exp\left(-\frac{25+V_m}{2.5}\right)}, \\
\dfrac{d[K]_0}{dt} = -\dfrac{1}{\tau}\left(I_{\mathrm{diff}} + 14 I_{\mathrm{pump}} + I_{\mathrm{glia}} - 7\gamma I_{\mathrm{K}}\right), \\
\dfrac{d[Na]_i}{dt} = -\dfrac{1}{\tau}\left(\gamma I_{\mathrm{Na}} + 3 I_{\mathrm{pump}}\right), \\
\dfrac{d\boldsymbol{y}}{dt} = 3\dfrac{y_\infty - \boldsymbol{y}}{\tau_y}.
\end{cases}
$$

$$
I_{\mathrm{Na}} = \left(G_{\mathrm{NaL}} + G_{\mathrm{Na}} m^3 h\right)(V_m - E_{\mathrm{Na}})
$$

Mathematical challenges

Multiphysics

Interaction between different tissues

- White/grey matter
- Cerebrospinal fluid (CSF)
- Skull

Coexistence of different processes

- Electrical signal excange
- Oxygen supply
- Waste clearance

Multiscale

Different dimensional scales

- Membrane scale
- Neuronal scale
- Tissue scale
- Brain scale

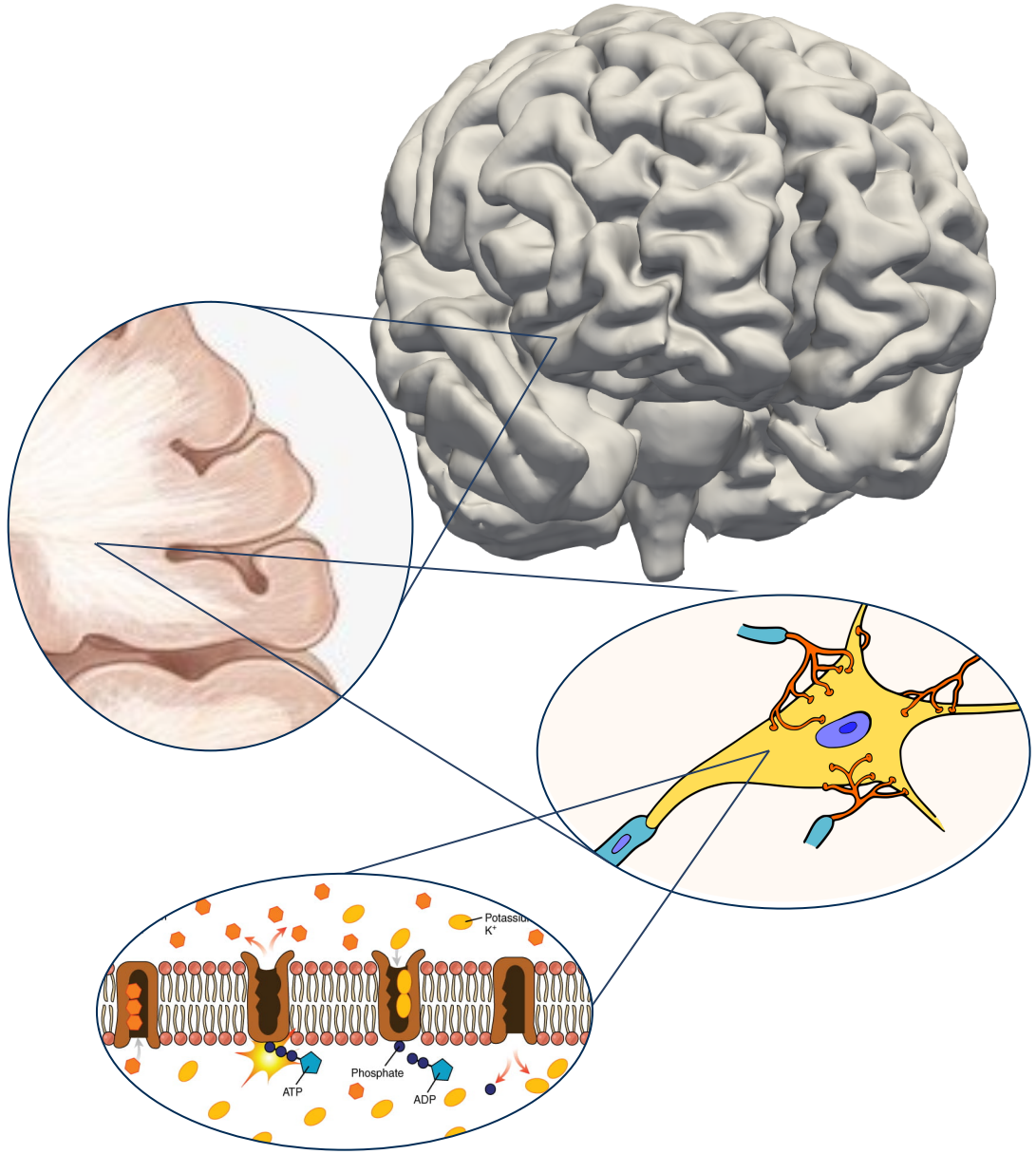

Mathematical challenges

Multiphysics

Interaction between different tissues

- White/grey matter
- Cerebrospinal fluid (CSF)
- Skull

Coexistence of different processes

- Electrical signal excange
- Oxygen supply
- Waste clearance

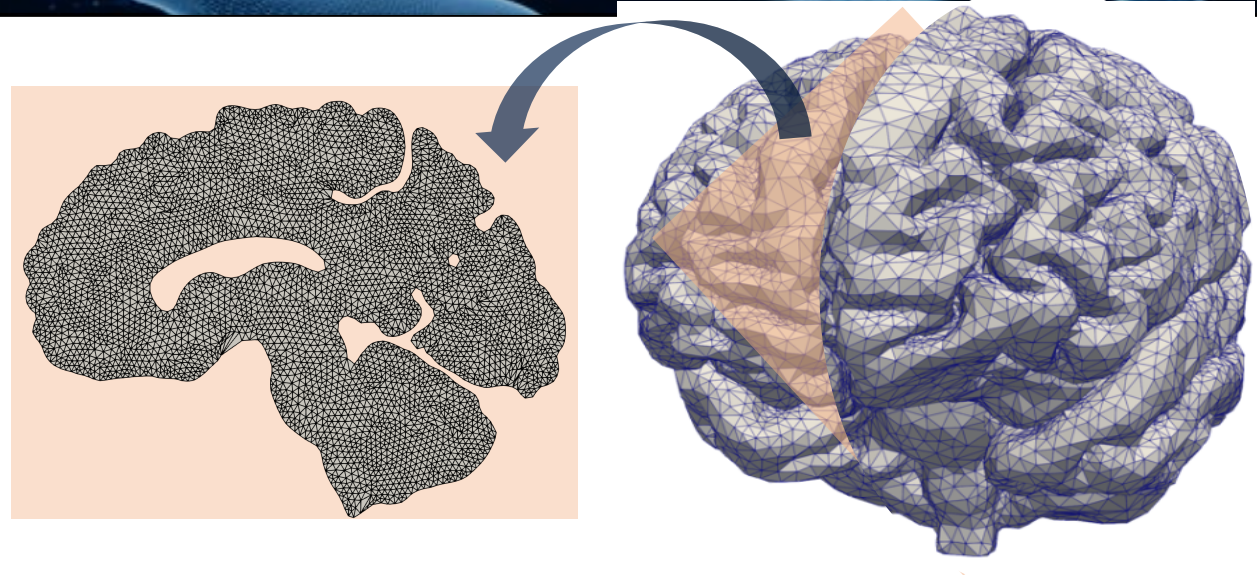

Multiscale

Different dimensional scales

- Membrane scale
- Neuronal scale
- Tissue scale
- Brain scale

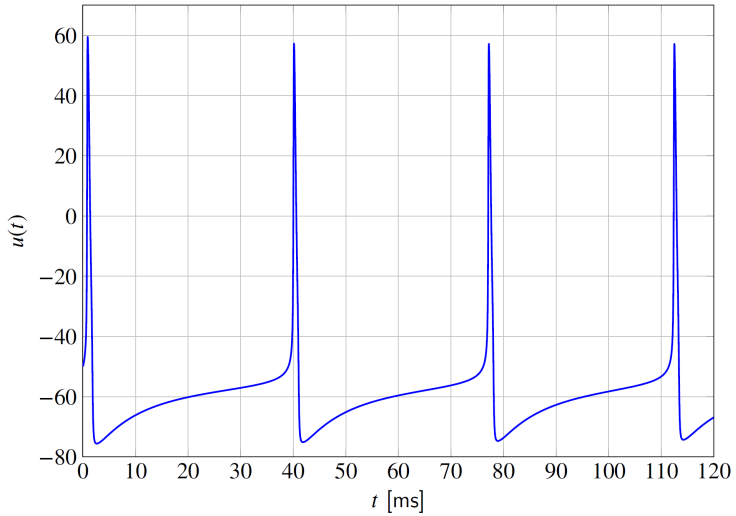

Computational challenges

Accuracy

- Extremely steep wavefronts
- Complex geometries

Mathematical challenges

Multiphysics

Interaction between different tissues

- White/grey matter
- Cerebrospinal fluid (CSF)
- Skull

Coexistence of different processes

- Electrical signal excange
- Oxygen supply
- Waste clearance

Multiscale

Different dimensional scales

- Membrane scale
- Neuronal scale
- Tissue scale
- Brain scale

Numerical level

Accuracy

- Extremely steep wavefronts
- Complex geometries

PolyDG solver

Discontinuous Galerkin finite element method on polytopal agglomerated meshes.

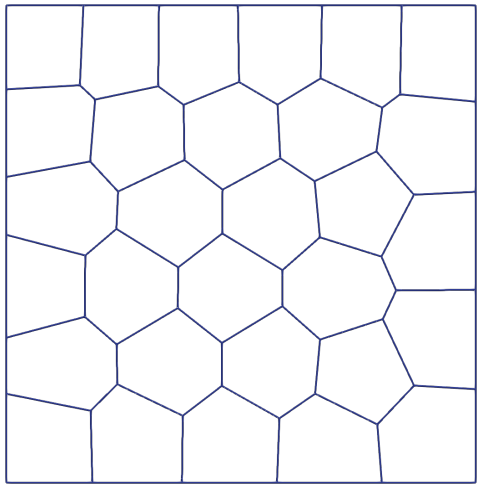

Literature review

Neuronal models

Hodgkin AL, Huxley AF (August 1952). "A quantitative description of membrane current and its application to conduction and excitation in nerve".

Mean-Field Models

Wilson, H.R.; Cowan, J.D. (1972). "Excitatory and inhibitory interactions in localized populations of model neurons". *Biophys. J.* 12 (1): 1–24

Single neuron

Cressman JR Jr, Ullah G, Ziburkus J, Schiff SJ, **Barreto E**. The influence of sodium and potassium dynamics on excitability, seizures, and the stability of persistent states: I. Single neuron dynamics. J Comput Neurosci. 2009 Apr;26(2):159-70.

Tissue models

Bidomain/Monodomain model :

- **O. H. Schmitt**, Information processing in the nervous system; proceedings of a symposium held at the State University of New York at Buffalo, 21st-24th October, 1968
- Electrical properties of anisotropic nerve-muscle syncytia-I. Distribution of the electrotonic potential., in Biofizika, vol. 22, n. 2, 1977
- Tung L, A bi-domain model for describing ischemic myocardial d-c potentials., in PHD Dissertation, MIT, Cambridge, Mass., 1978.

The monodomain model

The monodomain model allows us to define different tissues inside the brain and consider axonal directions.

$$\begin{cases} \chi_m C_m \frac{\partial u}{\partial t} - \nabla \cdot (\boldsymbol{\Sigma} \nabla u) + f(u, \boldsymbol{y}) = I^{\text{ext}} & \text{in } \Omega \times (0, T], \\ \frac{\partial \boldsymbol{y}}{\partial t} + \boldsymbol{m}(u, \boldsymbol{y}) = \mathbf{0} & \text{in } \Omega \times (0, T], \\ \boldsymbol{\Sigma} \nabla u \cdot \boldsymbol{n} = 0 & \text{on } \partial\Omega \times (0, T], \\ u(0) = u^0, \ \boldsymbol{y}(0) = \boldsymbol{y}^0 & \text{in } \Omega. \end{cases}$$

Variables:

$u = V_m(\boldsymbol{x}, t)$ ⟶ Transmembrane potential

$\boldsymbol{y}(\boldsymbol{x}, t) = [c,\ k,\ s,\ m,\ n,\ h]^\top$

$$f(u, \boldsymbol{y}) = I_{\text{ion}}(u, \boldsymbol{y}) = I_{\text{Na}}(u, \boldsymbol{y}) + I_{\text{K}}(u, \boldsymbol{y}) + I_{\text{Cl}}(u, \boldsymbol{y})$$

$$\boldsymbol{m}(u, \boldsymbol{y}) = \begin{bmatrix} \frac{c}{80} + \text{G}_{\text{Ca}} \frac{0.002(u - \text{E}_{\text{Ca}})}{1 + \exp\left(-\frac{25+u}{2.5}\right)} \\ \frac{1}{\tau}\left(I_{\text{diff}} - 14 I_{\text{pump}} - I_{\text{glia}} + 7\gamma I_{\text{K}}\right) \\ \frac{1}{\tau}\left(\gamma I_{\text{Na}} - 3 I_{\text{pump}}\right) \\ 3\frac{\boldsymbol{g} - \boldsymbol{g}_\infty}{\tau_g} \end{bmatrix}$$

$$\left.\begin{aligned} c &= [Ca]_i(\boldsymbol{x}, t) \\ k &= [K]_o(\boldsymbol{x}, t) \\ s &= [Na]_i(\boldsymbol{x}, t) \end{aligned}\right\} \text{Ion concentrations}$$

$$\boldsymbol{g} = \begin{bmatrix} m(\boldsymbol{x}, t) \\ n(\boldsymbol{x}, t) \\ h(\boldsymbol{x}, t) \end{bmatrix} \longrightarrow \text{Gating variables}$$

Cressman, John R., et al. *Journal of computational neuroscience* (2009)

Barreto-Cressman ionic model

Assumption 1 : The quantity of sodium within the system remains constant

$$[Na]_0 = 144mM - 7([Na]_i - 18mM),$$

Assumption 2 : A correlation subsists between the transport of sodium and that of potassium across the transmembrane space

$$[K]_i = 140mM + (18mM - [Na]_i).$$

The reversal potential can be defined via the Nerst equation:

$$E_{\mathrm{Ca}} = 120mV \qquad E_{\mathrm{Na}} = 26.64 \log\left(\frac{270 - [Na]_i}{[Na]_i}\right),$$

$$E_{\mathrm{K}} = 26.64 \log\left(\frac{[K]_0}{158 - [Na]_i}\right), \qquad E_{\mathrm{Cl}} = 26.64 \log\left(\frac{[Cl]_i}{[Cl]_0}\right),$$

Barreto-Cressman ionic model

Equivalent circuit for the Barreto-Cressman ionic model

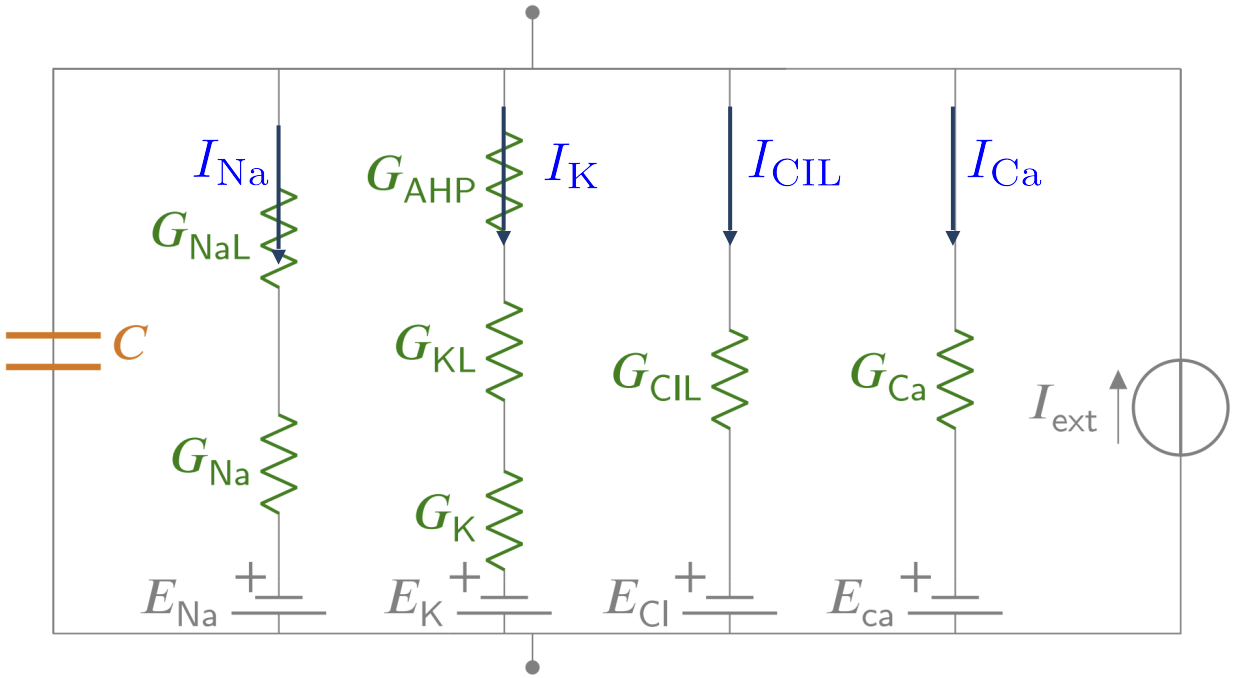

Principal ionic currents:

- Sodium channels depolarize nerve cell membranes.
- Calcium channels enhance overall neuronal excitability.
- Potassium channels restore resting potential post-action potential, regulating input-output balance in neurons.

$$I_{\mathrm{Na}} = \left(G_{\mathrm{NaL}} + G_{\mathrm{Na}} m^3 h\right)(V_m - E_{\mathrm{Na}}),$$

$$I_{\mathrm{K}} = \left(G_{\mathrm{K}} n^4 + G_{\mathrm{AHP}} \frac{[\mathrm{Ca}]_i}{1 + [\mathrm{Ca}]_i} + G_{\mathrm{KL}}\right)(V_m - E_{\mathrm{K}}),$$

$$I_{\mathrm{Cl}} = G_{\mathrm{CIL}}(V_m - E_{\mathrm{Cl}}).$$

Barreto-Cressman ionic model

The currents related to the ability of cells to remove excess potassium from the extracellular space (I_{glia}), the current representing potassium diffusion (I_{pump}) and the current that denotes the sodium-potassium pump (I_{diff})

$$I_{\text{pump}} = \frac{\rho}{1+\exp(5.5-[K]_o)}\left(\frac{1}{1+\exp(\frac{25-[Na]_i}{3})}\right),$$

$$I_{\text{Glia}} = \frac{G_{\text{glia}}}{1+\exp(\frac{18-[K]_o}{2.5})}, \quad I_{\text{diff}} = \epsilon([K]_0 - K_{\text{bath}})$$

$$\tau_y(u) = \frac{1}{a_y(u)+b_y(u)},$$

$$y_\infty(u) = \frac{a_y(u)}{a_y(u)+b_y(u)}$$

Supporting *rate equations* for the gating variables:

$$a_m = \frac{0.1(V_m+30)}{1-\exp(-0.1(V_m+30))}, \qquad b_m = 4\exp\left(-\frac{V_m+55}{18}\right),$$

$$a_h = 0.07\exp\left(-0.2(V_m+44)\right), \qquad b_h = \frac{1}{1+\exp(-0.1(V_m+14))},$$

$$a_n = \frac{0.01(V_m+34)}{1-\exp(-0.1(V_m+34))}, \qquad b_n = \frac{1}{8}\exp\left(-\frac{V_m+44}{80}\right).$$

The model

Find $V_m = \phi_i - \phi_e, [Ca]_i, [K]_0, [Na]_i, \boldsymbol{y}$ s.t. :

$$
\begin{cases}
C_m \dfrac{dV_m}{dt} = -(I_{\mathrm{Cl}} + I_{\mathrm{Na}} + I_{\mathrm{K}}), & \text{in } \Omega \times (0,T] \\
\dfrac{d[Ca]_i}{dt} = -\dfrac{[Ca]_i}{80} - G_{\mathrm{Ca}} \dfrac{0.002(V_m - E_{\mathrm{Ca}})}{1 + \exp\left(-\frac{25+V_m}{2.5}\right)}, & \text{in } \Omega \times (0,T] \\
\dfrac{d[K]_0}{dt} = -\dfrac{1}{\tau}\left(I_{\mathrm{diff}} + 14 I_{\mathrm{pump}} + I_{\mathrm{glia}} - 7\gamma I_{\mathrm{K}}\right), & \text{in } \Omega \times (0,T] \\
\dfrac{d[Na]_i}{dt} = -\dfrac{1}{\tau}\left(\gamma I_{\mathrm{Na}} + 3 I_{\mathrm{pump}}\right), & \text{in } \Omega \times (0,T] \\
\dfrac{d\boldsymbol{y}}{dt} = 3\dfrac{y_\infty - \boldsymbol{y}}{\tau_y} & \text{in } \Omega \times (0,T] \\
V_m(0) = V_m^0,\ \boldsymbol{g}(0) = \boldsymbol{g}^0,\ \boldsymbol{y}(0) = \boldsymbol{y}^0, & \text{in } \Omega
\end{cases}
$$

Where $\boldsymbol{g} = ([Ca]_i, [K]_0, [Na]_i)$ and $\boldsymbol{y} = (m, n, h)$ defines the gating variables.

J. Cressman, G. Ullah, J. Ziburkus, S. Schiff, and E. Barreto. The influence of sodium and potassium dynamics on excitability, seizure, and the stability of persistent states:i. single neuron dynamics. Journal of computational neuroscience, 26:159–70, 02 2009.

Numerical discretization

Identify steep wavefronts accurately and allows the **high-order approximation**

Allow for adaptivity in space and with respect to the polynomial order

Allow for dealing with **complex geometries** such as those related to the brain

PolyDG framework

Let us define $\mathbb{P}_p(K)$ as the space of polynomials of total degree $p \geq 1$ over a mesh element K.

Then we can introduce the following discontinuous finite element space:

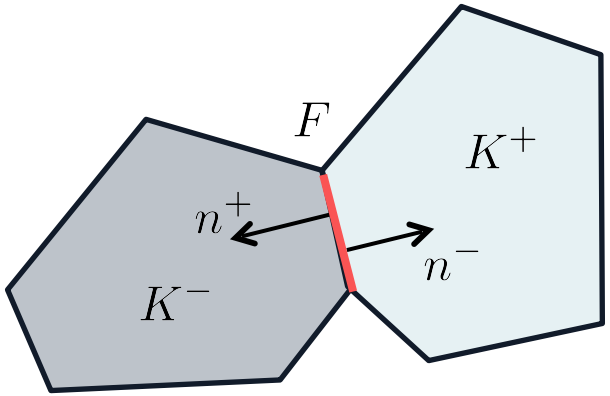

$$V_h^{\mathrm{DG}} = \{w \in L^2(\Omega) : w|_K \in \mathbb{P}_p(K)\ \forall K \in \mathcal{T}_h\}.$$

We define the trace operators as before

Semidiscrete PolyDG formulation

Find $u(t) \in V, \boldsymbol{y}(t) \in V^n$ such that $\forall\, t \in (0,T]$:

$$\begin{cases} \chi_m C_m \left(\dfrac{\partial u_h(t)}{\partial t}, v_h \right)_\Omega + \mathcal{A}(u_h(t), v_h) + \chi_{\mathrm{m}} r_{\mathrm{ion}}(u_h(t), v_h) = (I^{\mathrm{ext}}, v_h)_\Omega & \forall\, v \in V_h^{DG}, \\ \left(\dfrac{\partial \boldsymbol{y}_h(t)}{\partial t}, \boldsymbol{w}_h \right)_\Omega + r_{\mathrm{m}}(u_h(t), \boldsymbol{y}_h(t), \boldsymbol{w}_h) = 0 & \forall\, \boldsymbol{w}_h \in (V_h^{DG})^n, \\ u_h(0) = u_h^0,\ \boldsymbol{y}_h(0) = \boldsymbol{y}_h^0 & \text{in } \Omega. \end{cases}$$

where:

$$\mathcal{A}(u,v) = \int_\Omega \boldsymbol{\Sigma} \nabla_h u \cdot \nabla_h v \, dx + \sum_{F \in \mathcal{F}_h^I} \int_F (\eta [\![u]\!] \cdot [\![v]\!] - \{\!\{\boldsymbol{\Sigma} \nabla u\}\!\} \cdot [\![v]\!] - [\![u]\!] \cdot \{\!\{\boldsymbol{\Sigma} \nabla v\}\!\}) d\sigma \quad \forall\, u, v \in V_h^{\mathrm{DG}},$$

$$r_{\mathrm{ion}}(u, \boldsymbol{y}, v) = (f(u, \boldsymbol{y}), v)_\Omega \quad \forall\, v \in V$$

$$r_{\mathrm{m}}(u, \boldsymbol{y}, \boldsymbol{w}) = (\boldsymbol{m}(u, \boldsymbol{y}), \boldsymbol{w})_\Omega \quad \forall\, \boldsymbol{w} \in V^n$$

Theoretical analysis (for a simplified problem)

Simplified problem

$$\begin{cases} \chi_m C_m \frac{\partial u}{\partial t} - \nabla \cdot (\boldsymbol{\Sigma} \nabla u) + f(u) = I^{\text{ext}} & \text{in } \Omega \times (0, T], \\ \boldsymbol{\Sigma} \nabla u \cdot \boldsymbol{n} = 0 & \text{on } \partial\Omega \times (0, T], \\ u(0) = u^0 \end{cases}$$

$$f(u) = a(u - V_{\text{rest}})(u - V_{\text{thres}})(u - V_{\text{depol}})$$

$$u_{\text{ex}}(\boldsymbol{x}, t) = \frac{V_{\text{dep}} - V_{\text{rest}}}{2} \left[1 - \tanh\left(\frac{\boldsymbol{x} - \boldsymbol{c}t}{\epsilon} \right) \right] + V_{\text{rest}},$$

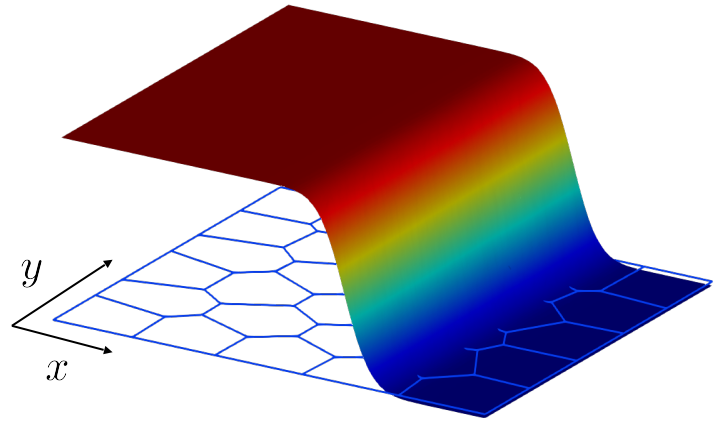

Semidiscrete PolyDG formulation

Find $u(t) \in V,\ \boldsymbol{y}(t) \in V^n$ such that $\forall\, t \in (0, T]$:

$$\begin{cases} \chi_m C_m \left(\frac{\partial u_h(t)}{\partial t}, v_h \right)_\Omega + \mathcal{A}(u_h(t), v_h) + \chi_m r_{\text{ion}}(u_h(t), v_h) = 0 & \forall\, v_h \in V_h^{\text{DG}}, \\ u_h(0) = u^0 & \text{in } \Omega. \end{cases}$$

lymph

Stability error estimate

Let us introduce the Sobolev spaces for $r \geq 1$: $H^r(\mathcal{T}_h) = \{v_h \in L^2(\Omega) : v_h|_K \in H^r(K)\ \forall K \in \mathcal{T}_h\}$.
Let us define the energy norm $\|\cdot\|_\epsilon : H^1(\mathcal{T}_h) \to \mathbb{R}$ is defined as:

$$\|v\|_\epsilon^2 = \|v\|^2 + \int_0^t \frac{2\mu}{C_m \chi_m} \|v\|_{\mathrm{DG}}^2 \mathrm{d}s + \int_0^t \frac{a}{C_m} \|v\|_{L^4(\Omega)}^4 \mathrm{d}s \quad \forall v \in H^1(\mathcal{T}_h),$$

Theorem: (stability error estimate)

Under suitable assumptions on the mesh regularity.
Let u_h be the solution of the semi-discrete problem for any $t \in (0,T]$. Let the stability parameter be large enough.
Then

$$\|u_h(t)\|_\epsilon^2 \lesssim \|u_h(0)\|^2 + a \frac{\|\omega\|_{L^\infty(\Omega)}^2 + \|\theta\|_{L^\infty(\Omega)}^2 + \|\phi\|_{L^\infty(\Omega)}^2}{C_m} |\Omega| t$$

where

$$\phi = (V_{\mathrm{thres}} + V_{\mathrm{depol}} + V_{\mathrm{rest}}),$$
$$\theta = (V_{\mathrm{thres}} V_{\mathrm{depol}} + V_{\mathrm{depol}} V_{\mathrm{rest}} + V_{\mathrm{rest}} V_{\mathrm{thres}}),$$
$$\omega = V_{\mathrm{thres}} V_{\mathrm{depol}} V_{\mathrm{rest}},$$

A-priori error estimate

Let us introduce the following norm:

$$|||v|||_{\mathrm{DG}} = \|v\|_{\mathrm{DG}} + \|\eta^{-\frac{1}{2}} \{\!\{\boldsymbol{\Sigma} \nabla_h v\}\!\}\|_{L^2(\mathcal{F}_h^I)} \quad \forall v \in H^2(\mathcal{T}_h),$$

Theorem: *(a-priori error estimate)*

Let u be the weak solution of the problem for any $t \in [0,T]$, and let it satisfy the following additional requirements:

$$u \in C^1((0,T]; H^n(\Omega) \cap L^\infty(\Omega)), \text{ for } n \geq 2$$

Let u_h be the solution of the DG formulation for any $t \in [0,T]$. Then, the following estimate holds:

$$\begin{aligned}
|||u(t) - u_h(t)|||_\epsilon^2 \lesssim & \sum_{K \in \mathcal{T}_h} h_K^{2\min\{p+1,n\}-2} \int_0^t \left(\|\dot{u}(s)\|_{H^n(K)}^2 + \|u(s)\|_{H^n(K)}^2 \right) \mathrm{d}s \\
& + \sum_{K \in \mathcal{T}_h} h_K^{4\min\{p+1,n\}-4} \int_0^t \|u(s)\|_{H^n(K)}^4 \mathrm{d}s \\
& + \sum_{K \in \mathcal{T}_h} \left(h_K^{2\min\{p+1,n\}-2} \|u(t)\|_{H^n(K)}^2 + h_K^{4\min\{p+1,n\}-4} \|u(t)\|_{H^n(K)}^4 \right) \quad t \in (0,T]
\end{aligned}$$

where $\mu - a\,\chi_m\,(M_I\,C_{E_2} + C_S\,C_{E_4})\phi_\infty - a\,\chi_m\,C_{E_2}\theta_\infty > 0$, and C_{E_q} is the discrete Sobolev embedding constant.

Numerical results

Verification

- Heterogeneity in tissues with white/grey matter

Idealised geometry

- Heterogeneity in tissues with white/grey matter
  - Analysis of potassium influence on seizures onset

Real geometry (2D)

- Brain stem 2D section with subdivision of grey/white matter

Numerical results: verification

Parameters	Values	Unit	Parameters	Values	Unit
σ_n	0.17	$\mathrm{mS \cdot mm^{-1}}$	a	$1.4e-5$	$\mathrm{mS \cdot mm^{-2} \cdot mV^{-2}}$
σ_t	0.62	$\mathrm{mS \cdot mm^{-1}}$	χ_m	140	$\mathrm{mm^{-1}}$
V_depol	30	mV	c	0.5	$\mathrm{mm \cdot ms^{-1}}$
V_rest	-85	mV	ϵ	0.2	mm
V_thres	-57.6	mV	$\mathrm{C_m}$	0.01	$\mu\mathrm{F \cdot mm^{-2}}$

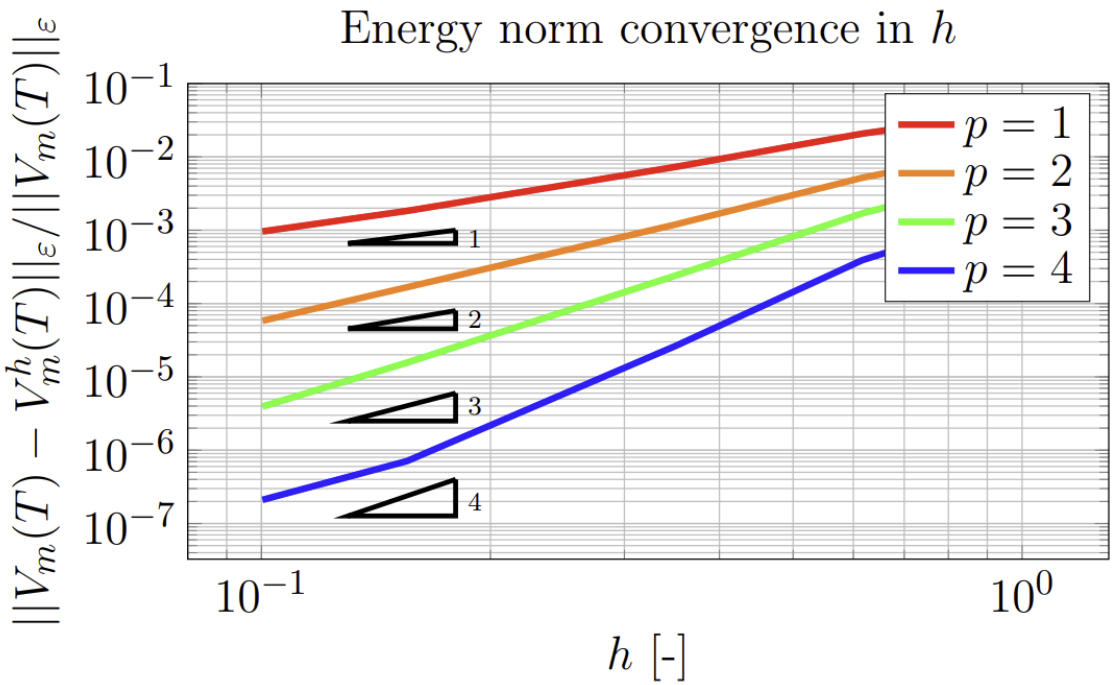

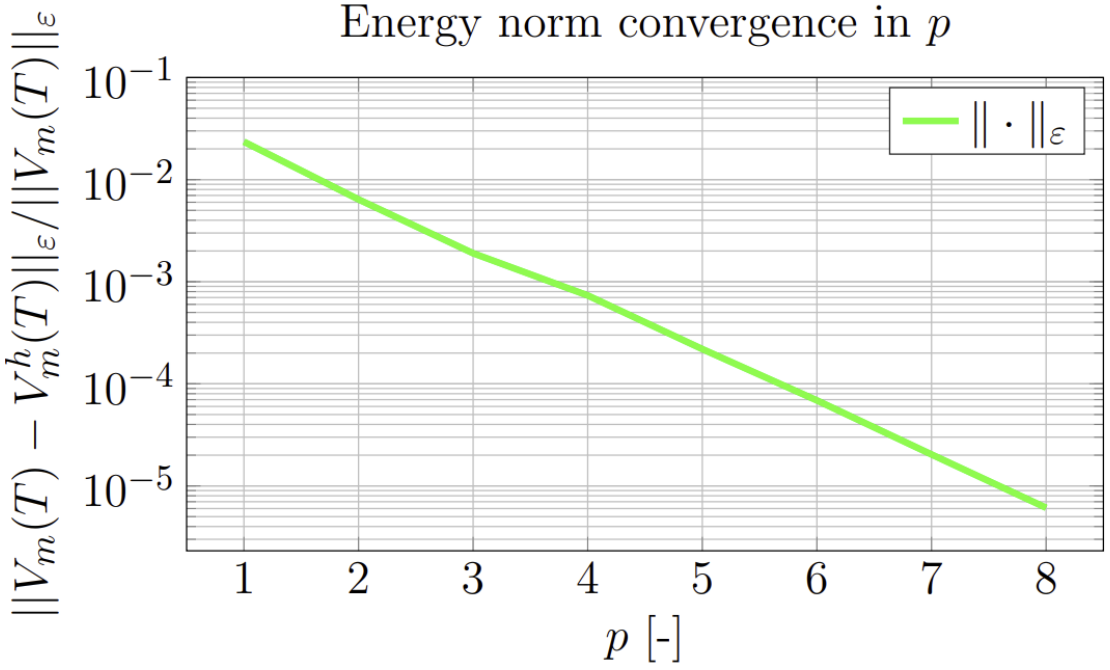

Pezzuto, Hake, Sundnes. "*International journal for numerical methods in biomedical engineering* (2016)

Numerical results

Gray-white matter tissue: evolution of the transmembrane potential in a squared section with unstable gray matter region for a general seizure simulation.

Tissue type	σ_n $[\mathrm{Sm}^{-1}]$	σ_t $[\mathrm{Sm}^{-1}]$
GM	0.0735	0.0735
HWM	0.0557	0.0139
VWM	0.0139	0.0557

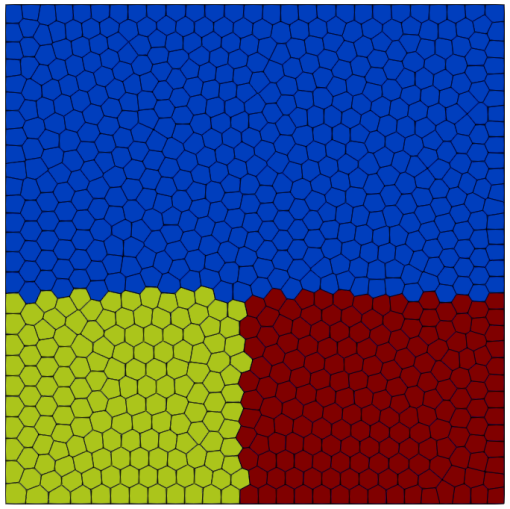

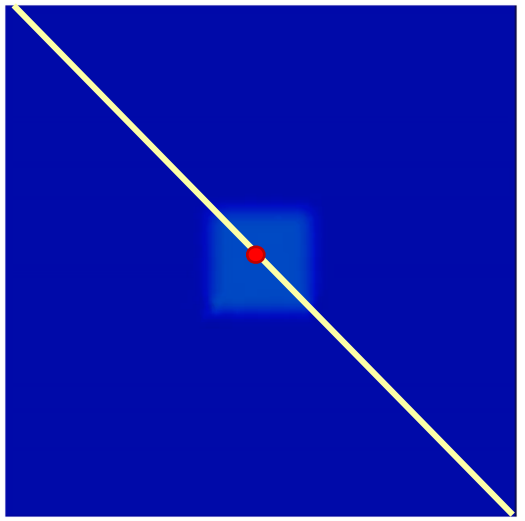

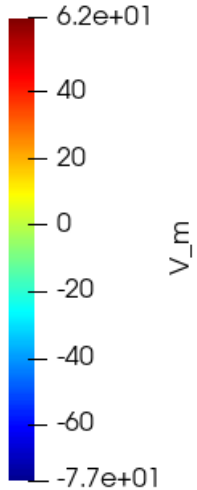

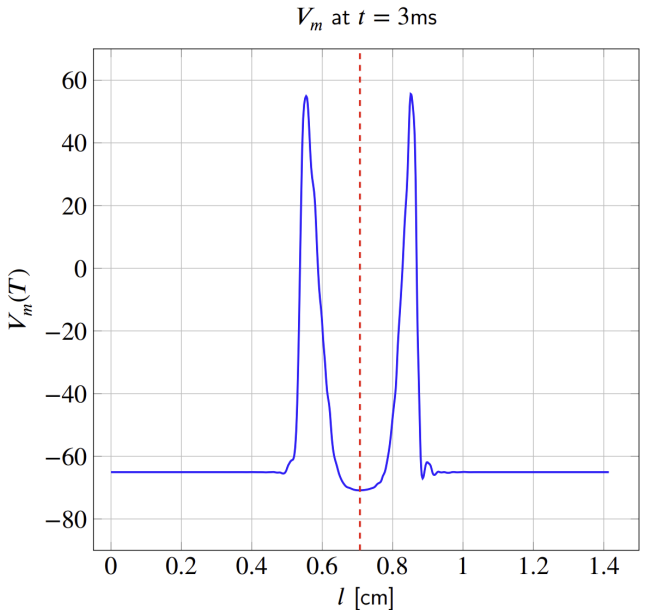

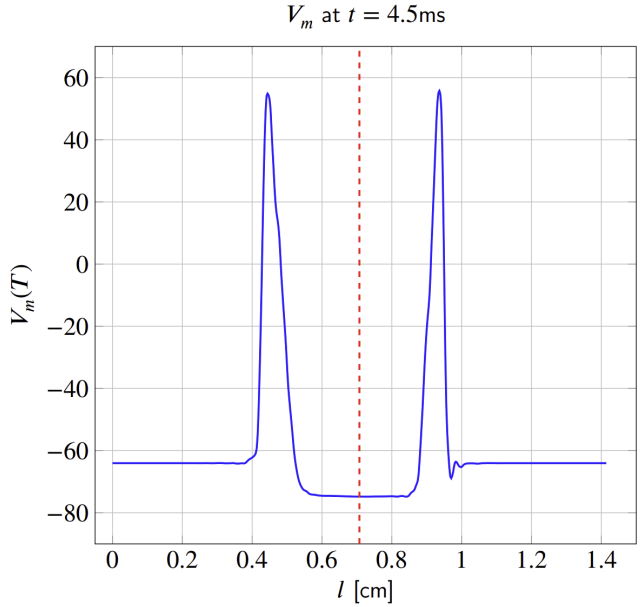

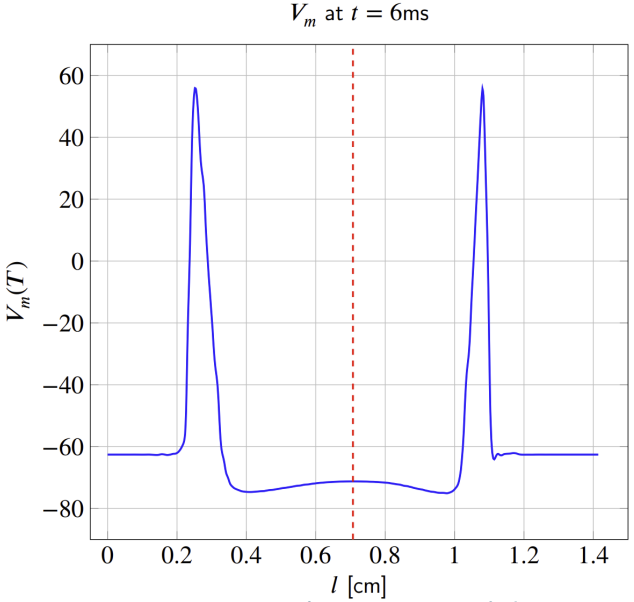

lymph

Schreiner Mardal, Scientific Reports (2022)

Numerical results

Analysis of the **conduction velocity** of the travelling wavefront:

Tissue type	σ_n $[\mathrm{Sm}^{-1}]$	σ_t $[\mathrm{Sm}^{-1}]$
GM	0.0735	0.0735

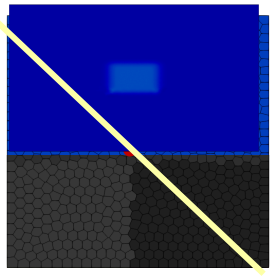

Grey matter

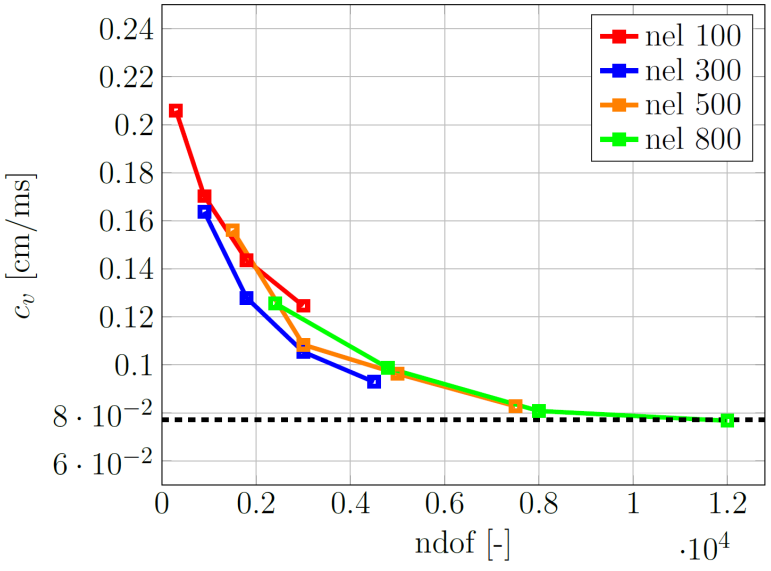

Tissue type	σ_n $[\mathrm{Sm}^{-1}]$	σ_t $[\mathrm{Sm}^{-1}]$
VWM	0.0139	0.0557

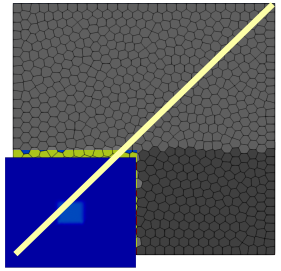

White matter with vertical anisotropy

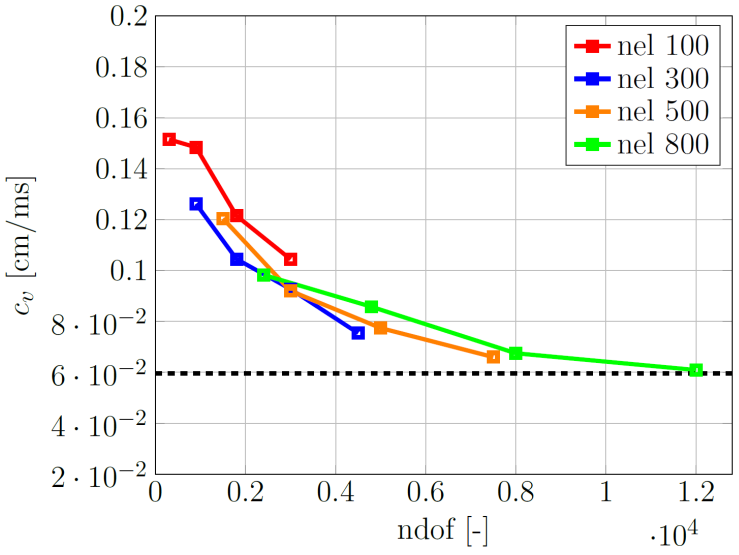

Tissue type	σ_n $[\mathrm{Sm}^{-1}]$	σ_t $[\mathrm{Sm}^{-1}]$
HWM	0.0557	0.0139

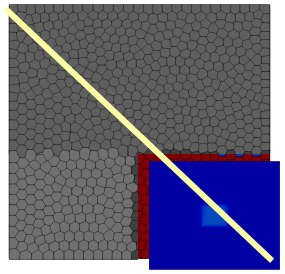

White matter with horizontal anisotropy

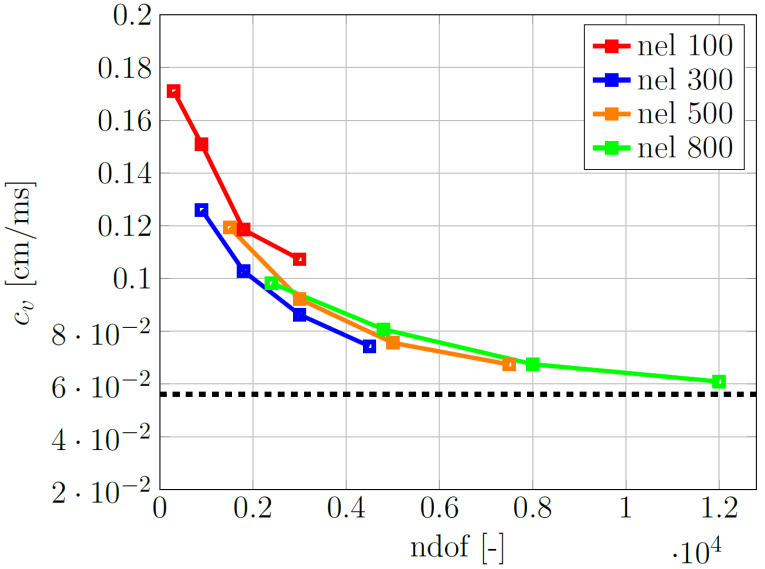

Influence of Potassium conductances

lymph

$K_{\text{bath}} = 4\text{mM}$

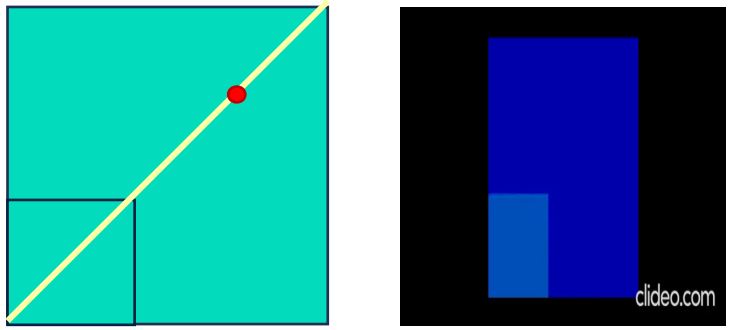

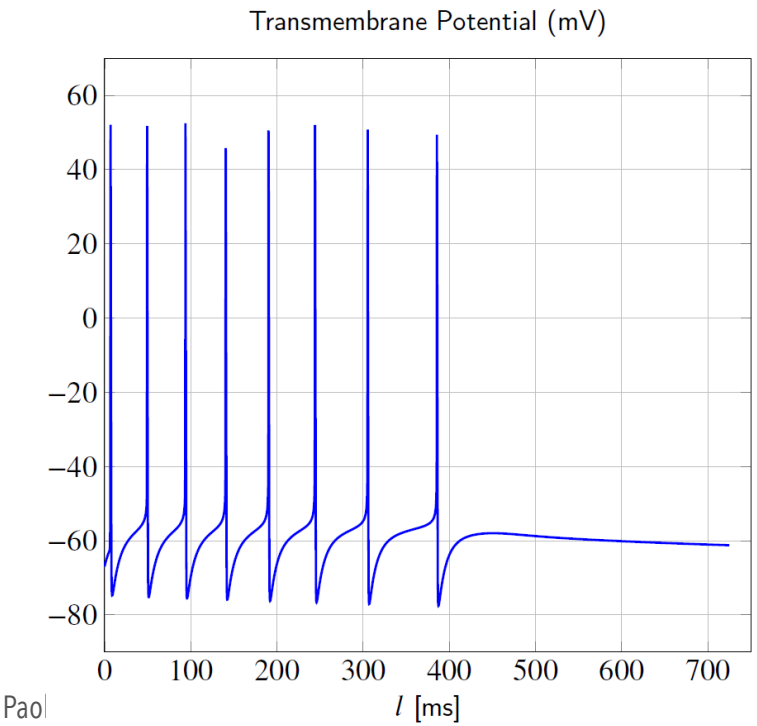

$K_{\text{bath}} = 8\text{mM}$

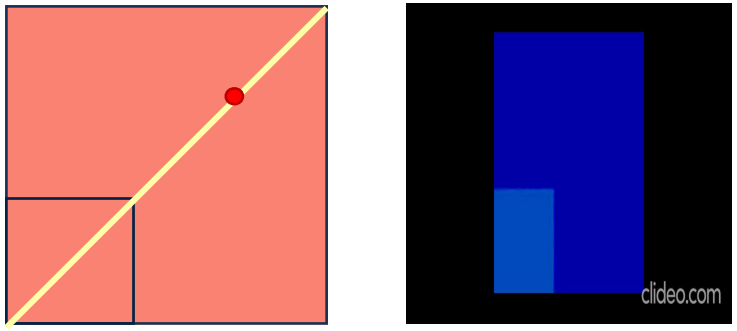

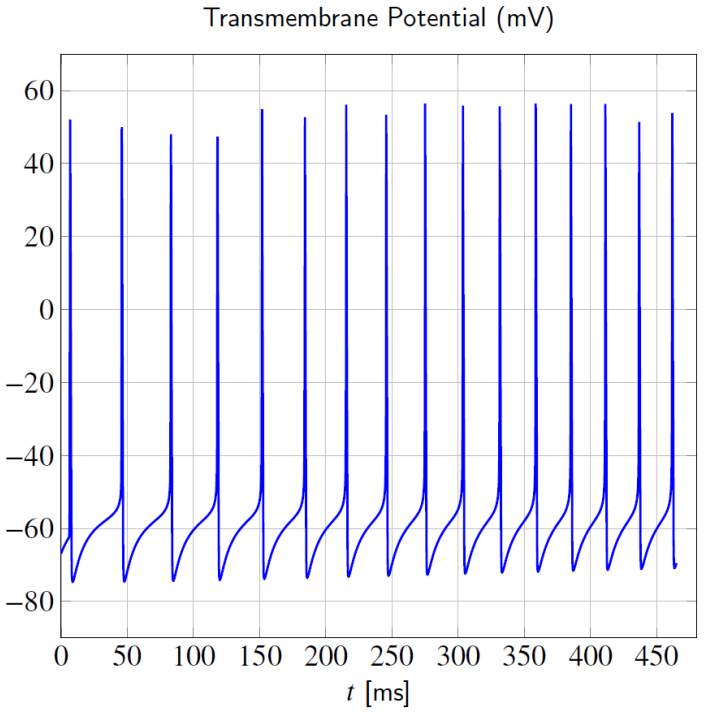

Mixed case

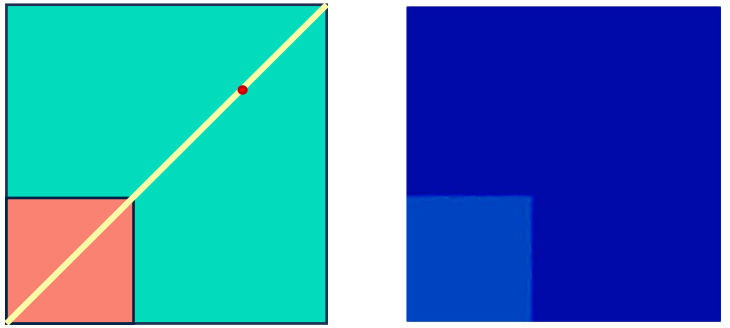

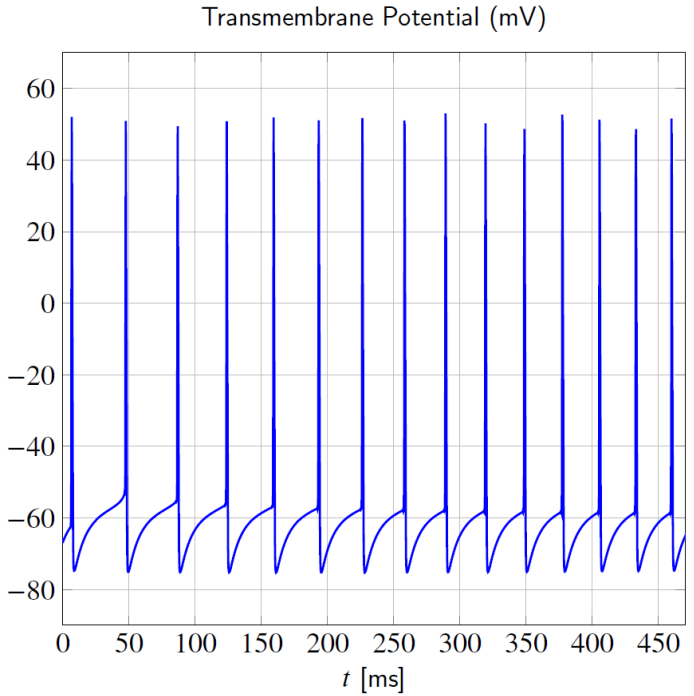

Numerical results: real geometry (2D)

Structured triangulated mesh

White-grey matter distinction

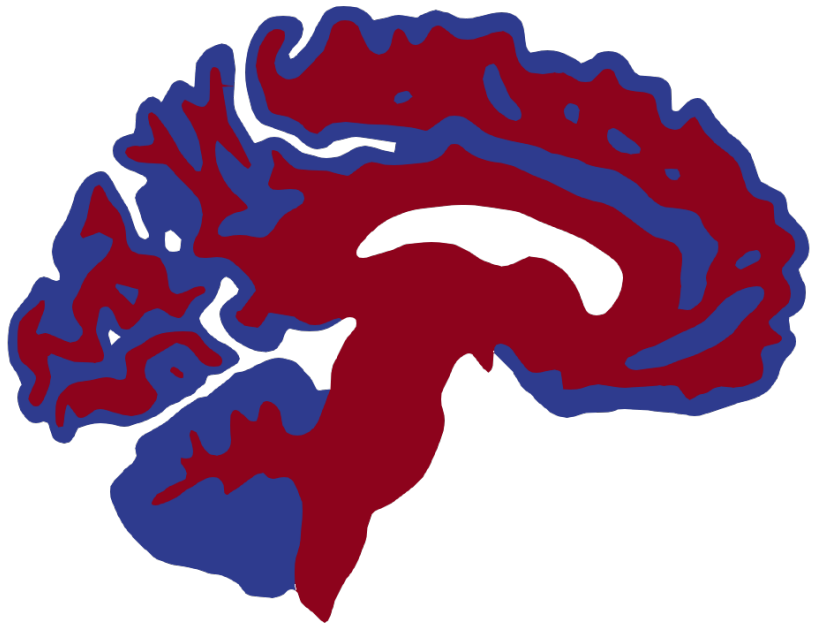

Agglomerated polytopal mesh

534 Elements

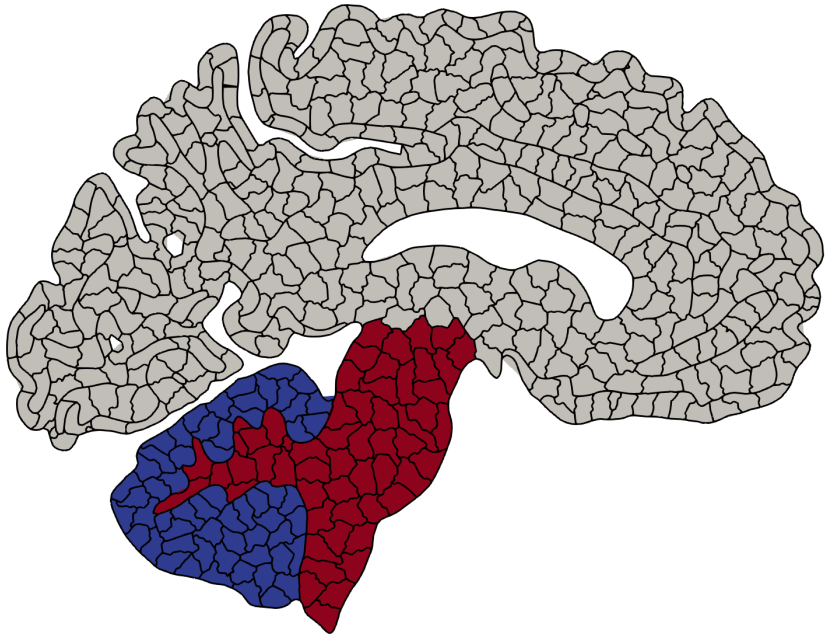

Brain stem section

3523 Elements

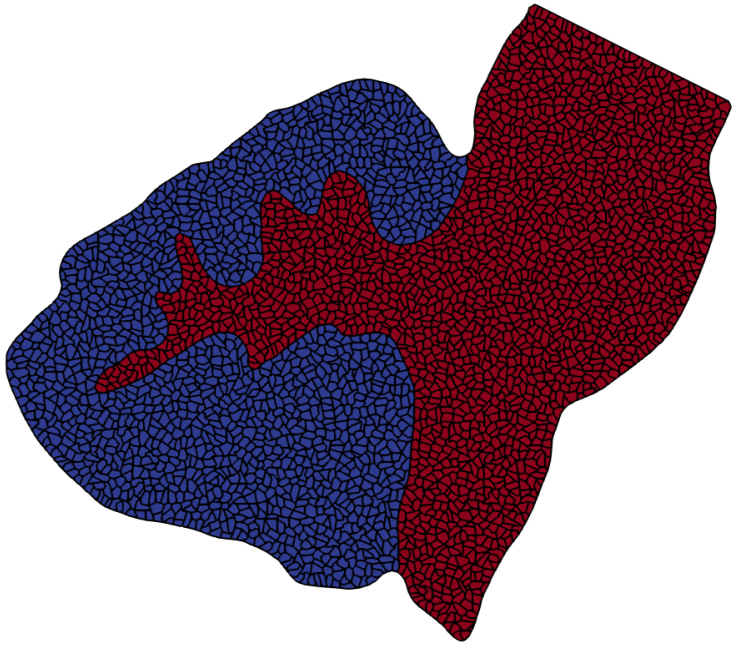

P. LaMontagne, T. Benzinger, J. Morris, S. Keefe, R. Hornbeck, C. Xiong, E. Grant, J. Hassenstab, K. Moulder, A. Vlassenko, M. Raichle, C. Cruchaga, and D Marcus. Oasis-3: Longitudinal neuroimaging, clinical, and cognitive dataset for normal aging and alzheimer disease, 12 2019.

Numerical results: real geometry (2D)

BrainStem with white-grey matter tissues: **evolution of the transmembrane potential in a brainstem section with unstable gray matter region for a general seizure simulation.**

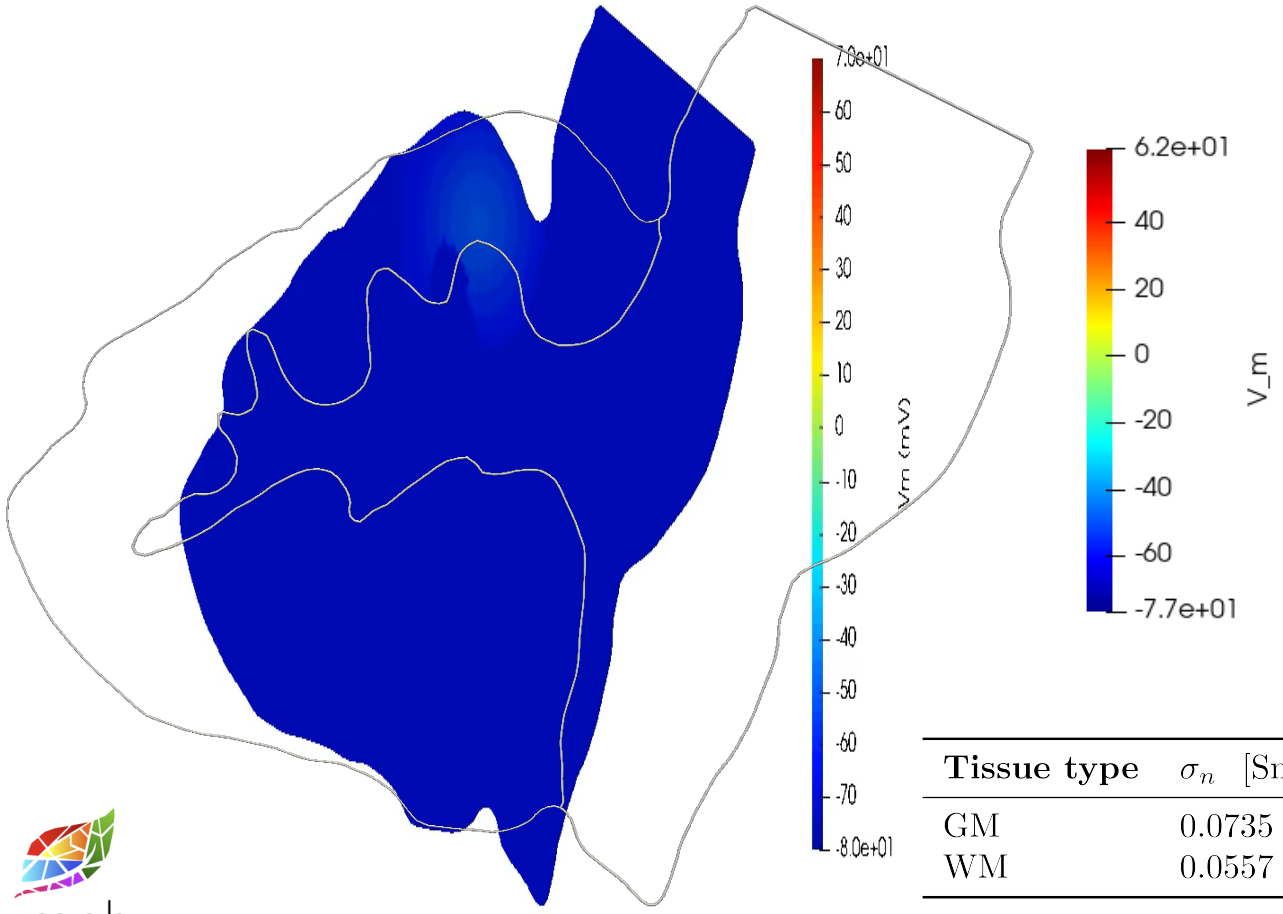

Initial condition:

$$u(0) = -67 + 17e^{-2(x-x_0)^2-2(y-y_0)^2}\chi_{\Omega_0}(x,y),$$

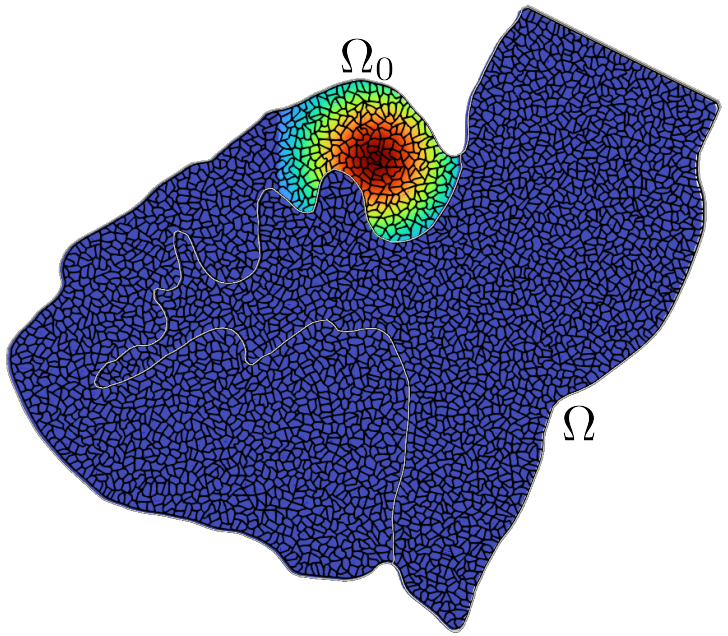

Tissue type	σ_n $[\mathrm{Sm}^{-1}]$	σ_t $[\mathrm{Sm}^{-1}]$
GM	0.0735	0.0735
WM	0.0557	0.0139

lymph

P. LaMontagne, T. Benzinger, J. Morris, S. Keefe, R. Hornbeck, C. Xiong, E. Grant, J. Hassenstab, K. Moulder, A. Vlassenko, M. Raichle, C. Cruchaga, and D Marcus. Oasis-3: Longitudinal neuroimaging, clinical, and cognitive dataset for normal aging and alzheimer disease, 12 2019.

Realistic geometry

BrainStem with white-grey matter tissues: evolution of the transmembrane potential in a brainstem section with unstable gray matter region for a general seizure simulation.

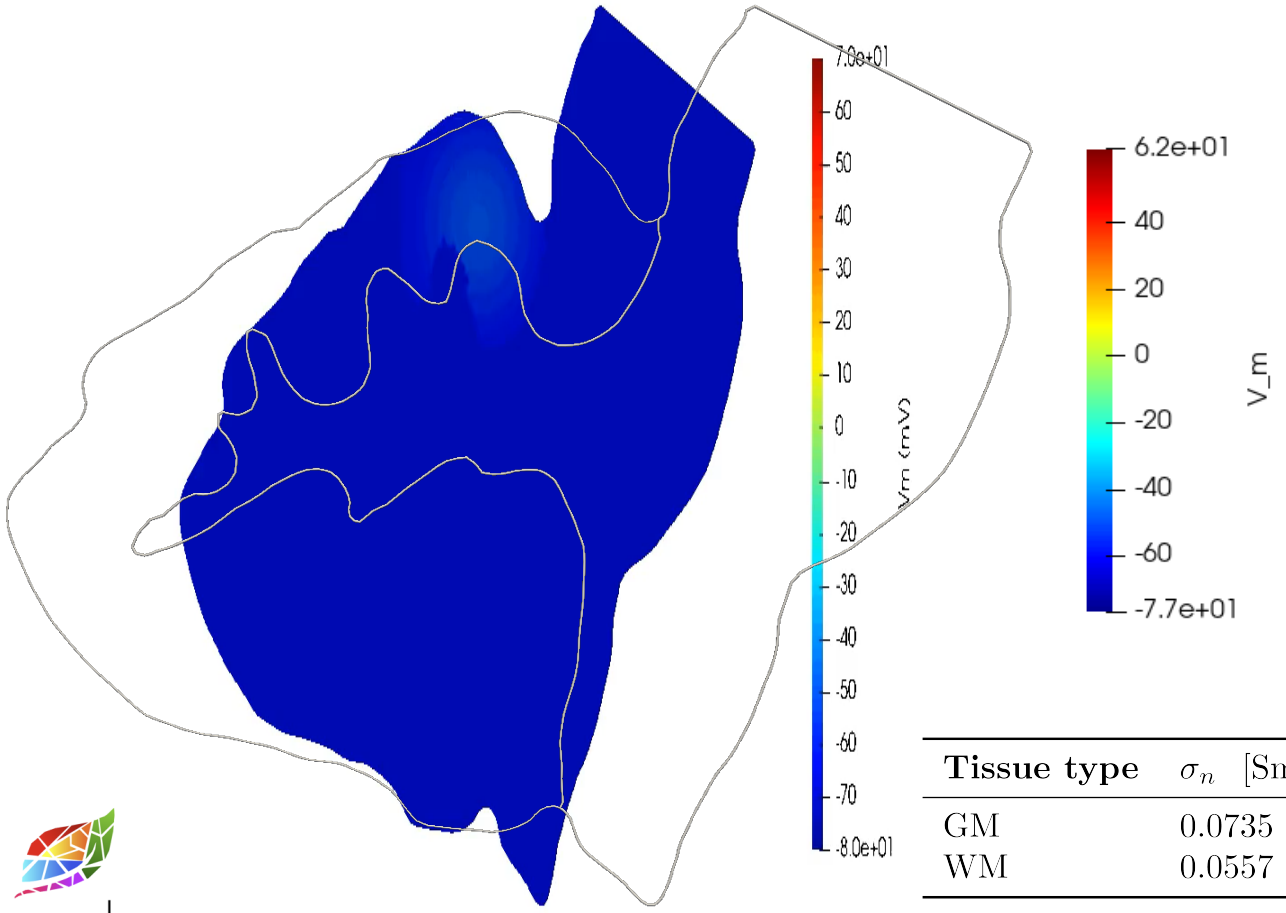

Tissue type	σ_n $[\mathrm{Sm}^{-1}]$	σ_t $[\mathrm{Sm}^{-1}]$
GM	0.0735	0.0735
WM	0.0557	0.0139

High computational costs of the simulations

High number of degrees of freedom

Adaptive PolyDG solver

lymph

P. LaMontagne, T. Benzinger, J. Morris, S. Keefe, R. Hornbeck, C. Xiong, E. Grant, J. Hassenstab, K. Moulder, A. Vlassenko, M. Raichle, C. Cruchaga, and D Marcus. Oasis-3: Longitudinal neuroimaging, clinical, and cognitive dataset for normal aging and alzheimer disease, 12 2019.

Taming complexity: adaptivity

PolyDG adaptive framework

Different methods, such as HP-adaptivity, have been proposed to overcome the complexities and reduce the cost of the simulations.

$h-$ adaptive

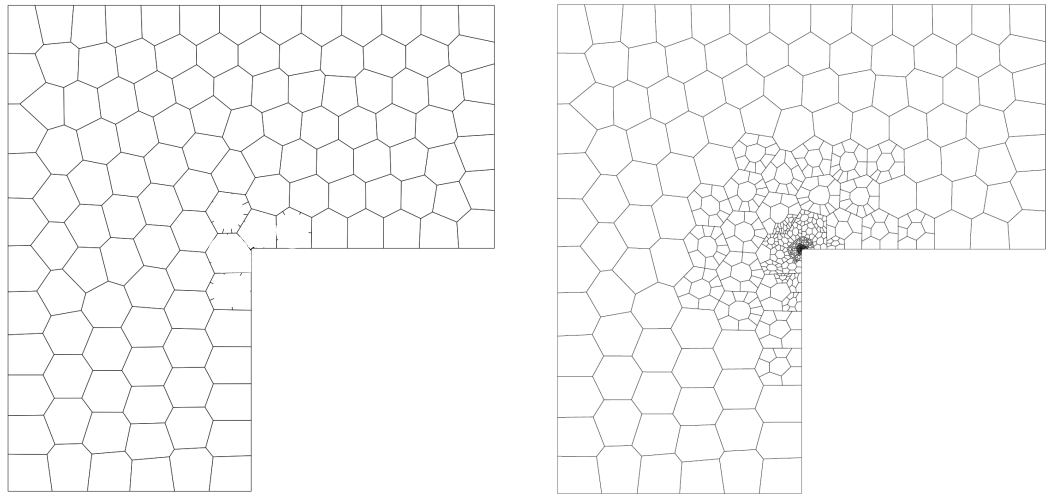

$p-$ adaptive

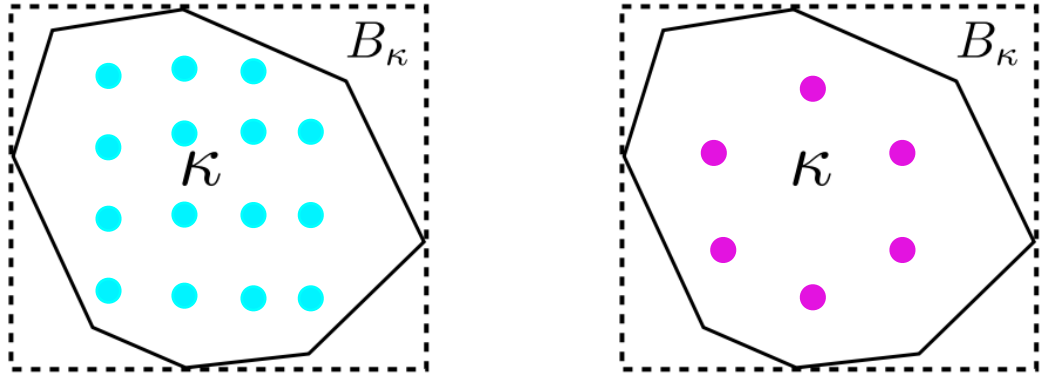

Re-meshing for traveling wavefronts is very expensive

The PolyDG method naturally supports the adaptation **of the local polynomial degree** for each element, allowing independent selection of polynomial degrees across neighbouring elements.

P-adaptive framework

Monodomain problem

$$\begin{cases} \chi_m C_m \frac{\partial u}{\partial t} - \nabla \cdot (\boldsymbol{\Sigma} \nabla u) + f(u) = I^{\text{ext}} & \text{in } \Omega \times (0,T], \\ \boldsymbol{\Sigma} \nabla u \cdot \boldsymbol{n} = 0 & \text{on } \partial\Omega \times (0,T], \\ u(0) = u^0 \end{cases}$$

Semidiscrete PolyDG formulation

$$\eta = \eta(p,h,\boldsymbol{\Sigma}) = \eta_0 \begin{cases} \{\boldsymbol{\Sigma}_K\}_A \dfrac{\{p_K^2\}_A}{\{h_K\}_H} & \text{on } F \in \mathcal{F}_h^I \\ \boldsymbol{\Sigma}_K \dfrac{p_K^2}{h_K} & \text{on } F \in \mathcal{F}_h^D \end{cases}$$

Find $u(t) \in V,\ \boldsymbol{y}(t) \in V^n$ such that $\forall\, t \in (0,T]$:

$$\begin{cases} \chi_m C_m \left(\dfrac{\partial u_h(t)}{\partial t}, v_h \right)_\Omega + \mathcal{A}(u_h(t), v_h) + \chi_m r_{\text{ion}}(u_h(t), v_h) = 0 & \forall\, v_h \in V_h^{\text{DG}}, \\ u_h(0) = u^0 & \text{in } \Omega. \end{cases}$$

$$\mathcal{A}(u,v) = \int_\Omega \boldsymbol{\Sigma} \nabla_h u \cdot \nabla_h v \, dx + \sum_{F \in \mathcal{F}_h^I} \int_F (\eta [\![u]\!] \cdot [\![v]\!] - \{\!\{\boldsymbol{\Sigma} \nabla u\}\!\} \cdot [\![v]\!] - [\![u]\!] \cdot \{\!\{\boldsymbol{\Sigma} \nabla v\}\!\}) d\sigma \quad \forall\, u, v \in V_h^{\text{DG}}$$

Adaptive indicator

A critical aspect of this approach is using an appropriate error indicator to determine the local polynomial order.

$$\tau_K^2(u) = \tau_{K,r}^2(u) + \tau_{K,n}^2(u) + \tau_{K,j}^2(u) + \tau_{K,t}^2(u)$$

$$\tau_K^2(u) = \sum_i \tau_{K,i}^2 + \sum_j \mathcal{O}_{K,j}^2$$

Residual indicator:

$$\tau_{K,r}(u_h^k) = \left\| h \left(\Pi f + \nabla_h \cdot (\boldsymbol{\Sigma} \nabla_h u_h^k) + \frac{\partial u_h^k}{\partial t} \right) \right\|_K$$

Jump indicator:

$$\tau_{K,j}(u_h^k) = \|\sqrt{\eta} [\![u_h^k]\!]\|^2_{\partial K \cap \mathcal{F}_h^I}$$

Normal jump gradient indicator:

$$\tau_{K,n}(u_h^k) = \left(\|\sqrt{h} [\![(\boldsymbol{\Sigma} \nabla_h u_h^k) \cdot \boldsymbol{n}]\!]\|^2_{\partial K \cap \mathcal{F}_h^I} + \|\sqrt{h} (\boldsymbol{\Sigma} \nabla_h u_h^k \cdot \boldsymbol{n} - \hat{g}_N)\|^2_{\partial K \cap \mathcal{F}_h^N} \right)^{\frac{1}{2}}$$

Tangential jump gradient indicator:

$$\tau_{K,t}(u_h^k) = \|\sqrt{h} [\![(\boldsymbol{\Sigma} \nabla_h u_h^k) \cdot \boldsymbol{t}]\!]\|_{\partial K \cup \mathcal{F}_h^I}$$

$$O_K^2(u) = O_{K,r}^2(u) + O_{K,j}^2(u)$$

Residual:

$$O_{K,r}(u) = \|h(\Pi f - f)\|_K,$$

Data:

$$O_{K,n}(u) = \|\sqrt{h}(g_N - \hat{g}_N)\|_{\partial K \cap \mathcal{F}_h^N}$$

Cangiani, A., Dong, Z., & Georgoulis, E. H. (2023)

Optimal threshold construction

The clustering with the k-means algorithm is done according to the value of the total indicator so that it is possible to identify the macro-region of elements presenting high indicator values.

Clustering made on the first iteration with maximum degree discretisation

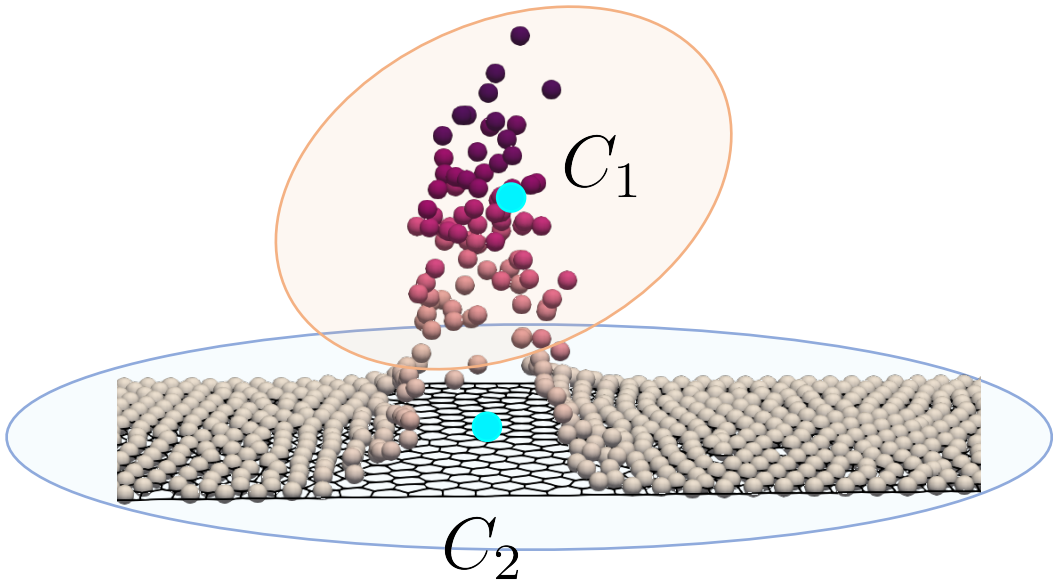

Algorithm 1 p-adaptive algorithm

1: **Input:** Initial conditions $\{u_0, \boldsymbol{y}_0\}$, Matrices
2: **Output:** $\forall t$ polynomial distribution, $\{u_h, \boldsymbol{y}_h\}$
3: Compute threshold with k-means algorithm
4: **for** time **do**
5: Compute forcing term $\boldsymbol{I}^{\text{ext}}$ and ionic therm $\boldsymbol{I}^{\text{ion}}$
6: Compute u_h^{k+1} with Crank-Nicholson scheme
7: Identify $S_K^k, S_{\text{neigh}}^k, S_K^{k+1}$ and compute $\tau_K(u_h^{k+1})$
8: Adapt polynomial degrees
9: Adapt Matrices, and reassemble SA.
10: Adapt $\boldsymbol{I}_{\text{ext}}^{k+1}$, $\boldsymbol{I}_{\text{ion}}^{k+1}$
11: Adapt solution u_h^{k+1}
12: **end for**

$$\tau_K^{\min} = \min C_i \ , \ \tau_K^{\text{mean}} = \frac{C_1 + C_2}{2}$$

Adaptive algorithm

Selection of a subsection of elements where to compute the indicator, depending on the elements modified in the iteration before and on the value of the indicator

High computational costs for the indicator

Selection of the elements where to compute the indicator

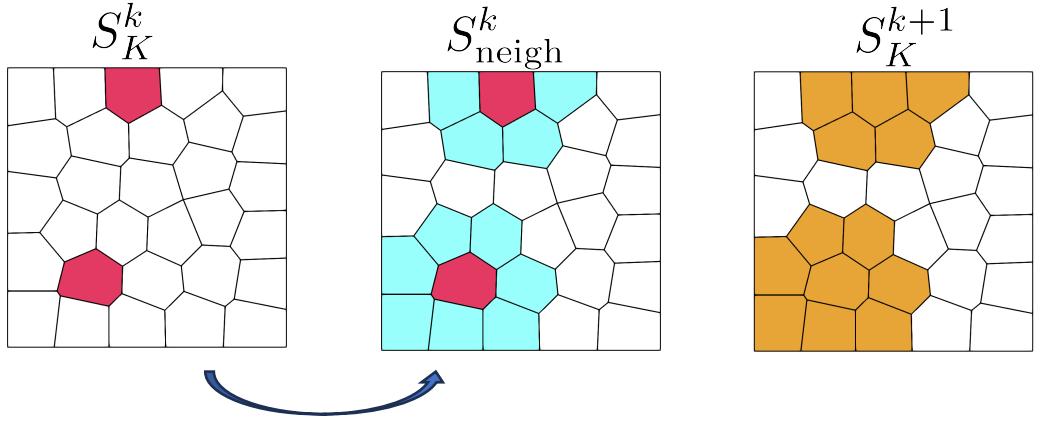

The final degree is defined also depending on the old polynomial degree of each element.

$$p_{\text{arctan}} = \left\lceil p_{\max} \frac{2}{\pi} \arctan\left(\frac{\tau_K}{\tau_{\text{threshold}}}\right) \right\rceil$$

Algorithm 1 p-adaptive algorithm

1: **Input:** Initial conditions $\{u_0, \boldsymbol{y}_0\}$, Matrices
2: **Output:** $\forall t$ polynomial distribution, $\{u_h, \boldsymbol{y}_h\}$
3: Compute threshold with k-means algorithm
4: **for** time **do**
5: Compute forcing term $\boldsymbol{I}^{\text{ext}}$ and ionic therm $\boldsymbol{I}^{\text{ion}}$
6: Compute u_h^{k+1} with Crank-Nicholson scheme
7: Identify $S_K^k, S_{\text{neigh}}^k, S_K^{k+1}$ and compute $\tau_K(u_h^{k+1})$
8: Adapt polynomial degrees
9: Adapt Matrices, and reassemble SA.
10: Adapt $\boldsymbol{I}_{\text{ext}}^{k+1}$, $\boldsymbol{I}_{\text{ion}}^{k+1}$
11: Adapt solution u_h^{k+1}
12: **end for**

$$p_{\text{new}} = \mathbb{1}_{\{p_{\text{old}} \leq p_{\text{arctan}}\}} \min(p_{\text{old}} + 1, p_{\text{arctan}}) + \mathbb{1}_{\{p_{\text{old}} > p_{\text{arctan}}\}} \max(p_{\text{old}} - 1, p_{\text{arctan}}).$$

Adaptivity of the matrices

High cost in reassembly the matrices

Exploit **hierarchical basis** function for the discretization

$$A = \begin{bmatrix} A_1 & A_2 & \cdots & A_{\text{nel}} \\ A_{\text{nel}+1} & \vdots & \vdots & A_{2\text{nel}} \\ \vdots & \vdots & \vdots & \vdots \\ A_{(\text{nel-1})\text{nel}} & \cdots & \cdots & A_{\text{nelnel}} \end{bmatrix}$$

$$A_i = \begin{bmatrix} a_{1,1} & a_{1,2} & a_{1,3} & a_{1,4} & a_{1,5} & a_{1,6} \\ & a_{2,2} & a_{2,3} & a_{2,4} & a_{2,5} & a_{2,6} \\ & & a_{3,3} & a_{3,4} & a_{3,5} & a_{3,6} \\ & & & a_{4,4} & a_{4,5} & a_{4,6} \\ & & & & a_{5,5} & a_{5,6} \\ & & & & & a_{6,6} \end{bmatrix}$$

$$A_1 = \begin{bmatrix} a_{1,1} & a_{1,2} & a_{1,3} & a_{1,4} & a_{1,5} & a_{1,6} \\ & a_{2,2} & a_{2,3} & a_{2,4} & a_{2,5} & a_{2,6} \\ & & a_{3,3} & a_{3,4} & a_{3,5} & a_{3,6} \\ & & & a_{4,4} & a_{4,5} & a_{4,6} \\ & & & & a_{5,5} & a_{5,6} \\ & & & & & a_{6,6} \end{bmatrix}$$

Re-assembly is made by "cutting" the local matrices of the problem depending of the polynomial degree

Algorithm 1 p-adaptive algorithm

1: **Input:** Initial conditions $\{u_0, \boldsymbol{y}_0\}$, Matrices
2: **Output:** $\forall t$ polynomial distribution, $\{u_h, \boldsymbol{y}_h\}$
3: Compute threshold with k-means algorithm
4: **for** time **do**
5: Compute forcing term $\boldsymbol{I}^{\text{ext}}$ and ionic therm $\boldsymbol{I}^{\text{ion}}$
6: Compute u_h^{k+1} with Crank-Nicholson scheme
7: Identify $S_K^k, S_{\text{neigh}}^k, S_K^{k+1}$ and compute $\tau_K(u_h^{k+1})$
8: Adapt polynomial degrees
9: Adapt Matrices, and reassemble SA.
10: Adapt $\boldsymbol{I}_{\text{ext}}^{k+1}$, $\boldsymbol{I}_{\text{ion}}^{k+1}$
11: Adapt solution u_h^{k+1}
12: **end for**

$$\mathcal{A}(u,v) = \int_\Omega \boldsymbol{\Sigma}\nabla_h u \cdot \nabla_h v \, dx + \sum_{F\in\mathcal{F}_h^I} \int_F (\eta[\![u]\!]\cdot[\![v]\!] - \{\!\{\boldsymbol{\Sigma}\nabla u\}\!\}\cdot[\![v]\!] - [\![u]\!]\cdot\{\!\{\boldsymbol{\Sigma}\nabla v\}\!\})d\sigma \quad \forall\, u,v \in V_h^{\text{DG}}$$

Numerical Results

Test case

Travelling wavefront in homogeneous medium

Analysis of the optimal indicator definition for keeping accuracy of the numerical solution

Double traveling wavefront with different speed in heterogeneous tissue

Neuronal electrophysiology application

Monodomain coupled problem for neuronal electrophysiology

Travelling wavefront

Traveling wave-front: **evolution of the transmembrane potential in p-adaptive context**

$$u_{\text{ex}}(\boldsymbol{x},t) = \frac{V_{\text{dep}} - V_{\text{rest}}}{2}\left[1 - \tanh\left(\frac{\boldsymbol{x} - \boldsymbol{c}t}{\epsilon}\right)\right] + V_{\text{rest}},$$

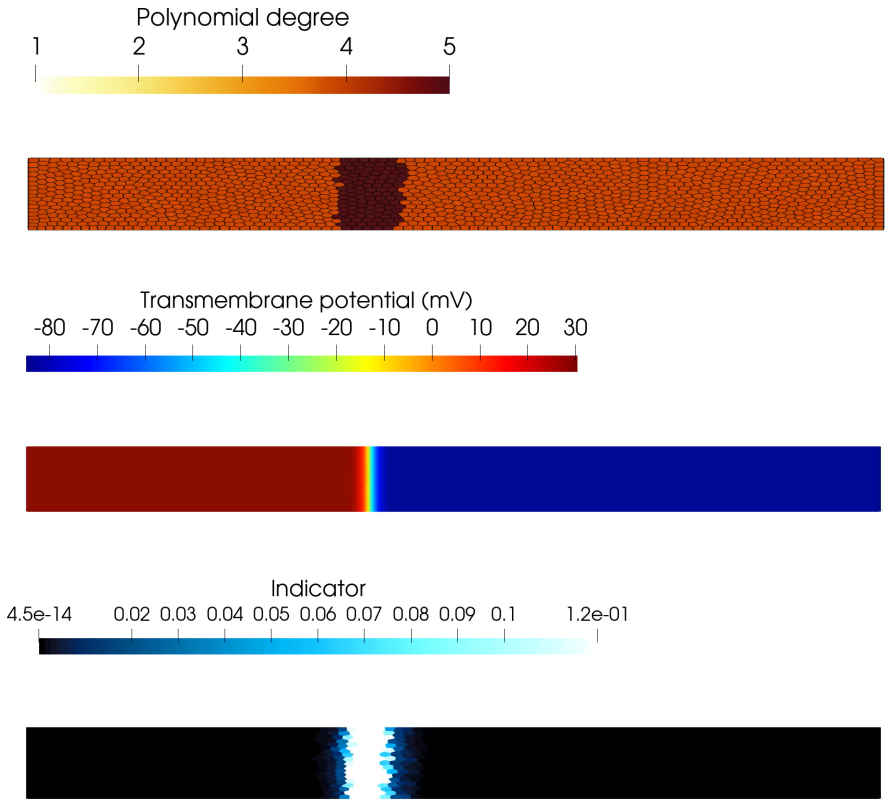

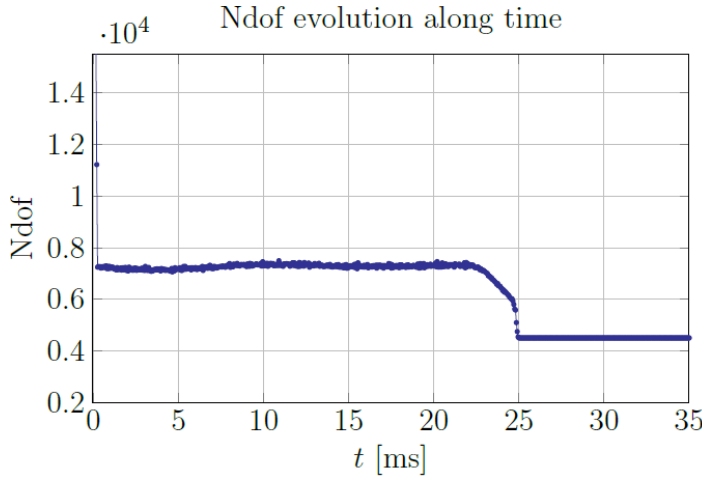

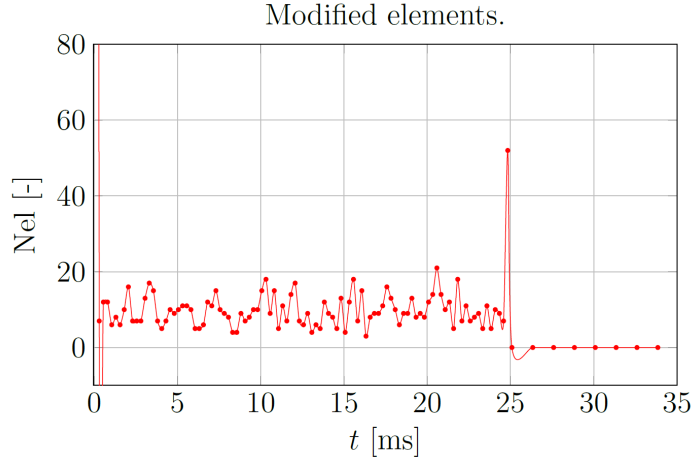

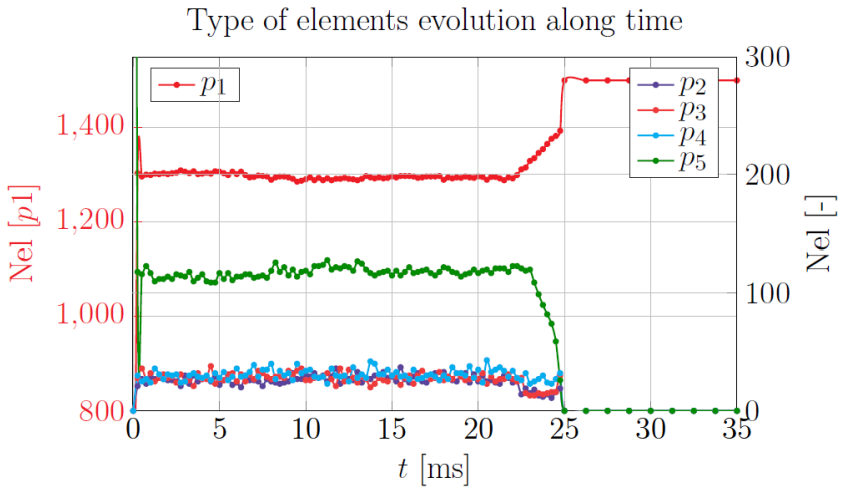

σ $[\text{Sm}^{-1}]$	c $[\text{ms}^{-1}]$
0.0081	0.0081

Optimal indicator comparison

Optimal indicator comparison: **Evolution of polynomial degree for different indicators**

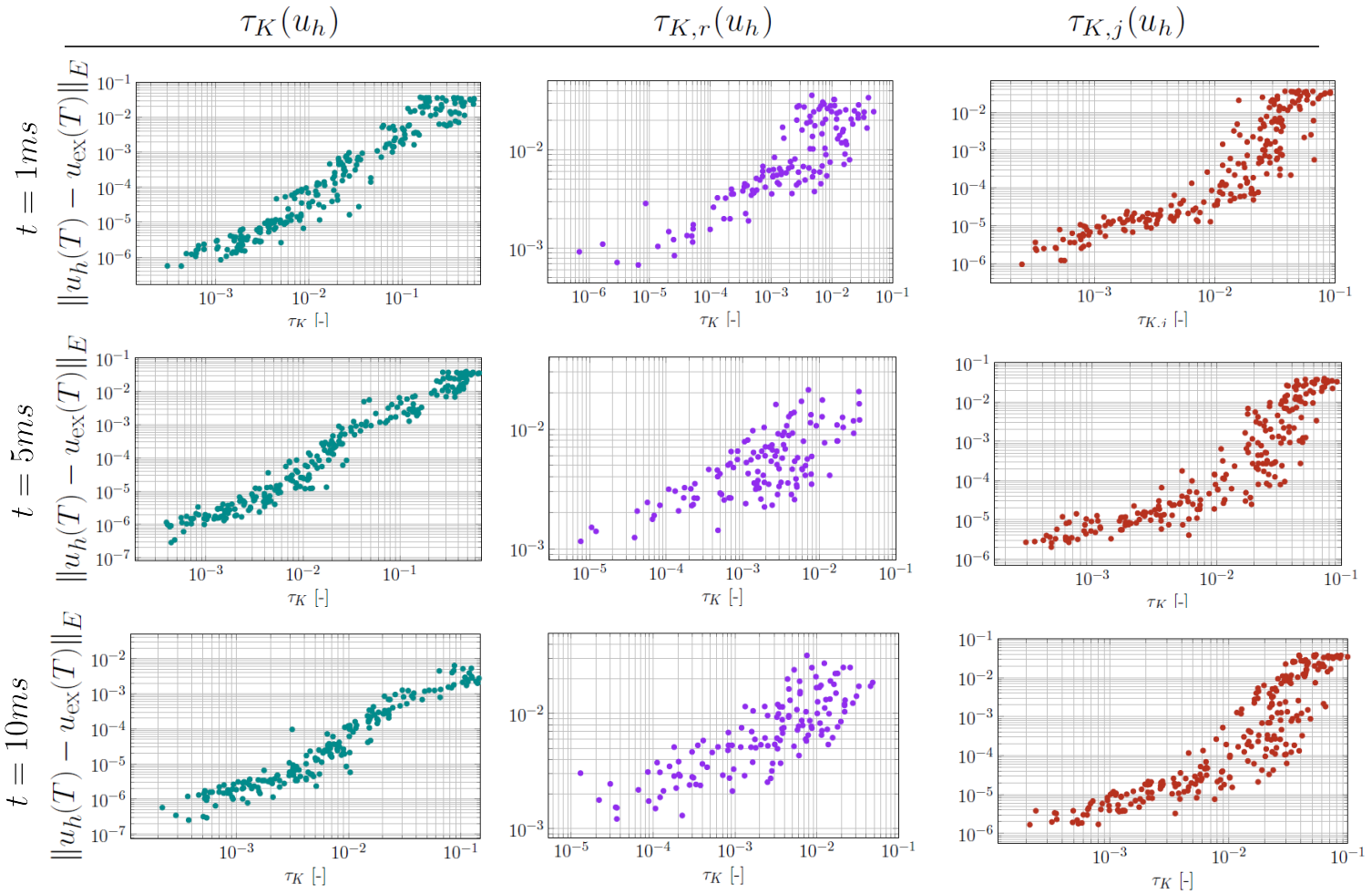

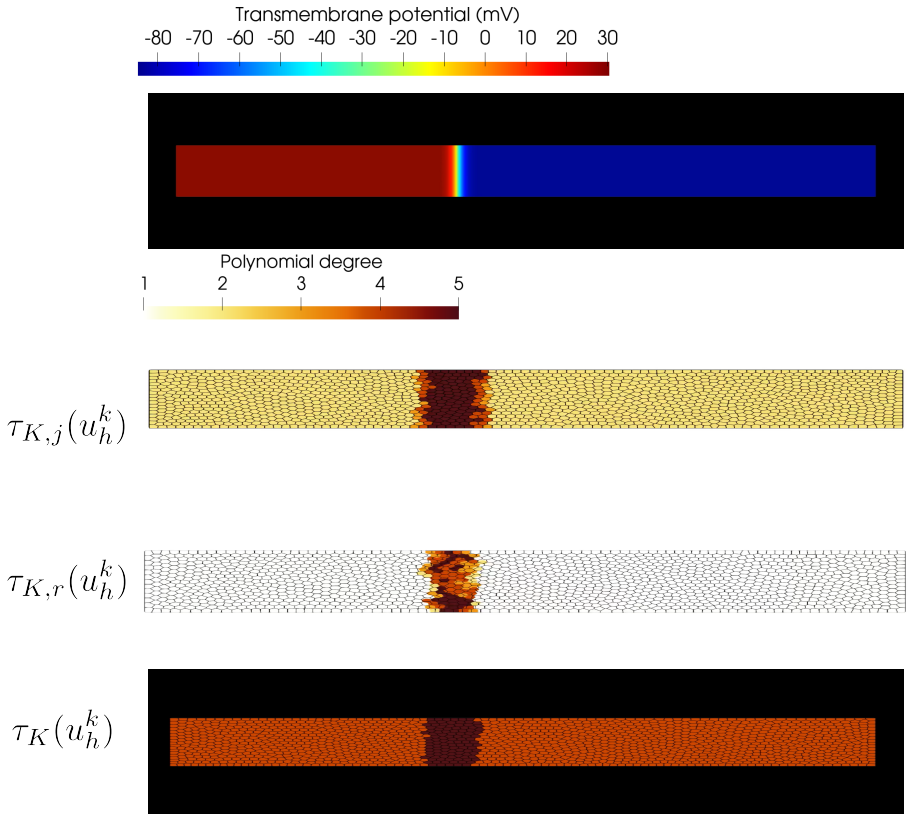

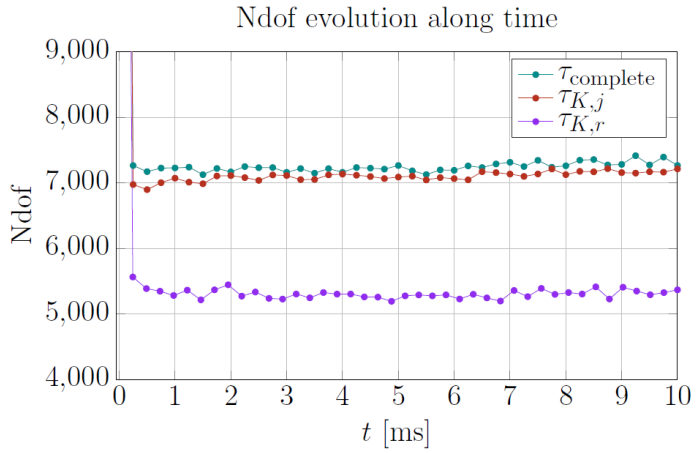

The complete and jump indicators can correctly identify the wave, maintaining the required accuracy.

Heterogeneous tissue

Heterogenous tissue: evolution of the transmembrane potential with p-adaptive context for double wavefront traveling with different speeds.

Tissue type	σ_n $[\mathrm{Sm}^{-1}]$	σ_t $[\mathrm{Sm}^{-1}]$
Ω_1	0.0081	0.0081
Ω_2	0.0551	0.0551

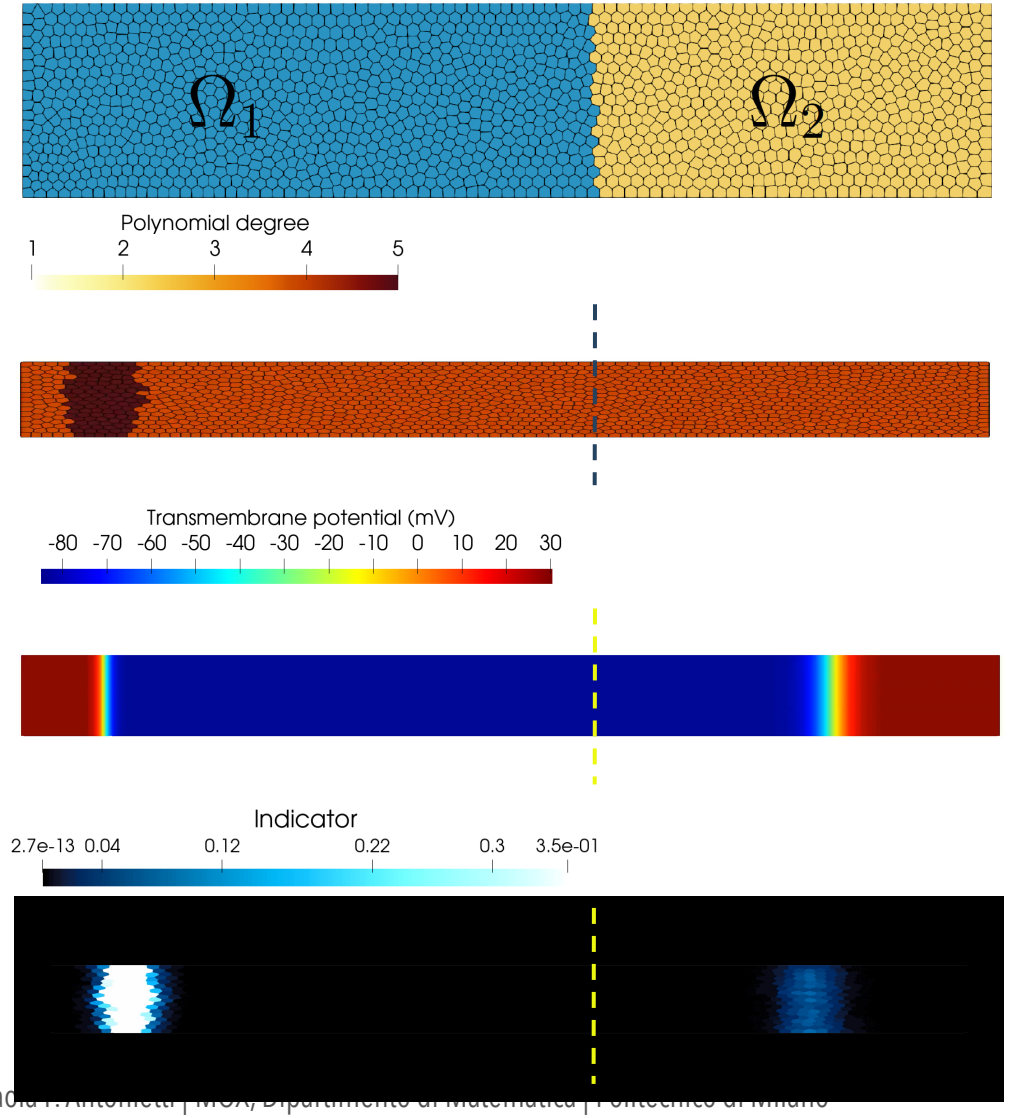

$$u^0(\boldsymbol{x}) = \frac{V_{\text{dep}} - V_{\text{rest}}}{2}\left(\tanh\left(\frac{\boldsymbol{x}+x_2}{\epsilon}\right) - \tanh\left(\frac{\boldsymbol{x}+x_1}{\epsilon}\right)\right) + V_{\text{dep}}.$$

Initial condition profile:

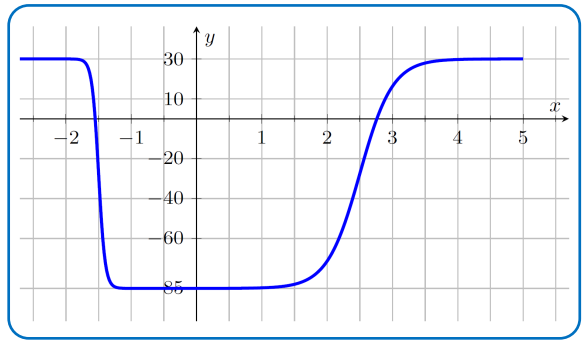

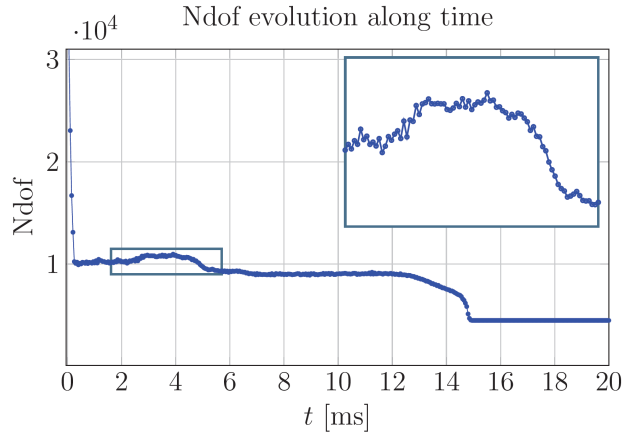

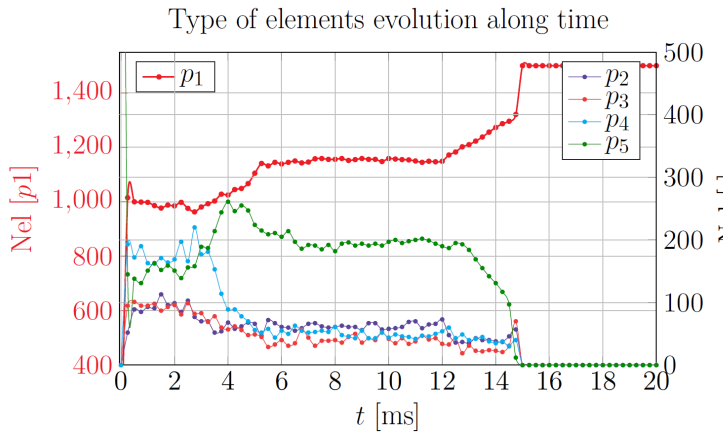

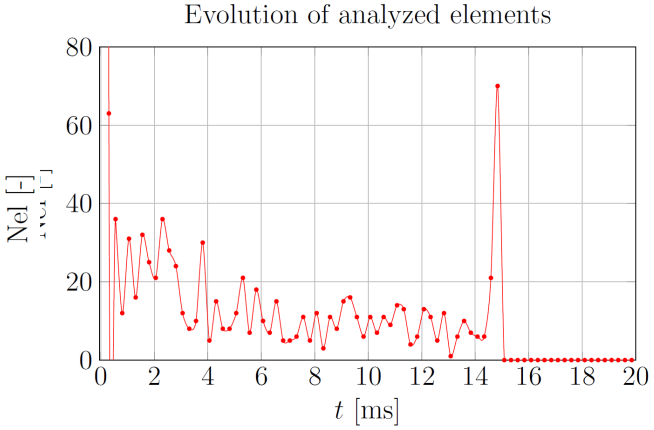

Monodomain coupled problem

Gray matter tissue: evolution of the transmembrane potential in a 2D slab section with unstable gray matter region for a general seizure simulation.

The pathological behavior is particularly accentuated by introducing an external forcing term so that the pathological grey matter zone is extremely excited.

$$I^{\text{ext}} = \frac{A}{1 + e^{\sin(t)}} \mathbb{1}_{\{\boldsymbol{x} \in \Omega_0\}}$$

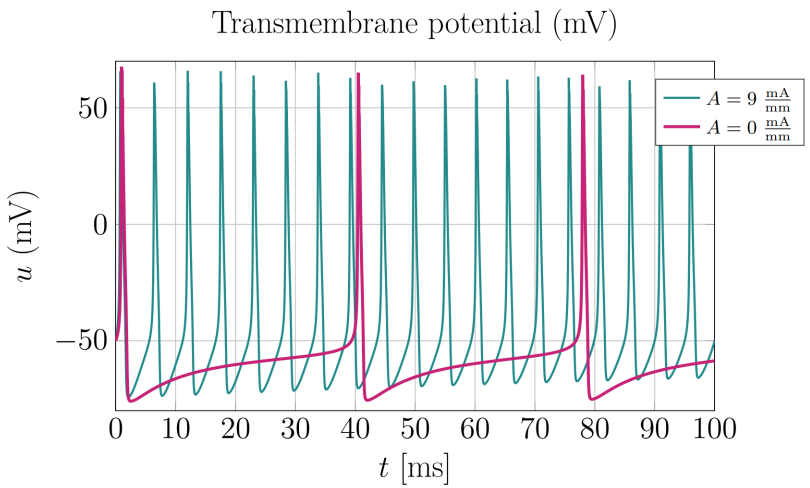

Initial condition: $u^0(\boldsymbol{x}) = 17\mathbb{1}_{(\Omega_0)} - 67\mathbb{1}_{(\Omega)}$

Tissue type	σ_n [Sm^{-1}]	σ_t [Sm^{-1}]
GM	0.0735	0.0735

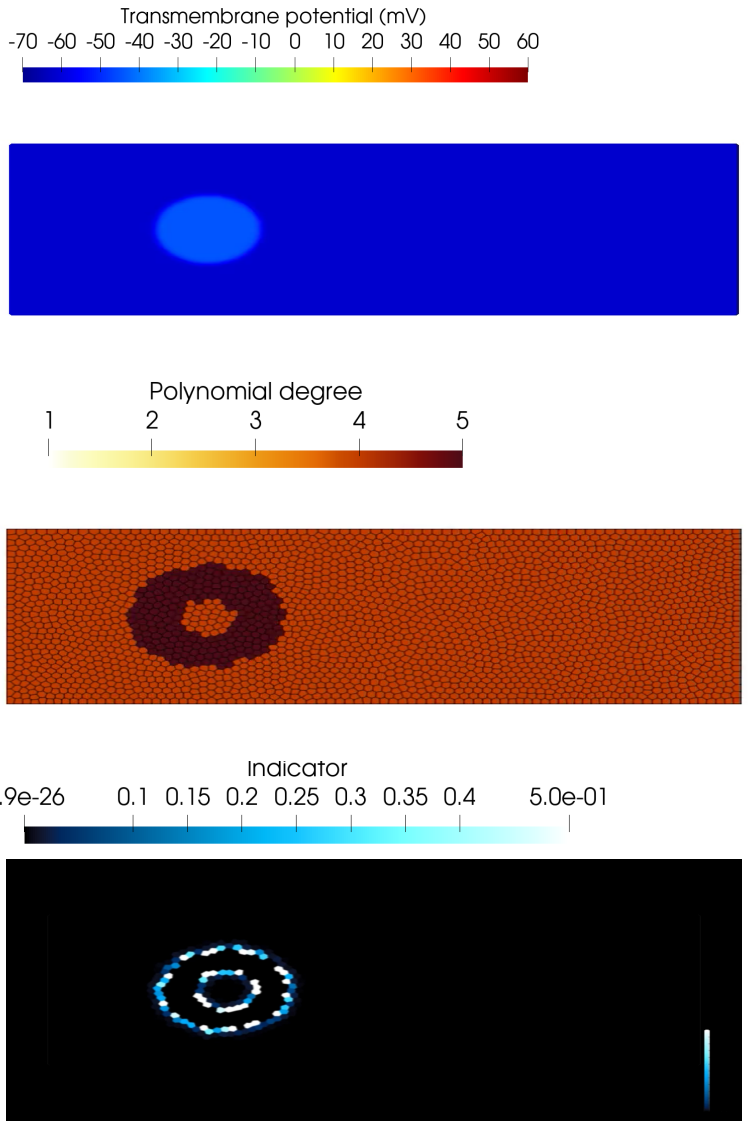

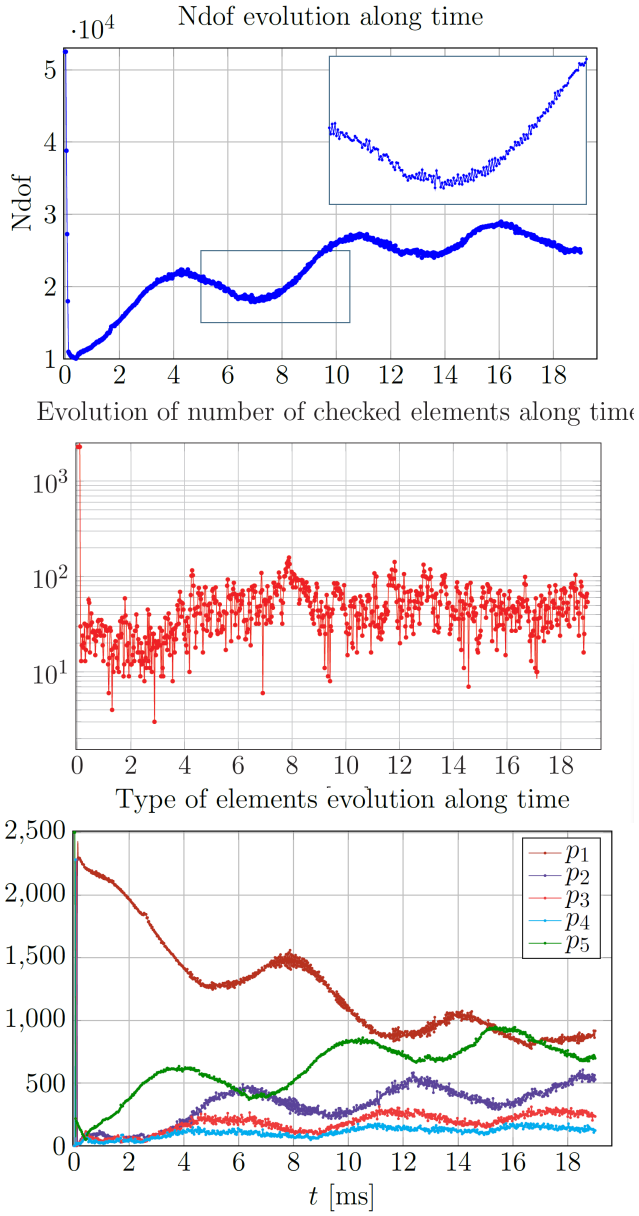

Real geometry

Gray-white matter tissue: evolution of the transmembrane potential in a 2D section of a brain stem with unstable gray matter region for a general seizure simulation.

Tissue type	σ_n [Sm^{-1}]	σ_t [Sm^{-1}]
GM	0.0735	0.0735
WM	1.0557	1.0139

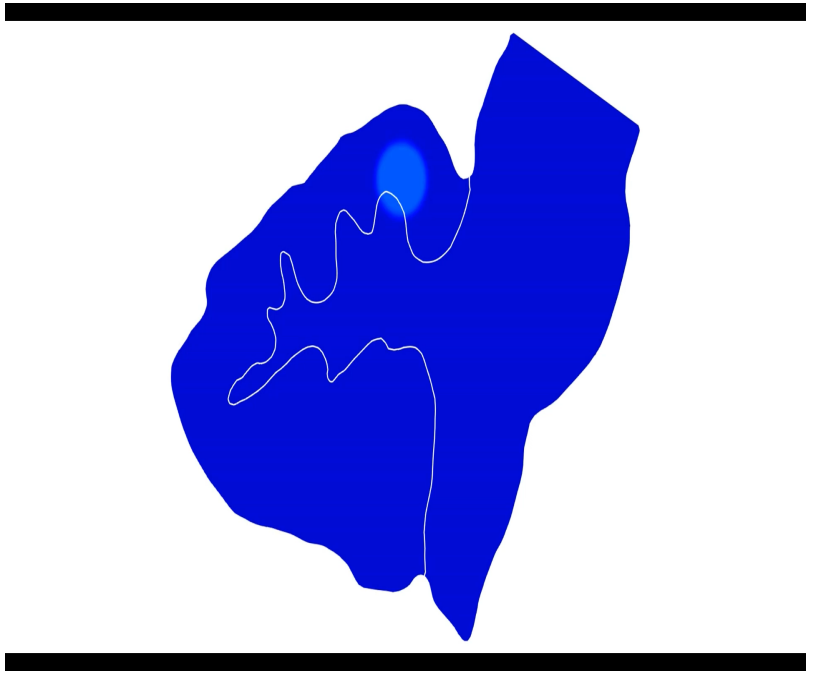

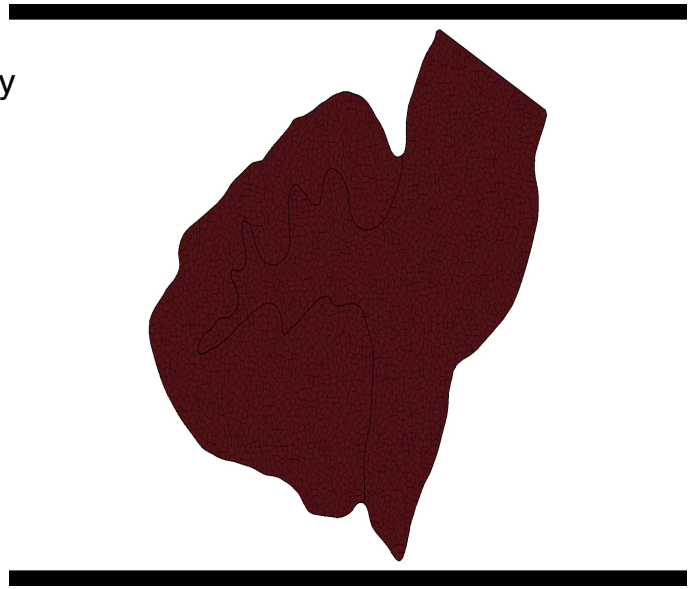

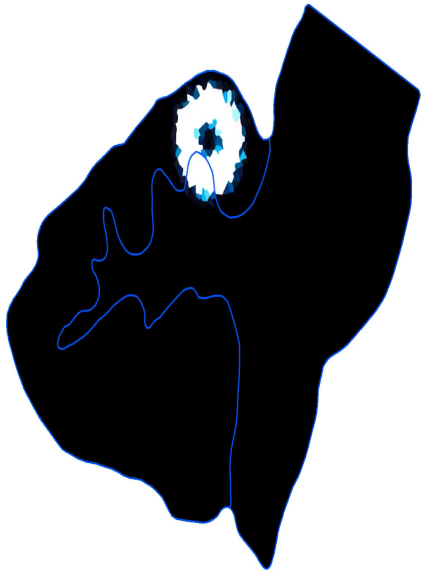

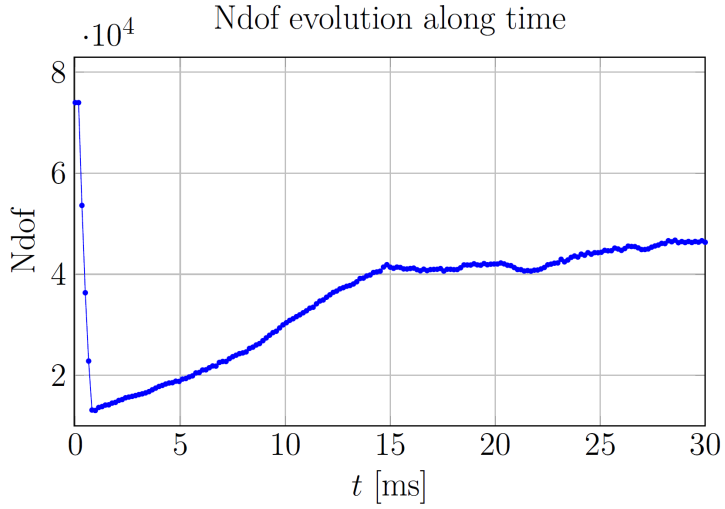

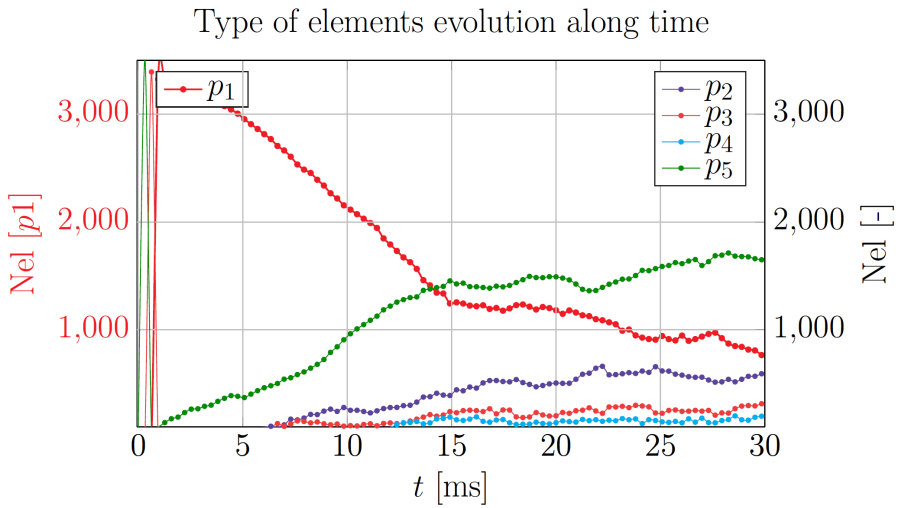

Acknowledgements